PERFORMANCE-BASED PLASTIC DESIGN OF EARTHQUAKE RESISTANT CONCENTRICALLY BRACED STEEL FRAMES

by

M. Reza Bayat

Subhash C. Goel

Shih-Ho Chao

Department of Civil and Environmental Engineering

The University of Michigan
College of Engineering

Ann Arbor, MI 48109-2125

Research Report UMCEE 10-02 September 2010

PERFORMANCE-BASED PLASTIC DESIGN
OF EARTHQUAKE RESISTANT
CONCENTRICALLY BRACED STEEL FRAMES

by

M. Reza Bayat

Subhash C. Goel

Shih-Ho Chao

A report on research sponsored by
American Institute of Steel Construction
and
NUCOR Research & Development

Department of Civil and Environmental Engineering

The University of Michigan
College of Engineering

Ann Arbor, MI 48109-2125

ACKNOWLEDGEMENT

The authors gratefully acknowledge financial support provided by the American Institute of Steel Construction (AISC), and NUCOR Research and Development (NUCOR R&D) for this study. Constant encouragement received from Tom Schlafly at AISC and Dave Samuelson and Walt Schultz at NUCOR R&D is also greatly appreciated. The opinions and views expressed in the report are solely those of the authors and do not necessarily reflect those of the sponsors.

TABLE OF CONTENTS

CHAPTER 1

Introduction

1.1 General

Concentrically braced frames (CBF) are very efficient and commonly used steel structures to resist forces due to wind or earthquakes because they provide complete truss action. Based on research performed during the last thirty years or so (for example, Goel, 1992a), current seismic codes (ANSI/AISC 341-05, 2005) include provisions for design of ductile concentric braced frames called Special Concentric Braced Frames (SCBF). Since the seismic forces are assumed to be entirely resisted by means of truss action, the columns are designed based on axial load demand only and simple shear connections are used to join the beams and columns (Tremblay and Robert, 2000; MacRae et al., 2004; ANSI/AISC 360-05, 2005). It has been estimated that CBF comprised about 40% of the newly built commercial construction in the last decade in California (Uriz, 2005). This is attributed to simpler design and high efficiency of CBF compared to other systems such as moment frames, especially after the 1994 Northridge Earthquake.

However, CBF are generally considered less ductile seismic resistant structures than other systems due to buckling or fracture of the bracing members under large cyclic displacements. These structures can undergo large story drifts after buckling of bracing members, which in turn may lead to early fractures of the bracing members, especially in those made of popular rectangular tube sections (HSS). Recent analytical studies have shown that SCBF designed by conventional elastic design method can suffer severe damage or even collapse under design level ground motions (Sabelli, 2000).

This report presents the application of the newly developed Performance-Based Plastic Design (PBPD) method to design of CBF with buckling type braces which exhibit somewhat "pinched" hysteretic loops. Pre-selected target drift and yield mechanism are used as performance limit states. In the PBPD method, design lateral forces are derived by using an energy equation where the energy needed to push the structure up to the target drift is calculated as a fraction of elastic input energy which is obtained from the selected elastic design spectra. Plastic design is then performed to detail the frame members in order to achieve the intended yield mechanism and behavior (Goel and Chao, 2008). In addition, modified brace and beam-to-column connection configurations are also suggested to further enhance the overall performance. Also, a fracture life criterion is employed for the HSS braces to prevent premature fracture. Results from nonlinear time history analyses carried out on example frames designed by the PBPD approach showed that the frames met all the desired performance objectives, including the intended yield mechanisms and story drifts while preventing brace fractures under varied hazard levels (Chao and Goel, 2006b).

Two alternative approaches are suggested for considering the pinched hysteretic behavior of CBF in the PBPD method. The first approach uses an energy modification factor, called η-factor and applied in the work-energy equation, to account for the reduced hysteretic energy due to pinching (Chao and Goel, 2006b; Goel and Chao, 2008). In this approach, the basic work-energy equation for elastic-perfectly plastic hysteretic systems is modified to account for the pinched hysteretic behavior of CBF (Goel and Chao, 2008). This method is presented in detail in Chapter 2.

Based on further research on the subject, a second approach to account for the pinched hysteretic behavior of CBF in calculation of the PBPD design base shear is proposed (Bayat, Chao, and Goel, 2010; Bayat, 2010). In this method, a modification factor, called λ-factor, is directly applied on the target drift to account for the effect of pinching. The λ-factor can be considered as ratio between the maximum displacement of a pinched SDOF system (representing CBF) to that of an equivalent elastic-plastic SDOF. By dividing the design target drift for the CBF by this factor, an effective target drift is obtained which is then used to calculate the PBPD design base shear. Pending further research on more accurate estimation of λ-factor for CBF, an estimation based on the C_2-factor values as proposed in FEMA-356 (FEMA, 2000a) and FEMA440 (FEMA, 2004) for stiffness and strength degrading systems in general are used herein. The application of this approach for design of CBF systems is presented in Chapter 3.

1.2 Scope and Organization of the Report

The scope of this report includes: (1) Development of the PBPD method for CBF; (2) Redesign of previously studied NEHRP SCBF by the PBPD method and comparison of their seismic performances; (3) Presentation of some new findings and modifications in the PBPD method for taller CBF; and (4) Reliability-based confidence level evaluation of the NEHRP and PBPD frames. The organization of the report is as follows:

- Chapter 1 introduces the background, scope and organization of the report.
- Chapter 2 presents in detail the application of PBPD method for design of CBF and also redesign of the 3 and 6-story NEHRP frames by using the PBPD method. The η-factor approach is utilized in this part of the study.
- Chapter 3 presents some new findings in further development of PBPD method in design of taller CBF such as: column design in CBF, λ-factor method to account for pinched hysteretic behavior in design base shear calculation, modification of yield drift to include column axial deformation, etc. Those findings and necessary modifications are incorporated in the method and used to design a mid-rise 9-story CBF.
- Chapter 4 presents the results of confidence level analysis of the previously studied 3, 6, and 9-story CBF structures, including NEHRP and PBPD designs. It should be mentioned that evaluation of confidence level against collapse in this study was performed by following the SAC methodology as used by Uriz (2005) for code designed frames, instead of the one currently suggested in FEMA P695 (2009). That was done for reasons of consistency and direct comparisons of the confidence levels for code designed (Uriz, 2005) versus corresponding PBPD frames.
- Chapter 5 presents the modifications applied for the 9-story CBF in order to improve its confidence level against collapse. These include modification in the

PBPD design base shear (DBS) calculations for taller CBF, and considering a different brace configuration of two story X-brace (Split-X). Also, the effect of increasing the brace fracture life, N_f, on the confidence level was studied.

- Chapter 6 presents the summary and conclusions of this study.

CHAPTER 2

PBPD Procedure for Design of CBF

2.1 AISC Seismic Design Criteria for CBF

Some key points for design of CBF in the AISC Seismic Provisions (ANSI/AISC 341-05, 2005) are also followed in the PBPD approach and summarized in the following:

- Bracing members should have $KL/r \leq 4\sqrt{E/F_y}$, where K and L are the effective length factor and the unbraced length for the member, respectively, and r is the governing radius of gyration.
- HSS bracing members should have b/t or $h/t_w \leq 0.64\sqrt{E/F_y}$. Columns in CBF are required to have adequate compactness as specified by Table I-8-1 in the AISC Seismic Provisions (ANSI/AISC 341-05, 2005), because they could undergo inelastic bending after buckling or fracture of the braces.
- For V-Type or Inverted-V (Chevron) bracing, the beams intersected by the braces should be designed assuming that braces do not provide support for gravity loads. The beam should be designed to support vertical and horizontal unbalanced forces resulting from the difference in the tension and compression brace forces after buckling. For this purpose, the tension and compression

forces in the braces are assumed to be equal to $R_y F_y A_g$ and $0.3P_{cr}$, respectively. Both flanges of beams need to be laterally braced, with a maximum spacing of $L_b = L_{pd} = \left[0.12 + 0.076\left(\frac{M_1}{M_2}\right)\right]\left(\frac{E}{F_y}\right) r_y$ for I-shaped beam members, where M_1 is the smaller moment at the end of unbraced length of beam and M_2 is the larger moment; r_y is the radius of gyration about minor axis. $\left(M_1 / M_2\right)$ is positive when moments cause reverse curvature and negative for single curvature.

2.2 Overall PBPD Procedure for CBFs

The design base shear and corresponding lateral force distribution are first determined according the flowchart shown in Figure 2.1 and using Equation (2.1) for V/W as given in the next section. Then the design of a typical concentrically braced frame is performed by following the flowchart given in Figure 2.2.

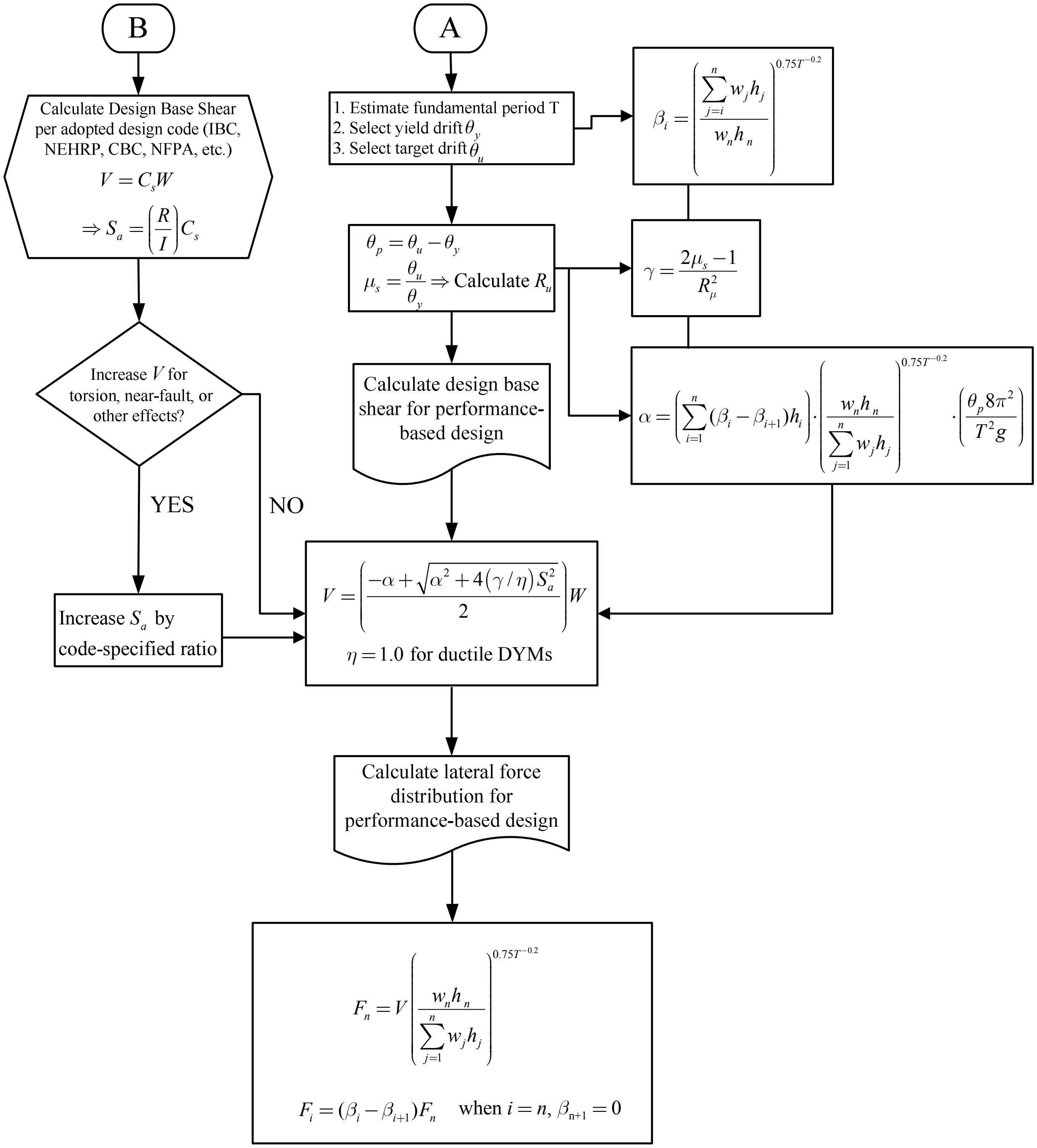

Figure 2.1. Performance-Based Plastic Design Flowchart: Determining Design Base Shear and Lateral Force Distribution

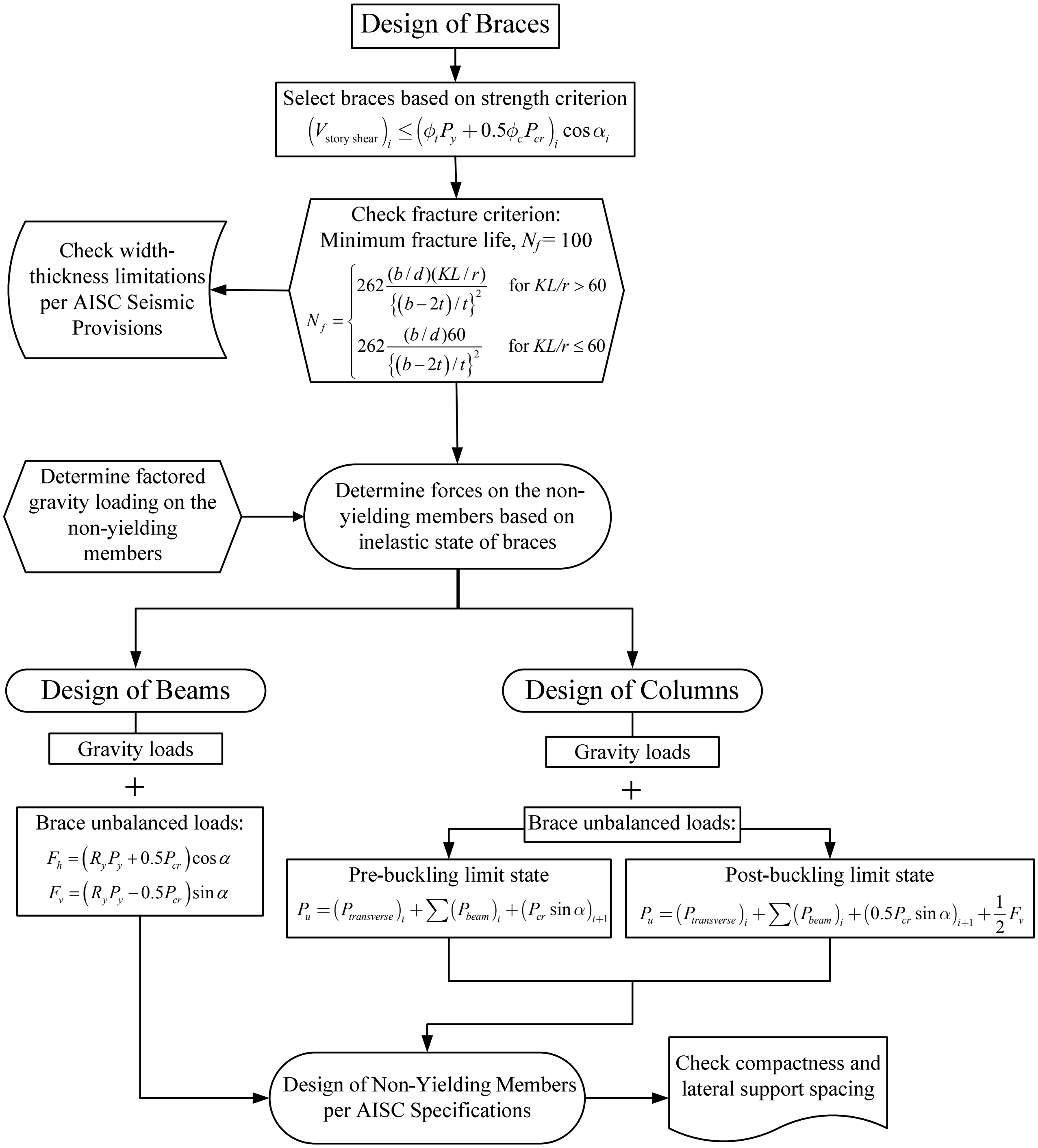

Figure 2.2. Performance-Based Plastic Design Flowchart for CBF: Element Design

2.2.1 Design Base Shear

The required design base shear in PBPD was derived by assuming elastic-plastic hysteretic behavior of structural systems, such as steel MF, EBF, BRBF, or STMF (Leelataviwat, 1998; Lee and Goel, 2001 ; Chao and Goel, 2006a; Goel and Chao, 2008). However, buckling of braces in concentrically braced frames (CBF) leads to "pinched" hysteretic loops. Therefore, using the same design base shear for a CBF would not be appropriate. A preliminary study based on a simple one-story one bay braced frame with pin-connected rigid beams and columns showed that the dissipated energy by CBF is approximately 35% of the energy dissipated by a corresponding frame with full elastic-plastic hysteretic loops, with both frames having equal strengths ($\eta = A_1 / A_2 = 0.35$ in Figure 2.3). Pending further study and considering that other structural members such as "gravity fames" will also resist earthquake forces, a slightly higher $\eta = 0.5$ is suggested at this time for design purposes. However, caution should be exercised as this suggested value for η is based on one data point. Thus, the work-energy equation for CBF can be modified as (Chao and Goel, 2006b):

$$\eta\left(E_e + E_p\right) = \frac{1}{2}\gamma M\left(\frac{T}{2\pi}S_a g\right)^2 \tag{2.1}$$

The solution leads to the following equation:

$$\frac{V}{W} = \frac{-\alpha + \sqrt{\alpha^2 + 4\left(\gamma/\eta\right)S_a^2}}{2} \tag{2.2}$$

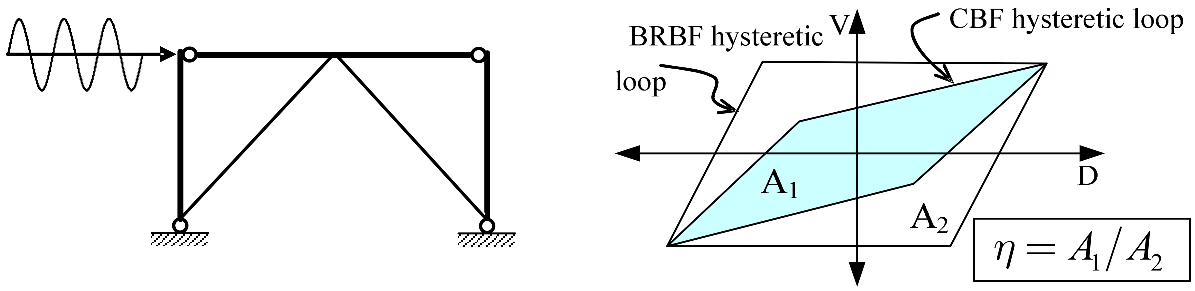

Figure 2.3. Typical Full EP and “Pinched” Hysteretic Loops

2.2.2 Target Yield Mechanism

Figure 2.4 shows a Chevron type CBF subjected to design lateral forces and pushed through its target plastic drift limit state. All inelastic deformations are intended to be confined to the braces in the form of yielding and buckling. The design yield mechanism of CBF is achieved through inelastic deformation of the bracing members and plastic hinges at the column bases, if permitted to form.

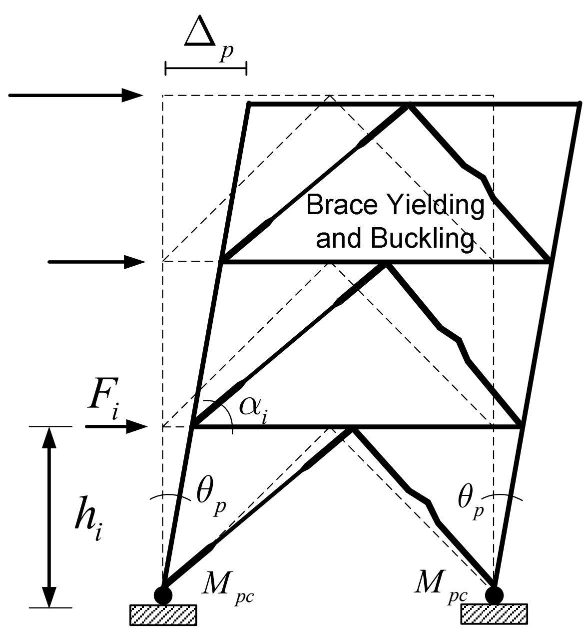

Figure 2.4. Target Yield Mechanism of CBF with Chevron Bracing

2.2.3 Recommended Brace and Beam-to-Column Connection Configurations

Rectangular tube (HSS) sections are very popular sections for bracing members because of their efficiency to carry axial compressive forces. Single tube sections with slots at the ends for welding to the gusset plate are most commonly used. Braces in this configuration generally buckle out-of-plane under compression, leading to large bending and rotation of the gusset plates. Thus, one plastic hinge forms in the bracing member with two end plastic hinges forming in the gusset plates with nearly pin-end conditions. Consequently, this results in less amount of energy dissipation in the bracing member. Other disadvantage of out-of-plane buckling of the braces includes the damage of non-structural elements, such as walls (Tremblay et al., 1996).

Special detailing is required (ANSI/AISC 341-05, 2005) in order to prevent premature failure in the gusset plates, which generally results in relatively large gusset plates. It has been observed in recent tests that large gusset plates change simple beam-to-column connections into somewhat rigid connections, creating significant moment and rotation demands on the columns. Because columns in CBF are commonly designed for axial force only, severe damage can occur at these locations (Figure 2.5, Uriz, 2005).

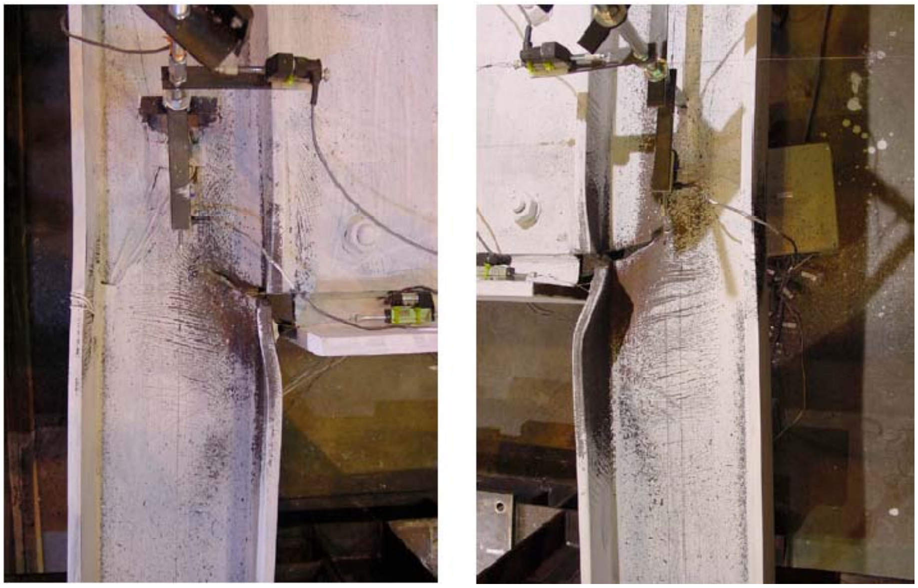

Figure 2.5. Fracture of beam-to-column connection in a two-story CBF specimen (Uriz, 2005)

Research conducted by Lee and Goel (1990) showed that the disadvantages of using single tube sections as bracing members can be overcome by using built-up double tube sections. Advantages of using double tube section for braces include the following (Lee and Goel, 1990; ANSI/AISC 341-05, 2005):

- Smaller width-thickness ratio for the same overall width of the section.
- In-plane buckling: three plastic hinges forming in the bracing member thus higher energy dissipation and compression strength (Goel, 1992a). The post-buckling strength can be taken as $0.5P_{cr}$ instead of $0.3P_{cr}$, along with effective length factor, K, of 0.5 (fixed end condition).
- More compact gusset plate connections due to elimination of out-of-plane bending of gusset plates.

- No slots in the tubes are needed, thus reducing the possibility of net section failure at the ends.
- Smaller unbalanced forces on beams due to higher post-buckling strength of the braces.
- Reduced damage to non-structural elements due to in-plane buckling of braces.

The detailed configuration of the double tube-to-gusset plate connection can be found elsewhere (Lee and Goel, 1990).

Furthermore, a beam shear splice is recommended to prevent moment transfer into the column, as shown in Figure 2.6. Another advantage of using this scheme is that the column-beam stub connection can be shop-fabricated, thereby enhancing the quality and reducing the field labor cost.

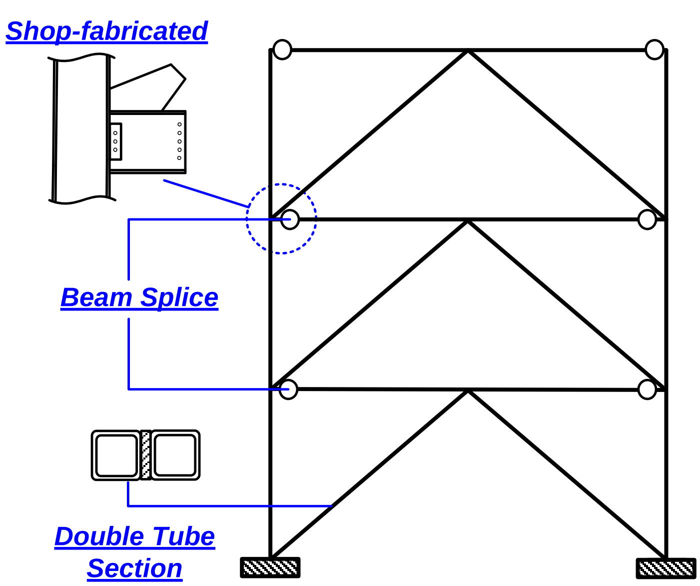

Figure 2.6. Recommended Connection Details for CBF

2.2.4 *Design of Bracing Members*

Three criteria are used in PBPD approach for design of bracing members, as described in the following sections.

2.2.4.1 Strength Criterion

It is desirable to have the distribution of bracing member strength along the building height closely follow the distribution of design story shears to minimize the possibility of concentration of inelastic deformation in one or few stories. The braces are designed based on their ultimate state (plastic design), i.e., tension yielding and post-buckling, to resist the total design story shear, neglecting the contribution from columns (conservative). Thus,

$$\left(V_{\text{story shear}}\right)_i \le \left(\phi_t P_y + 0.5\phi_c P_{cr}\right)_i \cos\alpha_i \tag{2.3}$$

or,

$$\frac{\left(V_{\text{story shear}}\right)_i}{0.9\cdot\cos\alpha_i} \le \left(P_y + 0.5P_{cr}\right)_i \tag{2.4}$$

where $V_{\text{story shear}}$ is the story shear at level i for an equivalent one-bay frame; P_y is the nominal axial tensile strength of bracing members; P_{cr} is the nominal axial compressive strength of bracing members; $\phi_t = \phi_c = 0.9$ (ANSI/AISC 360-05, 2005); α is the angle of bracing members with the horizontal (see Figure 7-3). The design is carried out by assuming that both bracing members reach their ultimate inelastic strength. Note that the post-buckling strength is taken as $0.5P_{cr}$ for braces buckling in-plane. A post-buckling strength of $0.3P_{cr}$ should be used for braces buckling out-of-plane. It is also noted that the effective length factor, *K*, is taken as 0.5 and 0.85 for the in-plane (K_x) and out-of-plane (K_y) directions, respectively (Lee and Goel, 1990). In order to ensure in-plane buckling, braces are selected such that $K_x L / r_x > K_y L / r_y$.

2.2.4.2 Fracture Criterion

Previous studies (Goel, 1992b; Sabelli, 2000) have shown that early brace fractures may lead to excessively large story drifts and ductility demand on beams and columns when subjected to strong earthquake ground motions. In order to prevent premature brace fractures, a fracture criterion for HSS braces is used in the PBPD approach for CBF. The brace fracture life, N_f, is estimated by the following empirical equation, which was derived from test results of HSS braces under cycling loading (Tang and Goel, 1987):

$$N_f = \begin{cases} 262 \dfrac{(b/d)(KL/r)}{\left\{(b-2t)/t\right\}^2} & \text{for } KL/r > 60 \\ 262 \dfrac{(b/d)60}{\left\{(b-2t)/t\right\}^2} & \text{for } KL/r \le 60 \end{cases} \tag{2.5}$$

where N_f is the fracture life representing the number of standard cycles, beyond which an HSS brace will fracture; *d* is the gross depth of the section; *b* is the gross width of the section ($b \ge d$); *t* is the wall thickness; $(b-2t)/t$ is the width-thickness ratio of compression flanges and the most important parameter affecting the fracture life of HSS braces (Goel, 1992a; Shaback and Brown, 2003); KL/r is the slenderness ratio. A minimum N_f = 100 for HSS braces is suggested herein. Nonlinear dynamic analysis results have shown that the performance of CBF is significantly enhanced (Chao and

Goel, 2006b) by using this criterion. Note that current design practice does not consider the brace fracture life in an explicit manner.

2.2.4.3 Compactness Criterion

The required compactness ratio specified by AISC Seismic Provisions (ANSI/AISC 341-05, 2005) is also checked for the braces. However, the compactness requirement is generally satisfied for HSS braces with a minimum $N_f = 100$.

2.2.5 Design of Non-Yielding Members

The design of non-yielding members, including beams and columns, is performed based on the capacity design approach. That is, non-yielding members should have design strengths to resist the combination of factored gravity loads and the forces due to braces in their ultimate state.

2.2.5.1 Design of Beams

Design of beams follows the criteria given in Section 2.1. It is noted that the post-buckling strength of a brace is taken as $0.5P_{cr}$ for in-plane buckling. Beams intersected by the braces should be designed assuming that no gravity loads are resisted by the braces. Those beams should also be designed to support vertical and horizontal unbalanced loads resulting from the force difference in the tension and compression braces as shown in Figure 2.7. A pin-supported beam model is used because shear splices are used at the ends. The design of beams should follow the beam-column design requirements due to the presence of high axial forces. Lateral supports need to be provided at a minimum spacing of L_{pd}, in the vicinity of mid-span. The unbalanced loads resulting from the braces are (see Figure 2.7):

$$F_h = \left(R_y P_y + 0.5 P_{cr}\right)\cos\alpha \tag{2.6}$$

$$F_v = \left(R_y P_y - 0.5 P_{cr}\right)\sin\alpha \tag{2.7}$$

where F_h is the horizontal unbalanced force; R_y is the ratio of the expected yield strength to the specified minimum yield strength and specified as 1.4 for ASTM A500 Grade B HSS (ANSI/AISC 360-05, 2005); P_y is the nominal yield strength = $F_y A_g$, in which F_y = 46 ksi for the A500 Grade B tube section; P_{cr} is the nominal compressive strength = $F_{cr} A_g$. The axial buckling stress, F_{cr} is specified as:

(a) when $F_e \geq 0.44 F_y$

$$F_{cr} = \left[0.658^{\frac{F_y}{F_e}}\right] F_y \tag{2.8}$$

(b) when $F_e < 0.44 F_y$

$$F_{cr} = 0.877 F_e \tag{2.9}$$

where $$F_e = \frac{\pi^2 E}{\left(KL/r\right)^2} \tag{2.10}$$

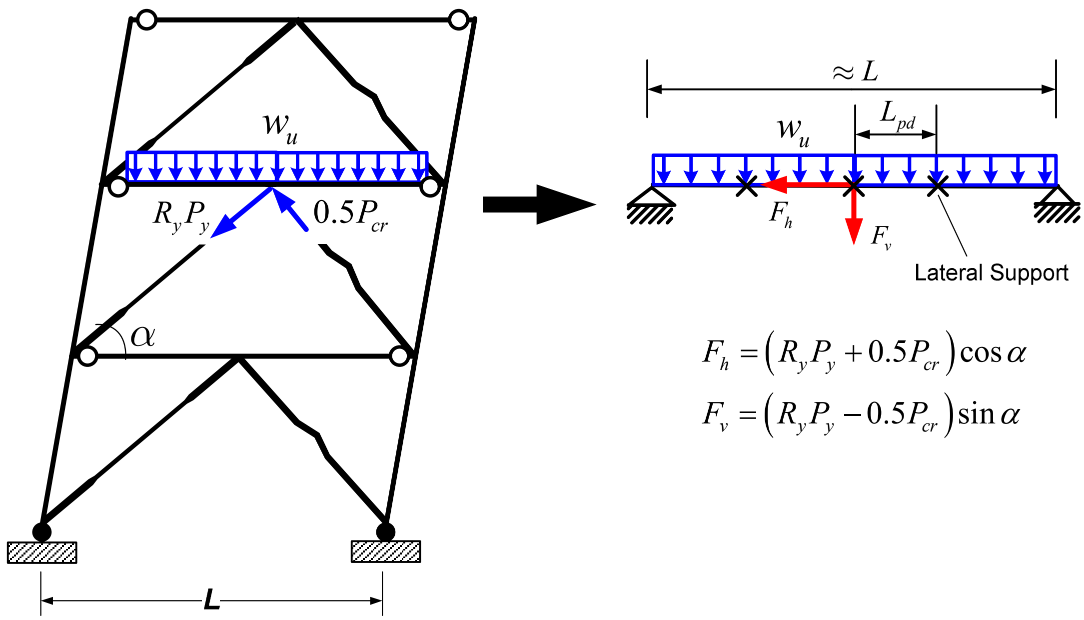

Figure 2.7. Beam Design Forces for a Chevron-Type CBF

2.2.5.2 Design of Columns

Due to the presence of beam shear splices, little or no moment is transferred into the columns, thus only axial loads are considered for column design, including the fixed base first story columns. Axial forces result primarily from the gravity loads and vertical component of brace forces. Two limit states are considered for the design of columns:

1. Pre-buckling limit state:

Prior to brace buckling, no unbalanced force occurs in the beam and the design axial force in a typical exterior column is (see Figure 2.8a):

$$P_u = \left(P_{transverse}\right)_i + \left(P_{beam}\right)_i + \left(P_{cr}\sin\alpha\right)_{i+1} \tag{2.11}$$

where $\left(P_{transverse}\right)_i$ is the tributary factored gravity load (1.2*DL*+0.5*LL*) on columns from the transverse direction at level *i*; $\left(P_{beam}\right)_i$ is the tributary factored gravity load from the beam at level i (= $\frac{1}{2}\left(w_u\right)_i L$); $\left(P_{cr}\right)_{i+1}$ is the buckling force of brace at $i+1$ level. Similarly, for a typical interior column, the axial force demand is determined by (Figure 2.8b):

$$P_u = \left(P_{transverse}\right)_i + \sum\left(P_{beam}\right)_i + \left(P_{cr}\sin\alpha\right)_{i+1} \quad (2.12)$$

2. Post-buckling limit state:

When a Chevron type CBF reaches its ultimate state, an unbalanced force is created in the beam (see Figure 2.7) and the axial force demand in a typical exterior column cab be determined by (see Figure 2.9a):

$$P_u = \left(P_{transverse}\right)_i + \left(P_{beam}\right)_i + \left(0.5P_{cr}\sin\alpha\right)_{i+1} + \frac{1}{2}F_v \quad (2.13)$$

where $\left(P_{transverse}\right)_i$ is the tributary factored gravity load (1.2DL+0.5LL) from the transverse direction at level i; $\left(P_{beam}\right)_i$ is the tributary factored gravity load from beam at level i (= $\frac{1}{2}\left(w_u\right)_i L$); $0.5\left(P_{cr}\right)_{i+1}$ is the post-buckling force of brace at i+1 level; F_v is the vertical unbalanced force.

Similarly, the axial force demand for a typical interior column is (Figure 2.9b):

$$P_u = \left(P_{transverse}\right)_i + \sum\left(P_{beam}\right)_i + \left(0.5P_{cr}\sin\alpha\right)_{i+1} + \frac{1}{2}F_v \quad (2.14)$$

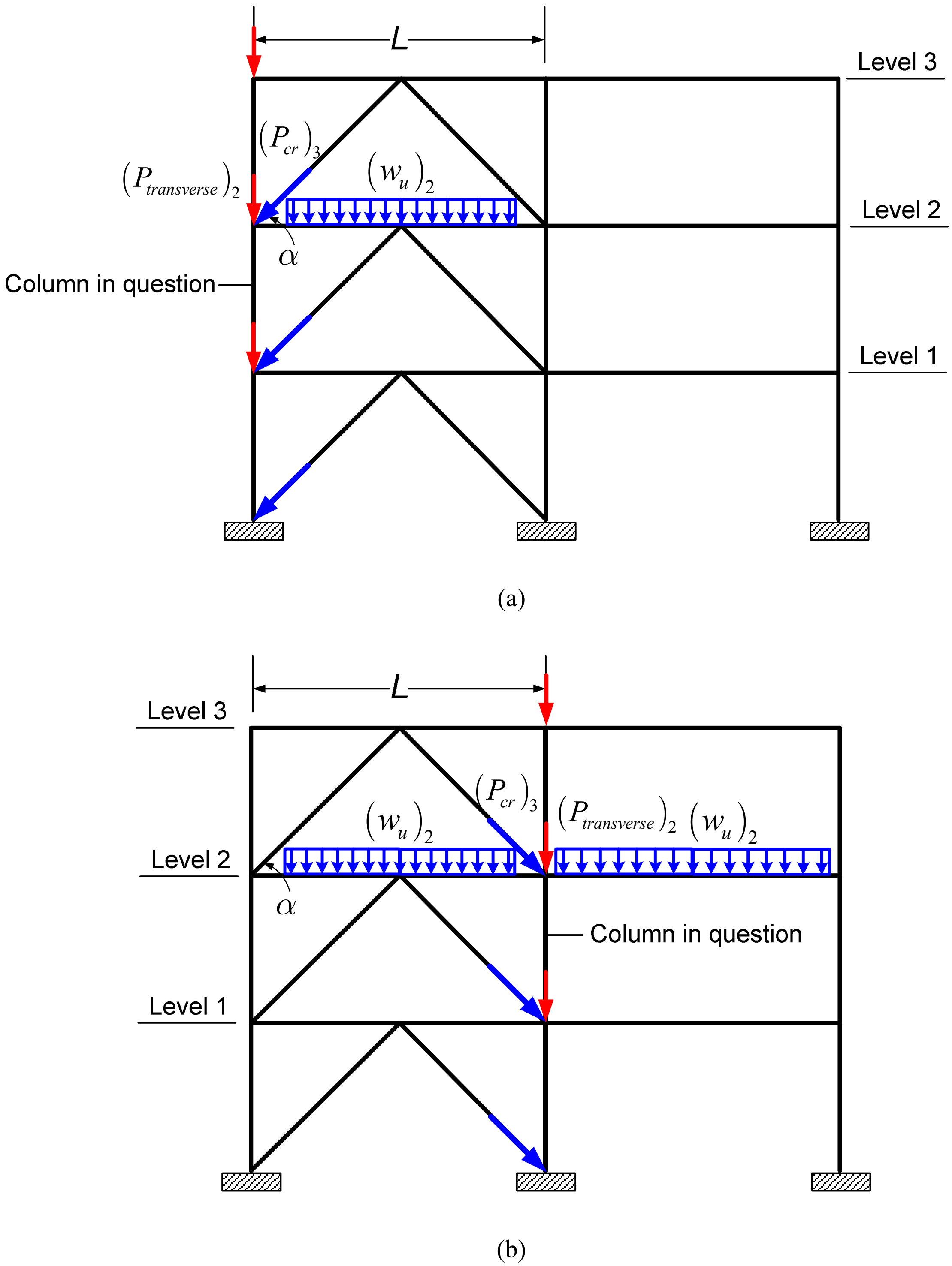

Figure 2.8. Axial Force Components for Brace Pre-Buckling Limit State:
(a) Exterior Column; (b) Interior Column

The design axial force demand is then determined by the governing pre-buckling or post-buckling limit state. It is noted that the above approach assumes that all braces reach their limit states simultaneously. This may be somewhat conservative for design of lower level columns, especially for high-rise buildings. In that case, the maximum probable axial force can be estimated by a more rational method, such as square root of the sum of squares method (SRSS, e.g. Redwood and Channagiri, 1991). Further research is needed on this issue of column design forces, especially in high-rise structures.

Column design is done by using Equations (2.8) to (2.10), with the effective length factor K = 1.0 (ANSI/AISC 360-05, 2005). Current AISC Seismic Provisions (ANSI/AISC 341-05, 2005) require that the compactness of columns in CBF meet the seismic width-thickness ratios given in the Provisions (e.g. $b/t \le 0.30\sqrt{E/F_y}$). This is supported by findings from previous studies (e.g. Sabelli et al., 2003), that columns in CBF can experience significant inelastic rotations. However, in CBF designed by PBPD approach, brace fractures are practically eliminated (especially for 10% in 50 years earthquake motions) by keeping the interstory drifts well within carefully selected limits. In addition, moments transferred to the columns are minimized by using the beam shear splices. Therefore, columns in CBF design by PBPD are expected to remain essentially free of bending. Yielding at the column bases may occur under severe ground motions but is generally quite limited. Therefore, the above mentioned b/t limitation is used for the first-level column only; whereas the limitation of $0.38\sqrt{E/F_y}$ as specified in the AISC *Specification* (ANSI/AISC 360-05, 2005c) is used for columns at all the other levels.

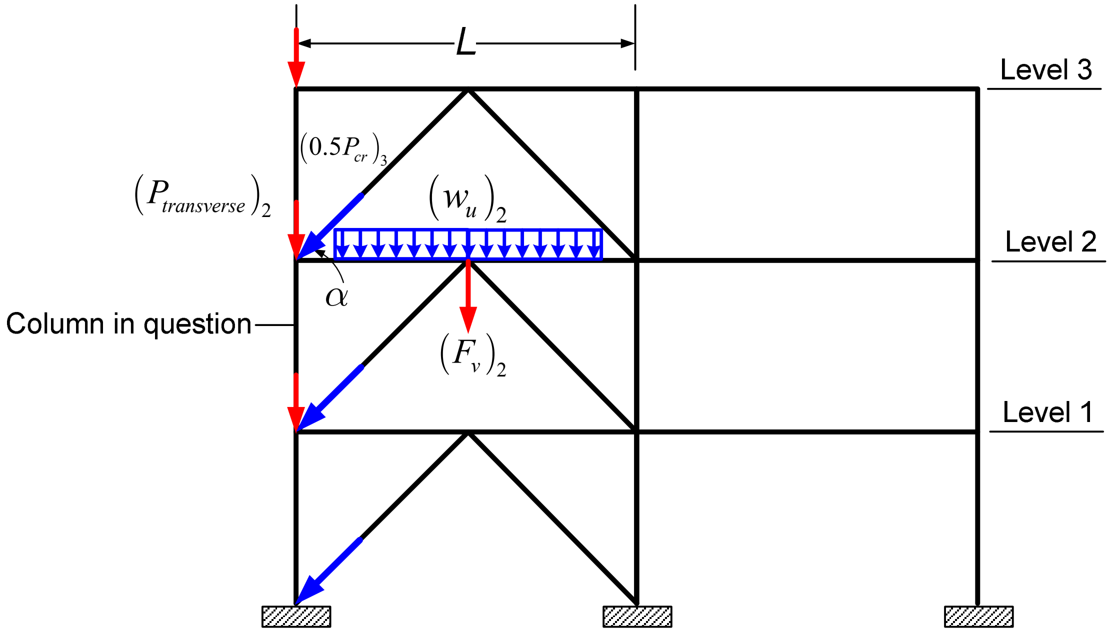

(a)

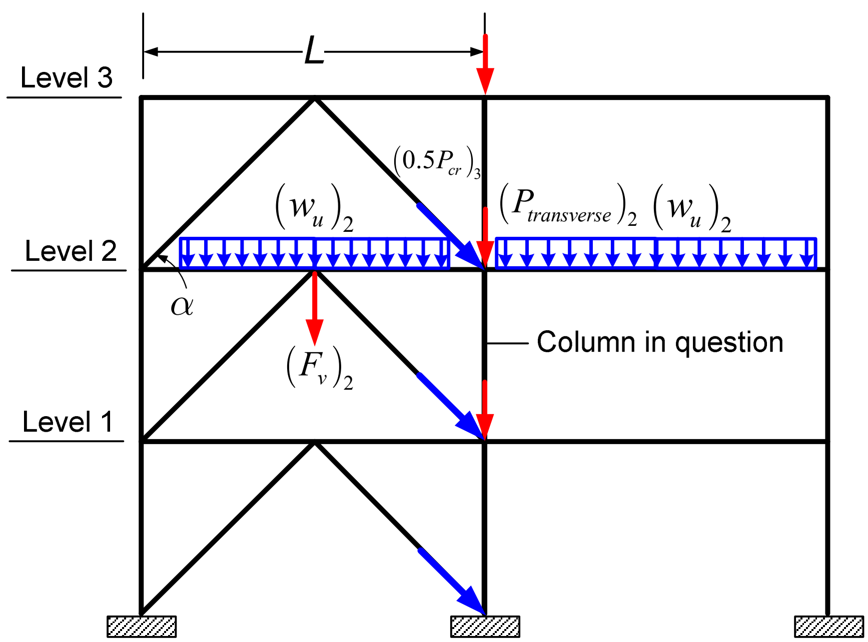

(b)

Figure 2.9. Axial Force Components for Brace Post-Buckling Limit State:
(a) Exterior Column; (b) Interior Column

2.3 Design Examples

Two Chevron type CBF, one with 3 stories and the other with 6 stories, were designed by using the PBPD procedure. These two frames were originally designed as SCBF according to current practice (Sabelli, 2000). Plan views of the example 3- and 6-story structures are shown in Figures 2.10 and 2.11, respectively. The 3-story structure is 120 ft by 180 ft in plan, and 39 ft in elevation. The floor-to-floor height is 13 ft for all three levels. The bays are 30 ft on centers, in both directions, with six and four bays in the two directions. The building's lateral force resisting system is comprised of two perimeter CBF bays in each direction. The interior frames of the structure consist of simple framing with composite floors.

The 6-story structure is 150 ft by 150 ft in plan, and 83 ft in height. The floor-to-floor heights are 13 ft for the first level and 18 ft for all the other levels. The bays are 30 ft on centers, in both directions, with five bays in each direction. The building's lateral force resisting system is comprised of three perimeter CBF bays in each direction. The interior frames of the structure consist of simple framing with composite floors.

The details of design weights of the building components can be found elsewhere (Sabelli, 2000). The calculated factored gravity loads (1.2*DL*+0.5*LL*) for the 3- and 6-story perimeter frames are shown in Figures 2.12 and 2.13, respectively, (with only two bays shown). The gravity loading is as follows:

- 3-story frame (pattern loading is not considered):

w_1 (level 1) = 1.13 kip/ft

w_2 (level 2, 3) = 0.95 kip/ft

L_1 (level 1, 2, exterior column) = 26.17 kips

L_2 (level 1, 2, interior column) = 37.56 kips

L_3 (level 3, exterior column) = 22.24 kips

L_4 (level 3, interior column) = 32.88 kips

- 6-story frame (pattern loading is not considered):

w_1 (level 1) = 1.21 kip/ft

w_2 (level 2, 3, 4, 5) = 1.13 kip/ft

w_3 (level 6) = 0.95 kip/ft

L_1 (level 1, exterior column) = 27.42 kips

L_2 (level 1, interior column) = 37.56 kips

L_3 (level 2, 3, 4, 5, exterior column) = 26.22 kips

L_4 (level 2, 3, 4, 5, interior column) = 37.56 kips

L_5 (level 6, exterior column) = 22.24 kips

L_6 (level 6, interior column) = 32.88 kips

The seismic design parameters for the two frames are based on the 1997 NEHRP Provisions (FEMA, 1997) and will be described in the following sections:

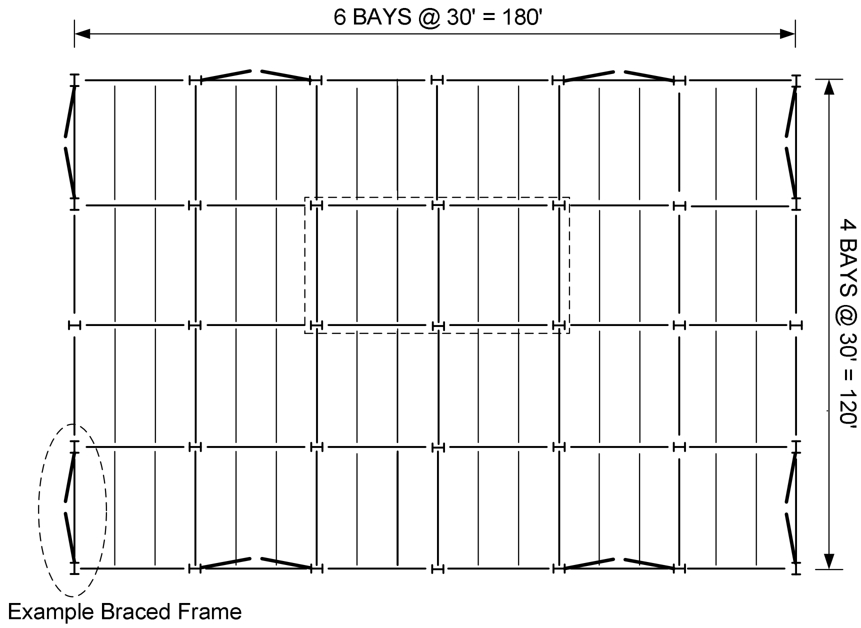

Figure 2.10. Plan View of 3-Story Example Building

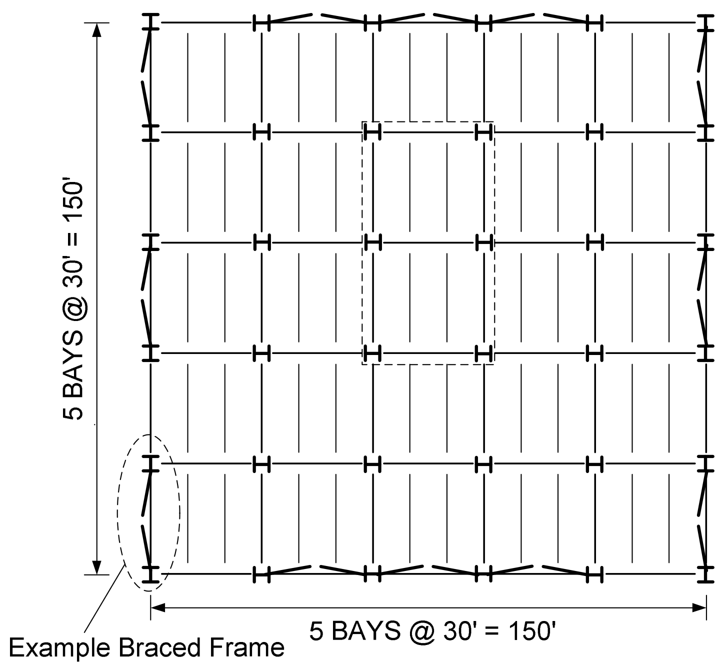

Figure 2.11. Plan View of 6-Story Example Building

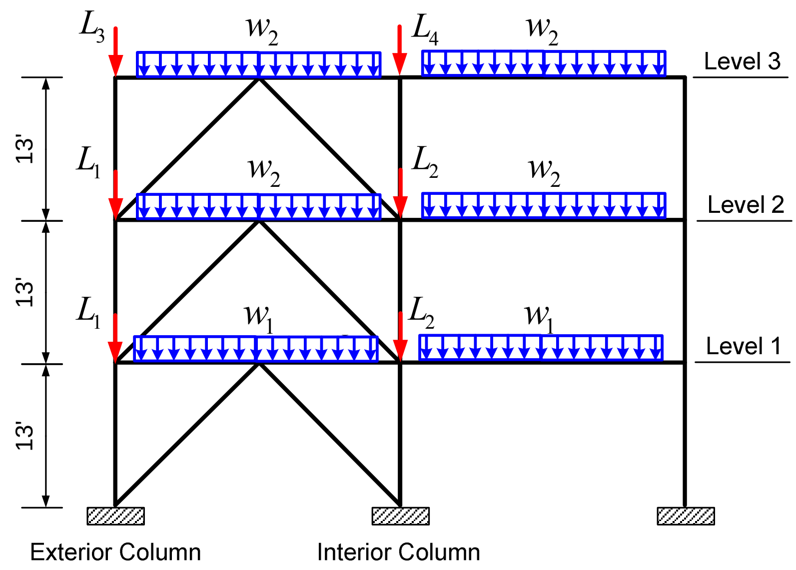

Figure 2.12. Gravity Loading Definition for 3-Story Example Building

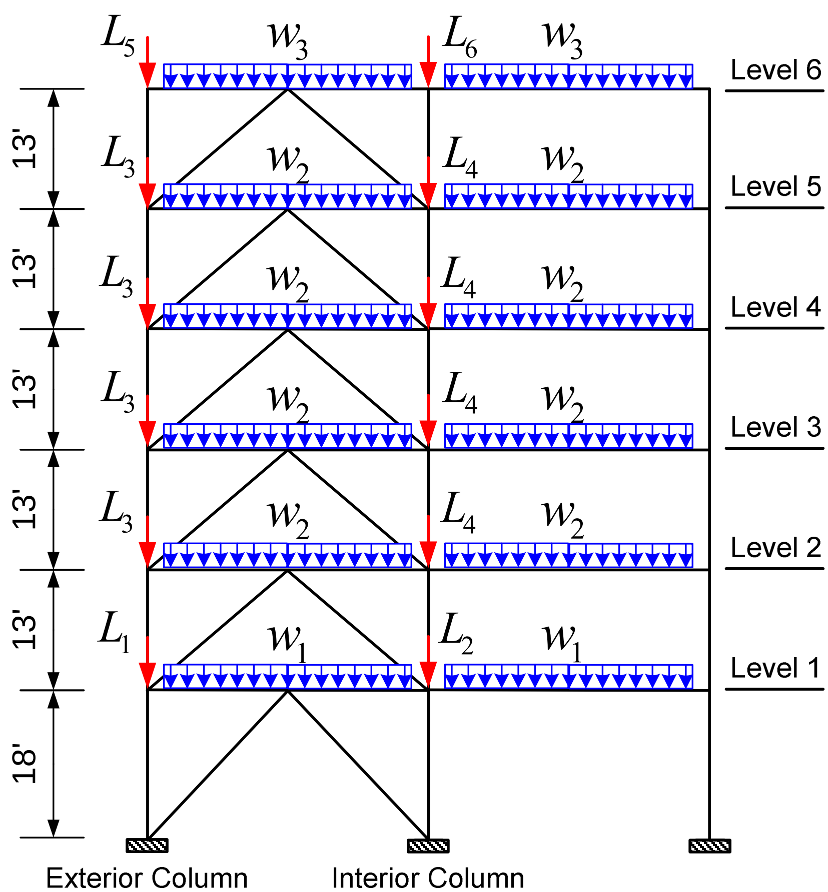

Figure 2.12. Gravity Loading Definition for 6-Story Example Building

2.3.1 *Design of 3-story CBF*

2.3.1.1 Design Base Shear and Lateral Force Distribution

Design parameters according to 1997 NEHRP Provisions (FEMA, 1997) for the 3-story CBF are listed in Table 2.1.

Table 2.1. Design parameters for the 3-story CBF according to 1997 NEHRP

Parameters	**3-story CBF**
MCE Short Period Spectral Response Acc., S_S	2.09 g
MCE One-Second Spectral Response Acc., S_1	0.77 g
Acceleration Site Coefficient, F_a	1.0
Velocity Site Coefficient, F_v	1.5
Short Period Design Spectral Response Acc., S_{DS}	1.393 g
One-Second Design Spectral Response Acc., S_{D1}	0.77 g
Site Class	D (Deep Stiff Soil)
Occupancy Importance Factor	I = 1.0
Seismic Design Category	D
Building Height	130 ft (above the base)
Approximate Building Period, T	0.31 sec.
Response Modification Factor	$R = 6$
Total Building Weight, W	6503 kips
Seismic Response Coefficient, $C_s = \dfrac{V}{W}$	0.232 g

The target drift is selected based on intended structural performance. For example, FEMA 356 (FEMA, 2000) specifies a Basic Safety Objective (BSO), which requires structures to meet the Life Safety Performance Level under 10%/50 year earthquake hazard level. For steel braced frames, the criteria are that the maximum transient and the permanent story drifts should be smaller than 1.5% and 0.5%, respectively. For the two design examples a slightly strict target, 1.25% maximum story drift for 10%/50 year (2/3MCE) hazard, was selected.

The elastic design spectral response acceleration, S_a, is calculated as:

$$S_a = C_s \cdot \left(\frac{R}{I}\right) = 0.232 \cdot \left(\frac{6}{1}\right) = 1.392 \tag{2.15}$$

By following the flowchart for the PBPD design procedure (Figure 2.1), all the corresponding parameters are calculated and listed in Tables 2.2 and 2.3. It can be seen that the base shear is 3150 kips for the full structure (787.5 kips for one CBF). Design lateral force at each floor level is then calculated and given in Table 2.4.

Note that the yield drift for CBF is generally in the range of 0.3% to 0.5% (ANSI/AISC 341-05), and is assumed as 0.3% herein.

Table 2.2. Design parameters for the 3-story CBF based on PBPD procedure

Parameters	10% in 50 year Hazard
S_a	1.392 g
T	0.31 sec.
Yield Drift θ_y	0.3%
Target Drift θ_u	1.25%
Inelastic Drift θ_p	0.95%
$\mu_s = \theta_u / \theta_y$	4.17
R_μ	2.71*
γ	1.00
α	7.52
η	0.5
V/W	0.484
Design Base Shear V	3150 kips (for four CBFs)

* See Table 3-1 of Goel and Chao (2008)

Table 2.3. Shear distribution factor for the 3-Story CBF

Floor	h_j (ft.)	w_j (kips)	$w_j h_j$ (k-ft)	$\sum w_j h_j$ (k-ft)	$\beta_i (=V_i / V_n)$	$(\beta_i - \beta_{i+1})h_i$
3	39	2283.0	89037.0	89037	1.000	39.00
2	26	2110.0	54860.0	143897	1.576	14.98
1	13	2110.0	27430.0	171327	1.860	3.69
Σ		6503				57.67

Table 2.4. Design lateral forces for the 3-Story CBF

Floor	$\beta_i - \beta_{i+1}$	F_i (kips), (full structure)	F_i (kips), (one CBF)	Story Shear V_i (kips), (one CBF)
3	1.000	1694	423.4	423.4
2	0.576	976	244.0	667.4
1	0.284	480	120.0	787.5
Σ		3150	787.5	

2.3.1.2 Design of Braces

The three criteria described in Section 2.2.4 are followed for the design of braces. ASTM A500 Grade B tubular section (HSS) with 46 ksi nominal yield strength were used. The selected brace sections are built-up double tube sections (see Figure 2.6) and shown in Table 2.3. The detailed calculations of fracture life and brace axial strength are given in Tables 2.6 and 2.7, respectively.

Table 2.3. Required brace strength and selected sections for the 3-story CBF

Floor	α^*	V_i (kips)	$\dfrac{\left(V_{\text{story shear}}\right)_i}{0.9 \cdot \cos\alpha_i}$ (kips)**	Brace Section	Brace Nominal strength $\left(P_y + 0.5P_{cr}\right)_i$ (kips)**
3	41°	423.4	623	2HSS4-1/2×4-1/2×3/8	683
2	41°	667.4	981	2HSS5 ×5 ×1/2	996
1	41°	787.5	1158	2HSS6 ×6 ×1/2	1266

*See Figure 2.4; ** Equation (2.4)

Table 2.6. Brace fracture life calculation for the 3-story CBF

Floor	Brace Length, L (in.)	r_x (in.)	r_y (in.)	$\frac{K_x L}{r_x}$ *	$\frac{K_y L}{r_y}$	$\frac{b-2t}{t}$	$0.64\sqrt{\frac{E}{F_y}}$ †	N_f §
3	238.2	1.67	3.06	71.3	66.2	10.0	16.1	187
2	238.2	1.82	3.35	63.6	60.5	8.0	16.1	268
1	238.2	2.23	3.99	53.5	50.7	10.0	16.1	157

*Governing slenderness ratio (K_x = 0.5; K_y = 0.85); †AISC compactness requirement; § Based on Equation (2.5), note that minimum design fracture value = 100

Table 2.7. Nominal axial strength of the braces selected for the 3-story CBF

Floor	Brace Cross Sectional Area (in^2)	F_e (ksi)	$0.44F_y$ (ksi)	F_{cr} (ksi)	$0.5P_{cr}$ (kips)	P_y (kips)
3	10.96	56.3	20.2	32.68	179.1	504.2
2	13.76	66.6	20.2	34.54	271.5	723.0
1	19.48	100.1	20.2	37.95	369.6	896.1

2.3.1.3 Design of Non-Yielding Members

Design of non-yielding members (beams and columns) is performed according to Section 7.3.3. ASTM A992 steel with 50 ksi nominal yield strength is used.

2.3.1.3.1 Beams

Table 2.8 gives the design parameters for beams intersected by the braces (see Figure 2.7). Beams are designed as beam-column elements due to high axial force and bending moment. The effective length factor, K, is taken as 1.0 because of the splice (simple connection) at both ends.

The final beam sections are shown in Table 2.9. The spacing of lateral supports in the vicinity of the mid-span (see Figure 2.7) is taken as 5ft for beams at all level. It can be seen from Table 2.9 that it meets the minimum requirement of the AISC Seismic Provisions.

Table 2.8. Design parameters for beams of the 3-story CBF

Floor	Uniformly Distributed gravity loading w_u (kips/ft)	$R_y P_y$ * (kips)	$0.5P_{cr}$ (kips)	F_h † (kips)	F_v ‡ (kips)	P_u (kips)	M_u (kips-ft)
3	0.95	703.9	179.1	669	345	334.5	2689
2	1.13	1013.0	271.5	972	487	486.0	3723
1	1.13	1254.5	369.6	1227	580	613.5	4433

* $R_y = 1.4$ (ANSI/AISC 341-05); †Equation (2.6); ‡Equation (2.7)

Table 2.9. Determination of lateral support spacing for beams of the 3-story CBF

Floor	Selected Beam Section	r_y (in.)	M_1 * (kips-ft)	M_2 ** (kips-ft)	L_{pd} † (ft)	L_b (ft)
3	W40 $\times$ 183	2.49	1838	2689	8.19	5
2	W40 $\times$ 235	2.54	2530	3723	8.39	5
1	W40 $\times$ 278	2.52	3013	4433	8.32	5

*5ft from mid-span; **at mid-span; † $L_{pd} = \left[0.12 + 0.076\left(M_1 / M_2\right)\right]\left(E / F_y\right) r_y$

Design calculations for the third level beam are given below for illustration. Assuming a trial section W40$\times$183, the design check is carried out according to AISC *Specifications* (ANSI/AISC 360-05, 2005b).

- Design beam moment = 2689 kip-ft
  Design axial force = 334.5 kips

- $K_x = K_y = 1.0$
- $r_x = 15.7$ in.; $r_y = 2.49$ in.
- $L_x = 30$ ft; $L_y = 5$ ft

- $K_x L_x / r_x = 22.93 < K_y L_y / r_y = 24.10$ => The minor axis controls $\phi_c F_{cr}$.
- $K_y L_y / r_y = 24.1 \le 4.71\sqrt{E / F_y} = 4.71\sqrt{29,000/50} = 113.4$

$$\Rightarrow F_{cr} = \left[0.658^{\frac{F_y}{F_e}} \right] F_y = 47.92 \text{ ksi} \tag{2.16}$$

- The compressive strength is:

$\phi_c P_n = \phi_c F_{cr} A_g = 2299$ kips ($\phi_c = 0.9$, $A_g = 53.3$ in^2.)

The flexural strength is:

$\phi_b M_n = \phi_b M_p = 2903$ kip-ft

For $P_u / \phi_c P_n = 0.15 < 0.2$, the member strength must satisfy:

$$\frac{P_u}{2\phi_c P_n} + \left(\frac{M_{ux}}{\phi M_{nx}} \right) \le 1.0 \tag{2.17}$$

where $M_{ux} = B_1 M_{nt}$

$$B_1 = \frac{C_m}{1 - \frac{P_u}{P_{e1}}} \ge 1 \tag{2.18}$$

$$P_{e1} = \frac{\pi^2 EI}{(K_1 L)^2} = 26274 \text{ kips} \tag{2.19}$$

where C_m is conservatively taken as 1.0 for beam-columns subjected to transverse loading; K_1 is the effective length factor in the plane of bending = 1.0.

Hence:

$$B_1 = \frac{1.0}{1 - \frac{334.5}{26274}} = 1.01$$

and

$$\frac{P_u}{2\phi_c P_n} + \left(\frac{B_1 \times M_u}{\phi_b M_{nx}}\right) = \frac{334.5}{2 \times 2299} + \frac{1.01 \times 2689}{2903} = 1.0 \qquad \text{(o.k.)}$$

2.3.1.3.2 Columns

The design of columns is done as described in Section 2.2.3.2. The required axial strengths for exterior and interior columns are determined according to Equations (2.11) to (2.14) and listed in Tables 2.10 and 2.11, respectively. Note that post-buckling limit state of the braces governs the design of the columns.

Table 2.10. Design parameters for exterior columns of the 3-story CBF

Exterior Columns									
			Pre-buckling Limit State			Post-buckling Limit State			
FL	$P_{transverse}$ (kips)	P_{beam} (kips)	$P_{cr}\sin\alpha$ (kips)	P_u (total) (kips)	P_u (cumulative) (kips)	$0.5P_{cr}\sin\alpha$ (kips)	$\frac{1}{2}F_v$ (kips)	P_u (total) (kips)	P_u (cumulative) (kips)
3	22.24	14.25	0	36	36	0	173	209	209
2	26.17	16.95	235	278	314	117	243	404	613
1	26.17	16.95	356	399	713	178	290	511	1124†

†Governing force

Table 2.11. Design parameters for interior columns of the 3-story CBF

Interior Columns									
			Pre-buckling Limit State			Post-buckling Limit State			
FL	$P_{transverse}$ (kips)	P_{beam} (kips)	$P_{cr} \sin\alpha$ (kips)	P_u (total) (kips)	P_u (cumulative) (kips)	$0.5P_{cr} \sin\alpha$ (kips)	$\frac{1}{2}F_v$ (kips)	P_u (total) (kips)	P_u (cumulative) (kips)
3	32.88	28.5	0	61	61	0	173	234	234
2	37.56	33.9	235	306	367	117	243	432	666
1	37.56	33.9	356	427	795	178	290	539	1205†

†Governing force

As mentioned in Section 2.2.3.2, only axial forces are considered for column design. For this example, the same section is used in all stories. That is, the maximum axial force (1205 kips) is used and it leads to a column section of W12 $\times$ 120 (axial strength = 1325 kips). The width-thickness ratio of the selected column section also meets the compactness requirement. The final member sections for the 3-story CBF are shown in Figures 2.14. Note that beam sizes are governed by span length and unbalanced forces from the braces.

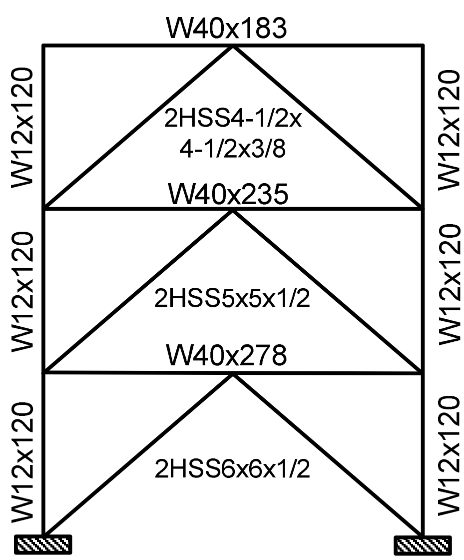

Figure 2.14. Member Sections for 3-Story CBF Designed by PBPD

2.3.2 Design of 6-story CBF

2.3.2.1 Design Base Shear and Lateral Force Distribution

Design parameters according to 1997 NEHRP Provisions (FEMA, 1997) for the 6-story CBF are listed in Table 2.12.

Table 2.12. Design parameters for the 6-story CBF according to 1997 NEHRP

Parameters	**6-Story CBF**
MCE Short Period Spectral Response Acc., S_S	2.09 g
MCE One-Second Spectral Response Acc., S_1	0.77 g
Acceleration Site Coefficient, F_a	1.0
Velocity Site Coefficient, F_v	1.5
Short Period Design Spectral Response Acc., S_{DS}	1.393 g
One-Second Design Spectral Response Acc., S_{D1}	0.77 g
Site Class	D (Deep Stiff Soil)
Occupancy Importance Factor	I = 1.0
Seismic Design Category	D
Building Height	130 ft (above the base)
Approximate Building Period, T	0.55 sec.
Response Modification Factor	$R = 6$
Total Building Weight, W	13332 kips
Seismic Response Coefficient, $C_s = \dfrac{V}{W}$	0.232 g

A target drift of 1.25% for 10%/50 year (2/3MCE) hazard, is selected for the 6-story CBF and the elastic design spectral response acceleration, S_a, is calculated as:

$$S_a = C_s \cdot \left(\frac{R}{I}\right) = 0.232 \cdot \left(\frac{6}{1}\right) = 1.392 \tag{2.20}$$

The corresponding parameters are calculated and listed in Tables 2.13 and 2.14. It can be seen that the base shear is 4507 kips for the full structure (751.2 kips for one CBF). Design lateral force at each floor level is then calculated and given in Table 2.13.

Table 2.13. Design parameters for the 6-story CBF based on PBPD procedure

Parameters	**10% in 50 year Hazard**
S_a	1.392 g
T	0.55 sec.
Yield Drift θ_y	0.3%
Target Drift θ_u	1.25%
Inelastic Drift θ_p	0.95%
$\mu_s = \theta_u / \theta_y$	4.17
R_μ	4.02*
γ	0.454
α	4.86
η	0.5
V/W	0.338
Design Base Shear V	4507 kips (for six CBFs)

* See Table 3-1 of Goel and Chao (2008)

Table 2.14. Shear distribution factors for the 6-Story CBF

Floor	h_j (ft.)	w_j (kips)	$w_j h_j$ (k-ft)	$\sum w_j h_j$ (k-ft)	$\beta_i (=V_i / V_n)$	$(\beta_i - \beta_{i+1}) h_i$
6	83	2358	195714.0	195714	1.000	83.00
5	70	2187	153090.0	348804	1.630	44.08
4	57	2187	124659.0	473463	2.110	27.38
3	44	2187	96228.0	569691	2.467	13.72
2	31	2187	67797.0	637488	2.713	7.63
1	18	2226	40068.0	677556	2.857	2.58
Σ		13332				180.39

Table 2.15. Design lateral forces for the 6-Story CBF

Floor	$\beta_i - \beta_{i+1}$	F_i (kips), (full structure)	F_i (kips), (one CBF)	Story Shear V_i (kips), (one CBF)
6	1.000	1578	263.0	263.0
5	0.630	994	163.6	428.6
4	0.480	758	126.3	554.8
3	0.357	564	93.9	648.8
2	0.246	388	64.7	713.5
1	0.143	226	37.7	751.2
Σ		4507	751.2	

2.3.2.2 Design of Braces

The three criteria described in Section 2.2.4 are followed for the design of braces. ASTM A500 Grade B tube sections (HSS) with 46 ksi nominal yield strength were used. The selected brace sections are built-up double tube sections (see Figure 2.6) and shown in Table 2.16. The detailed calculations of fracture life and brace axial strength are given in Tables 2.17 and 2.18, respectively.

Table 2.16. Required brace strength and selected sections for the 6-story CBF

Floor	α *	V_i (kips)	$\dfrac{\left(V_{\text{story shear}}\right)_i}{0.9 \cdot \cos \alpha_i}$ (kips)**	Brace Section	Brace Nominal strength $\left(P_y + 0.5P_{cr}\right)_i$ (kips)**
6	41°	263.0	387	2HSS3-1/2 $\times$ 3-1/2 $\times$ 5/16	415
5	41°	428.6	630	2HSS4-1/2 $\times$ 4-1/2 $\times$ 3/8	683
4	41°	554.8	816	2HSS4-1/2 $\times$ 4-1/2 $\times$ 1/2	861
3	41°	648.8	954	2HSS5 $\times$ 5 $\times$ 1/2	996
2	41°	713.5	1049	2HSS6 $\times$ 6 $\times$ 1/2	1266
1	50°	751.2	1304	2HSS6 $\times$ 6 $\times$ 5/8	1483

*See Figure 2.4; ** Equation (2.4)

Table 2.17. Brace fracture life calculation for the 6-story CBF

Floor	Brace Length, L (in.)	r_x (in.)	r_y (in.)	$\frac{K_x L}{r_x}$ *	$\frac{K_y L}{r_y}$	$\frac{b-2t}{t}$	$0.64\sqrt{\frac{E}{F_y}}$ †	N_f §
6	238.2	1.29	2.43	92.5	83.3	9.2	16.1	286
5	238.2	1.67	3.06	71.3	66.2	10.0	16.1	187
4	238.2	1.61	3.03	73.8	66.9	7.0	16.1	395
3	238.2	1.82	3.35	63.6	60.5	8.0	16.1	268
2	238.2	2.23	3.99	53.5	50.7	10.0	16.1	157
1	281.2	2.17	3.96	64.7	60.3	7.6	16.1	293

*Governing slenderness ratio (K_x = 0.5; K_y = 0.85); †AISC compactness requirement; § Based on Equation (2.5), note that minimum design fracture life = 100

Table 2.18. Nominal axial strength of the braces for the 6-story CBF

Floor	Brace Cross Sectional Area (in^2)	F_e (ksi)	$0.44F_y$ (ksi)	F_{cr} (ksi)	$0.5P_{cr}$ (kips)	P_y (kips)
6	7.04	33.5	20.2	23.88	91.1	323.8
5	10.96	56.3	20.2	32.68	179.1	504.2
4	13.9	52.6	20.2	31.89	221.6	639.4
3	13.76	66.6	20.2	34.45	271.5	723.0
2	19.48	100.1	20.2	37.95	369.6	896.1
1	23.4	68.4	20.2	34.72	406.2	1076.4

2.3.2.3 Design of Non-Yielding Members

Design of non-yielding members (beams and columns) is performed as described in Section 2.2.3. ASTM A992 steel with 50 ksi nominal yield strength is used.

2.3.2.3.1 Beams

Table 2.19 gives the design parameters for beams intersected by the braces (see Figure 2.7). Beams are designed as beam-column elements due to large axial forces. The effective length factor, K , is taken as 1.0 because of the simple connection at both ends.

The final beam sections are shown in Table 2.20. The spacing of lateral supports in the vicinity of the mid-span (see Figure 2.7) is taken as 5ft for beams at all level. It can be seen from Table 2.20 that it meets the minimum requirement of the AISC Seismic Provisions.

Table 2.19. Design parameters for beams of the 6-story CBF

Floor	Uniformly Distributed gravity loading w_u (kips/ft)	$R_y P_y$ * (kips)	$0.5P_{cr}$ (kips)	F_h † (kips)	F_v ‡ (kips)	P_u (kips)	M_u (kips-ft)
6	0.95	453.3	91.1	411	237	203.5	1866
5	1.13	703.9	179.1	669	345	334.5	2689
4	1.13	893.2	221.6	844	441	422.0	3401
3	1.13	1013.0	271.5	972	487	486.0	3743
2	1.13	1254.5	369.6	1227	580	613.5	4433
1	1.21	1507.0	406.2	1225	846	612.5	6408

* $R_y = 1.4$ (ANSI/AISC 341-05); †Equation (2.6); ‡Equation (2.7)

Table 2.20. Determination of lateral support spacing for beams of the 6-story CBF

Floor	Selected Beam Section	r_y (in.)	M_1 * (kips-ft)	M_2 ** (kips-ft)	L_{pd} † (ft)	L_b (ft)
6	$W33 \times 130$	2.39	1280	1866	7.84	5
5	$W36 \times 182$	2.55	1838	2689	8.39	5
4	$W40 \times 211$	2.51	2318	3401	8.27	5
3	$W40 \times 235$	2.54	2548	3743	8.38	5
2	$W40 \times 278$	2.52	3013	4433	8.32	5
1	$W40 \times 397$	3.64	4343	6408	12.05	5

*5ft from mid-span; **at mid-span; † $L_{pd} = \left[0.12 + 0.076\left(M_1 / M_2\right)\right]\left(E / F_y\right) r_y$

2.3.2.3.2 Columns

Design of columns is done as described in Section 2.2.3.2. The required axial strengths for exterior and interior columns are determined according to Equations (2.11) to (2.14) and listed in Tables 2.21 and 2.22, respectively. It should be noted that the post-buckling limit state of the braces governs the design of the columns.

Table 2.21. Design parameters for exterior columns of the 6-story CBF

Exterior Columns									
			Pre-buckling Limit State			Post-buckling Limit State			
FL	$P_{transverse}$ (kips)	P_{beam} (kips)	$P_{cr}\sin\alpha$ (kips)	P_u (total) (kips)	P_u (cumulative) (kips)	$0.5P_{cr}\sin\alpha$ (kips)	$\frac{1}{2}F_v$ (kips)	P_u (total) (kips)	P_u (cumulative) (kips)
6	22.24	14.25	0	36	36	0	119	155	155
5	26.22	16.95	119	162	199	60	173	275	430
4	26.22	16.95	235	278	477	117	221	381	811‡
3	26.22	16.95	290	333	810	145	243	432	1243
2	26.22	16.95	356	399	1209	178	290	511	1754
1	27.42	18.15	484	530	1739	242	423	710	2464†

†Governing force for first to third level; ‡ Governing force for fourth to sixth level

Table 2.22. Design parameters for interior columns of the 6-story CBF

Interior Columns									
			Pre-buckling Limit State			Post-buckling Limit State			
FL	$P_{transverse}$ (kips)	P_{beam} (kips)	$P_{cr}\sin\alpha$ (kips)	P_u (total) (kips)	P_u (cumulative) (kips)	$0.5P_{cr}\sin\alpha$ (kips)	$\frac{1}{2}F_v$ (kips)	P_u (total) (kips)	P_u (cumulative) (kips)
6	32.88	28.5	0	61	61	0	119	180	180
5	37.56	33.9	119	191	252	60	173	304	484
4	37.56	33.9	235	306	558	117	221	409	893‡
3	37.56	33.9	290	362	920	145	243	460	1353
2	37.56	33.9	356	427	1347	178	290	539	1892
1	37.56	36.3	484	558	1905	242	423	739	2631†

†Governing force for first to third level; ‡ Governing force for fourth to sixth level

As mentioned in Section 2.2.3.2, only axial forces are considered for column design. For this example, column sections were changed after every three stories. That is, the force of 2631 kips was used for the first to the third story columns, and 893 kips for the fourth to the sixth story. This led to a column size of W14 $\times$257 (axial strength = 2785 kips) for the lower three levels and W14 $\times$109 (axial strength = 1267 kips) for the upper three levels. It is noted that although a lighter section such as W14 $\times$90 or W14 $\times$ 99 could have been used for the upper three stories to meet the strength requirement, their width-thickness ratios do not meet the limit of $0.38\sqrt{E/F_y}$ (see discussion in Section 2.4.3.2). The final member sections for the 6-story CBF are shown in Figures 2.13.

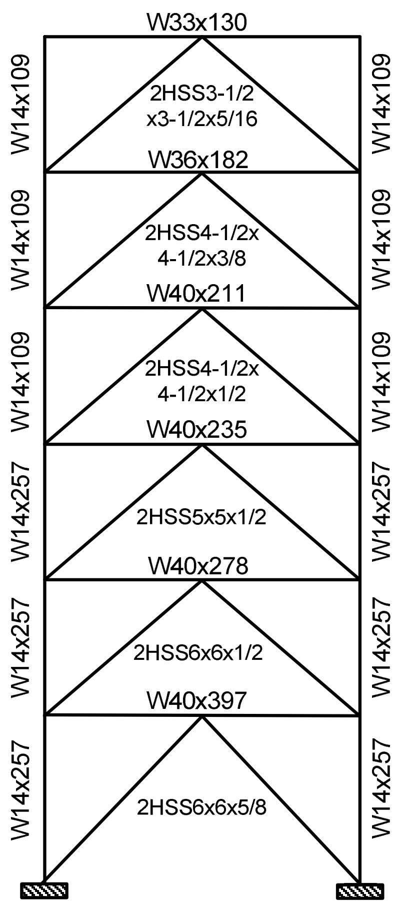

Figure 2.13. Member Sections for 6-Story CBF Designed by PBPD

2.4 Verification by Nonlinear Analysis

2.4.1 Frames Designed by Elastic Method

The three- and six-story Chevron type CBF described in Section 2.3 were originally designed (Sabelli, 2000) as SCBF according to 1997 NEHRP design spectra (FEMA, 1997) and 1997 AISC Seismic Provisions (AISC, 1997). The beams were designed based on the difference of nominal yield strength (P_y) and post-buckling strength ($0.3\phi_c P_{cr}$, assuming out-of-plane buckling). The material overstrength factor, R_y (the ratio of the expected yield strength to the specified minimum yield strength), was not specified for design of beams in the 1997 Provisions, which could in turn lead to yielding in the beam at the location of brace intersection under major earthquakes (Sabelli, 2000). For comparison purposes those frames were re-designed according to the 2005 AISC Seismic Provisions (ANSI/AISC 341-05, 2005a), where the beams are required to be designed based on the difference of expected yield strength ($R_y P_y$) and nominal post-buckling ($0.3P_{cr}$).

The final sections of the 3- and 6-story CBF (termed “NEHRP” frame) are given in Figures 2.16 and 2.17, respectively. Table 2.23 gives the corresponding design parameters for the 3-stoy NEHRP frame. It should be noted that the braces were designed based on initial buckling strength ($2\phi_c P_{cr} \cos\alpha$). The column design forces were based on gravity loading, post-buckling strength of braces, and vertical unbalanced load on the beams from the braces.

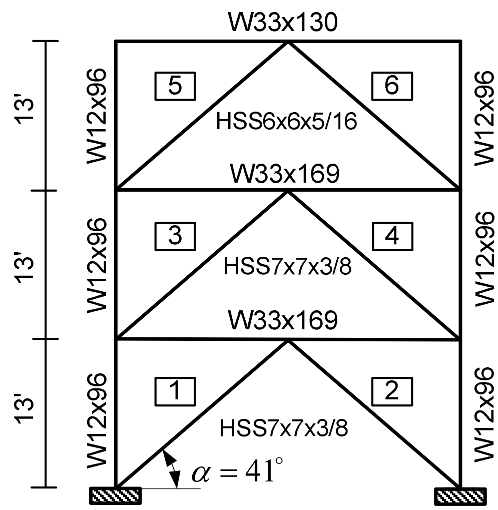

Figure 2.16. Member sections for the 3-story CBF designed by current design practice

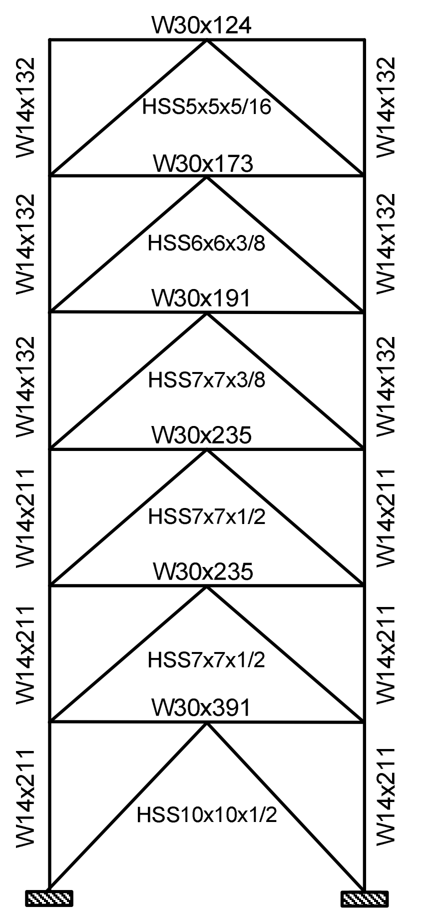

Figure 2.17. Member sections for the 6-story CBF designed by current design practice

Table 2.23. Selected design parameters of 3V-NEHRP frame

FL	Required Story Shear, V_i (kips)	Brace Size (A_g, in^2)	Design Strength, $2\phi_c P_{cr} \cos\alpha$ (kips)	Difference between Tensile and Post-buckling Strengths, $P_y - 0.3P_{cr}$ (kips)	Fracture Life, N_f
3rd	203	HSS6$\times$6$\times$5/16 (6.43)	241	243	78
2nd	320	HSS7$\times$7$\times$3/8 (8.97)	386	328	71
1st	377	HSS7$\times$7$\times$3/8 (8.97)	386	328	71

*Note: the braces of 3V- NEHRP frame were chosen based on strength demand, compactness requirement, and weight (lightest among available sections).

The comparison of material weights is given in Tables 2.24 and 2.25 for the 3- and 6-story frames, respectively. Although the PBPD frames are somewhat heavier than the NEHRP frames, the merit of PBPD method is justified by their performance as shown by nonlinear analysis.

Table 2.24. Material weight for one braced frame of the 3-story building

Weight Calculation	3V-NEHRP (lbs)	3V-PBPD (lbs)	3V-PBPD/3V-NEHRP
Braces	3505	6598	1.88
Beams	14040	20880	1.49
Column	7488	9360	1.25
Total	25033	36838	1.47

Table 2.25. Material weight for one braced frame of the 6-story building

Weight Calculation	6V-NEHRP (lbs)	6V-PBPD (lbs)	6V-PBPD/6V-NEHRP
Braces	9379	13124	1.40
Beams	40470	42990	1.06
Column	28860	31118	1.08
Total	78709	87232	1.11

2.4.2 *Nonlinear Analysis Results*

Nonlinear analyses were carried out by using the SNAP-2DX program, which has the ability to model brace behavior under large displacement reversals, as well as the fracture of braces with tubular sections (Rai et al., 1996). Gravity columns were included in the modeling by using a lumped continuous leaning column, which was connected to the braced frame through rigid pin-ended links (e.g. see Figures 2.18 to 2.23). $P-\Delta$ effect due to the gravity loads was also accounted for in the analysis. All beams and columns of the frame were modeled as beam-column elements.

2.4.2.1 3-story CBF

The beam-to-column connections at the first and second levels of the 3-story NEHRP frame were modeled as moment resisting connections due to the presence of gusset plates. On the other hand, the beam-to-column connections at all levels of the 3-story PBPD frame were modeled as pin connections due to the introduction of beam splices (Figure 2.6).

Selected responses of the 3V-NEHRP frame are shown in Figures 2.18, 2.20, and 2.22, under either 10% in 50 years or 2% in 50 years ground motions. In one of these responses, *i.e.*, due to LA 02 record (Figure 2.18a), the structure collapsed after 20 seconds due to early brace fractures (*i.e.*, short fracture life) in the first story. Significant yielding was also observed in the columns due to rigid connections (Figure 2.18b). This agrees with recent test results which showed that severe damage can occur in the vicinity of connection regions of CBF designed by current practice (Uriz, 2005; see Figure 2.5).

In the other responses, although collapse did not occur, the NEHRP frame subjected to severe damage and considerable residual drifts due to early brace fractures and plastic hinging in the columns.

Typical responses of the 3V-PBPD frame are shown in Figures 2.19, 2.21, and 2.23 under the same ground motions. It can be seen that the behavior is quite stable and drift was considerably less as compared with the 3V-NEHRP frame. The damage in terms of yielding and buckling was generally confined to the braces only and no brace fracture occurred, thus the intended yield mechanism and response was achieved. It is also noticed that the PBPD frame exhibited smaller residual drifts as compared to those in the NEHRP frame, even due to 2% in 50 years ground motions.

Figure 2.24 shows maximum interstory drifts for both 3V-NEHRP and 3V-PBPD frames due to eleven 10% in 50 years SAC ground motion records. As can be seen, the 3V-NEHRP frame experienced large concentrated drift in the first story, due to brace fractures and column hinging. On the other hand, the frame designed by PBPD method resulted in more uniformly distributed story drifts along the height of the frame, and generally within the design target drift, while eliminating brace fractures and column yielding.

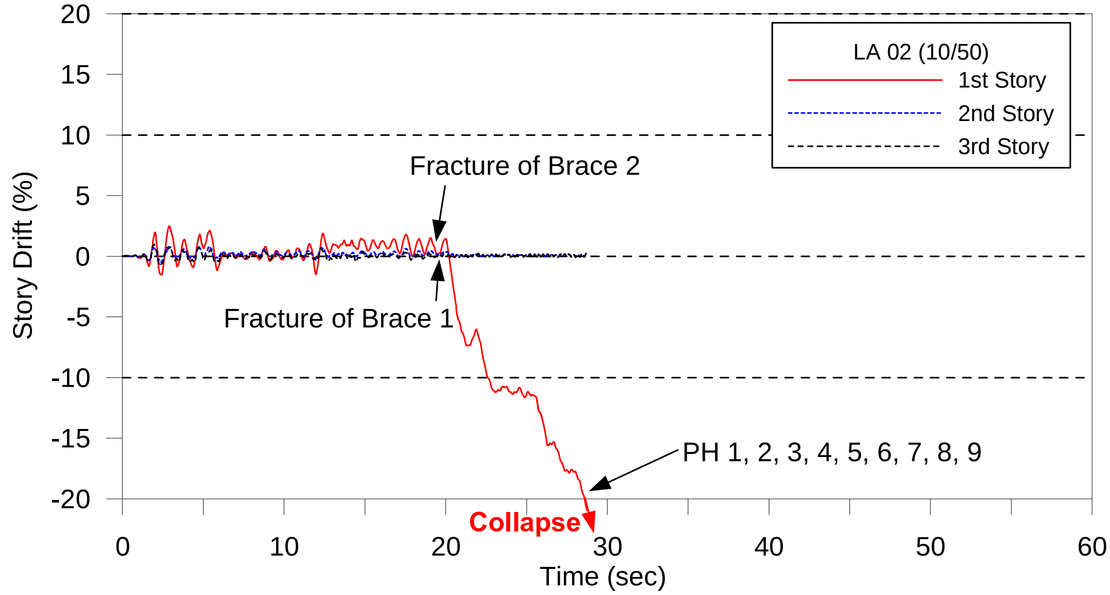

(a)

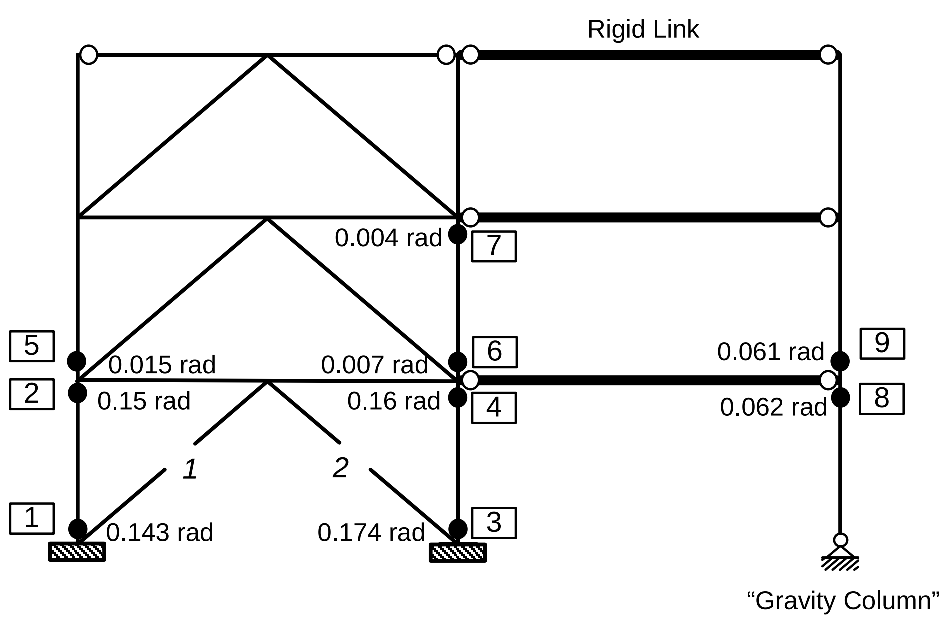

(b)

Figure 2.18.
LA02 ground motion (10% in 50 years)
3V-NEHRP. The sequence of brace fractures and plastic hinge formation along with maximum plastic rotations are also shown.

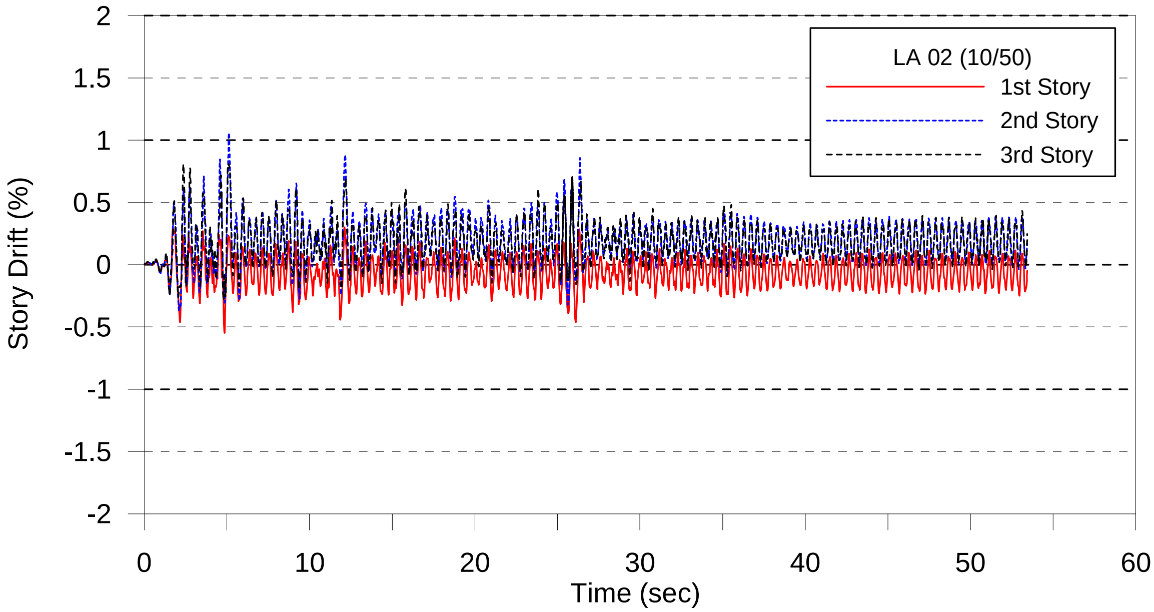

(a)

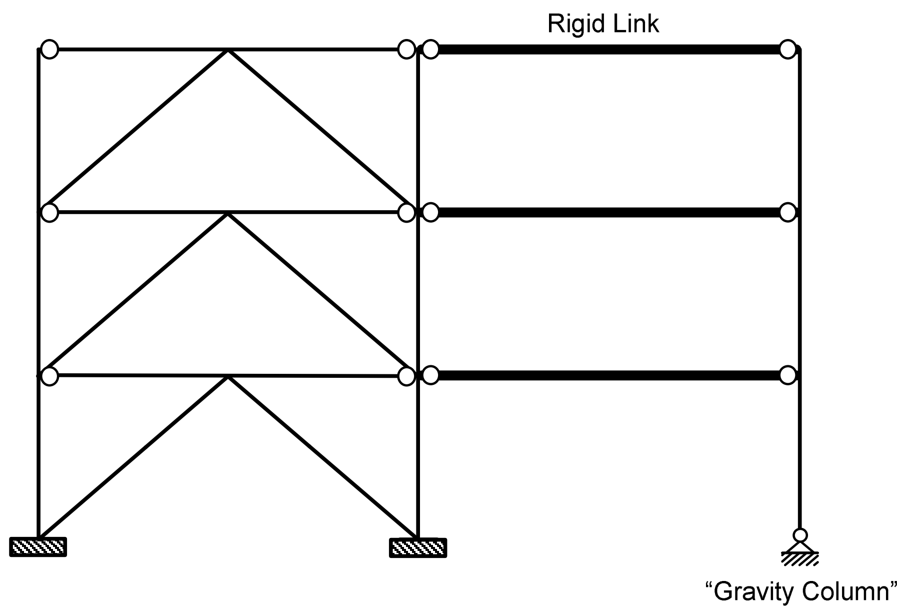

(b)

Figure 2.19. LA02 ground motion (10% in 50 years), 3V-PBPD.

(Note absence of brace fracture and plastic hinging.)

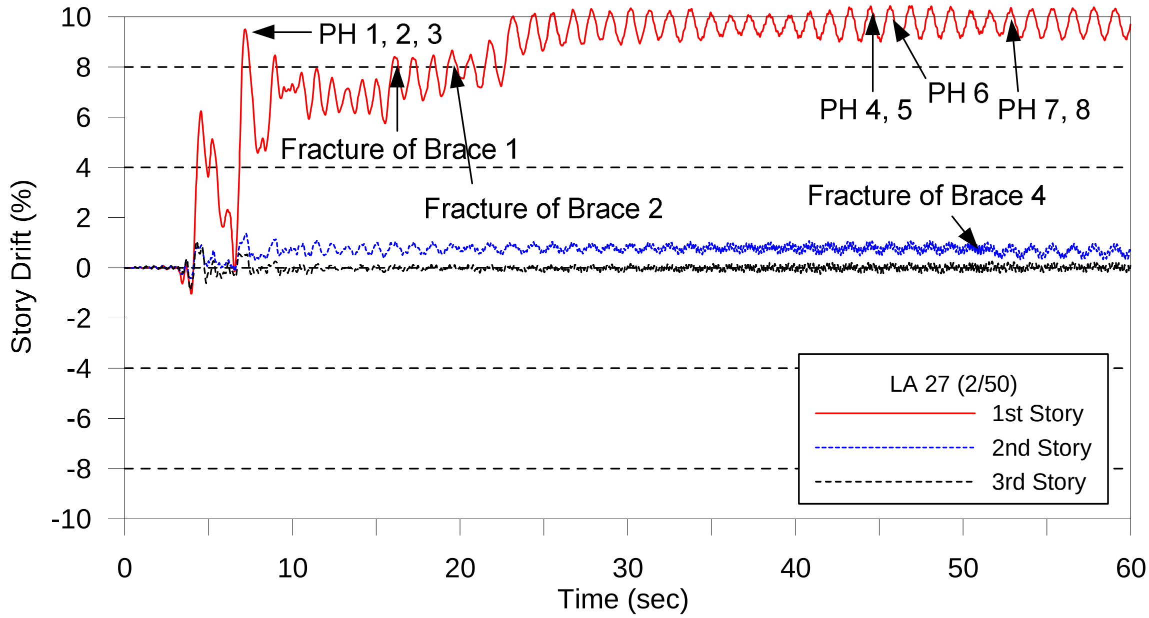

(a)

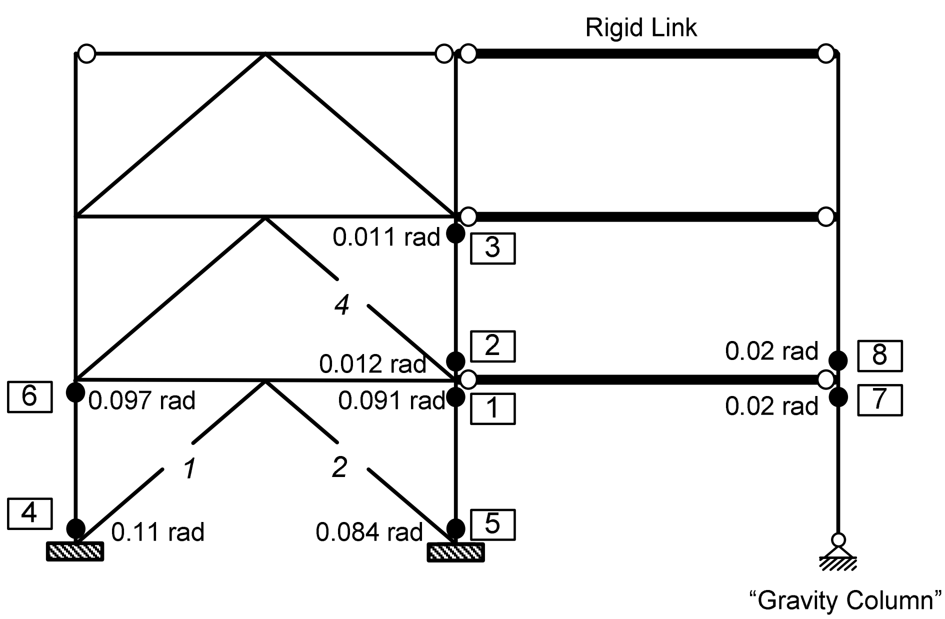

(b)
Figure 2.20. LA27 ground motion (2% in 50 years), 3V-NEHRP.

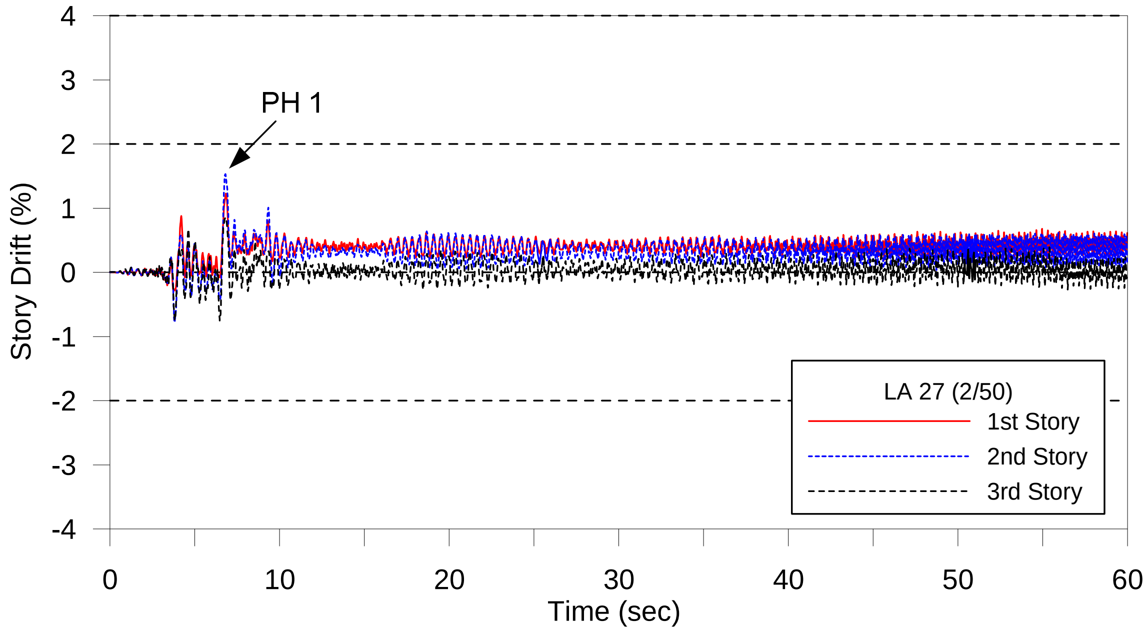

(a)

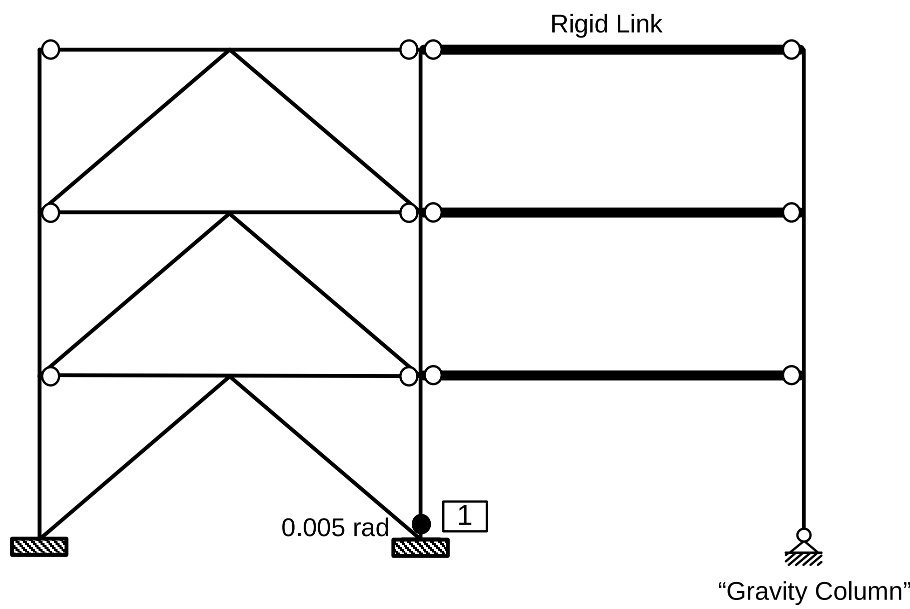

(b)

Figure 2.21. LA27 ground motion (2% in 50 years).

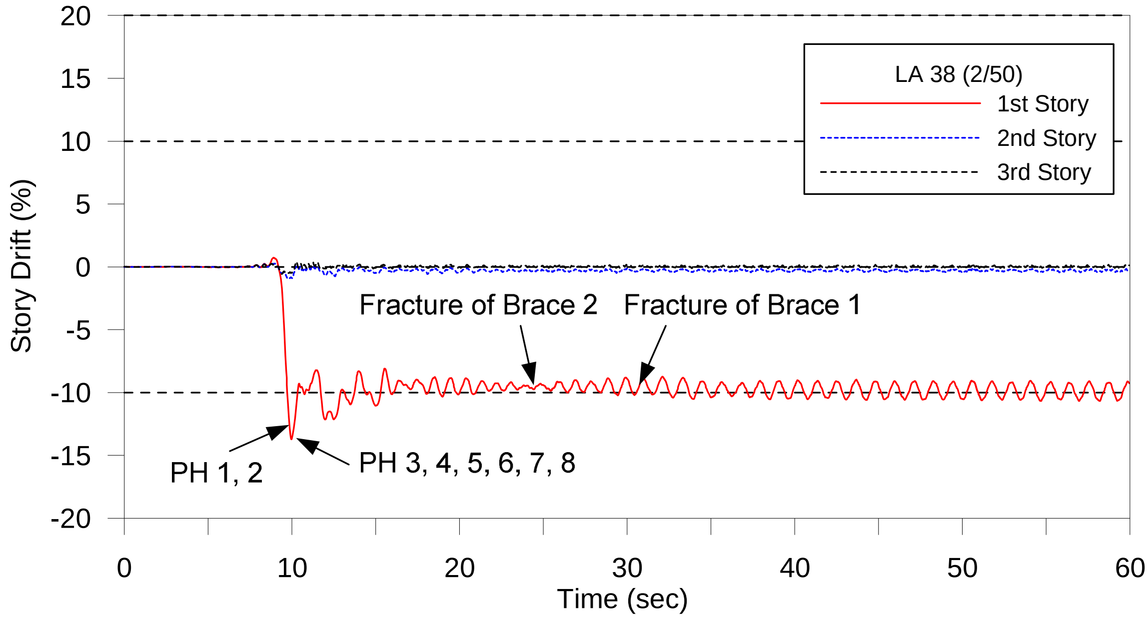

(a)

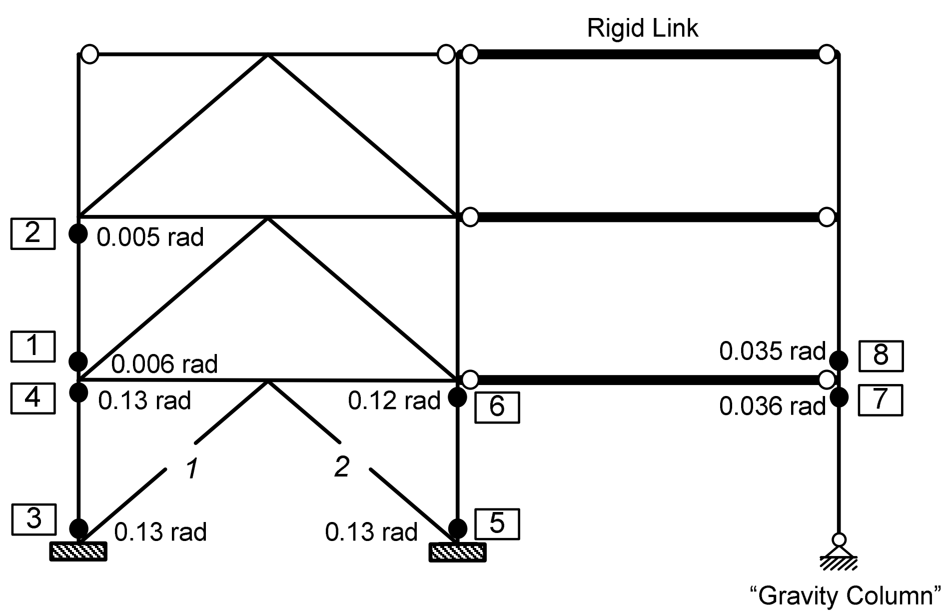

(b)

Figure 2.22. LA38 ground motion (2% in 50 years), 3V-NEHRP. The sequence of brace fractures and plastic hinge formation along with maximum plastic rotations are also shown.

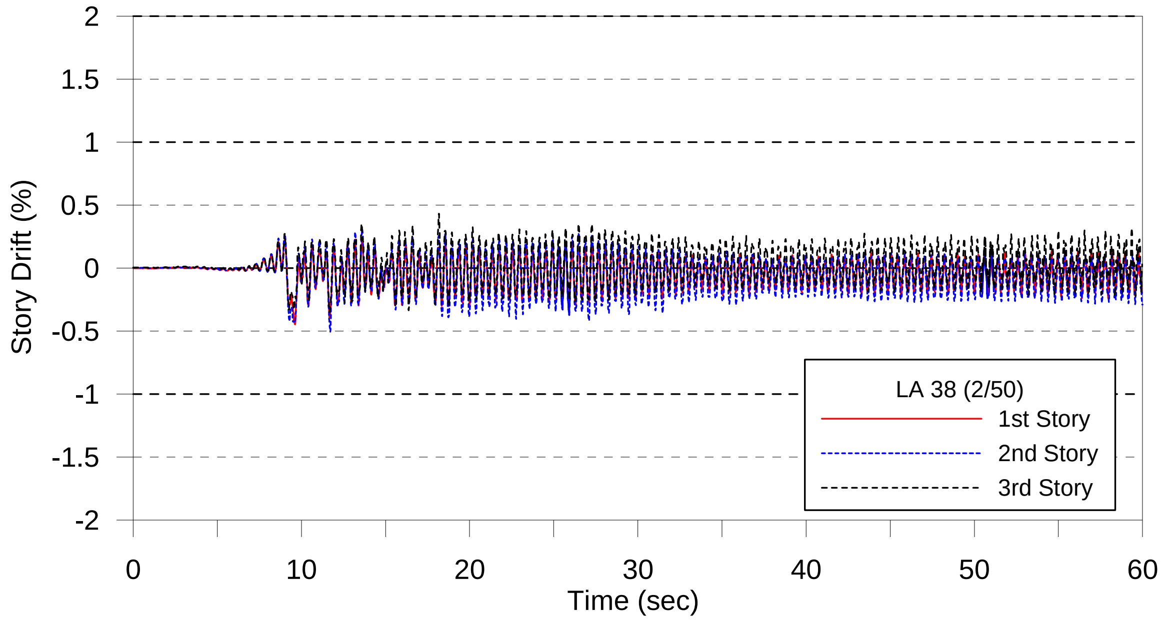

(a)

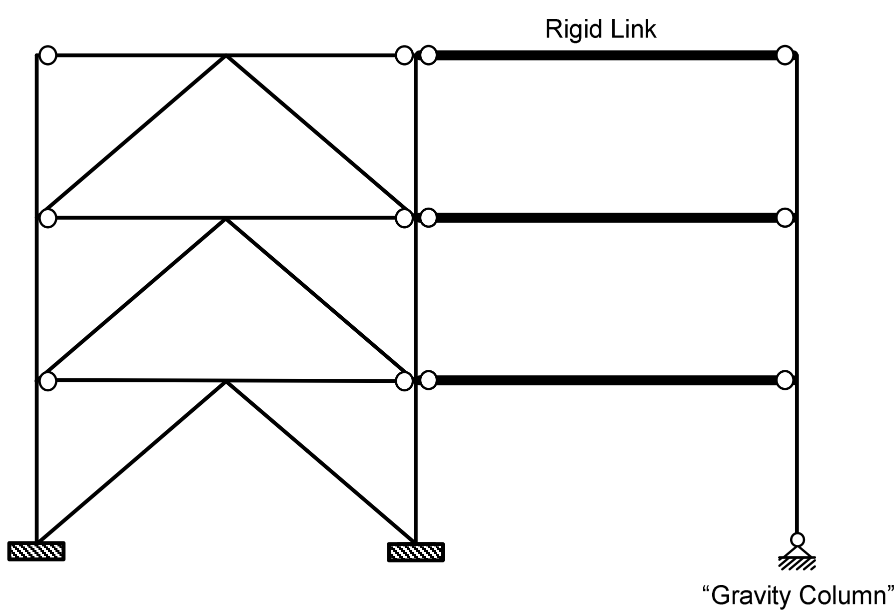

(b)

Figure 2.23. LA38 ground motion (2% in 50 years), 3V-PBPD

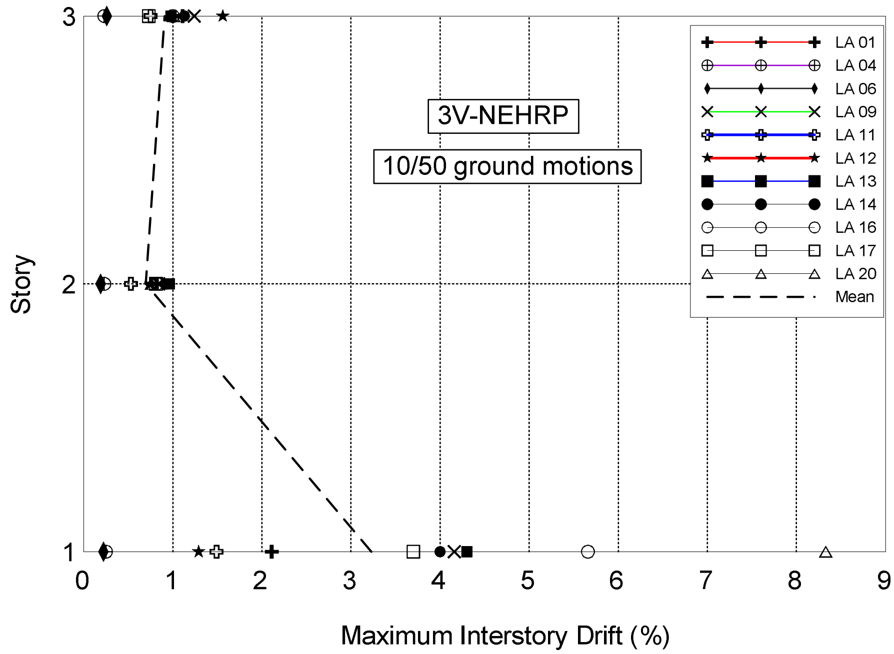

(a) NEHRP frame

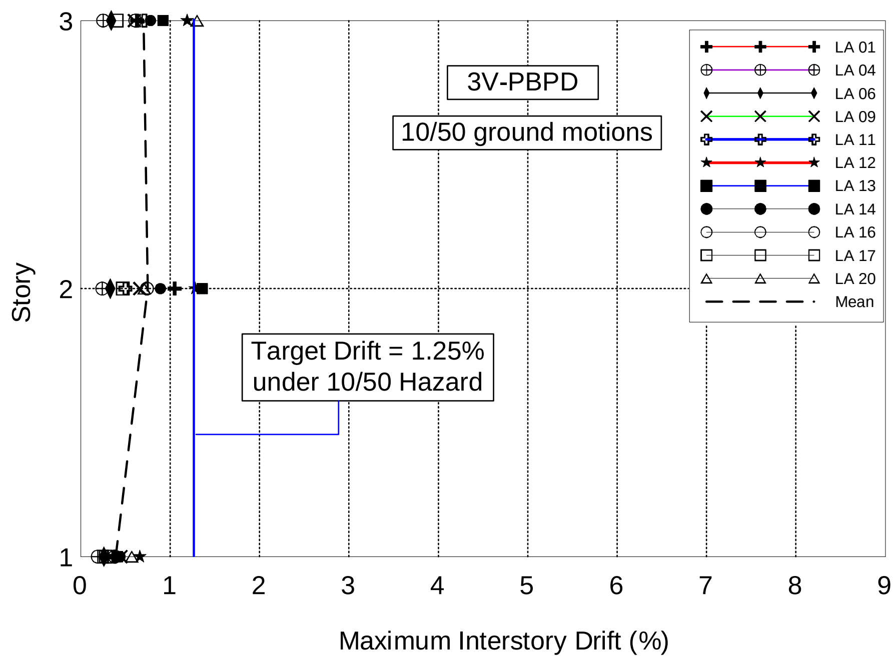

(b) PBPD frame

Figure 2.24. (a) Maximum story drifts of 3V-NEHRP under 10% in 50 years ground motions; (b) Maximum story drifts of 3V-PBPD under 10% in 50 years ground motions

2.4.2.1.1 Redesign of the 3-Story CBF

It should be noted that the design base shear for 3V-PBPD frame was approximately twice that of the 3V-NEHRP frame. This large difference is attributed to short period (T = 0.31 second), strict drift control (1.25% for 2/3 MCE design spectrum), and adjustment due to “pinched” hysteretic behavior of bucking type braces, which are part of the PBPD method needed to ensure the targeted performance. The differences in the performance of those two frames as presented in the previous section clearly showed that. In order to study the effect of the difference in the design base shear, the 3V-PBPD frame was redesigned (called 3V-PBPD-1 frame) by using the same design base shear as for the 3V-NEHRP frame. All other design criteria as presented in Section 2.2 for the PBPD procedure remained unchanged. Tables 2.26 and 2.27 give comparison of some selected parameters between the 3V-NEHRP and 3V-PBPD-1 frames, and the final design sections are shown in Figure 2.23. It can be seen that the two frames have equal material weight.

Selected responses of the 3V-PBPD-1 frame are shown in Figures 2.26, 2.27, and 2.28. It is seen that although the behavior is still better than that of 3V-NEHRP frame, in terms of damage control (no collapse, relatively smaller column hinge rotations, and no early brace fractures), the 3Vf-PBPD-1 frame exhibited much larger story drifts than those of the 3V-PBPD frame. This becomes evident when the maximum story drifts due to eleven ground motions (10% in 50 years) are plotted as shown in Figure 2.29. These results clearly show the merits of the PBPD method in order to achieve the intended seismic performance.

Table 2.26. Design fracture life of brace members

Fracture Life of Braces	3V-NEHRP	3V-PBPD-1
3rd level	78	499
2nd level	71	461
1st level	71	283

Table 2.27. Material weight for one braced frame (NEHRP design base shear)

Weight Calculation	3V-NEHRP (lbs)	3V-PBPD-1 (lbs)	3V-PBPD-1/3V-NEHRP
Braces	3505	3359	0.96
Beams	14040	13530	0.96
Column	7488	7488	1.00
Total	25033	24377	0.97

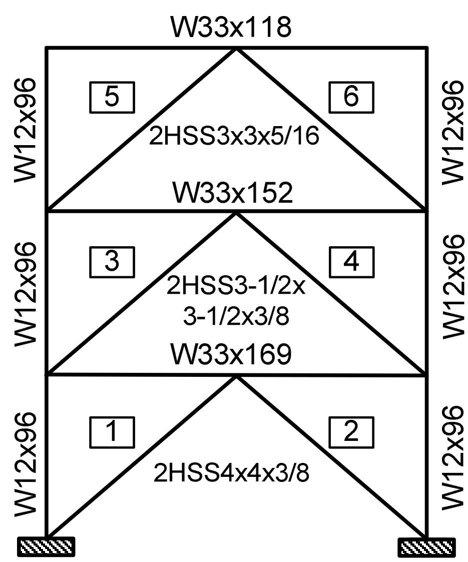

Figure 2.25. Final member sections of 3V-PBPD-1 (using the NEHRP design base shear)

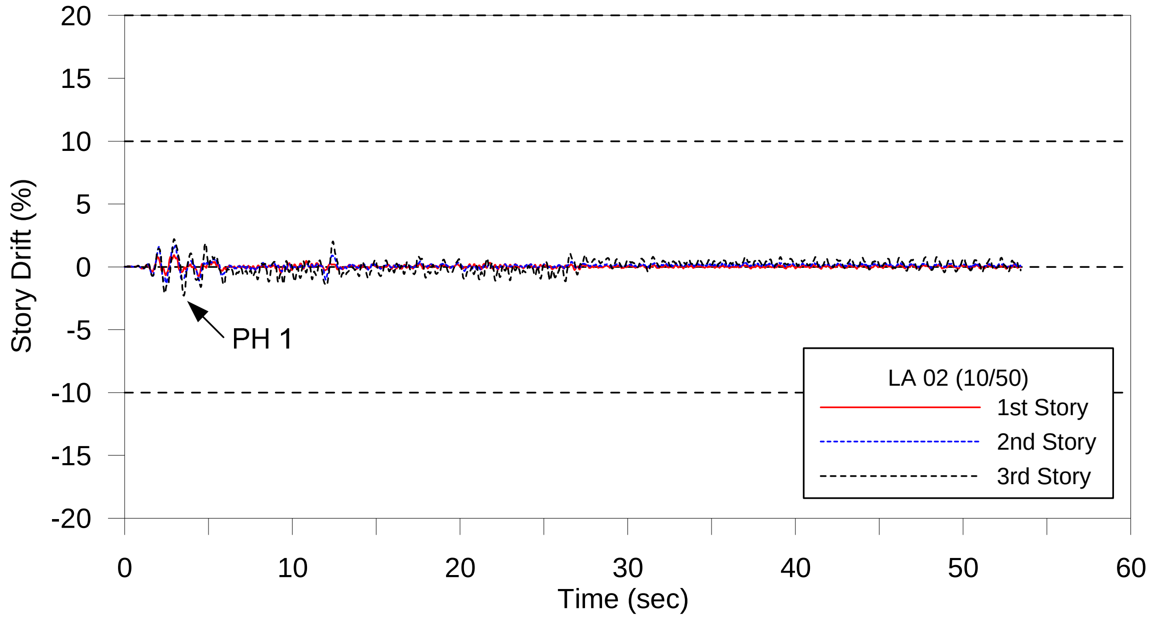

(a)

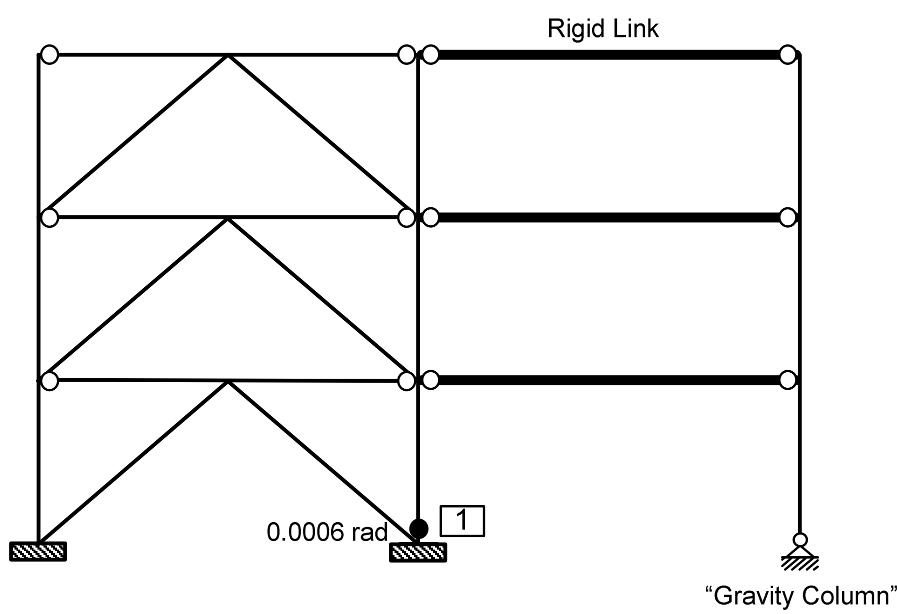

(b)

Figure 2.26. LA02 ground motion (10% in 50 years), 3V-PBPD-1

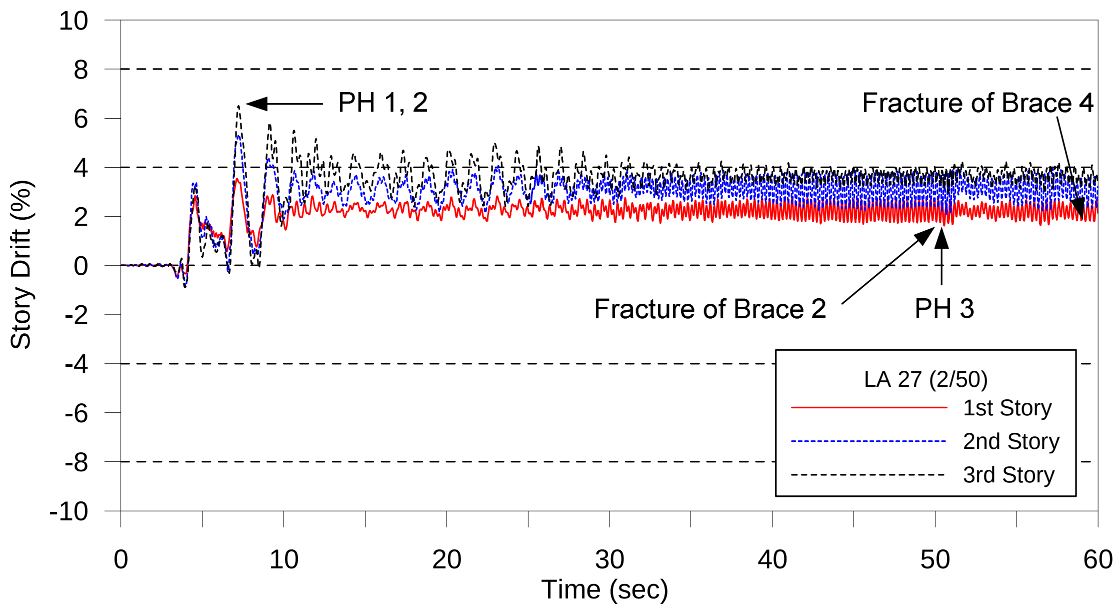

(a)

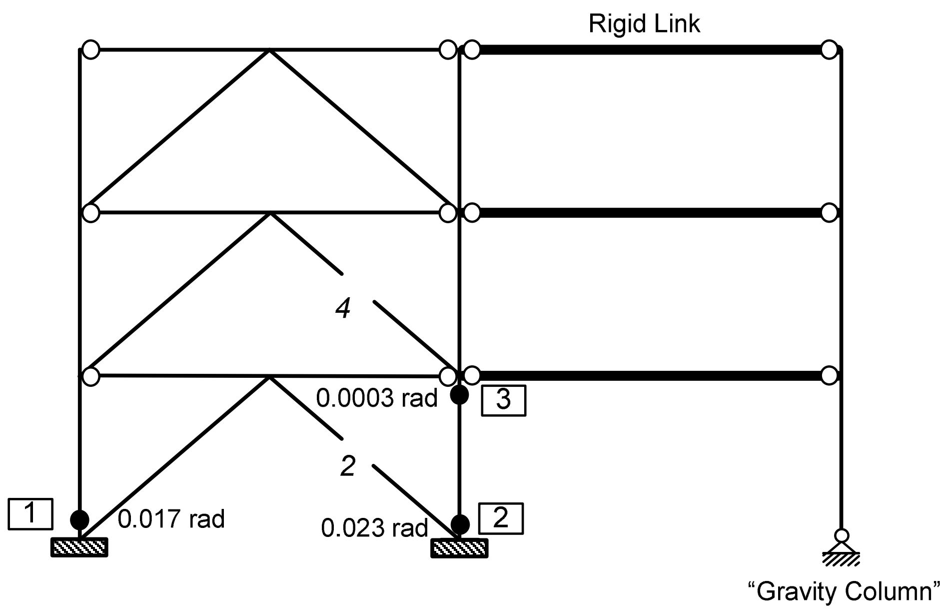

(b)

Figure 2.27. LA27 ground motion (2% in 50 years), 3V-PBPD-1. The sequence of brace fractures and plastic hinge formation along with maximum plastic rotations are also shown.

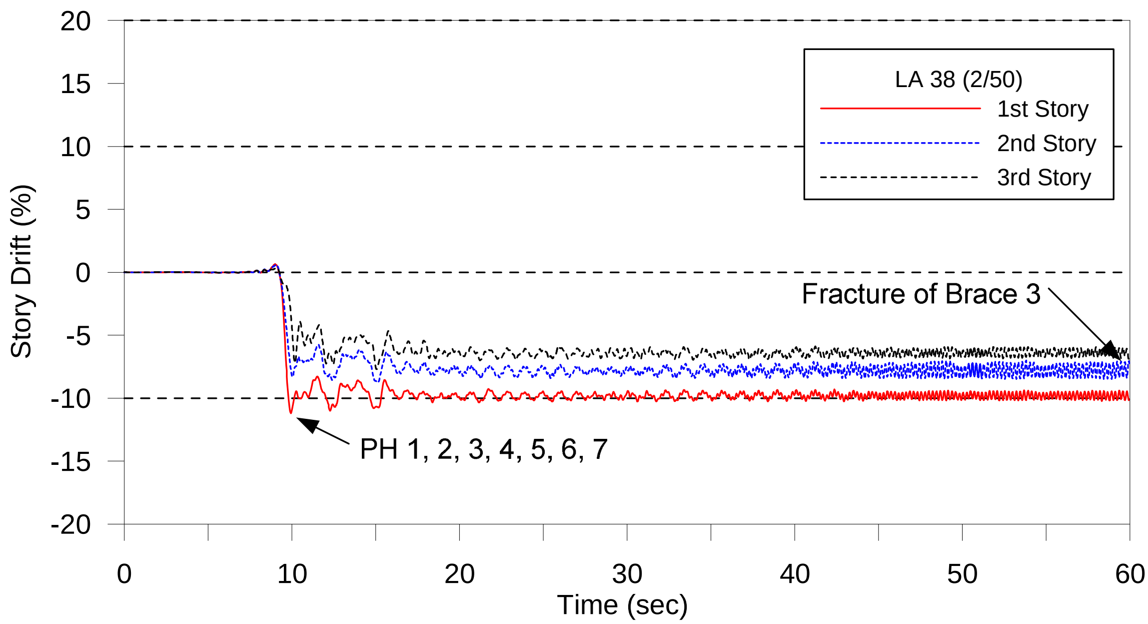

(a)

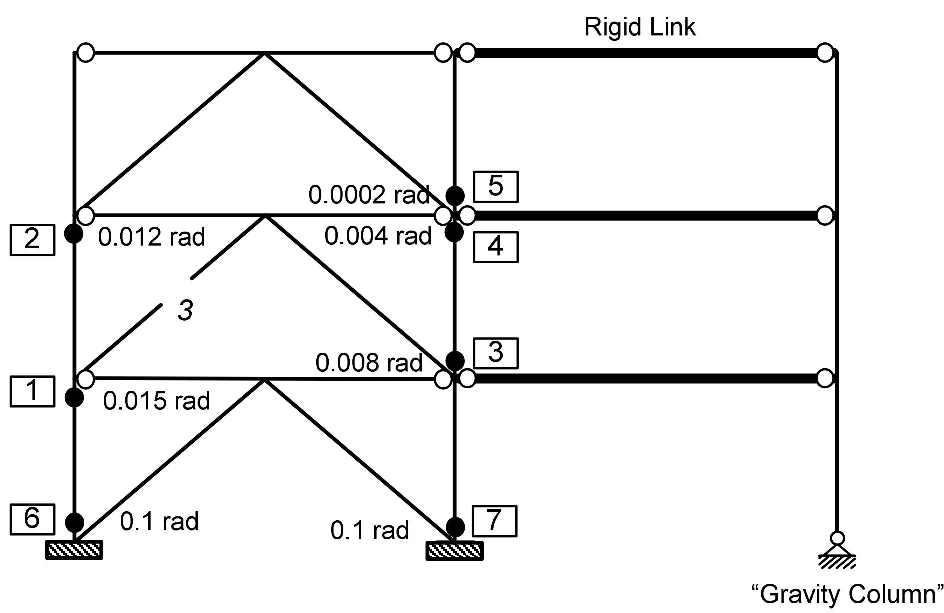

(b)

Figure 2.28. LA38 ground motion (2% in 50 years), 3V-PBPD-1. The sequence of brace fractures and plastic hinge formation along with maximum plastic rotations are also shown.

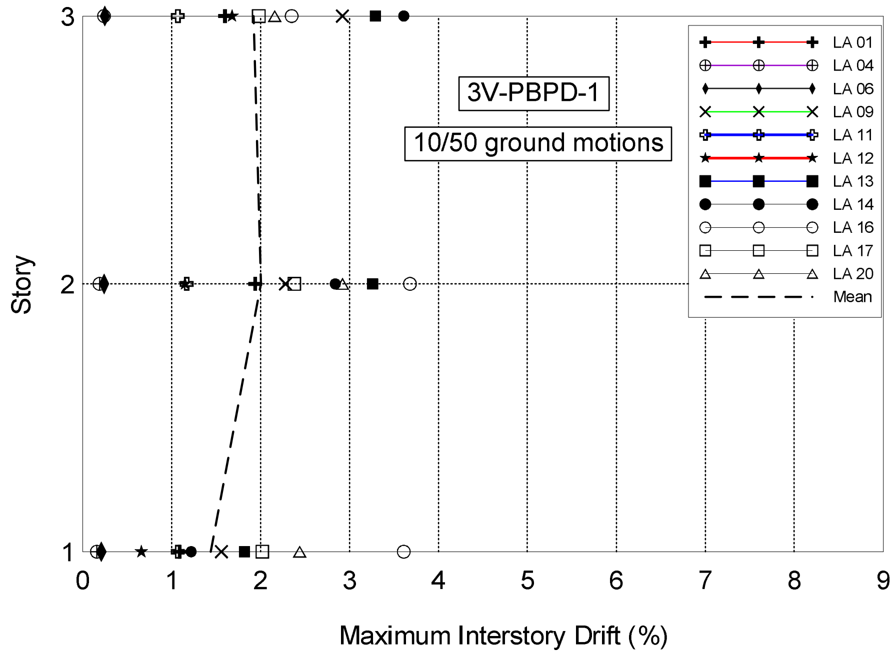

Figure 2.29. Maximum story drifts of 3V-PBPD-1 under 10% in 50 years ground motions

2.4.2.2 6-story CBF

Similar to the 3-story CBF, the beam-to-column connections at the first to fifth levels of the 6-story NEHRP frame were modeled as moment resisting connections due to the presence of gusset plates, while the beam-to-column connections at all levels of the 6-story PBPD frame were modeled as pin connections due to the introduction of beam splices. The maximum story drifts due to twelve 10% in 50 year ground motions for the two frames are shown in Figure 2.30. It is seen that the performance of the 6V-NEHRP and 6V-PBPD frames are similar when subjected to the design level hazard. However, the differences become more significant when subjected to 2% in 50 year ground motions. For example, as can be observed in Figures 2.31 and 2.32, the 6V-NEHRP frame showed poor performance and large story drifts for LA 38 record. On the other hand, the 6V-PBPD frame remained stable during the entire excitation with a maximum story drift slightly higher than the 2% target value, and no brace fracture occurred.

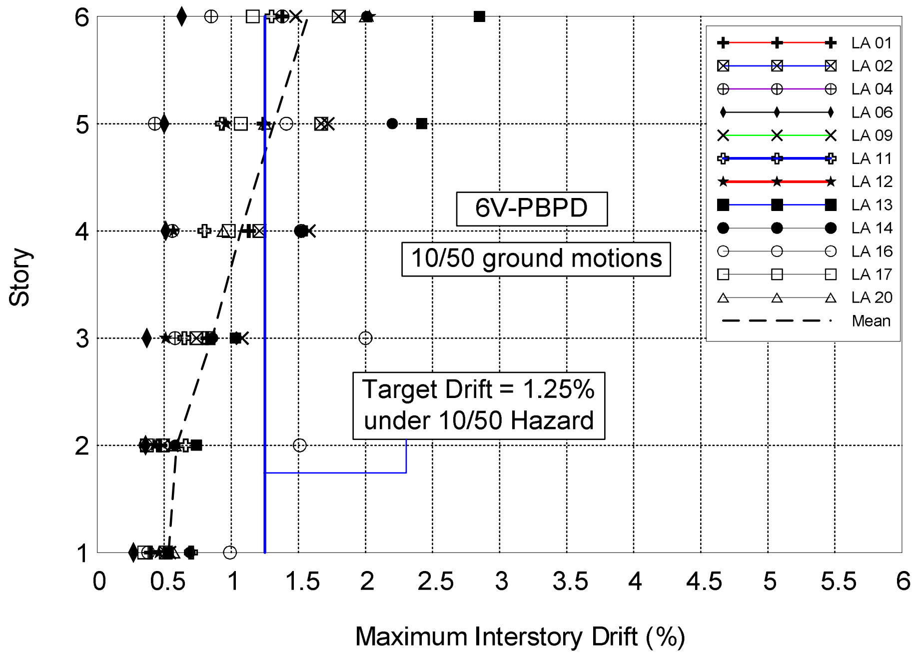

(a)

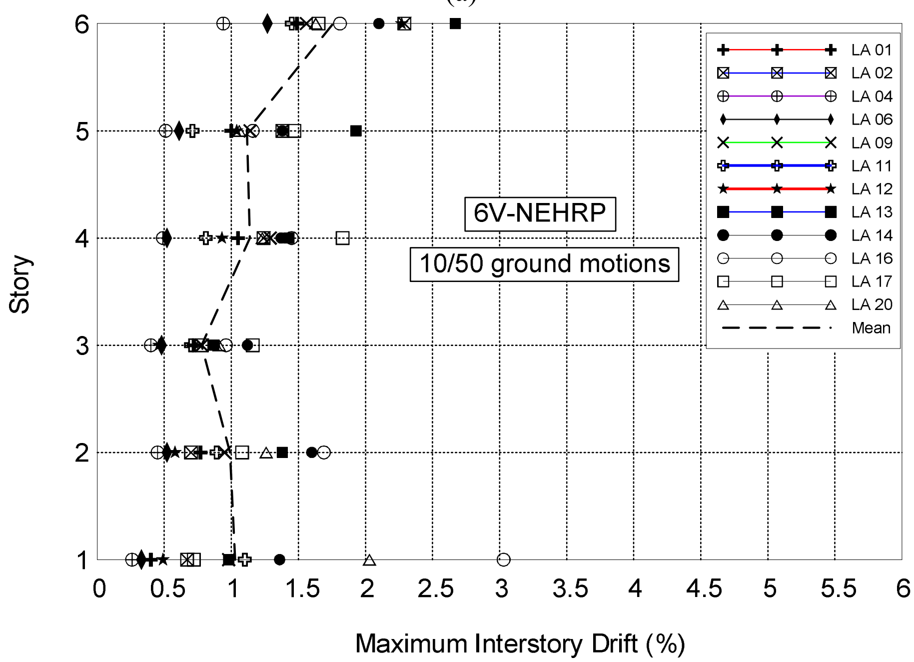

(b)

Figure 2.30. Maximum story drifts under 10% in 50 years ground motions:
(a) 6V-NEHRP; (b) 6V-PBPD

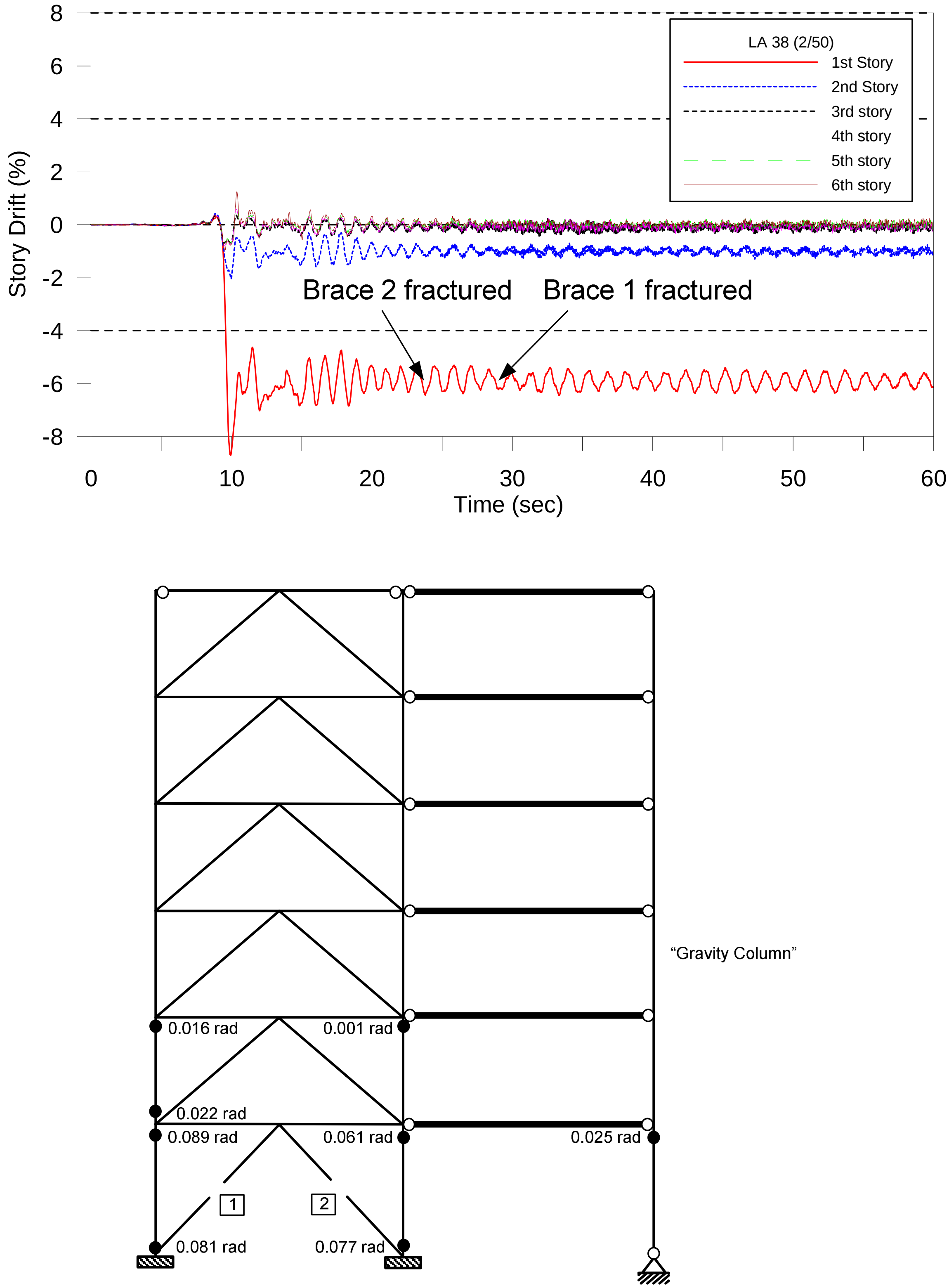

Figure 2.31. Drift responses and plastic hinge/brace fracture locations of 6V-NEHRP frame under LA 38 ground motion (2% in 50 years)

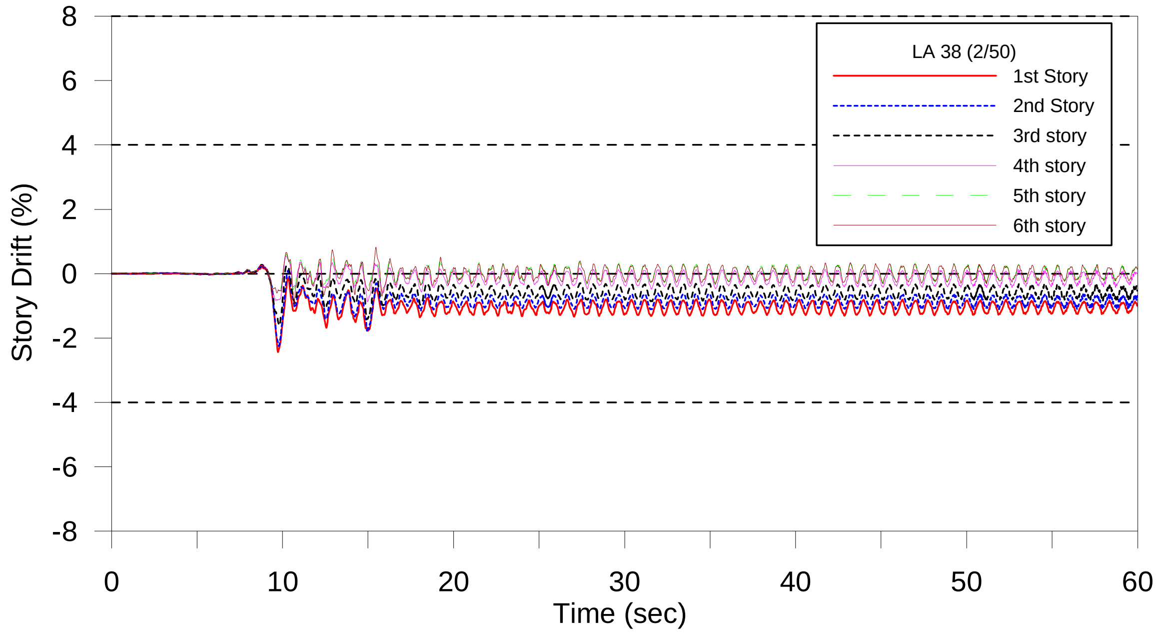

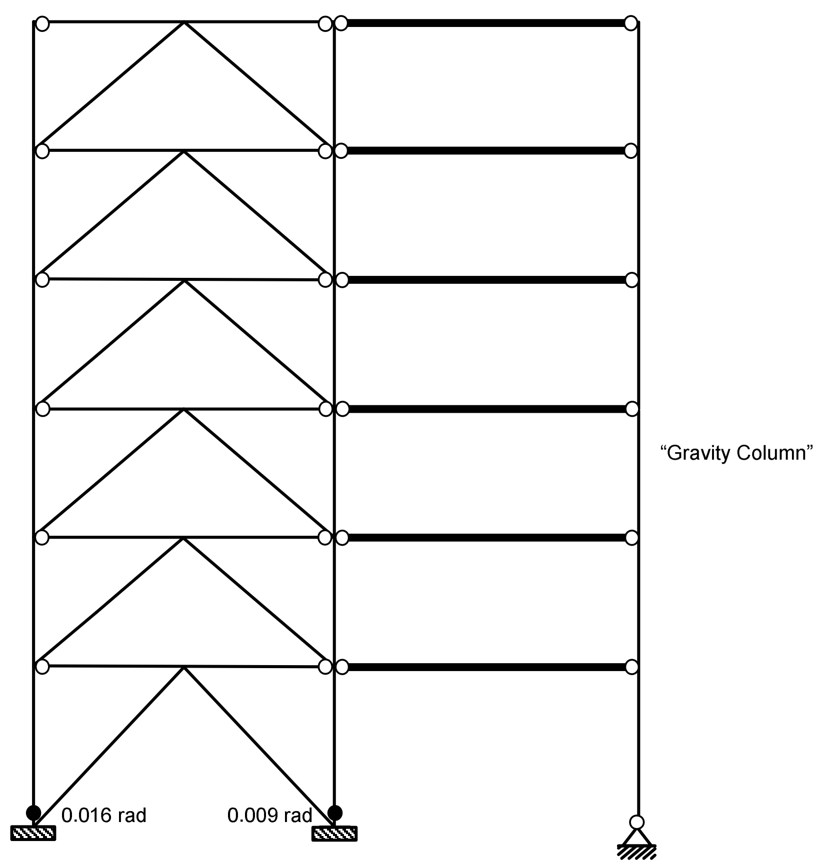

Figure 2.32. Drift responses and plastic hinge locations of 6V-PBPD frame under LA 38 ground motion (2% in 50 years)

CHAPTER 3

Further Development of PBPD Method for Design of CBF

3.1 General

The current PBPD procedure for design of CBFs was described in Chapter 2. The 3-story and 6-story CBFs, originally designed by Sabelli (2001) based on NEHRP guidelines (1997), were re-designed by using the PBPD procedure explained in Chapter 2 (Goel and Chao, 2008). It was shown that the PBPD designed CBFs have much better performance under design level (2/3MCE) as well as MEC level ground motions compared to the NEHRP frames.

As part of the current PBPD procedure for CBFs, the beam to column connection detail was modified by using shear splice in the beam such that the large moments produced in the beams would not transfer in to the columns. However, since the shear splice has to be placed with an offset from the column face at least equal to the length of gusset plate over the beam flange, there are concerns that this eccentricity of the shear splice combined with the large shear force caused by the vertical component of the unbalanced force in chevron CBFs may produce large bending moments at the centerline of the column. A new configuration for the gusset plate connection is proposed in Section 3.2. The gusset plate in this configuration is only connected to the column such that the total unbalanced moment on the column would be reduced.

In Section 3.3, the current capacity design method for columns in CBFs based on the accumulative axial forces is evaluated by comparing the column moments from pushover and dynamic analyses. A more accurate design method for columns using pushover analysis is proposed.

An alternative method to account for pinched hysteretic behavior of CBFs in the PBPD approach is introduced in Section 3.4. This method is also applicable to other types of systems with degrading hysteretic behavior.

It is realized that the yield drift in slenderer braced frames such as CBFs, does not have a constant value due to the significant amount of flexural deformation caused by axial deformation of columns. Because of importance of having a good estimation of yield drift in PBPD method, a procedure is presented in Section 3.5 to analytically estimate the yield drift for slender braced frames.

Unlike MFs, a significant amount of the story drift in slender braced frames comes from the axial deformation of the columns. This is basically an elastic type of deformation which is not imposing additional deformation demand on bracing members as the main seismic components in braced frames. To address this issue, an approach is introduced in Section 3.6 in order to obtain the proper target drift for CBFs. In this method, an effective target drift is calculated based on the original definition of the target drift used in the work-energy equation in PBPD.

In Section 3.7, the suggested PBPD approach is utilized to design the 9-story SAC building by using CBFs as the lateral load resisting system. The performance of this design is then evaluated by using 10%/50yrs and 2%/50yrs SAC LA ground motions (Somerville et al, 1997). Based on the observed maximum story drift profile along the height, the possibility of considering a different lateral load distribution in the PBPD procedure for CBFs is investigated. Using the new lateral load distribution, the provided strength and stiffness would be greater in upper stories which can be helpful in reducing the large story drifts observed under dynamic analyses. Extensive dynamic analyses were carried out to study the effect of varying lateral distribution on the performance of CBFs.

3.2 Proposed Gusset Plate Configuration

As part of the current PBPD procedure for CBF, the beam-to-column connection detail is modified by using shear splice in the beam such that the large moments produced in the beams would not transfer in to the columns (Chao and Goel, 2006b). However, since the shear splice has to be placed with an offset from the column face at least equal to the length of gusset plate over the beam flange, there are concerns that this eccentricity of the shear splice combined with the large shear force caused by the vertical component of the unbalanced force in chevron CBF may produce large bending moments at the centerline of the column. A new configuration for the gusset plate connection is presented in this section. The gusset plate in this configuration is only connected to the column such that the total unbalanced moment on the column can be reduced.

Figure 3.1.a shows the current detail for gusset plate connection, called connection Type I. The proposed configuration, called connection Type II, is shown in Figure 3.1.b. As can be seen in this figure, the gusset plate is only connected to the column. The top flange of the beam is coped in order to reduce the eccentricity between the line of action of brace force and the intersection of beam and column. Although there is some eccentricity in the proposed connection (Type II), the total unbalanced moment

transferred to the column is smaller in this configuration. This is due to the fact that the shear splice in this configuration is much closer to the column centerline. More importantly, the moments produced by the axial force in the brace and the one produced by the shear force at the shear splice act oppositely to each other. This would further reduce the unbalanced moment on the column. Since the columns are designed solely based on their accumulative axial force in the PBPD procedure, having lesser moment demand on columns would ensure their better performance and safety.

The analysis results for this proposed configuration are shown in the following section along with the results without considering and eccentricity to investigate the importance of the unbalanced transferred moments on the performance of the columns.

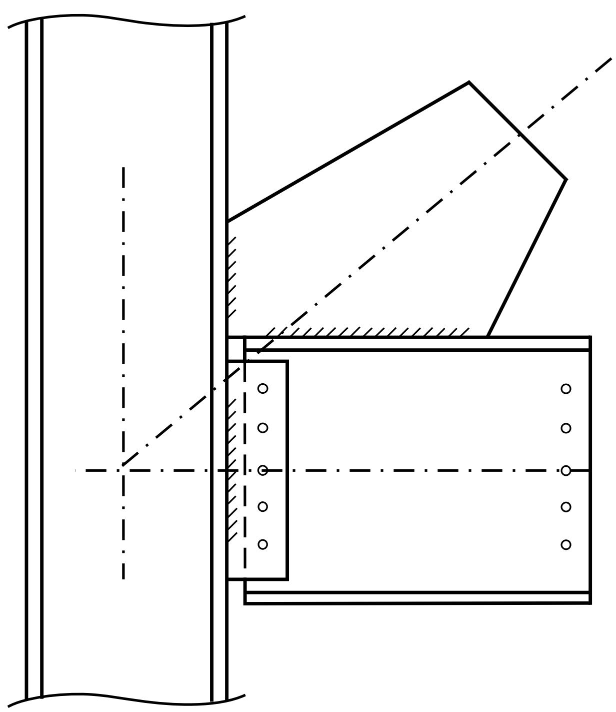

a) Connection Type I

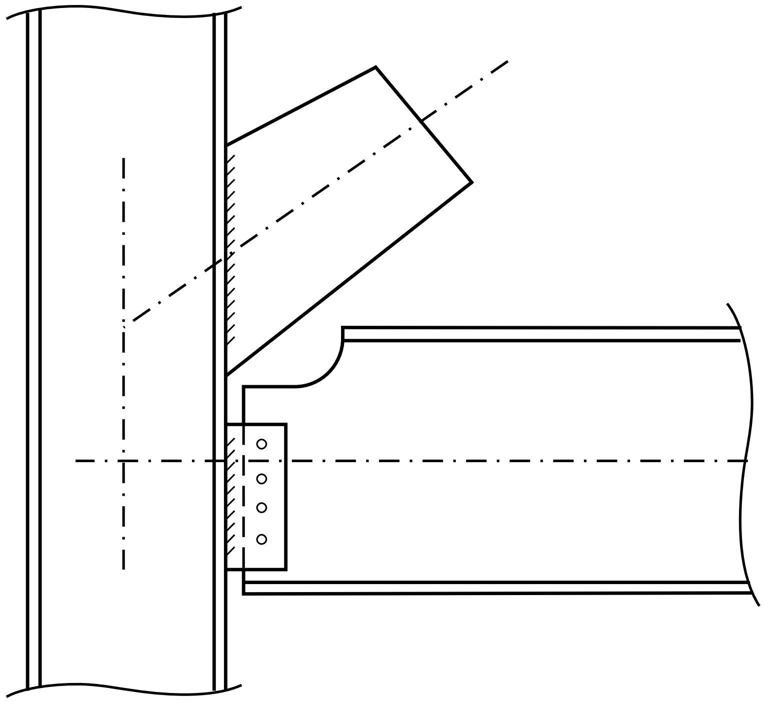

b) Connection Type II (proposed)

Figure 3.1. Gusset Plate Connection Configurations: (a) Type I; (b) Type II (proposed)

3.3 Capacity Design of Columns in CBFs

Previously, the CBF frames were modeled in SNAP-2DX program with pin-ended beams due to presence of shear splices. Since the shear splices are being placed beyond the gusset plate connection region, there is an eccentricity between the shear splice and the centerline of the column. Because of large vertical component of the unbalanced force at the shear splice, the transferred moment to the column can be significant. The purpose of this part of the study is to investigate how large such transferred moments can be, and whether or not they affect the overall design procedure for columns. Also, the possible effect of these moments on the performance of the structure will be studied. In addition, the behavior and performance of two alternative gusset plate connections to the beam-column joint are compared.

Table 3.1 shows the properties of the CBF models used in this section. The brace, beam, and column sections in all these models are similar to the PBPD designs (3V-PBPD and 6V-PBPD) obtained in Chapter 2. The models were analyzed by using the SNAP-2DX program.

Table 3.1 Description of the Studied CBF Models

CBF Model	Design Method	Modeling of G.P./ Beam-Column Connection
3V-PBPD	PBPD	Type I connection, without Ecc. for shear splices
3V-PBPD01	PBPD	Type I conn., with Ecc. for shear splices (Ecc.=20 inches)
3V-PBPD02	PBPD	Type II connection , with G.P. connected to the column
6V-PBPD	PBPD	Type I connection, without Ecc. for shear splices
6V-PBPD01	PBPD	Type I conn., with Ecc. for shear splices (Ecc.=20 inches)
6V-PBPD02	PBPD	Type II connection, with G.P. connected to the column

As can be seen in Figure 3.2, modeling the eccentricity of the shear splice is resulting in larger column moments for both the design level earthquake LA01, as well as MCE level earthquake of LA27. As can be seen, considerable moments are transferred from beams to column due to the end eccentricities. Therefore, these eccentricities should be properly modeled in order to obtain more realistic moment demands in columns.

In terms of the overall performance, no significant change was observed by adding the eccentricities in the models (for both 3-story and 6-story models). Still no plastic hinge formed in the columns except at the base. For the models with eccentricity, plastic hinge rotation at the column base shows an increase of about 10-15% which is not significant.

Comparing the column moments for connections Type I and Type II, it can be seen that for most of the stories these moments are somewhat larger in the Type II case (Figure 3.3 and Figure 3.5). On the other hand, the axial forces at the time of maximum moments are generally lower for Type II, and hence the available moment capacity is larger (Figure 3.4 and Figure 3.6).

It can also be seen from Figure 3.5.b Figure 3.6.b that for the 6-story CBF under 2/50 ground motion of LA38, the behavior of the Type I and Type II frames are practically the same (in terms of column axial forces and moments).

In summary, practically similar performances were seen for connections Type I and the proposed connection Type II under time-history analysis. However, connection Type II does not need an extra shear splice connection (like the one in Type I to reduce the transferred moment) and as a result can be considered to be a more cost-effective alternative.

A more accurate design method for columns would be the one where moments obtained from pushover analysis of the frame are taken into account along with the axial forces in the design of columns. This method is investigated in the next sub section.

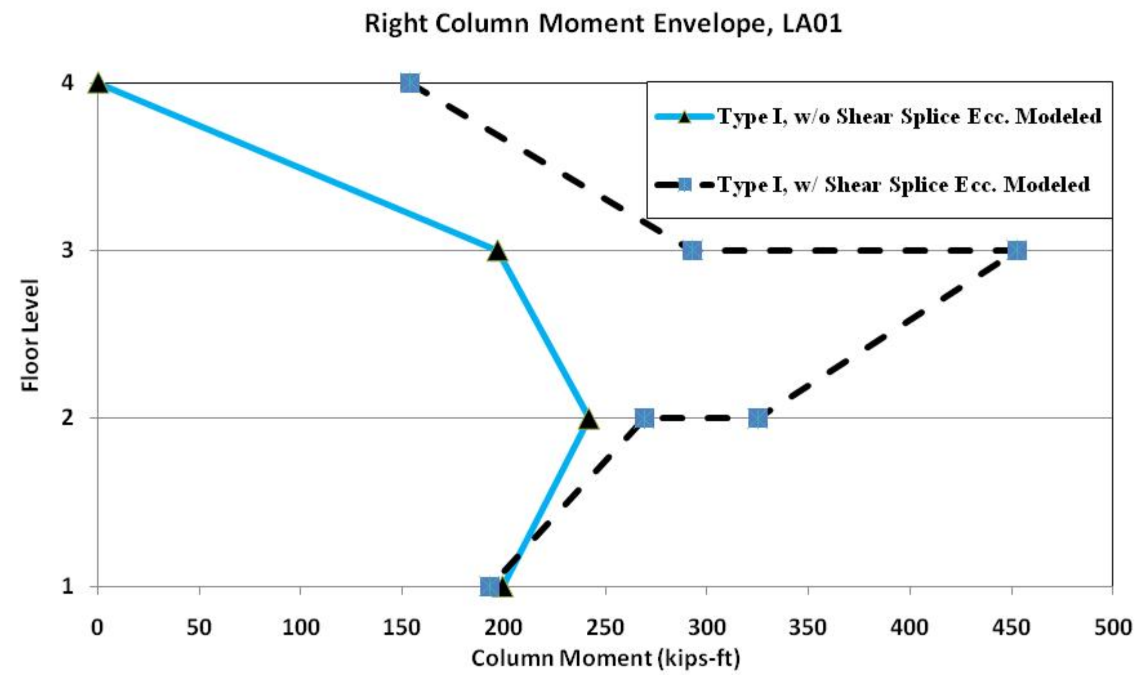

a)

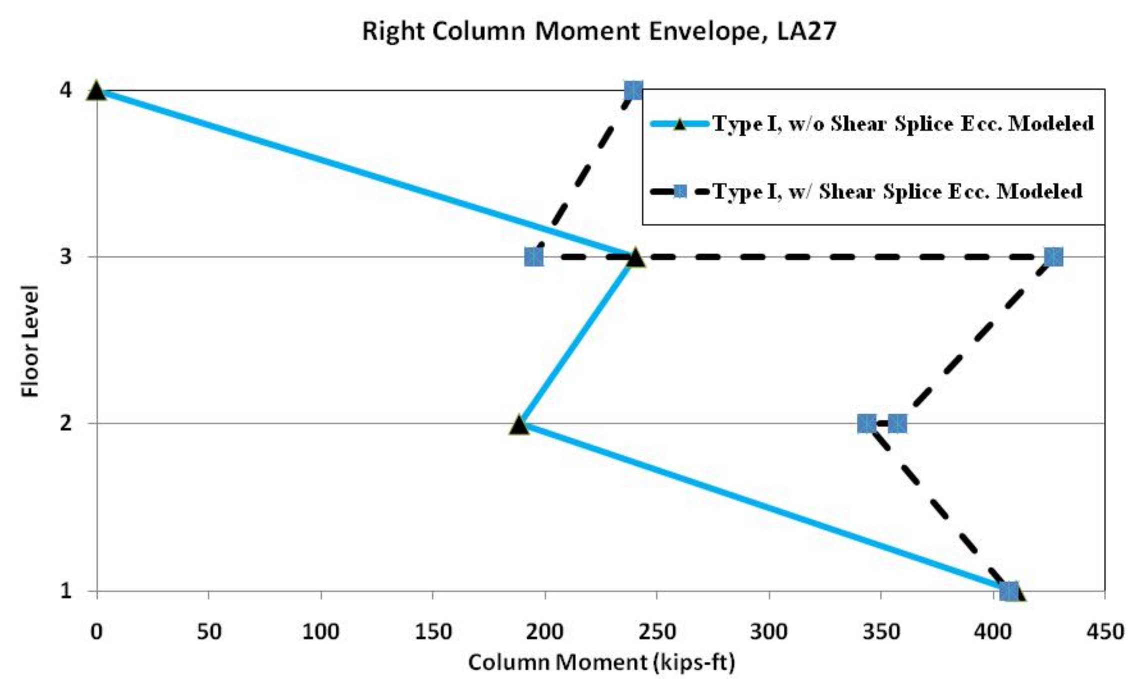

b)

Figure 3.2. The Effect of Modeling Shear Splice Eccentricity on Column Bending Moments under: (a) LA01; and (b) LA27

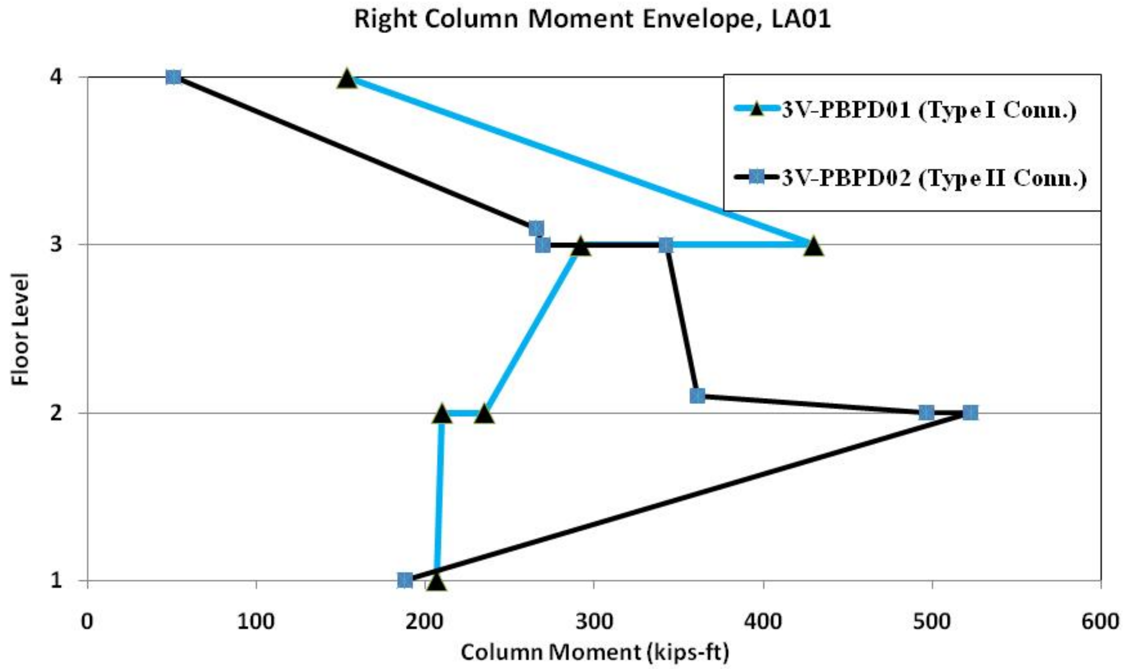

a)

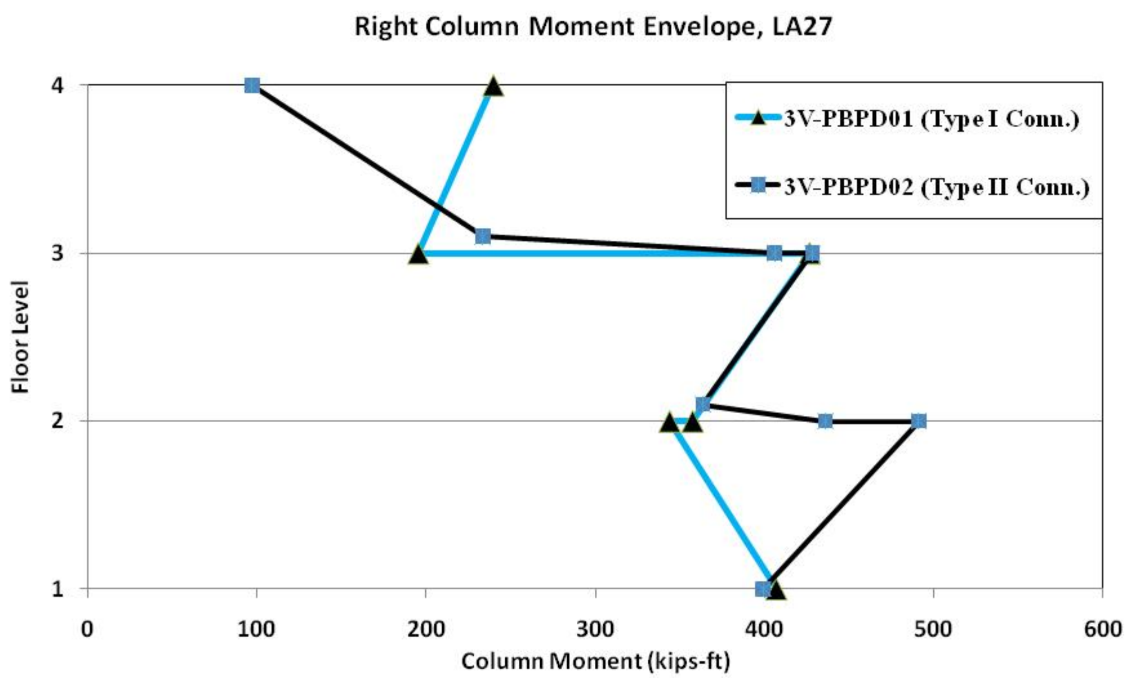

b)

Figure 3.3. Right Column, Moment Envelops for Models 3V-PBPD01 (Type I) and 3V-PBPD02 (Type II) under: (a) LA01; and (b) LA27

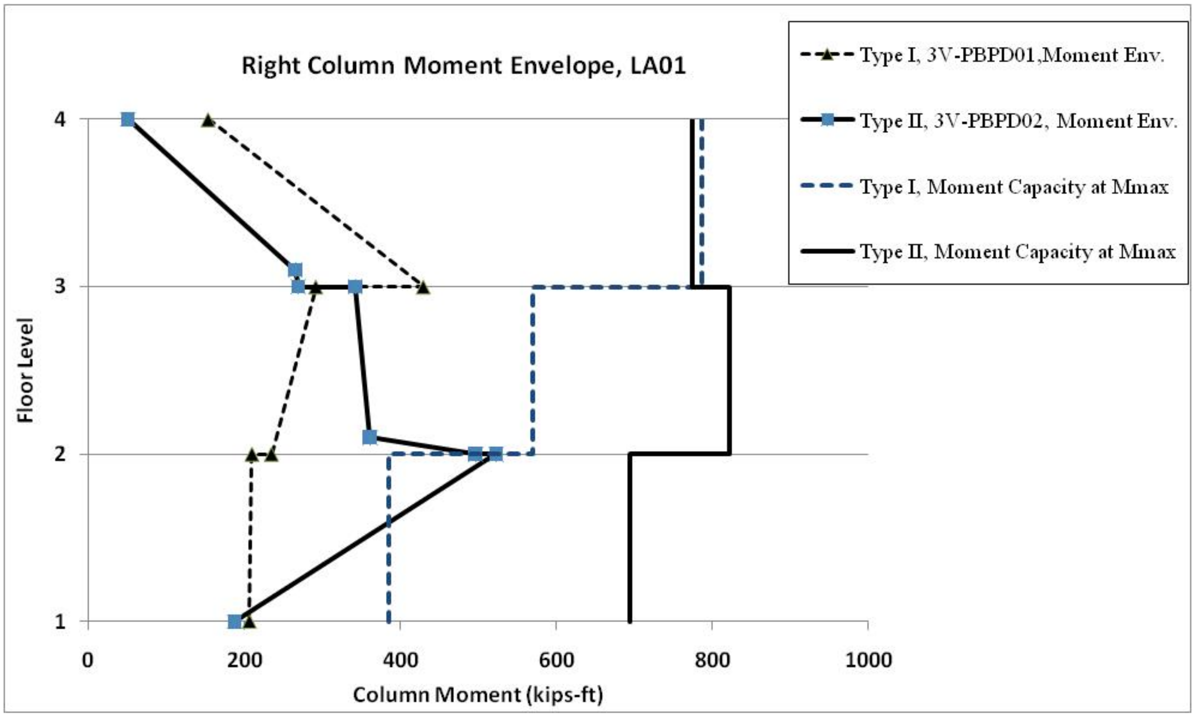

a)

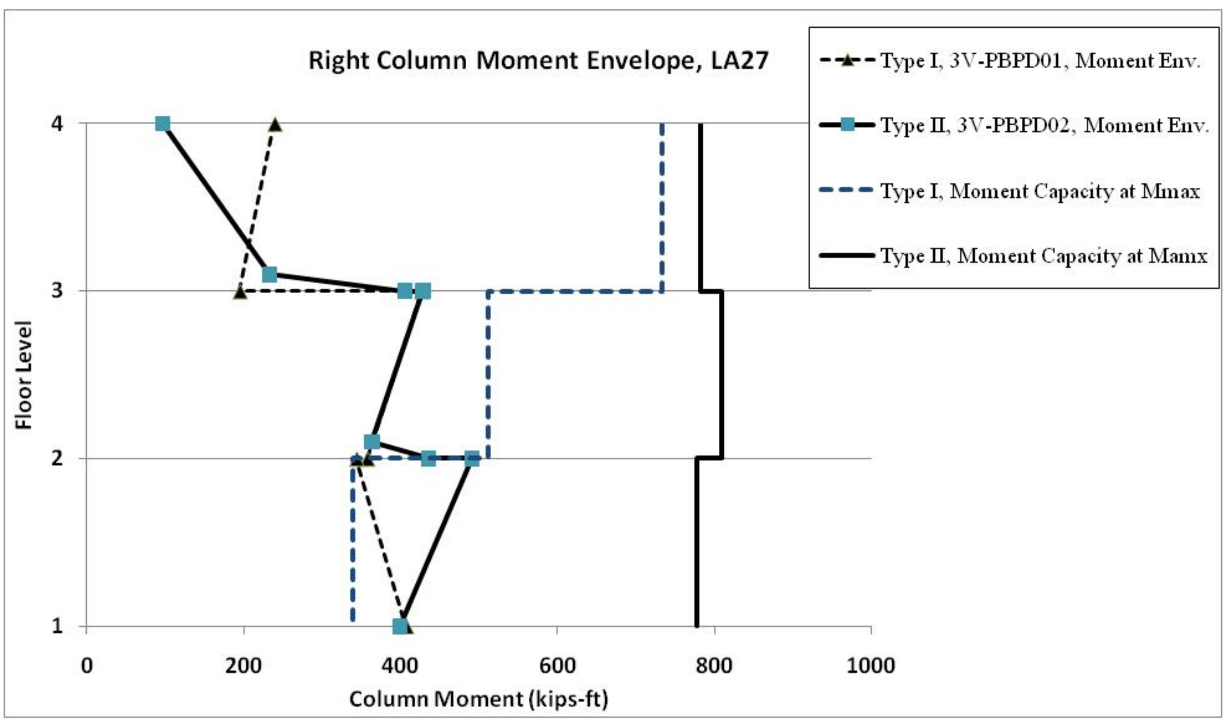

b)

Figure 3.4. Column Moments for connection Type I and Type II in 3-Story CBF and Available Moment Capacities under: (a) LA01; and (b) under LA27.

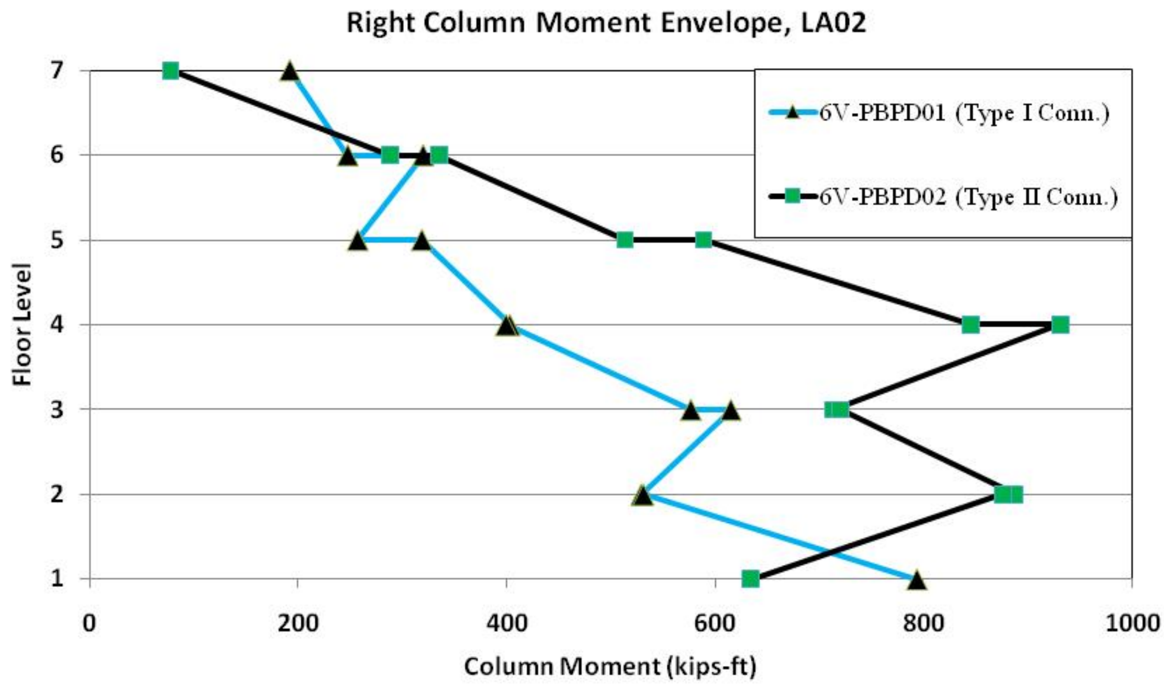

a)

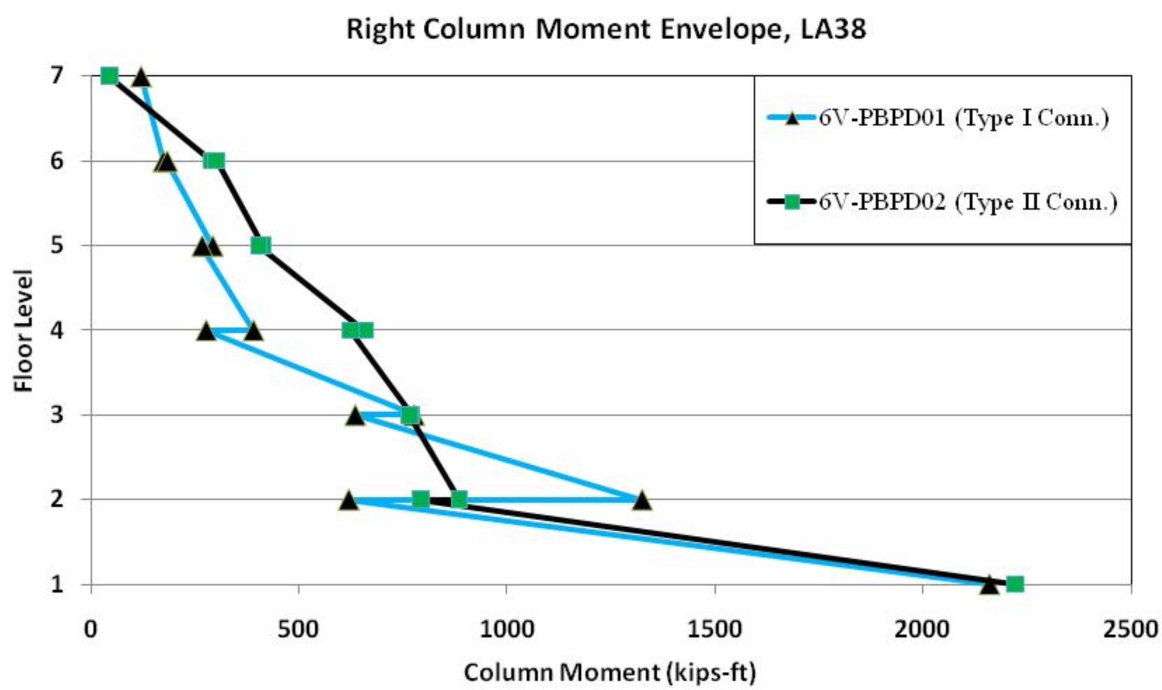

b)

Figure 3.5. Right Column, Moment Envelops for Models 6V-PBPD01 (Type I) and 6V-PBPD02 (Type II) under: (a) LA02; and (b) LA38

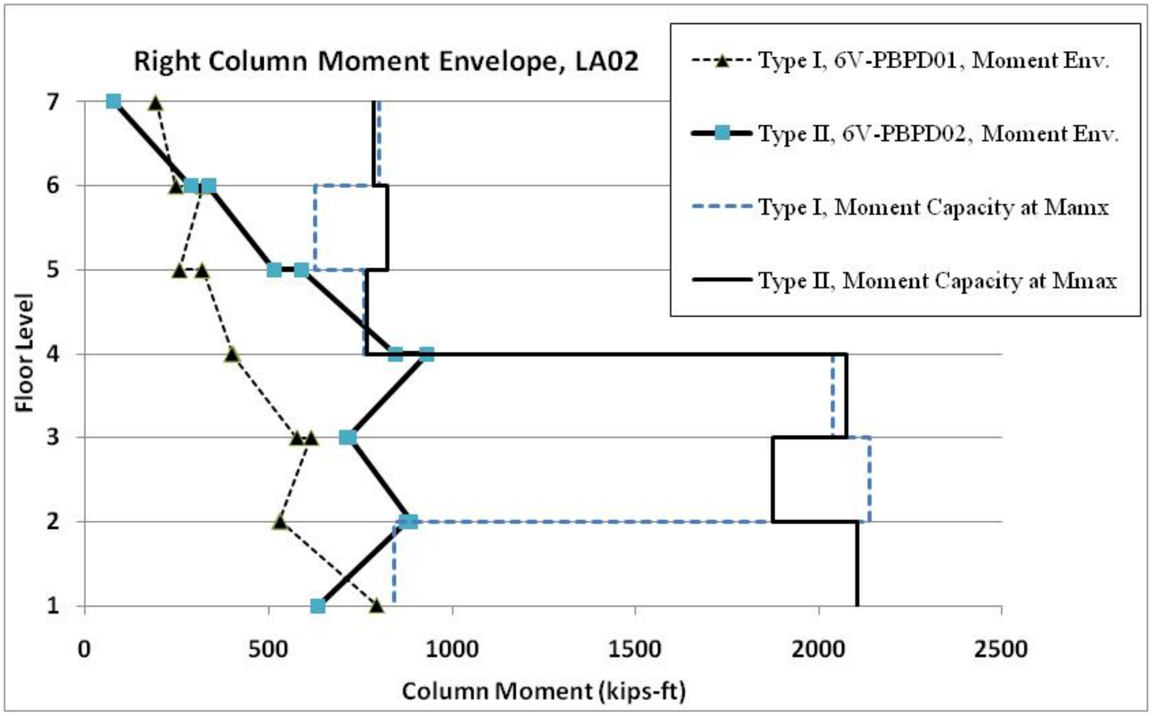

a)

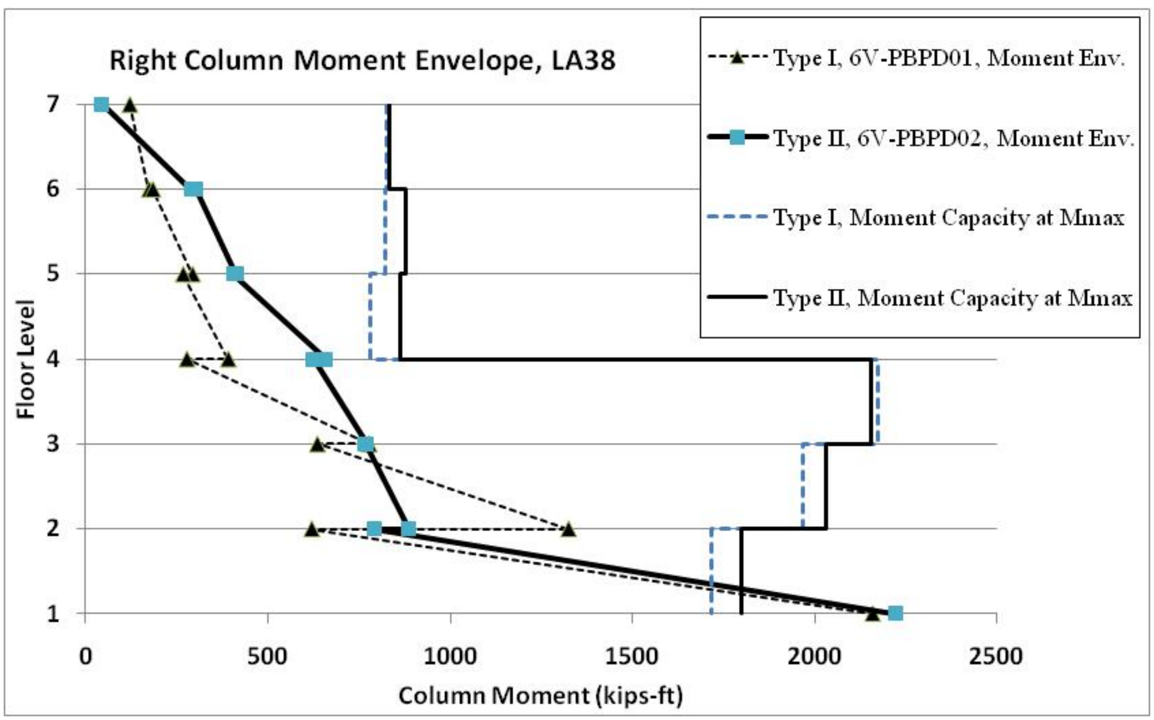

b)

Figure 3.6. Column Moments for connection Type I and Type II in 6-Story CBF and Available Moment Capacities under: (a) LA02; and (b) under LA38.

3.3.1 Re-Design of Columns in CBF Based on Combined Axial Forces and Moments Obtained from Pushover Analysis (3-Story and 6-Story)

The design of columns in CBFs based on only cumulative axial forces has proven to be satisfactory under both 10/50 and 2/50 ground motions. The goal here is to introduce a more accurate design method for columns which takes the moments as well as axial forces into account. The results of pushover analysis for the case of Type II Connection are used for this purpose. For pushover analysis, the column is considered to be elastic except for a PMM plastic hinge modeled at the base of columns. The frames are then pushed to the DBE target drift of 1.25%. A typical target drift value of 1.75% was also selected for comparison purposes to MCE level results. The moments and axial forces obtained from these analyses are then used to redesign the columns of the 3V-PBPD and 6V-PBPD frames.

Table 3.2 to Table 3.4 show the column sections obtained by using the two design methods: 1) Considering cumulative axial forces from column tree; 2) considering combined axial and moments from pushover analysis. It can be seen from the Table 3.2, that by using pushover results for column design in 3-story CBF (i.e., combined axial force and moment) a section with the same weight but larger depth (W14x120) would be required. The additional moment capacity of W14x120 versus W12x120 can be quite beneficial in case larger than expected bending moments occur in the columns. It is seen from Table 3.3 and Table 3.4 that the effect of bending moments in column design becomes more important by the increase in the number of stories. For the 6-story frame, a

W14x283 is required for the three lower stories if moments are considered in the design whereas W14x257 section was adequate considering only the cumulative axial forces.

Also, as shown in Figure 3.7 and Figure 3.8, the column moments at DBE target drift (1.25%) obtained from pushover analysis can be used with reasonable accuracy to account for column moments during the design. It should be noted that although the column moments obtained from pushover analysis are smaller than the ones under ground motions, they occur simultaneously with large axial forces under pushover analysis. As shown in the previous section, the maximum axial force and maximum moments are not occurring at the same time under time-history analysis.

Based on observation from this preliminary study, one may conclude that even by considering only axial forces in capacity design of columns, good performance can still be expected for the PBPD frame. Two main reasons that even with using only axial forces in design of columns, still a good performance can be achieved are:1) P_{max} and M_{max} in columns are not occurring at the same time; and 2) the axial force used in column design is based on the fact that all braces buckle and yield at the same time, which applies the largest possible axial demand on columns. But this does not generally occur during dynamic response; therefore the axial force demand is lower than the value used for design.

A practical conclusion is that since it is known that there would be some bending moments in columns due to unbalanced moments transferred to the column and also from the continuity of the column itself under dynamic analysis, it would be better to use a W-sections with larger depth (with almost the same weight) whenever possible, so that additional bending capacity can be provided.

In addition, based on the preliminary study in this section, designing columns in CBF by using the demands obtained from pushover analysis was seen to be a more accurate method. The accuracy of pushover method however decreases with the increase in the number of stories. A more comprehensive study on the subject can be done by comparing the demand ratios obtained from pushover to those from time-history analysis results.

Table 3.2. Column Design for 3-Story CBF

Design Method	Pu (kips)	Mu (k-ft)	Design Section	Design Ratio
Cum. Axial Forces	1124	0	W12X120	0.848
Combined Axial and Moments	906	385	W14X120	1.05

Table 3.3. Column Design for 6-Story CBF (Lower Three Stories)

Design Method	Pu (kips)	Mu (k-ft)	Design Section	Design Ratio
Cum. Axial Forces	2464	0	W14X257	0.885
Combined Axial and Moments	1970	900	W14X283	1.01

Table 3.4. Column Design for 6-Story CBF (Top Three Stories)

Design Method	Pu (kips)	Mu (k-ft)	Design Section	Design Ratio
Cum. Axial Forces	811	0	W14X109	0.640
Combined Axial and Moments	640	196	W14X109	0.958

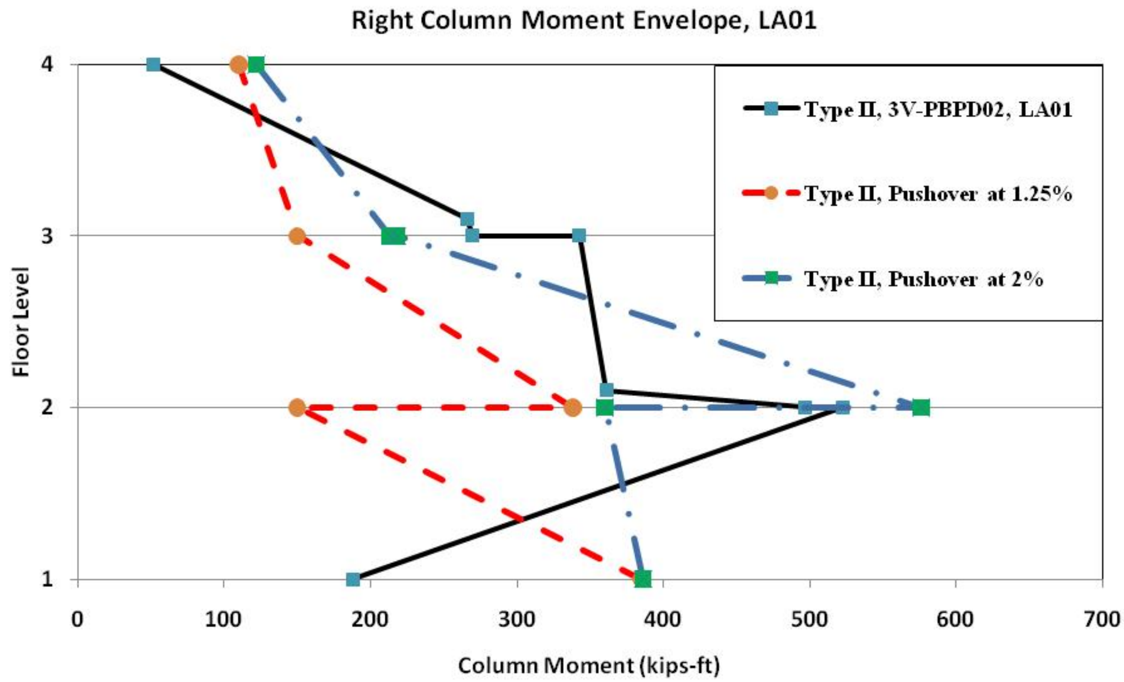

(a)

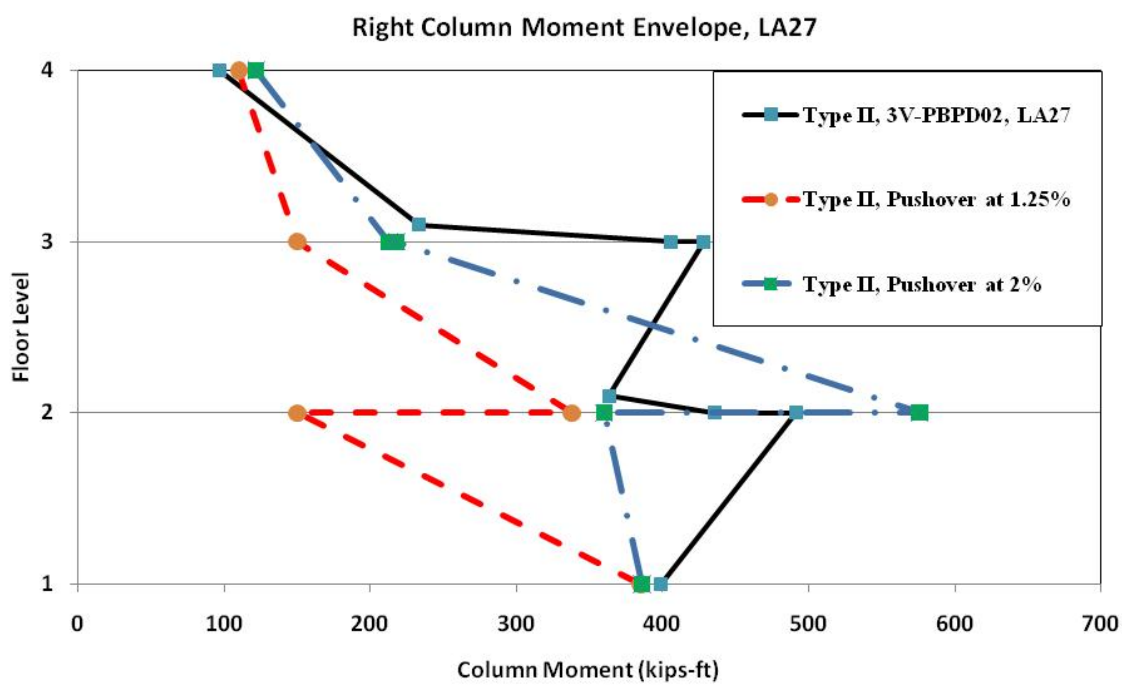

(b)

Figure 3.7. Column Moments for 3V-PBPD02: (a) Under LA01; and (b) Under LA27 Ground Motions.

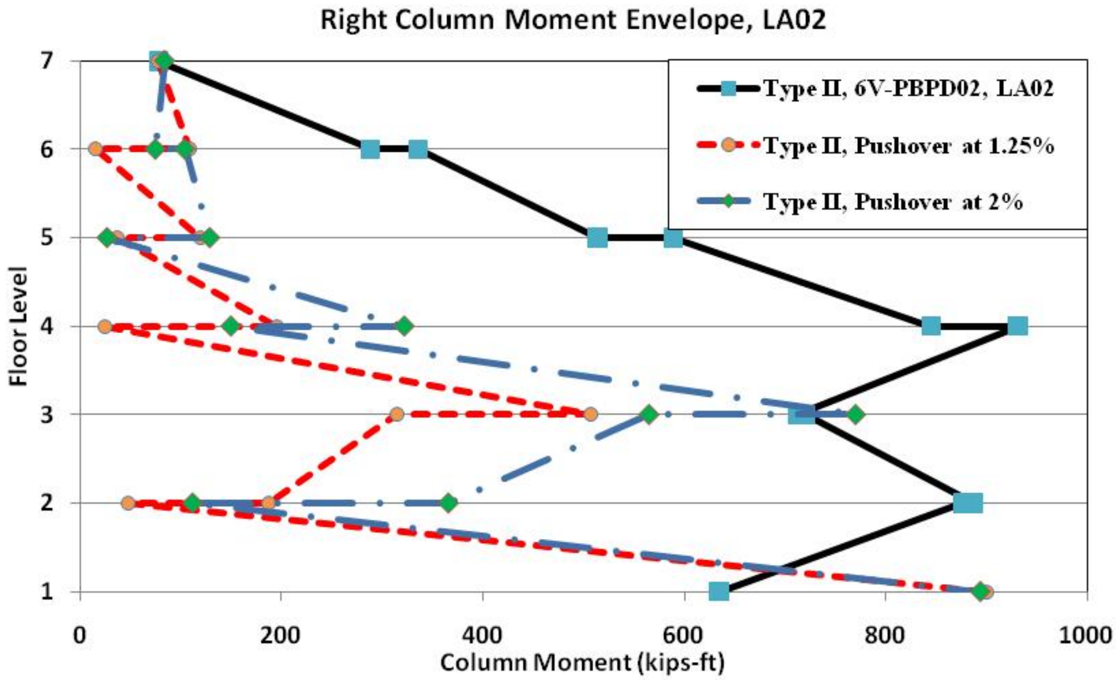

(a)

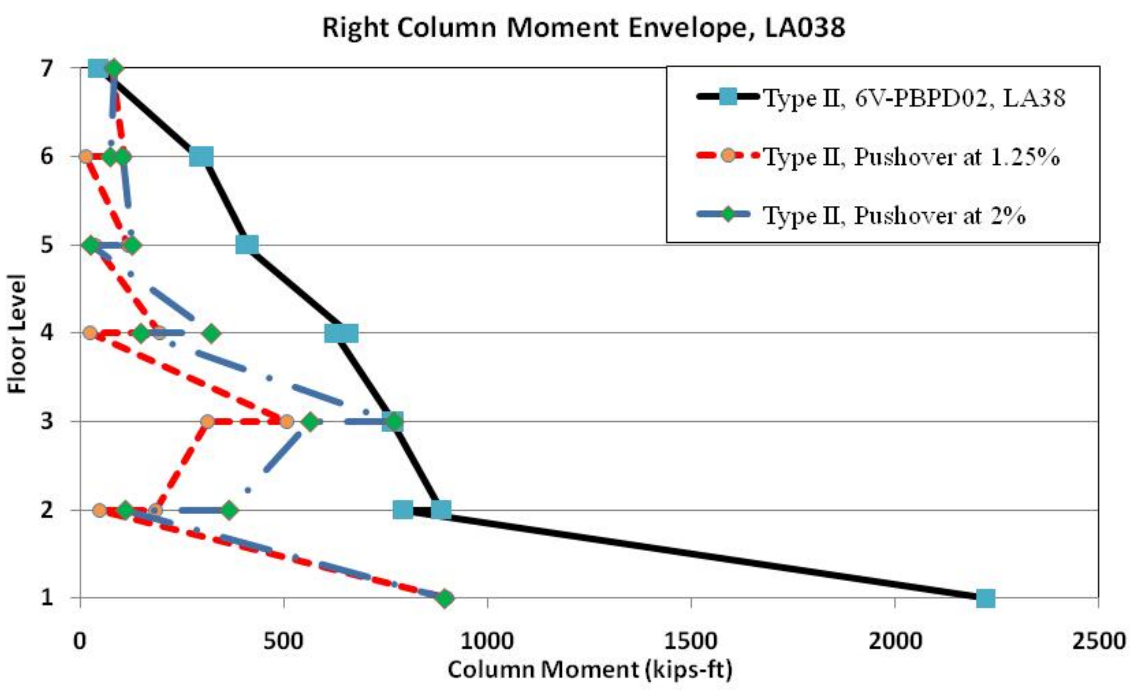

(b)

Figure 3.8. Column Moments for 6V-PBPD02: (a) Under LA02; and (b) Under LA38 Ground Motions.

3.4 Proposed λ-Factor Method to Account for Pinched Hysteretic Behavior

It is expected that the response of a degrading Single Degree Of Freedom (SDOF) will be different from that of an equivalent Elastic-Plastic (EP) system under the same earthquake ground motion. The degrading behavior, although normally caused by the behavior of components, can be expected in the system behavior as well. The degrading behavior can be Strength Degradation (STRD), Stiffness Degradation (SD), or pinched hysteretic behavior.

CBFs show somewhat pinched hysteretic behavior under cyclic as well as dynamic loadings due to buckling of the bracing members. Since the original PBPD approach was developed for MFs, and the strength and stiffness of the braces in CBFs decrease under cyclic compression, using the same design base shear as MFs would not be appropriate. In the PBPD approach for CBF (Chapter 2) an energy modification factor, η, is used to account for pinched hysteretic behavior (Chao and Goel, 2006b and Goel and Chao, 2008), Equation (3.1).

$$\eta(E_e + E_p) = \frac{1}{2}\gamma M(\frac{T}{2\pi}S_a g)^2 \tag{3.1}$$

The solution of this equation leads to:

$$\frac{V}{W} = \frac{-\alpha + \sqrt{\alpha^2 + 4(\gamma/\eta)S_a^2}}{2} \tag{3.2}$$

By using the energy modification factor, η, the design base shear for the system with pinched hysteretic behavior is increased with respect to the one for EPP system to compensate for the pinching effect.

In this approach, the energy modification factor η remains independent of the fundamental period. Figure 3.9 shows the ratio of the PBPD design base shear for the pinched system to that of the benchmark EPP system for different values of η. As shown in this figure, using the same η values, increase in the EPP design base shear is almost the same for short and long periods. It can also be seen that by using $\eta = 0.5$, the design base shear for the pinched system is almost twice that of the EPP system.

On the other hand, several studies (e.g. Rahnama and Krawinkler, 1993, Gupta and Krawinkler, 1998, Gupta and Kunnath, 1998, Foutch and Shi, 1998, Medina and Krawinkler, 2004; Ruiz-Garcia and Miranda, 2005) have shown that, although pinching alone or in combination with stiffness degradation increases the peak displacement demands for short period SDOFs (periods less than 0.7 sec) but not for longer periods, as long as post-yield stiffness remains positive. It can be seen in Figure 3.10, taken from Ruiz-Garcia and Miranda (2005), that the mean displacement ratio of SD to EPP system is larger than 1.0 for short periods and can be taken practically equal to 1.0 for longer periods. The results in this figure are obtained for site Class D. Also, the ratio increases with increase in the *R* value. Larger *R* value corresponds to a weaker system. Therefore, the significance of the effect of pinching (SD and STRD) on the overall performance of structures varies with the period.

An alternative approach, called λ-factor method, to take this variation into account for design of SD and pinched systems by the PBPD approach is presented herein.

In this approach, the target ductility (corresponding to the target drift) is directly modified to account for the SD, pinching, or other degradation effects. An effective ductility for the degrading system can be obtained by dividing the actual target ductility by a factor called the λ-factor. The λ-factor in general can be considered as the average ratio of the peak displacement of a degrading system to that of an equivalent EPP system under the same earthquake ground motion. Therefore, $\lambda = (\mu_{pinched}/\mu_{EPP})$.

CBFs show somewhat moderate pinching behavior due to buckling of bracing members. λ-R-T curves (with constant R-values) can be obtained by applying suitable sets of ground motion to pinched systems with different periods and the corresponding equivalent EPP systems as benchmark.

The procedure to obtain λ-R-T curves is as follows:

- Select the period for pinched system, T. For this period to be achieved, mass can be taken equal to 1.0 and the stiffness k can be changed to get the desired T.
- Find the pseudo spectral acceleration at the selected period T for each ground motion in the set.
- Find maximum elastic base shear as $V_e = M \times S_a = 1.0 \times S_a = S_a$.
- Select the desired constant R value (e.g. $R=4$).
- Since the actual R value from dynamic analysis is $R = V_e/V_y$, in order to get constant R values under all ground motions in the set, either the V_y or the ground motion intensity should be adjusted. If V_y is taken as constant, then a

proper scale factor should be applied to each ground motion such that $V_e = M \times S_a = 1.0 \times S_a = S_a = R \times V_y$.

- Find $\lambda = (\Delta_{pinched}/\Delta_{EPP})$.
- With the same R value, select a new period and repeat the above steps to obtain λ values.
- When the λ-R-T curve for an R value is obtained, select a different R value and follow the above procedure.

Alternatively and pending further study to obtain λ-R-T curves for pinched systems representing CBFs, the C_2 factor introduced in FEMA 356 (FEMA, 2000a) for SD systems can be used as a preliminary approximation. The coefficient C_2 is the modification factor to represent the effect of pinching, SD, and STRD on the peak displacement response according to FEMA 356. In FEMA 356, values of C_2 depend on the structural framing system and the structural performance levels. Those values, taken from Table 3-3 in FEMA 356, are drawn in FEMA 440 (FEMA, 2005) and are shown in Figure 3.11.

These approximations for C_2 are obtained for systems with rather severe pinching behavior and also systems with STRD. For CBF which have moderate pinching behavior slightly different λ-factors based on C_2 values are suggested in this study, as shown in Figure 3.13.

The PBPD procedure to obtain the design base shear for such systems is as follows:

- *Estimate the fundamental period, T.*
- *Estimate the yield drift* θ_y .
- *Select the target drift* θ_u .
- *Find* $\mu_0=\theta_u/\theta_y$*, then calculate* R_{EPP} *from R-μ-T equation for EPP-SDOF (e.g. Newmark-Hall).*
- *Get* λ *from* λ*-R-T.*
- *Find the effective target ductility* $\mu_D= \mu_0/\lambda$.
- *Find R form R-μ-T equations for EPP-SDOF.*

After this step, the following steps are the same as presented in Chapter 3.

- *Calculate* γ *using Equation (3-7), as usual in PBPD.*
- *Find* α*, then calculate V/W (use* η *=1.0).*

With modifications for Y.D. and T.D. in CBFs, the above procedure will be used in the next section of this chapter to obtain PBPD design base shear for CBFs with different heights. These design base shears will be also compared to the values obtained by using IBC code (Figure 3.14). It can be seen from this figure that the PBPD design base shear is generally greater than the code value, especially for shorter periods. For longer periods (more than 0.7sec), the PBPD design base shear although still greater than the code value, but the difference is small.

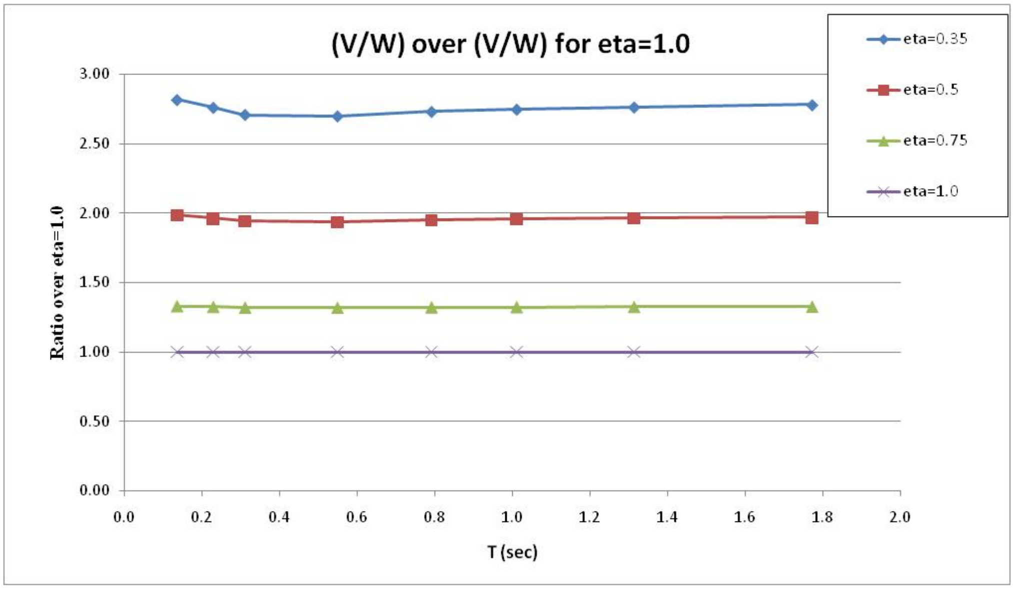

Figure 3.9. Ratio of the PBPD Calculated Design Base Shear for the Pinched System vs. The Benchmark EPP System.

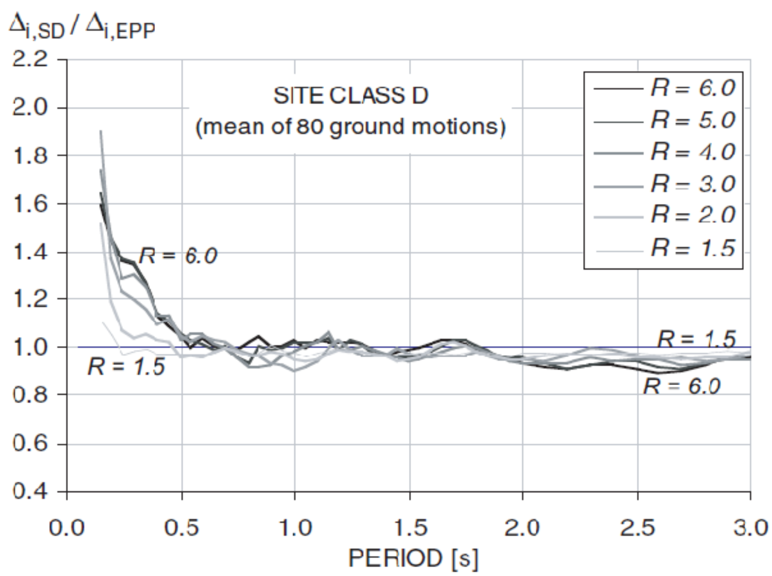

Figure 3.10. Mean Displacement Ratio of SD to EPP Models Computed with Ground Motions Recorded on Site Class D (from Ruiz-Garcia and Miranda, 2005).

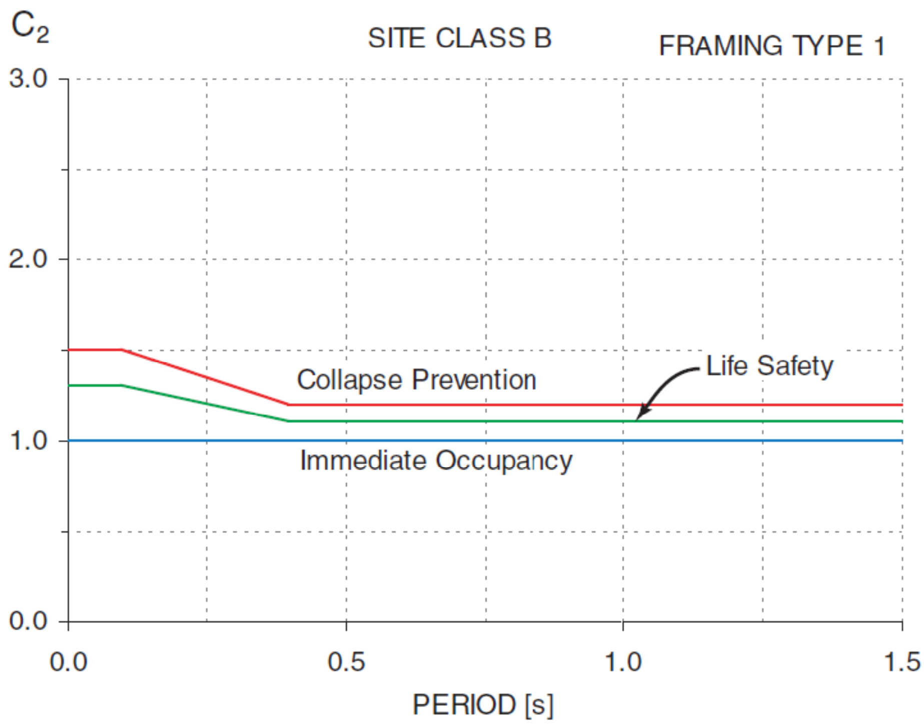

Figure 3.11. Variation of C_2 Factor According to FEMA440 (FEMA, 2005).

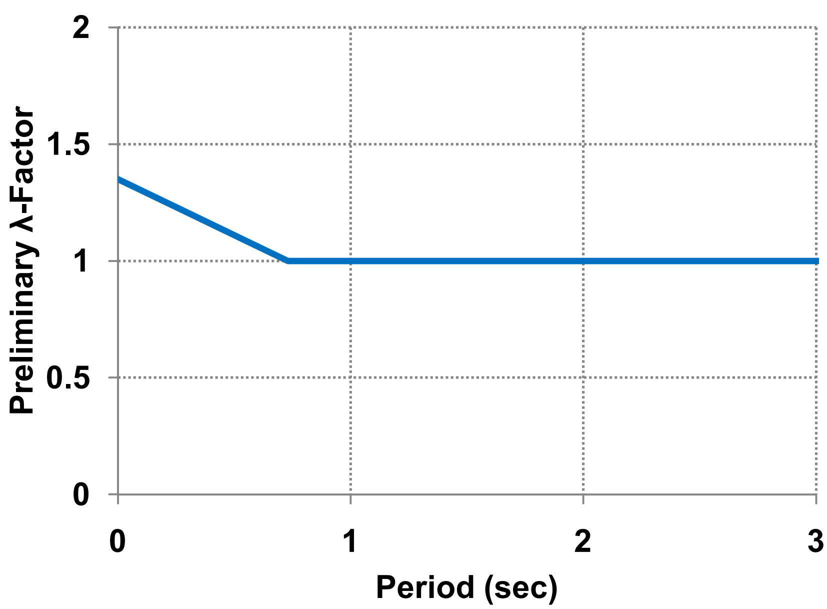

Figure 3.12. Preliminary Suggested λ-Factor Values for CBF (used in Chapter 3)

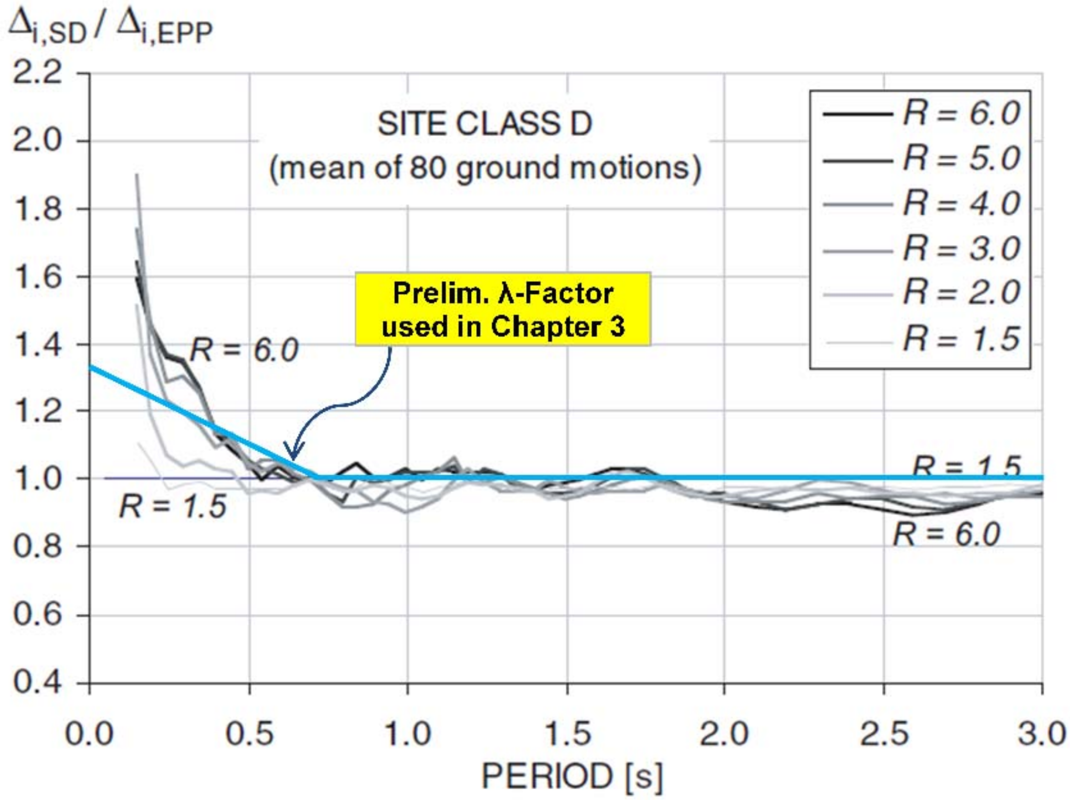

Figure 3.13. Suggested λ-factor values for CBF versus Mean Displacement Ratios obtained by Ruiz-Garcia and Miranda (2005)

Table 3.5. Preliminary λ-Factor Values as Function of T (used only in Chapter 3)

$0 \leq T \leq 0.73\,\text{sec}$	$T > 0.73\,\text{sec}$
$\lambda = -0.48T + 1.35$	$\lambda = 1.00$

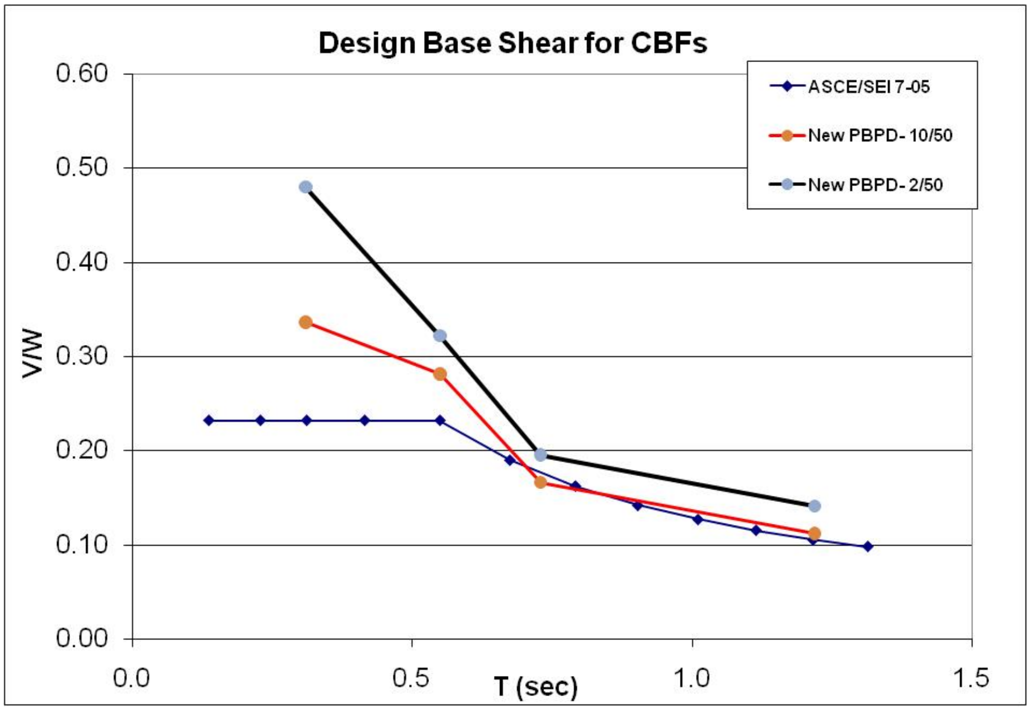

Figure 3.14. Comparison of Design Base Shear Using Different Methods.

3.5 Yield Drift

Yield drift is one of the main parameters used in the PBPD method for calculation of the design base shear, as discussed in Chapter 3. The system target ductility demand will change with the yield drift. Therefore, having a good estimation of the yield drift is required in order to find the appropriate design base shear for a system that can meet the desired performance objectives. In general, the yield drift for SDOFs is defined at the intersection point of the two lines of the equivalent bi-linear pushover (capacity) curve. This definition has also been used in the PBPD method.

In case the yield drift obtained from pushover analysis turns out different from the initially assumed value, iterations would be necessary until reasonable convergence on this parameter is achieved.

It should be noted that in the PBPD method, it would be unconservative if a smaller than the actual value for yield drift is used in design base shear calculation. That is because a smaller yield drift would give a larger ductility ratio and therefore a smaller design base shear. The actual value for the yield drift can be obtained from pushover analysis under the same lateral force distribution used in design.

It has been observed in several studies that regular Moment Frames (MFs) show practically constant yield drift of about 1.0% regardless of their height or bay width (Lee, 2002 and Goel and Chao, 2008). This is mainly due to the fact that in regular MFs, the contribution of stiffness of the beams is significantly larger than that of the columns, and also axial deformation of columns is negligible (Miranda and Akkar, 2006). On the other hand, it is known that the flexural type of deformation caused by axial deformation of columns in slender braced frames (i.e. CBFs, BRBFs, EBFs, and SPSWs) results in significant change in the yield drift. For instance, it has been observed from the results of the study by Richard (2009) that the yield drift for BRBFs, CBFs, and EBFs significantly increases with the increase in the height of the frame. The yield drift for the 3-story frame is about 0.3%, whereas the yield drift for the 9-story and 18-story frames are approximately 0.5% and 1.1%, respectively (Figure 3.15).

A building structure can be considered as a vertical cantilever beam which has shear as well as flexural modes of deformation. Therefore, the lateral deflection of frames can be obtained by adding the deformations from the shear and flexural modes together. In order to obtain the shear deformation, one can assume the columns to be axially rigid (Figure 3.16.a). Therefore, there would be no axial deformation for columns in this mode which basically means that there is no flexural lateral deformation. In the flexural mode of deformation, the braces are considered to be axially rigid. Columns are axially flexible so their length can change. In this mode, plane sections remain plane and perpendicular to the fictitious neutral axis (similar to the assumption in the beam theory). The flexural mode of deformation is illustrated in Figure 3.16.b. As can be seen, the braced frame in this mode is deflecting similar to a cantilever beam. In a frame with dominant mode of shear deformation, the drifts at different stories are almost equal, whereas the total story drifts increase from bottom to top in a frame with dominant flexural deformation mode.

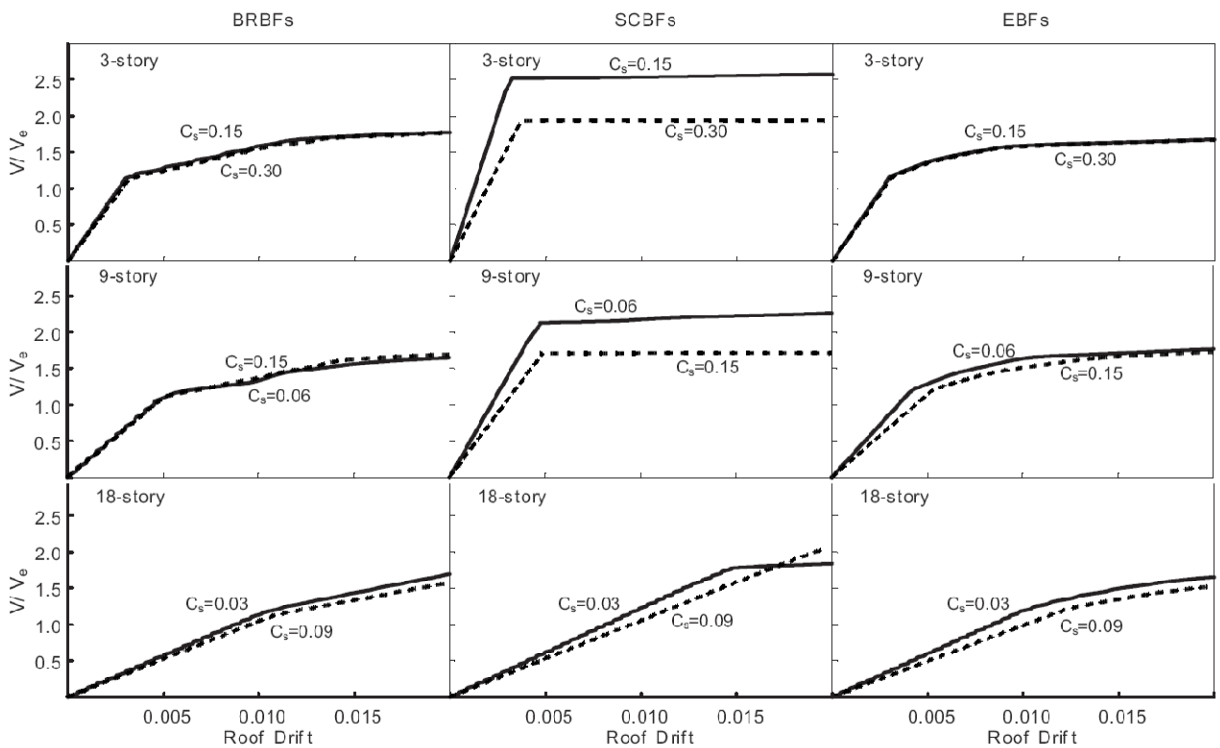

Figure 3.15. Pushover Analysis Results for different Braced Frames (from Richard, 2009).

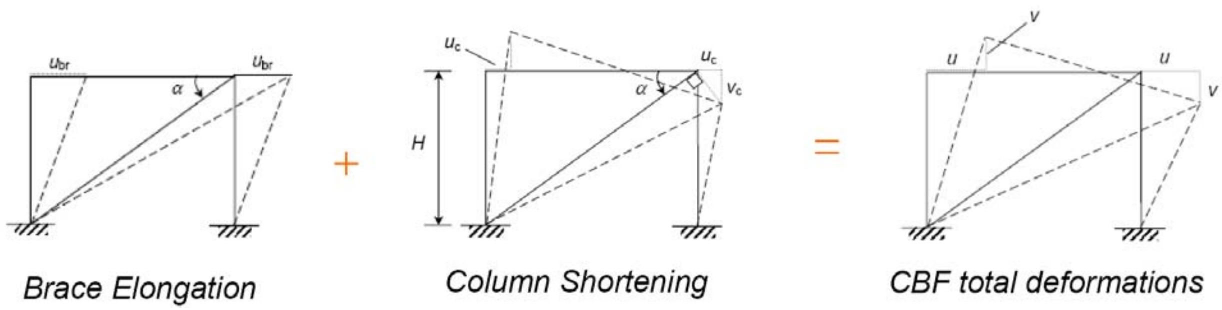

a) b) c)

Figure 3.16. Different Components of Lateral Drift in a Braced Frame: (a) Shear Mode of Deformation; (b) Flexural Mode of Deformation; and (c) Total Deformations (from Calvi, M.J.N. Priestley, 2006 (presentation)).

There are several reasons for the fact that in a typical MF, the deflection due to the flexural mode of deformation is negligible (unless we have only a one bay MF). First of all, in a MF the lateral loads are mainly resisted by bending action in beams and columns as opposed to the axial action in braced and columns of a braced frame. As a result, the axial forces in columns of a MF are relatively smaller than those in a braced frame and thus the change in the length of the columns due to lateral loads would be smaller. The other reason is that there are usually several bays in a typical MF system which carry the lateral loads. The axial forces in the interior columns due to lateral loads are very small (negligible) and therefore there is no axial deformation in these columns. Exterior columns may have significant axial forces, but due to the presence of several bays, the moment arm against the overturning moment is large resulting in much smaller axial forces compared to braced frames with single bay. Also, for the beam lines to rigidly rotate in order to produce flexural deformation, they have to overcome the axial stiffness of the interior columns.

On the other hand, in braced systems like CBFs, there is usually a single bay resisting the lateral loads. Therefore, both columns are exterior and both carry significant axial forces (tension and compression). The two column lines are acting as the flanges of a cantilever beam. Therefore, the beams can rotate due to shortening of columns on one side and elongation on the other side resulting in the so called flexural deformation.

Therefore, the story drift in CBFs (and other braced systems) can be obtained by adding the shear and flexural components (Englekirk, 1994, Bertero et al, 1991):

$$\Delta_{\substack{Story\\Drift}} = \Delta_{\substack{Flexural\\Deformation}} + \Delta_{\substack{Shear\\Deformation}} = \Delta_f + \Delta_s \qquad (3.3)$$

It should be noted that since the objective here is to find the yield drift of the system, the deformations at the yield state of the system are considered. For a CBF, the shear component of deformation comes from axial deformation of the braces, and the flexural component is caused by axial deformation of the columns (Figure 3.16). For a one-story one-bay CBF (Figure 3.17), the shear component of the yield drift can be obtained as:

$$\begin{aligned}\Delta_{y,s} &= \delta_y \big/ \cos\alpha = \delta_y \left(\frac{l_b}{L}\right) = \varepsilon_y l_b \left(\frac{l_b}{L}\right) = \varepsilon_y\, l_b^2 \big/ L \\ &= \varepsilon_y \big/ L \times \left((L)^2 + h^2\right)\end{aligned} \qquad (3.4)$$

since $L \times \tan\alpha = h$, then:

$$\begin{aligned}\Delta_{y,s} &= \varepsilon_y \big/ L \times (L)^2 \times (1 + \tan^2\alpha) \\ &= \varepsilon_y \times h \times (1 + \tan^2\alpha) / \tan\alpha\end{aligned} \qquad (3.5)$$

therefore the shear component of the yield drift can be obtained as:

$$YD_{shear} = \frac{2\varepsilon_y}{\sin 2\alpha} \qquad (3.6)$$

As can be seen from Equation (3.6), the yield drift due to shear deformations only depends on the yield strength of the braces and the geometry parameter α. For a regular

CBF, the angle α is almost the same in all stories. Hence, somewhat equal story drift due to shear at the yield state can be expected for different stories in a multistory CBF.

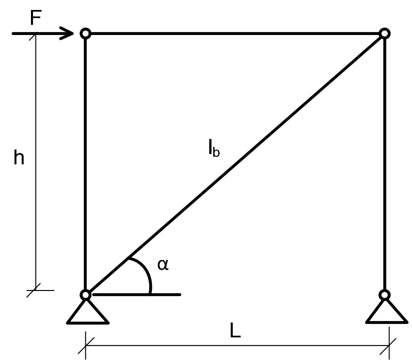

Figure 3.17. One-Story One-Bay CBF.

The flexural component of the story drift at yield state for the one-story one-bay CBF shown in Figure 3.17 can be obtained by considering the frame as a cantilever beam in which the two columns are acting as flanges in tension and compression. Then the flexural deformation of the frame can be obtained as follows:

$$\sigma = \frac{Mc}{I} \tag{3.7}$$

where σ is the average axial stress in columns due to the overturning moment, M, caused by the lateral loads. If the frame is assumed to behave like a beam, the moment of inertia, I can be estimated as:

$$I \simeq 2 \times A_c \times L^2 / 4 = \frac{A_c L^2}{2} \tag{3.8}$$

where A_c is the area of the column cross section and $c = L/2$. Therefore, the average strain in columns can be estimated as:

$$\varepsilon = \frac{\sigma}{E} = \frac{(Fh) \times L/2}{EA_c \times L^2/2} = \frac{Fh}{EA_c L} \tag{3.9}$$

where E is the modulus of elasticity. The vertical axial deformation of the columns can be obtained as:

$$\Delta_{vert} = \int_0^h \varepsilon dy = \frac{Fh^2}{EA_c L} \tag{3.10}$$

The horizontal drift due to this vertical deflection, which is basically the flexural component of the story drift, can be obtained as:

$$\Delta_{horiz} = \Delta_{vert} \times \frac{h}{L} = \frac{Fh^3}{A_c EL^2} \tag{3.11}$$

In order to obtain the horizontal deflection at any level in a multistory CBF due to flexural mode of deformation, the above approach can be followed. The vertical deflection can be calculated from Equation (3.12) by assuming an approximate constant average axial strain in columns, ε_{avg}. This axial strain should be only due to the lateral loads. Then, the horizontal deflections can be found by multiplying vertical deflections by h/L.

$$\Delta_{vert} = \int_0^h \varepsilon dy = \int_0^h \varepsilon_{avg} dy = \varepsilon_{avg} \times h \tag{3.12}$$

$$\Delta_{horiz} = \varepsilon_{avg} \times h \times \frac{h}{L} = \varepsilon_{avg} \times \frac{h^2}{L} \tag{3.13}$$

Thus, the flexural component of the yield drift can be estimated as:

$$YD_{flex} = \varepsilon_{avg} \times \frac{h}{L} \tag{3.14}$$

As can be seen from the above equation, the yield drift caused by flexural deformation depends on the height of the frame and also the bay width.

A reasonable estimate of the average axial strain in columns is needed for the yield drift calculation. First, it is assumed that about 20% of the axial capacity of columns is utilized by the gravity loads. Then, assuming that the column sections are the same for every three stories, axial force design ratios of 1.00, 0.75, and 0.50 can be assumed at mechanism for these columns. The bending moments in the columns are assumed to be negligible compared to the axial forces in these estimations. Since these design ratios are under combined gravity and lateral loading, the ratios utilized only by lateral loads are 0.80, 0.55, and 0.30. Hence, the average axial stress in these three columns due to the lateral loads would be *(0.80 + 0.55 + 0.30) / 3 = 0.53.* The column axial stress capacity can be estimated as:

$$\phi\sigma_{cr} \simeq (0.9)\times(0.85)\times\sigma_y \tag{3.15}$$

where the approximation $F_{cr} \approx 0.85\ \sigma_y$ has been used. Therefore, the following estimate can be obtained for average axial stress in the columns:

$$\sigma_{avg} \simeq (0.55)\times\phi\sigma_{cr} = (0.55)\times(0.9)\times(0.85)\sigma_y = 0.42\sigma_y \tag{3.16}$$

As a result, the following expressions can be derived for the yield drift due to flexural deformation:

$$\varepsilon_{avg} = 0.42\varepsilon_y \tag{3.17}$$

and

$$
\begin{aligned}
YD_{flex} &= \frac{\sigma_{avg}}{E} \times \frac{h}{L} = \frac{0.42\sigma_y}{E} \times \frac{h}{L} = \frac{0.42 \times 46}{29000} \times \frac{h}{L} \\
&= 0.000761 \times \frac{h}{L}
\end{aligned}
\tag{3.18}
$$

The yield stress of 46 ksi for HSS sections was used to obtain the numerical values in the above equation.

It should be noted that in Chevron braced frames the effective *h* can be considered from the base to the bottom of top story (i.e. very small contribution of column axial deformation from the top story). Table 3.6 shows the calculated yield drift values for four CBFs of different heights. The geometrical information for theses frames is shown in Figure 3.18. The 6-story frame is assumed to have plan and elevation properties similar to the 9-story one frame. The effective height, h_{eff}, which is basically the total height minus the height of top story, is used in yield drift calculation. As can be seen, the calculated yield drifts are quite close to the ones obtained from a pushover analysis of the final designs shown in Figure 3.15. These yield drifts will be used in the following sections to calculate the design base shear for example CBF frames.

Table 3.6. Yield Drift for CBFs.

CBF Frame	h_{eff} (ft)	L (ft)	α (deg)	Y.D.$_f$	Y.D.$_s$	Y.D.$_{total}$	Y.D. from pushover
3-Story (SAC)	25	30	40.9	0.055%	0.317%	0.37%	0.35-0.4%
6-Story (Guideline)	70	30	40.9	0.155%	0.317%	0.47%	0.48%
9-Story (SAC)	109	30	40.9	0.242%	0.317%	0.56%	0.5-0.6%
18-Story (SAC)	226	20	52.4	0.753%	0.328%	1.08%	1.1-1.4%

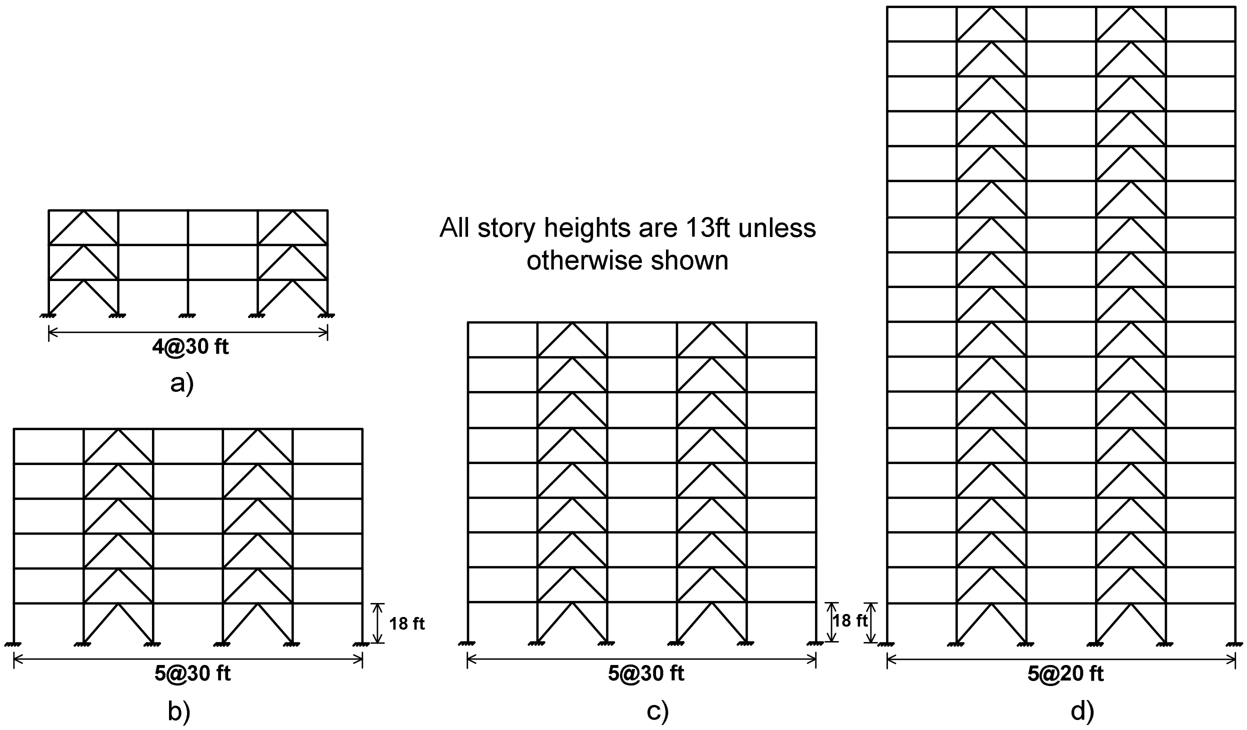

Figure 3.18. Elevation Views of CBF Buildings: (a) 3-Story; (b) 9-Story; and (c) 18-Story.

3.6 Selection of Proper Target Drift for CBFs

In MFs, the roof drift can be considered as a good representative of story drifts since the shear mode of deformation governs the behavior. However, in braced frames (e.g. CBFs), the roof drift may not be an accurate estimation of the story drifts (especially as the height increases) due to the presence of flexural deformations.

In the previously studied 3-story and 6-story CBFs (Sabelli, 2000; Chao and Goel, 2006b; Chao, Bayat, and Geol, 2008; and Goel and Chao, 2008), the flexural deformations caused by axial deformation of columns were rather small compared to the shear deformations. This is the main reason that although such flexural deformations were neglected in the PBPD design of 3-story and 6-story CBFs, the frames showed satisfactory performance under 2/3MCE and MCE ground motions. In those designs the Y.D. was assumed to be 0.3% and the T.D. was taken as 1.25%.

However, for taller CBFs, the flexural deformations become more significant and it would be unconservative to neglect their effect on the system Y.D. As explained in Section 3.5, the effect of flexural deformations on system Y.D. for CBFs increases with height. Such flexural deformations are also present in the T.D. A method is proposed in this section to find the proper T.D. for taller CBFs.

As was assumed in the yield drift derivation in the previous section, columns were considered to be axially rigid in order to obtain the shear deformations (Figure 3.16). On the other hand, braces should be considered axially rigid to obtain the flexural deformations (due to axial deformation of columns only).

Therefore, the length of the braces would remain unchanged while the flexural deformation takes place (i.e. no shear deformation). Hence, flexural deformations do not produce deformation (ductility) demand on braces.

This fact can be utilized in order to obtain the proper Target Drift (T.D.) for CBFs. For a given CBF the original T.D. of 1.25% (associated with shear deformation or deformation demand of braces) can be increased by the amount of the flexural component of the Y.D. The reason as mentioned above is that the flexural drift does not cause additional deformation demand on the braces.

For instance, the flexural component of Y.D. for the 18-story CBF is obtained to be 0.75% (Table 3.7). The adjusted T.D. for PBPD design of this frame would then be $T.D._{adj}$ =1.25% + 0.75% = 2.00%. This means that when the roof drift of the frame under lateral loading reaches 2.0%, the story drifts due to brace deformation are approximately 1.25%. In other words, roof drift of 2.0% is approximately equivalent to 1.25% story drift caused by brace deformation.

The inelastic drift θ_p represents the amount of inelastic deformation demand on braces. By using the adjusted target drift $T.D._{adj}$, as explained above in PBPD procedure, the inelastic deformation, θ_p, would remain unchanged. The reason is that $\theta_p = \theta_u - \theta_y = T.D._{adj} - Y.D.$, and since the $T.D._{adj}$ already includes the term $Y.D._{flex}$ in it, this term would be eliminated and the inelastic drift would become $\theta_p = 1.25\% - Y.D._{shear}$, which is basically a constant value for CBFs with different heights.

The value of 1.25% for T.D. was considered suitable for DBE (10%/50yrs) hazard level (Goel and Chao, 2008). Based on the results from pseudo dynamic tests on full scale CBFs at NCREE (http://w3.ncree.org/), a story drift of 1.75% can be assumed for the shear target drift under MCE (2%/50yrs) hazard level. The NCREE tests showed that fracture in braces can start when the story drifts are about 2% under cyclic loading. The 0.25% was kept as the margin of safety.

The above procedure was then utilized to obtain the required PBPD design base shears for four different CBFs (Table 3.7 and Table 3.8). These are the same frames as shown in Sec. 3.5 (Figure 3.18 and Table 3.6). Two different hazard levels are considered in these two tables to see which one would govern the design.

Table 3.7. PBPD Design Base Shear Under DBE (2/3MCE) Hazard Level.

CBF	***h (total)***	***h (eff)***	***L***	***α (deg)***	***$Y.D._f$ (%)***	***$Y.D._s$ (%)***	***$Y.D._{total}$ (%)***	***T.D.***	***$T.D._{total}$***	***λ***	***PBPD V/W***

	ft	***for Y.D.***	***ft***					***(10/50)***	***(10/50)***		
3-Story	39	26	30	40.9	0.06	0.32	0.37	1.25%	1.31%	1.2	**0.336**
6-Story	83	70	30	40.9	0.16	0.32	0.47	1.25%	1.41%	1.09	**0.281**
9-Story	122	109	30	40.9	0.24	0.32	0.56	1.25%	1.49%	1.0	**0.166**
18-Story	239	226	20	52.4	0.75	0.33	1.08	1.25%	2.00%	1.0	**0.111**

Table 3.8. PBPD Design Base Shear Under MCE Hazard Level.

CBF	***h (total)***	***h (eff)***	***L***	***α (deg)***	***Y.D.$_f$ (%)***	***Y.D.$_s$ (%)***	***Y.D.$_{total}$ (%)***	***T.D.***	***T.D.$_{total}$***	***λ***	***PBPD V/W***
	ft	***for Y.D.***	***ft***					***(2/50)***	***(2/50)***		
3-Story	39	26	30	40.9	0.06	0.32	0.37	1.75%	1.81%	1.2	**0.480**
6-Story	83	70	30	40.9	0.16	0.32	0.47	1.75%	1.91%	1.09	**0.322**
9-Story	122	109	30	40.9	0.24	0.32	0.56	1.75%	1.99%	1.0	**0.195**
18-Story	239	226	20	52.4	0.75	0.33	1.08	1.75%	2.50%	1.0	**0.141**

As can be seen from the design base shear values in these tables, the MCE hazard level base shear governs for all cases, and should therefore be used if a dual hazard level performance objective is expected.

In Figure 3.19, a comparison between the calculated PBPD design base shears and the ASCE 7-05 code (SEI, 2005) values is shown. As can be seen, the DBE base shears are larger than the code values for short period, but almost the same for longer periods. The MCE base shears are much larger than the code values for shorter periods and slightly larger for longer periods.

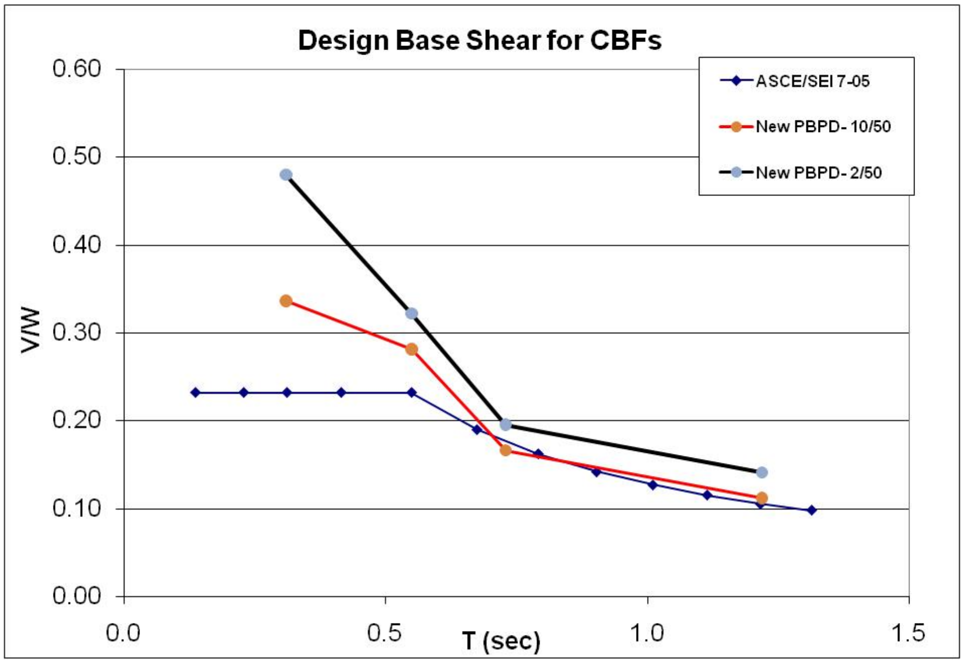

Figure 3.19. Comparing PBPD Design Base Shears with Current Code Values.

Table 3.9. Design Base Shear for CBFs Using Different PBPD Approaches.

CBF	New PBPD V/W (2/3 MCE)	New PBPD V/W (MCE)	Current PBPD (η=0.5) V/W (2/3 MCE)
3-Story	0.336	0.480	0.484
6-Story	0.281	0.322	0.338

It can also be seen from Table 3.9 that the V/W value for 3-story and 6-story CBFs obtained by the proposed PBPD approach in this Chapter are quite close to the values previously obtained by using η = 0.5 as the energy modification factor. Therefore, there was no need to redesign the 3-story and 6-story CBFs with the new design base shears, because the remaining steps of the PBPD procedure (after design base shear calculations) are essentially unchanged. This means that by using the proposed approach and including the MCE hazard level, the previous designs for 3-story and 6-story CBF can be used.

It should be noted that in the energy modification approach the design base shear values would be quite large and over-estimated if MCE hazard level was also included.

In the following sections, the proposed PBPD procedure for CBFs will be applied to the 9-story SAC building (Figure 3.18) as an example of a mid-rise CBF structure.

3.7 PBPD Design of a Mid-Rise CBF (9-Story SAC Building)

The merits of the proposed approach to obtain the design base shear in the PBPD method become more evident when the method is applied to mid-rise to tall CBFs. This is due to the fact that the significance of the flexural deformations increases with the increase in the height of the frame.

In this section, the proposed approach will be used to obtain the required design base shear for CBF as the lateral load resisting system in the 9-story SAC building. The building was originally designed with perimeter MFs as the lateral load resisting system. Instead of the original MFs, four CBFs are used in this design in each direction to resist the lateral loads.

It should be noted that the main difference between the proposed PBPD approach and the current one is in calculation of the design base shear. The other PBPD steps after the design base shear is determined are the same. Those design steps were explained in Chapter 4.

Plan view of the example 9-story structure is shown in Figure 3.20. The 9-story structure is 150 ft by 150 ft in plan, and 83 ft in height. The floor-to-floor heights are 18 ft for the first level and 13 ft for all the other levels. The bays are 30 ft on centers, in both directions, with five bays in each direction. The building's lateral force resisting system is comprised of two perimeter CBF bays in each direction. The interior frames of the structure consist of simple framing with composite floors. The details of the design weights of the building components can be found elsewhere (Sabelli, 2000).

As previously mentioned in Chapter 3, The calculation of the PBPD design base shear is also based on a lateral force distribution proposed by Chao, Goel, and Lee (2007), which can be expressed as $F_i = C'_{vi}V$, where:

$$C'_{vi} = (\beta_i - \beta_{i+1})\left(w_n h_n \Big/ \sum_{j=1}^{n} w_j h_j \right)^{kT^{-0.2}} \tag{3.19}$$

and

$$\beta_i = V_i / V_n = \left(\sum_{j=1}^{n} w_j h_j \Big/ w_n h_n \right)^{kT^{-0.2}} \tag{3.20}$$

In the above equations, β_i represents the shear distribution factor at level i; V_i and Vn, respectively, are the story shear forces at level i and at the top (nth) level; w_j is the seismic weight at level j; h_j is the height of level j from the base; F_i is the lateral force at level i; and V is the total design base shear. The value of factor k in the exponent term was taken equal to 0.75.

The initial PBPD design of the 9-story CBF is performed in Section 3.7.1 using k = 0.75 as the lateral load distribution parameter. The performance of this design is then evaluated and recommendations for performance improvement are suggested. In the subsequent section, k = 0.50 is used as the lateral load distribution parameter in order to provide more strength and stiffness in the upper stories. This change in the lateral load distribution appears to enhance the performance of the frame, especially in the upper stories.

3.7.1 PBPD Design of 9-Story CBF Using k = 0.75 as the Lateral Load Distribution Parameter

Design parameters according to 1997 *NEHRP Provisions* (FEMA, 1997) for the 9-story CBF are listed in Table 3.10. A basic target drift (shear target drift) of 1.25% for 10%/50 year (2/3MCE) hazard, and 1.75% for 2%/50 year (MCE) hazard is selected. The elastic design spectral response acceleration, S_a, is calculated as:

$$S_a = C_s \cdot \left(\frac{R}{I} \right) = 0.175 \cdot \left(\frac{6}{1} \right) = 1.05 \qquad (3.21)$$

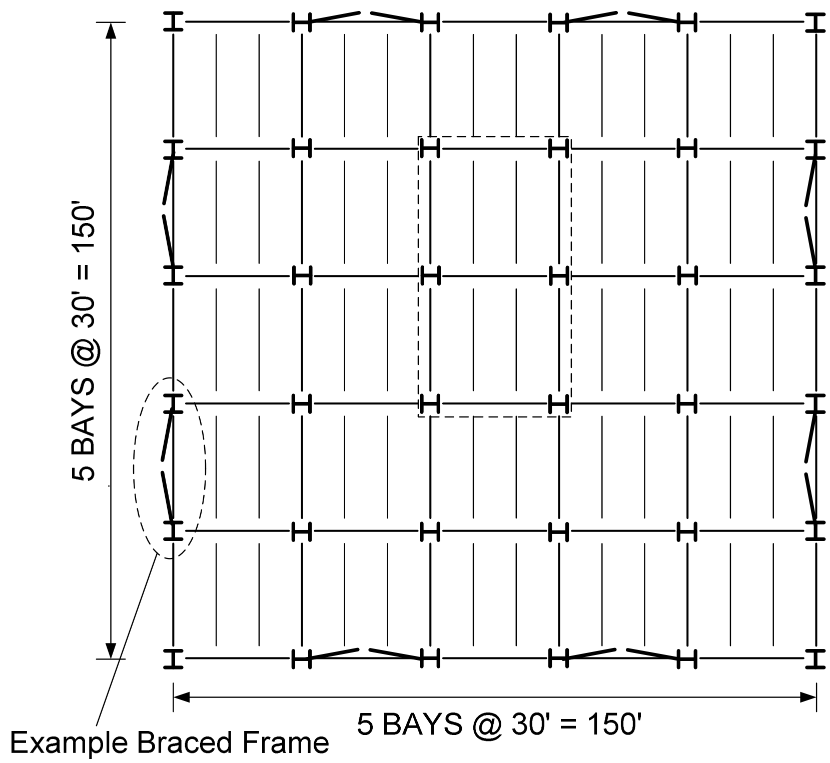

Figure 3.20. Plan View of 9-Story SAC Building.

Table 3.10. Design Parameters For the 9-Story CBF According to 1997 NEHRP.

Parameters	**9-story CBF**
MCE Short Period Spectral Response Acc., S_S	2.09 g
MCE One-Second Spectral Response Acc., S_1	1.155 g
Acceleration Site Coefficient, F_a	1.0
Velocity Site Coefficient, F_v	1.5
Short Period Design Spectral Response Acc., S_{DS}	1.393 g
One-Second Design Spectral Response Acc., S_{D1}	0.77 g
Site Class	D (Deep Stiff Soil)
Occupancy Importance Factor	$I = 1.0$
Seismic Design Category	D
Building Height	122 ft (above the base)
Approximate Building Period, T	0.734 sec.
Response Modification Factor	$R = 6$
Total Building Weight, W	19893 kips
Seismic Response Coefficient, $C_s = \frac{V}{W}$	0.175 g

The corresponding parameters are calculated and listed in Table 3.10 and Table 3.11. It can be seen that the MCE hazard level governs the design. The governing base shear is 3871 kips for the full structure (967.8 kips for one CBF). Design lateral force at each floor level is then calculated and given in Table 3.12.

Table 3.11. Design Parameters For the 9-Story CBF Based on PBPD Procedure ($k = 0.75$)

Parameters	**10% in 50 year Hazard**	**2% in 50 year Hazard**
S_a	1.049 g	1.574 g
T	0.734 sec.	0.734 sec.
k (Lat. Dist. Parameter)	0.75	0.75
Yield Drift, θ_y	0.56%	0.56%
$\theta_{y,flex}$	0.24%	0.24%
Basic Target Drift, θ_u	1.25%	1.75%
λ	1.0	1.0
Effective Target Drift, $\theta_{u,eff} = \theta_u + \theta_{y,flex}$	1.49%	1.99%
Inelastic Drift, $\theta_p = \theta_{u,eff} - \theta_y$	0.93%	1.43%
$\mu_s = \theta_{u,eff} / \theta_y$	2.66	3.55
R_μ	2.66	3.55
γ	0.610	0.484
α	3.88	3.96
η	1.0	1.0
V/W	0.166	0.195 (governs)
Design Base Shear V	3302 kips (for four CBFs)	3871 kips (for four CBFs)

Table 3.12. Lateral Force Distribution ($k = 0.75$).

Floor	F_i (kips)	F_i (kips)	Story Shear (kips)
	Full Structure	one CBF	one CBF
9	1093.7	273.9	273.9
8	677.8	169.4	443.4
7	544.9	136.2	579.6
6	443.8	111.5	691.1
5	362.2	90.5	781.6
4	287.2	71.8	853.4
3	217.5	54.4	907.8
2	151.3	37.8	943.6
1	88.7	22.2	967.8

The design of braces as the yielding members is performed based on the strength, fracture, and compactness criteria, as explained in Chapter 2. ASTM A500 Grade B tube sections (HSS) with 46 ksi nominal yield strength are used. The selected brace sections are built-up double tube sections and shown in Table 3.13. After design of braces, the non-yielding members, which are beams and columns, can be designed.

Table 3.13. Required Brace Strength and Selected Sections for 9-Story CBF ($k = 0.75$).

Floor	α	***Vi/0.9cos(α)*** **kips**	**Brace Section**	**Strength** $P_y+0.5P_{cr}$	**Area**	F_{cr}	$0.5P_{cr}$	P_y	N_f
9	41	403	**2HSS3-1/2×3-1/2×5/16**	415	7.04	23.88	91.1	323.8	241
8	41	653	**2HSS4-1/2×4-1/2×3/8**	683	10.96	32.68	179.1	504.2	157
7	41	853	**2HSS4-1/2×4-1/2×1/2**	861	13.9	31.89	221.6	639.4	329
6	41	1017	**2HSS5×5×1/2**	996	13.76	34.45	271.5	723.0	224
5	41	1151	**2HSS6×6×1/2**	1266	19.48	37.95	369.6	896.1	132
4	41	1256	**2HSS6×6×1/2**	1266	19.48	37.95	369.6	896.1	132
3	41	1336	**2HSS6×6×5/8**	1483	23.4	34.72	406.2	1076.4	245
2	41	1392	**2HSS6×6×5/8**	1483	23.4	34.72	406.2	1076.4	245
1	50	1673	**2HSS7×7×5/8**	1815	28	37.67	527.4	1288.0	156

Table 3.14. Design of Beams ($k = 0.75$).

Floor	w_u (k/ft)	R_yP_y	$0.5P_{cr}$	F_h	F_v	P_u	M_u	Beam Section
9	0.95	453.4	91.1	410.9	237.7	203.5	1872.4	W33x130
8	1.13	703.8	179.1	667.9	343.6	333.9	2698.6	W36x182
7	1.13	893.2	221.6	842.9	441.9	421.4	3420.9	W40x211
6	1.13	1014.9	271.5	970.9	487.8	483.4	3763.1	W40x235
5	1.13	1254.5	369.6	1223.8	580.5	612.9	4460.8	W40x278
4	1.13	1254.5	369.6	1223.8	580.5	612.9	4460.8	W40x278
3	1.13	1507.0	406.2	1443.9	722.1	721.9	5522.9	W40x397
2	1.13	1507.0	406.2	1443.9	722.1	721.9	5522.9	W40x397
1	1.21	1803.2	527.4	1498.1	977.3	749.0	7444.4	W40x431

Table 3.15. Design of Columns ($k = 0.75$).

Floor	$P_{trans.}$	P_{beam}	$0.5P_{cr}Sin\ \alpha$	$0.5F_v$	P_u	P_u (cumulative)	Column Section
9	32.88	28.5	0	119	180	180	W14x109
8	37.56	33.9	60	173	304	484	W14x109
7	37.56	33.9	117	221	410	894	W14x109
6	37.56	33.9	145	244	461	1355	W14x211
5	37.56	33.9	178	290	540	1895	W14x211
4	37.56	33.9	243	290	604	2499	W14x211
3	37.56	33.9	243	361	675	3174	W14x426
2	37.56	33.9	267	361	699	3873	W14x426
1	37.56	36.3	267	489	829	4702	W14x426

Generally, capacity design approach is used for design of non-yielding members, which are columns and beams in CBFs. For columns, the post-buckling limit state of the braces governs the design. Table 3.14 and Table 3.15 show the design parameters as well as the final design sections for beams and columns, respectively. Only cumulative axial forces are considered for design of columns. Column sections are changed after every three stories.

3.7.2 Evaluation of 9-Story CBF Designed by the Lateral Load Distribution Parameter k = 0.75

Nonlinear analyses were carried out by using the SNAP-2DX program, which has the ability to model brace behavior under large displacement reversals, as well as the fracture of braces with tubular sections (Rai et al., 1996). Gravity columns were included in the modeling by using a lumped continuous leaning column, connected to the braced frame through rigid pin-ended links. *P-Δ* effect due to the gravity loads was also accounted for in the analysis. All beams and columns of the frame were modeled as beam-column elements.

Maximum story drifts under 2/3MCE and MCE level SAC ground motions are shown in Figure 3.21. Under the design level (2/3MCE) ground motion, although some ground motions induce somewhat large drifts in middle stories, the response is generally good and the median response is within the target drift limit except for the top story. However, under MCE level ground motions, both middle stories and also upper stories show quite large story drifts. In addition, brace fractures at lower and middle stories were observed under a couple of MCE ground motions. Further investigation showed that the main reason for brace fractures were large story drifts.

Large story drifts (and subsequent brace fractures) in lower and middle stories under MCE ground motions are mainly due to large velocity pulses in these records. However, large story drifts at upper stories are mainly due to the effect of higher modes on dynamic response and somewhat low strength/stiffness of these stories.

In order to reduce the upper story drifts, a smaller k value can be used. By doing this, larger forces are assigned at the upper stories which eventually make them stronger and stiffer. It should be noted that there is significant change in the story shears at lower stories by using a different k value, since all the upper story forces are added to the lower stories' shear. Basically, by using $k = 0.5$, larger portion of the design base shear is assigned at upper stories.

A recommendation is made for improving the performance of this frame, which is by using $k = 0.50$ as the lateral load distribution parameters. Upper story drifts, as will be seen in the following section, can be significantly reduced by using the lower value of 0.5 for the lateral distribution parameter, k.

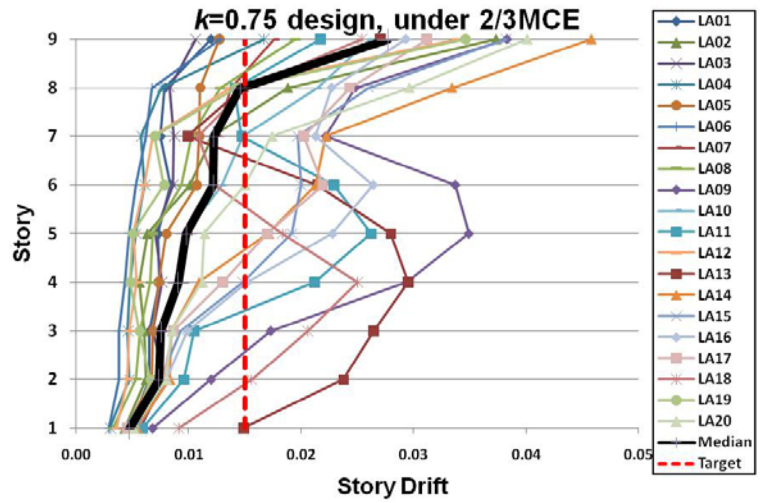

(a)

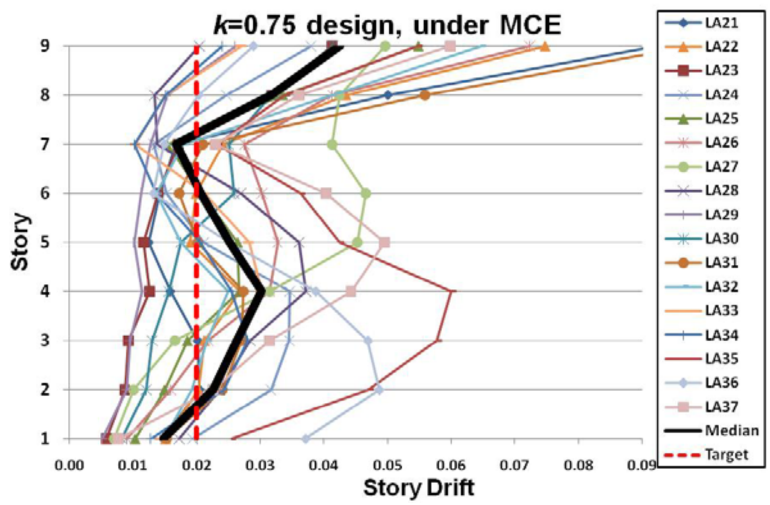

(b)

Figure 3.21. Story Drifts for 9V-PBPD Designed with k = 0.75 Under: (a) 2/3MCE; and (b) MCE Level SAC Ground Motions.

3.7.3 PBPD Design of 9-Story CBF Using k = 0.50 as the Lateral Load Distribution Parameter

The previous design steps are followed here as well except that $k = 0.50$ is used for the lateral force distribution. This is done to assign larger lateral forces at the upper levels in order to provide adequate strength and stiffness in those stories.

A preliminary study was done to compare the story shears obtained by using k = 0.75 and k = 0.50. The results are shown in Figure 3.22. As can be seen in part (a) of this figure, the story shears for k = 0.50 are larger in upper stories and somewhat smaller (less than 10%) in the lower stories. Figure 3.22.b compares the story shears better by showing the ratio of the story shears obtained with k = 0.50 to those with k = 0.75. As can be seen, with k = 0.50, the story shears in the top two stories are significantly greater than those with k = 0.75. In lower stories, the shears obtained by using k = 0.50 are slightly smaller (less than 10%) than the ones with k = 0.75. From the results shown in Figure 3.22, it is expected that the 9-story CBF designed by using k = 0.50 show smaller drifts at upper levels.

The 9-story frame was then redesigned by using k = 0.50 for the lateral distribution parameter. The design parameters for base shear calculations are shown in Table 3.16. The MCE hazard level governs the design with $V/W = 0.180$. The frame showed dynamic instability (due to P-Delta effect) under a few SAC LA MCE ground motions. Therefore, it was decided to include P-Delta forces in the design of yielding members (braces).

These P-Delta forces can be estimated as horizontal forces in the fictitious rigid links connecting main frame to the lumped gravity column, assuming a linear deflected shape at the target drift of 1.99%. These forces are shown in Table 3.17, along with the original lateral forces without the P-Delta forces. By adding these P-Delta forces, total design base shear was increased to *0.206V/W*. This value is closer to the *0.195V/W* obtained for design with $k = 0.75$. Therefore, a better and fair performance comparison can be made between the two frames.

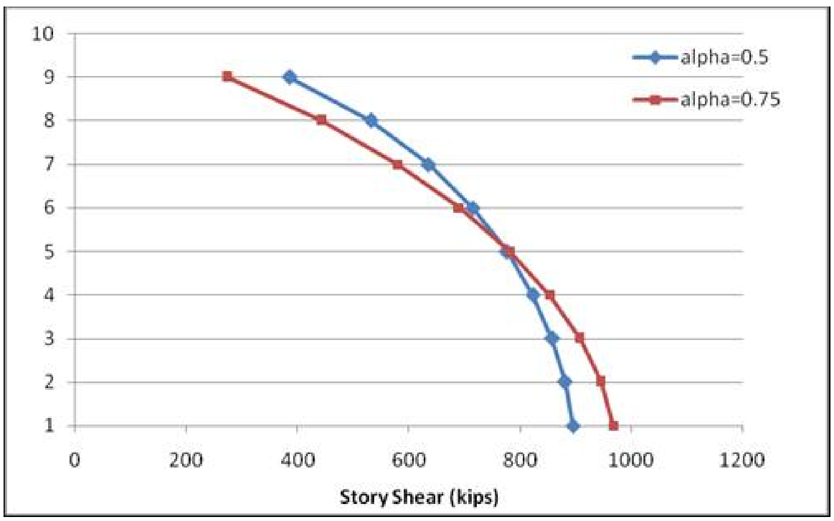

(a)

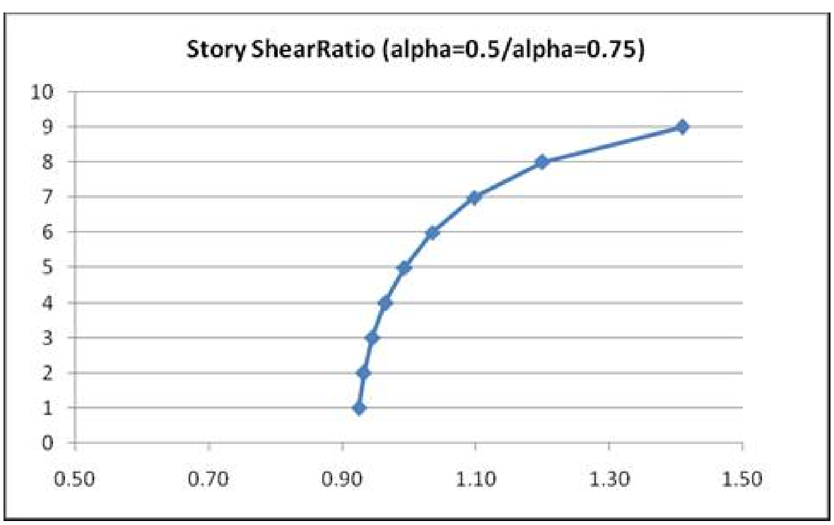

(b)

Figure 3.22. Comparison of the Story Shears with k = 0.50 and k = 0.75.

The final sections for braces, beams and column are shown in Table 3.18, Table 3.19, and Table 3.20, respectively. As can be seen, the sizes of upper story braces were increased compared to the design with k = 0.75, but brace sizes for lower stories are the about the same. It should also be noted that the weight of the frame with k = *0.5* (designated as 9V-PBPD-A henceforth) is about 10% more than the frame with k = 0.75, which is mostly due to increase in the brace sizes and the supporting non-yielding members in the upper stories. However, this is only the comparison between the weights of seismic frames, not the entire structure including gravity frames.

As will be seen later in Chapter 5, P-Delta effects can be indirectly compensated for by modification of the λ-factor. Using the modified λ-factor in Chapter 5, the structure will have adequate design base shear from the beginning without the need to add approximate P-Delta forces as done herein.

Table 3.16. Design Parameters For the 9-Story CBF Based on PBPD Procedure (k = *0.50*): 9V-PBPD-A

Parameters	**10% in 50 year Hazard**	**2% in 50 year Hazard**
S_a	1.049 g	1.574 g
T	0.734 sec.	0.734 sec.
k (Lat. Dist. Parameter)	0.50	0.50
Yield Drift, θ_y	0.56%	0.56%
$\theta_{y,flex}$	0.24%	0.24%
Basic Target Drift, θ_u	1.25%	1.75%
λ	1.0	1.0
Effective Target Drift, $\theta_{u,eff} = \theta_u + \theta_{y,flex}$	1.49%	1.99%

Inelastic Drift, $\theta_p = \theta_{u,eff} - \theta_y$	0.93%	1.43%
$\mu_s = \theta_{u,eff} / \theta_y$	2.66	3.55
R_μ	2.66	3.55
γ	0.610	0.484
α	4.209	6.472
η	1.0	1.0
V/W	0.154	0.180 (governs)
Design Base Shear V	3063 kips (for four CBFs)	3581 kips (for four CBFs)

Table 3.17. Lateral Force Distribution ($k = 0.50$) : 9V-PBPD-A

Floor	**F_i (kips)**	**F_i (kips)**	**Story Shear (kips)**	**P-Delta Lateral Forces (kips)**	**Story Shear- w/ P-Delta (kips)**
	Full Structure	**one CBF**	**one CBF**	**at T.D.= 1.99%**	**one CBF**
9	1543.8	386.0	386.0	15.0	400.9
8	584.4	146.1	532.1	14.9	561.9
7	416.2	104.1	636.1	14.9	680.8
6	316.5	79.1	715.3	14.9	774.8
5	244.7	61.2	776.5	14.9	850.8
4	187.4	46.8	823.3	14.9	912.5
3	138.5	34.6	857.9	14.9	962.0
2	94.7	23.7	881.6	14.9	1000.5
1	54.9	13.7	895.3	15.0	1029.2

Table 3.18. Required Brace Strength and Selected Sections for 9-Story CBF ($k = 0.50$) : 9V-PBPD-A

Floor	**α**	***Vi/0.9cos(α)* kips**	**Brace Section**	**Strength P_y+0.5P_{cr}**	**Area**	**F_{cr}**	**0.5P_{cr}**	**P_y**	**N_f**
9	41	400.9	**2HSS4-1/2×4-1/2×3/8**	683	10.96	32.68	179.1	504.2	157
8	41	561.9	**2HSS4-1/2×4-1/2×1/2**	861	13.9	31.89	221.6	639.4	329
7	41	680.8	**2HSS5×5×1/2**	996	13.76	34.45	271.5	723.0	224
6	41	774.8	**2HSS6×6×1/2**	1266	19.48	37.95	369.6	896.1	132
5	41	850.8	**2HSS6×6×1/2**	1266	19.48	37.95	369.6	896.1	132
4	41	912.5	**2HSS6×6×5/8**	1483	23.4	34.72	406.2	1076.4	245

3	41	962.0	**2HSS6×6×5/8**	1483	23.4	34.72	406.2	1076.4	245
2	41	1000.5	**2HSS6×6×5/8**	1483	23.4	34.72	406.2	1076.4	245
1	50	1029.2	**2HSS7×7×5/8**	1815	28	37.67	527.4	1288.0	156

Table 3.19. Design of Beams (k = 0.50): 9V-PBPD-A

Floor	w_u (k/ft)	R_yP_y	$0.5P_{cr}$	F_h	F_v	P_u	M_u	Beam Section
9	0.95	703.8	179.1	667.9	343.6	333.9	2681.6	**W36x182**
8	1.13	893.2	221.6	842.9	441.9	421.4	3420.9	**W40x211**
7	1.13	1014.9	271.5	970.9	487.8	483.4	3763.1	**W40x235**
6	1.13	1254.5	369.6	1223.8	580.5	612.9	4460.8	**W40x278**
5	1.13	1254.5	369.6	1223.8	580.5	612.9	4460.8	**W40x278**
4	1.13	1507.0	406.2	1443.9	722.1	721.9	5522.9	**W40x397**
3	1.13	1507.0	406.2	1443.9	722.1	721.9	5522.9	**W40x397**
2	1.13	1507.0	406.2	1443.9	722.1	721.9	5522.9	**W40x397**
1	1.21	1803.2	527.4	1498.1	977.3	749.0	7444.4	**W40x431**

Table 3.20. Design of Columns (k = 0.50): 9V-PBPD-A

Floor	$P_{trans.}$	P_{beam}	$0.5P_{cr}Sin\ \alpha$	$0.5F_v$	P_u	P_u *(cumulative)*	Column Section
9	32.88	28.5	0	173	234	234	**W14x109**
8	37.56	33.9	117	221	410	644	**W14x109**
7	37.56	33.9	145	244	461	1105	**W14x109**
6	37.56	33.9	178	290	540	1645	**W14x257**
5	37.56	33.9	243	290	604	2249	**W14x257**
4	37.56	33.9	243	361	675	2924	**W14x257**
3	37.56	33.9	267	361	699	3623	**W14x455**
2	37.56	33.9	267	361	699	4322	**W14x455**
1	37.56	36.3	267	489	829	5151	**W14x455**

3.7.4 Evaluation of 9-Story CBF Designed By the Lateral Load Distribution Parameter k = 0.50

As was done before for 3-story and 6-story frames earlier in this chapter, nonlinear analyses were carried out by using the SNAP-2DX program. The same modeling techniques were used. The results for maximum story drifts under 2/3MCE and MCE level SAC ground motions are shown in Figure 3.23.

It can be seen that by using k = 0.50, the upper story drifts become quite smaller compared to the case of k = 0.75. In addition, the story drift profile matches much better with the target drift limit in the case of k = 0.50 and also tends to be more uniform along the height.

Under the design level (2/3MCE) ground motions, the response is generally good and the median response is well within the target drift limit. This is consistent with the fact that the MCE level governed the design, therefore it is expected that the story drifts under MCE level ground motions are closer to the drift limit. Under a couple of MCE ground motions, lower stories show large drifts. In addition, brace fracture at lower and middle stories occurred under a couple of MCE ground motions.

Figure 3.24 show comparison between story drift response under different ground motions for the two designs; one with k = 0.75 and the other with k = 0.50. Also, the median story drifts under the two sets of SAC LA ground motions (2/3MCE and MCE) for the two designs are shown in Figure 3.25. From these figures, it is evident that by using k = 0.50 much smaller story drifts in the upper stories and more uniform story drift profile can be expected.

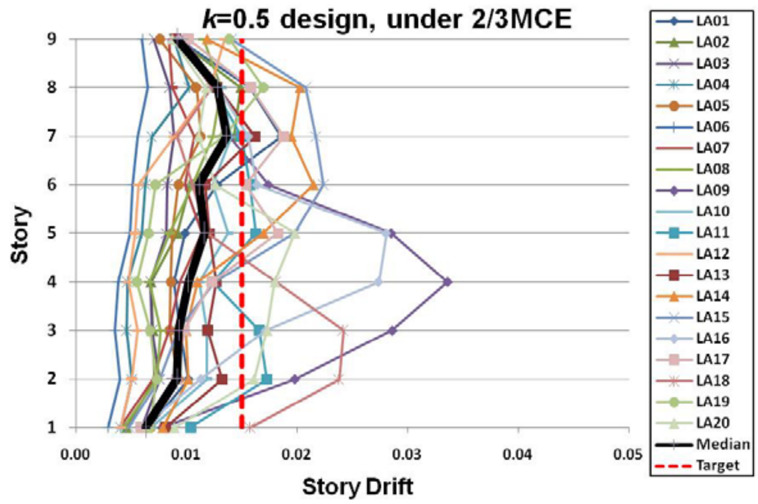

(a)

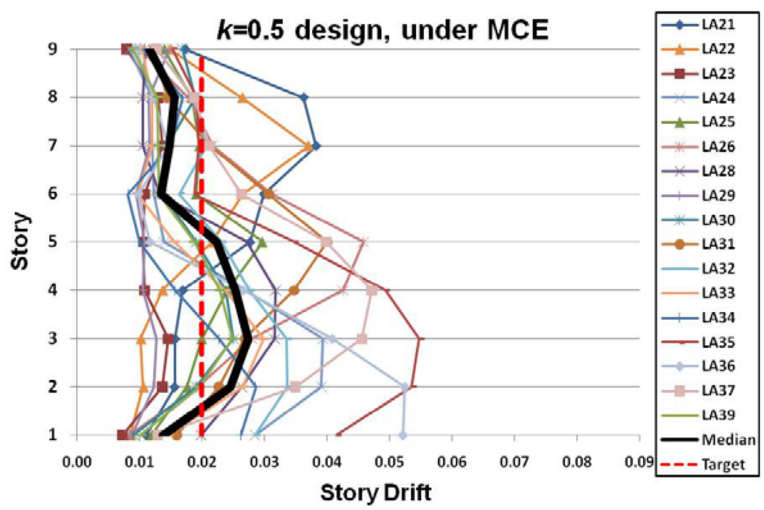

(b)

Figure 3.23. Story Drifts for 9V-PBPD-A Designed with k = 0.50 under: (a) 2/3MCE; and (b) MCE Level SAC Ground Motions.

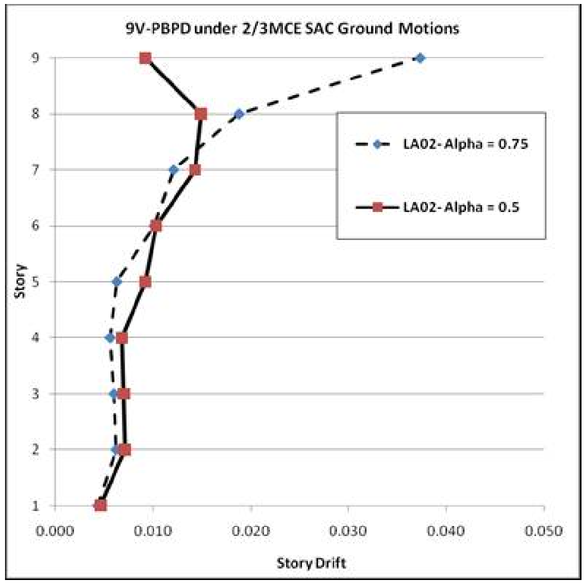

9V-PBPD under 2/3MCE SAC Ground Motions
LA02- Alpha = 0.75
LA02- Alpha = 0.5
Story
Story Drift
0.000
0.010
0.020
0.030
0.040
0.050
1
2
3
4
5
6
7
8
9

(a)

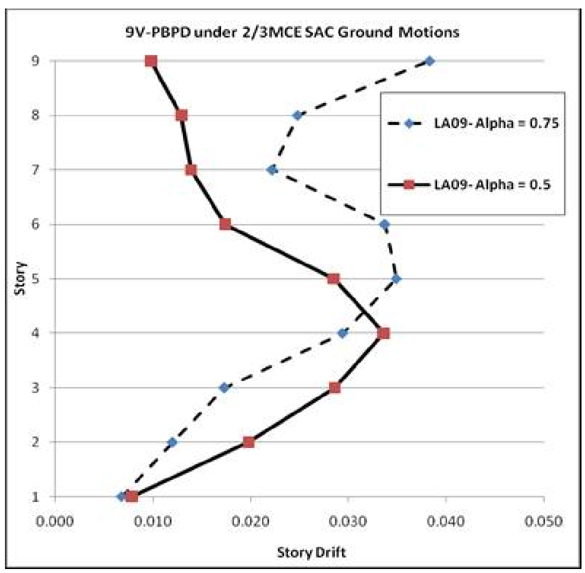

9V-PBPD under 2/3MCE SAC Ground Motions
LA09- Alpha = 0.75
LA09- Alpha = 0.5
Story
Story Drift
0.000
0.010
0.020
0.030
0.040
0.050
1
2
3
4
5
6
7
8
9

(b)

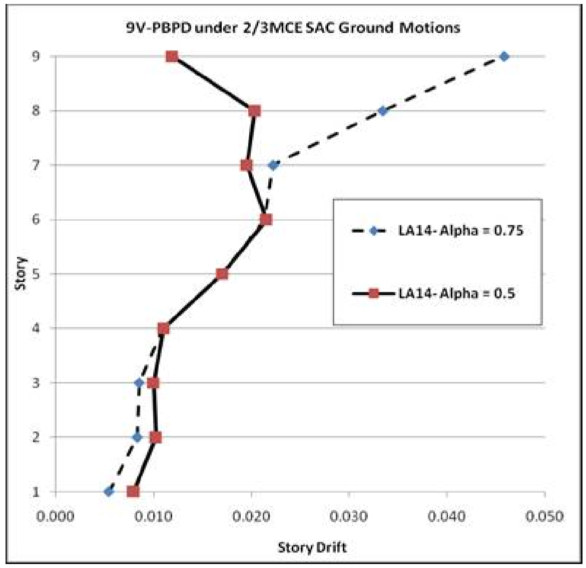

(c)

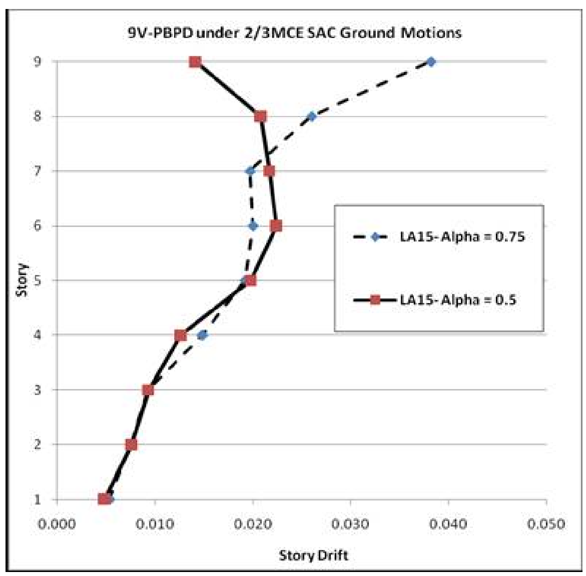

(d)

Figure 3.24. Comparison of the Story Drift Profile for Design with $k = 0.50$ vs. $k = 0.75$ Under: (a) LA02; (b) LA09; (c) LA14; and (d) LA15 Ground Motions.

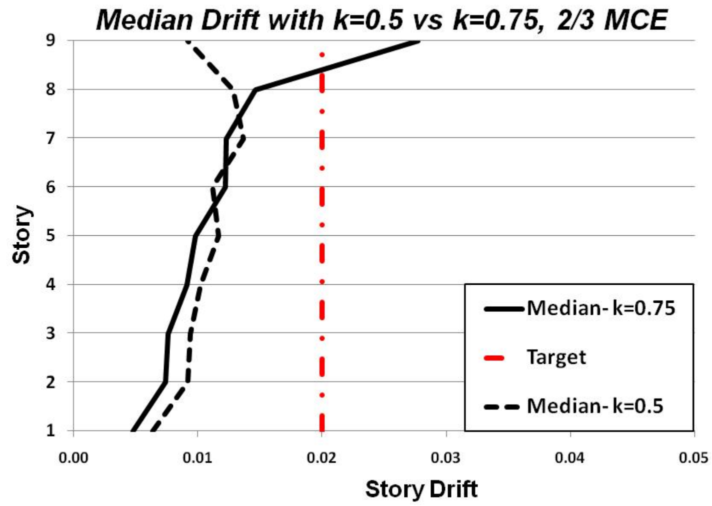

(a)

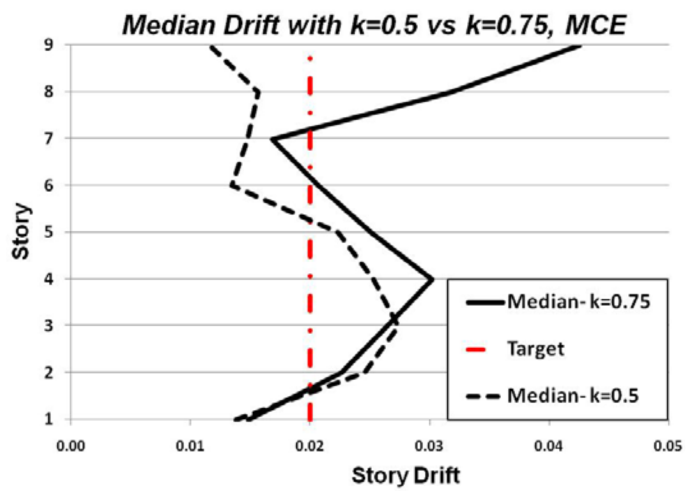

(b)

Figure 3.25. Comparison of the Median Story Drifts for 9-Story CBF under SAC LA Ground Motions; (a) Under 2/3 MCE; and (b) Under MCE Hazard Level.

3.8 Performance Comparison Between Beam Shear Splice vs. Conventional Connection

As was discussed in Section 2.2 (Chapter 2), beam shear splices are recommended for CBF in order to minimize moment transfer into the columns (Figure 2.6). For analysis purposes such shear splices can be modeled as pin connections at the beam ends. On the other hand, the conventional gusset plate detail provides considerable flexural constraint in the beam-to-column connection region. Therefore, the conventional beam-to-column connections need to be treated as rigid connections with moment transfer capability.

In this section, the effect of recommended beam shear splice detail, i.e., moment release, on the seismic performance of the 9V-PBP-A frame is studied. Two models of the 9V-PBPD-A frame are considered. One, which is the original model, has beam shear splices at the ends of the beams (9V-PBPD-A-Pin), while the other model has the usual gusset plate connection (9V-PBPD-A-Rigid). Hence, the only difference between these two frames is their beam-to-column connection detail. The two models were subjected to the DBE and MCE SAC ground motion records.

Figures 3.28 and 3.29 show the analysis results of these two frames under the LA01 record which is a DBE ground motion. No brace fractures were observed and the maximum story drifts are quite similar. However, several plastic hinges formed in the columns of the frame with rigid connections (9V-PBPD-A-Rigid). Column plastic hinges (PH) rotations are more significant in 5th, 6th , and 7th stories as shown in Figure 3.29a. Formation of the column plastic hinges is due to large moments transferred from beam to columns when conventional gusset plate connections are used (Refer to Figure 2.5).

Figures 3.30, 3.31, and 3.32 show the results of dynamic analysis of the two frames under LA21 (MCE) ground motion. As can be seen in Figure 3.30, significant column plastic hinging occurred as the largest pulse of the LA21 ground motion hit the 9V-PBPD03-Rigid frame. The column plastic hinge rotations are most significant in stories 5 to 8. In addition, several brace fractures occurred in the 9V-PBPD-A-Rigid frame. On the other hand, very little column plastic hinge formation can be seen in 9V-PBPD-A-Pin frame. Also, one brace fractured, albeit near the end of the ground motion (Figure 3.30a). It should be noted that the residual drifts are also larger for 9V-PBPD-A-Rigid frame as shown in Figure 3.32.

The performance under another MCE level ground motion record, LA36, is shown in Figures 3.33 and 3.34. As was the case for other ground motions, significant column plastic hinging and larger residual story drifts can be observed for the 9V-PBPD-A-Rigid frame. The plastic hinge rotations of columns are quite large in the first two stories and also some beam plastic hinges can be seen, Figure 3.34a.

It is worth mentioning that although the maximum 2nd story drifts under LA36 are about the same for both frame models, i.e., 5.25% for Pin model and 4.85% for Rigid model (Figure 3.33b), the 9V-PBPD-A-Pin frame was able to accommodate such deformation without formation of column plastic hinges. But, such deformation caused undesirable plastic hinges in the columns of 9V-PBPD-A-Rigid frame. This shows that the frame with pin connections has more deformation capacity or ductility.

It should be noted that although the story drifts were much larger in the case of LA36 compared to LA21, no brace fracture was seen under LA36 for either frame. This can be attributed to shorter duration of the LA36 ground motion (see Table 3.17), which resulted in less low-cycle fatigue in the braces.

Figures 3.35 to 3.37 show the story drifts under the two sets of DBE and MCE level SAC LA ground motions. The median drifts are shown in Figure 3.37. As can be seen, the median drifts under DBE ground motions (LA01-LA20) are quite close for the two frames. Under MCE ground motions (LA21-LA40) the 9V-PBPD-A-Pin frame shows larger story drifts in the lower stories except for the 1st story. Although the median drifts are somewhat larger for the Pin model, there is much less plastic hinging in the columns, which again indicates larger deformation capacity and hence larger ductility of the 9V-PBPD-A-Pin frame.

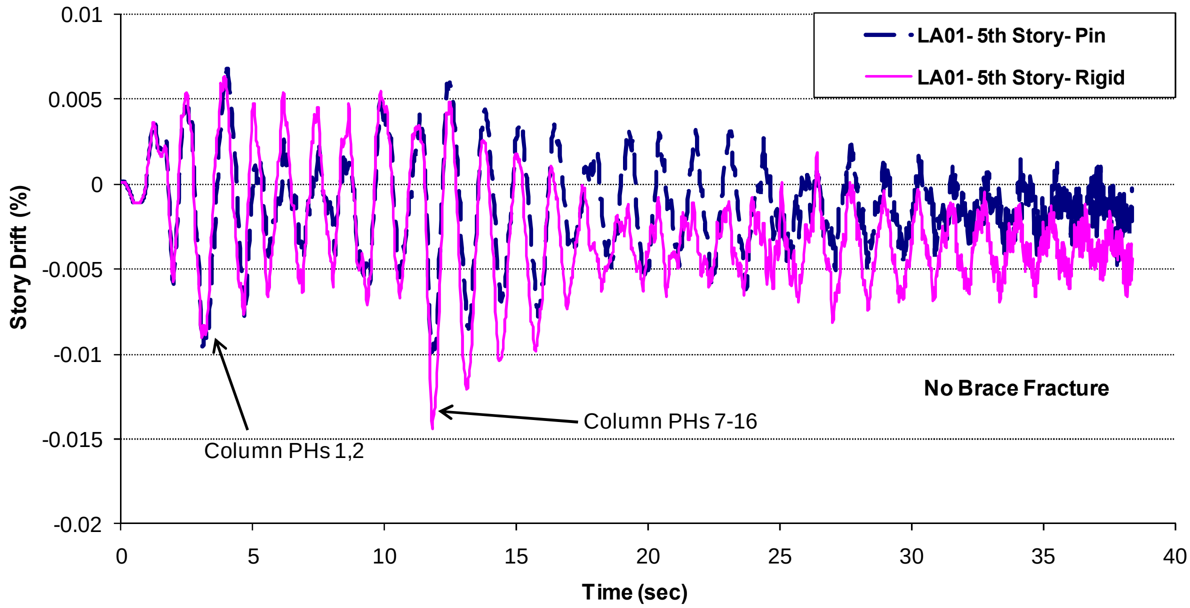
LA01- 5th Story- Pin
LA01- 5th Story- Rigid
Story Drift (%)
0.01
0.005
0
-0.005
-0.01
-0.015
-0.02
No Brace Fracture
Column PHs 7-16
Column PHs 1,2
0
5
10
15
20
25
30
35
40
Time (sec)

(a)

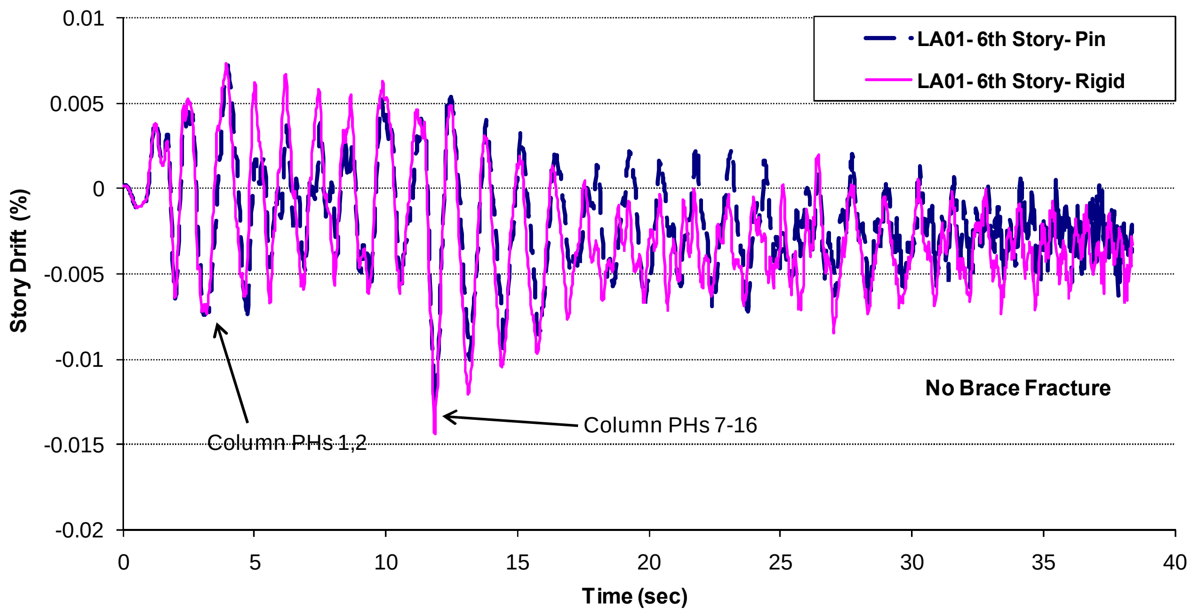
LA01- 6th Story- Pin
LA01- 6th Story- Rigid
Story Drift (%)
0.01
0.005
0
-0.005
-0.01
-0.015
-0.02
No Brace Fracture
Column PHs 7-16
Column PHs 1,2
0
5
10
15
20
25
30
35
40
Time (sec)

(b)

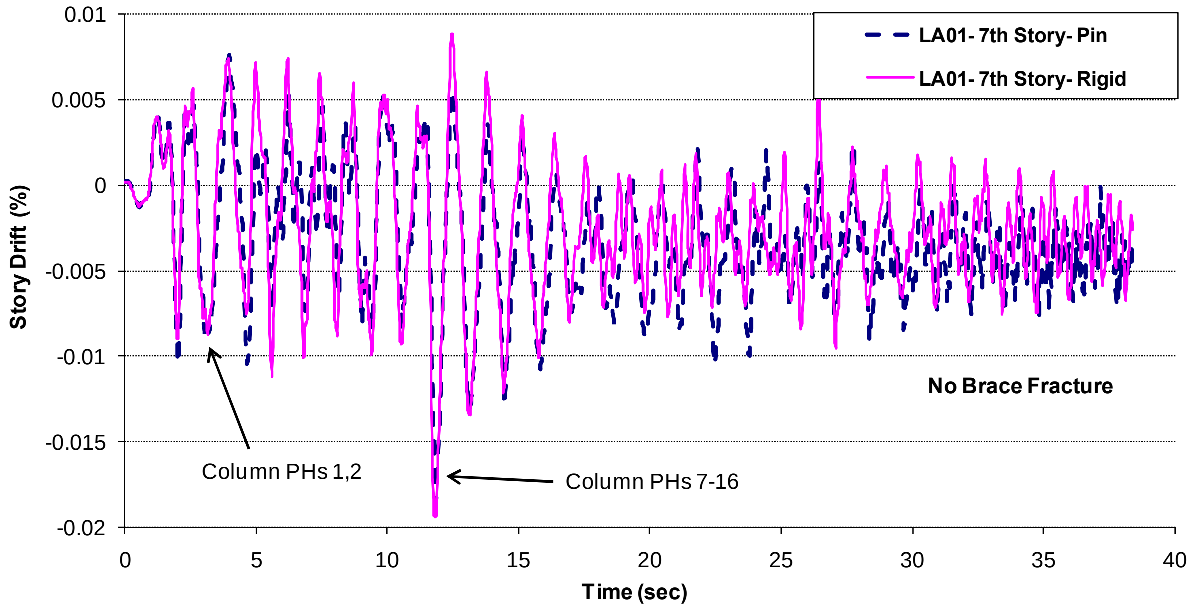

(c)

Figure 3.28. Story Drift vs. Time under LA01 for 9V-PBPD-A-Pin and 9V-PBPD-A-Rigid

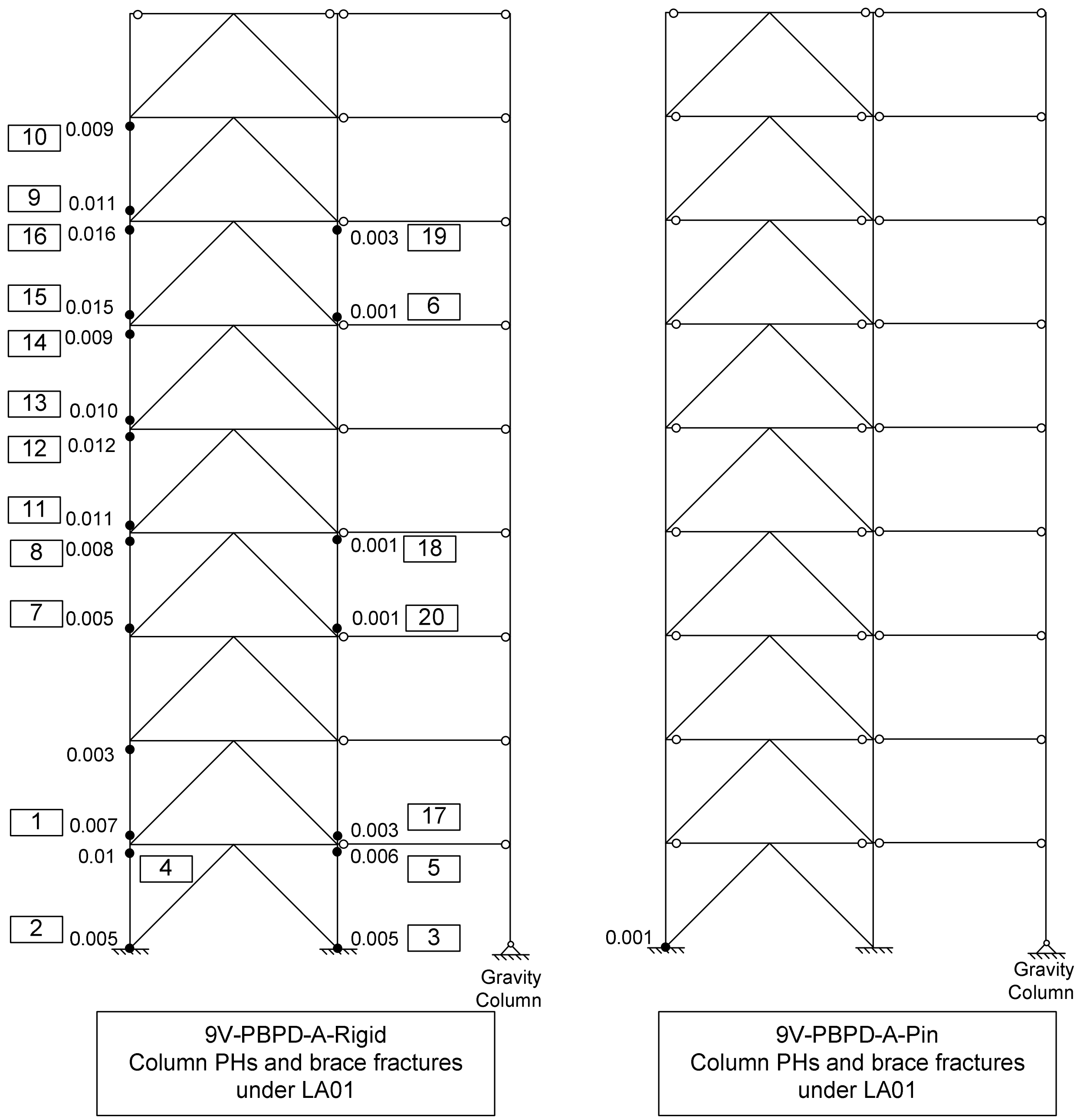

(a) (b)

Figure 3.29. Column PHs and No Brace Fractures under LA01 for: (a) 9V-PBPD-A-Pin; and (b) 9V-PBPD-A-Rigid Frames

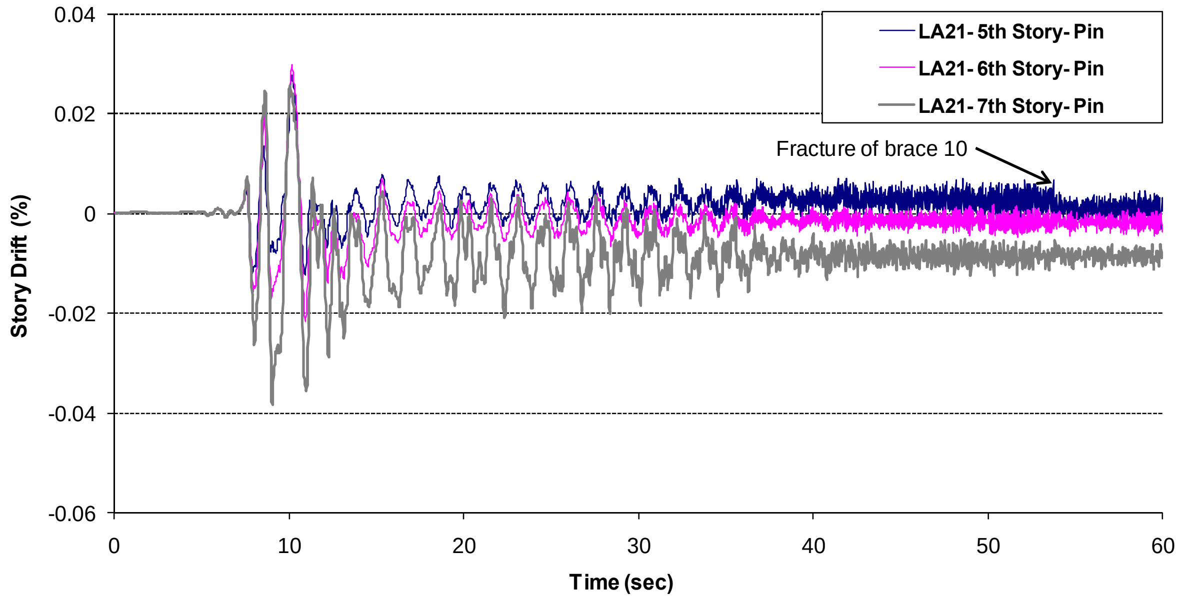

(a)

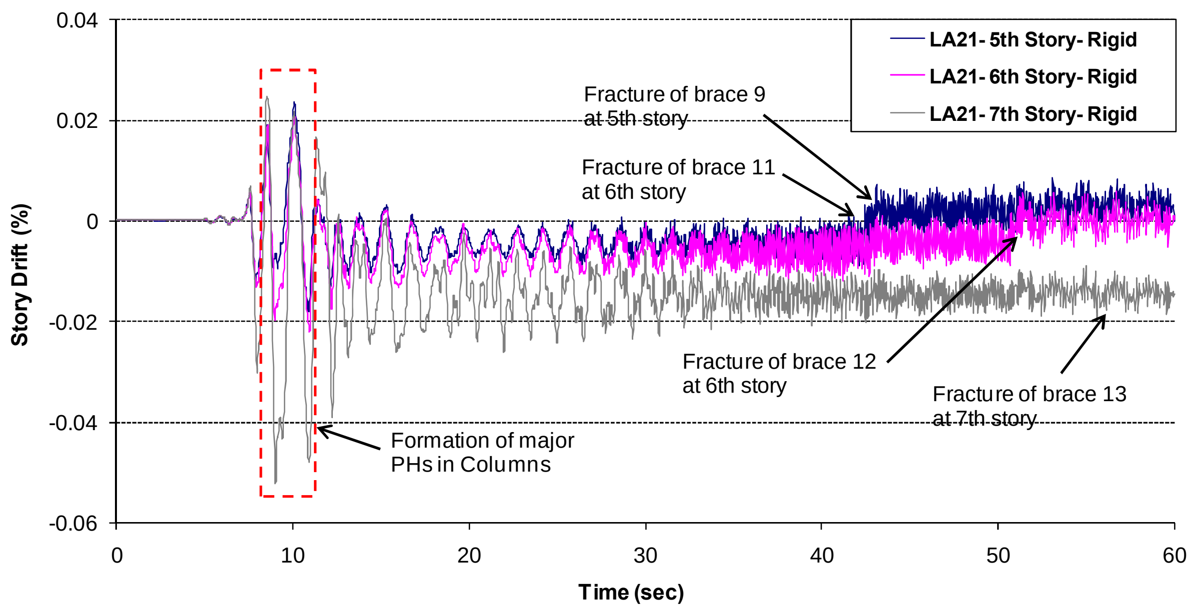

(b)

Figure 3.30. Sequence of Brace Fractures and PH Formation under LA21 for: (a) 9V-PBPD-A-Pin; and (b) 9V-PBPD-A-Rigid Frame

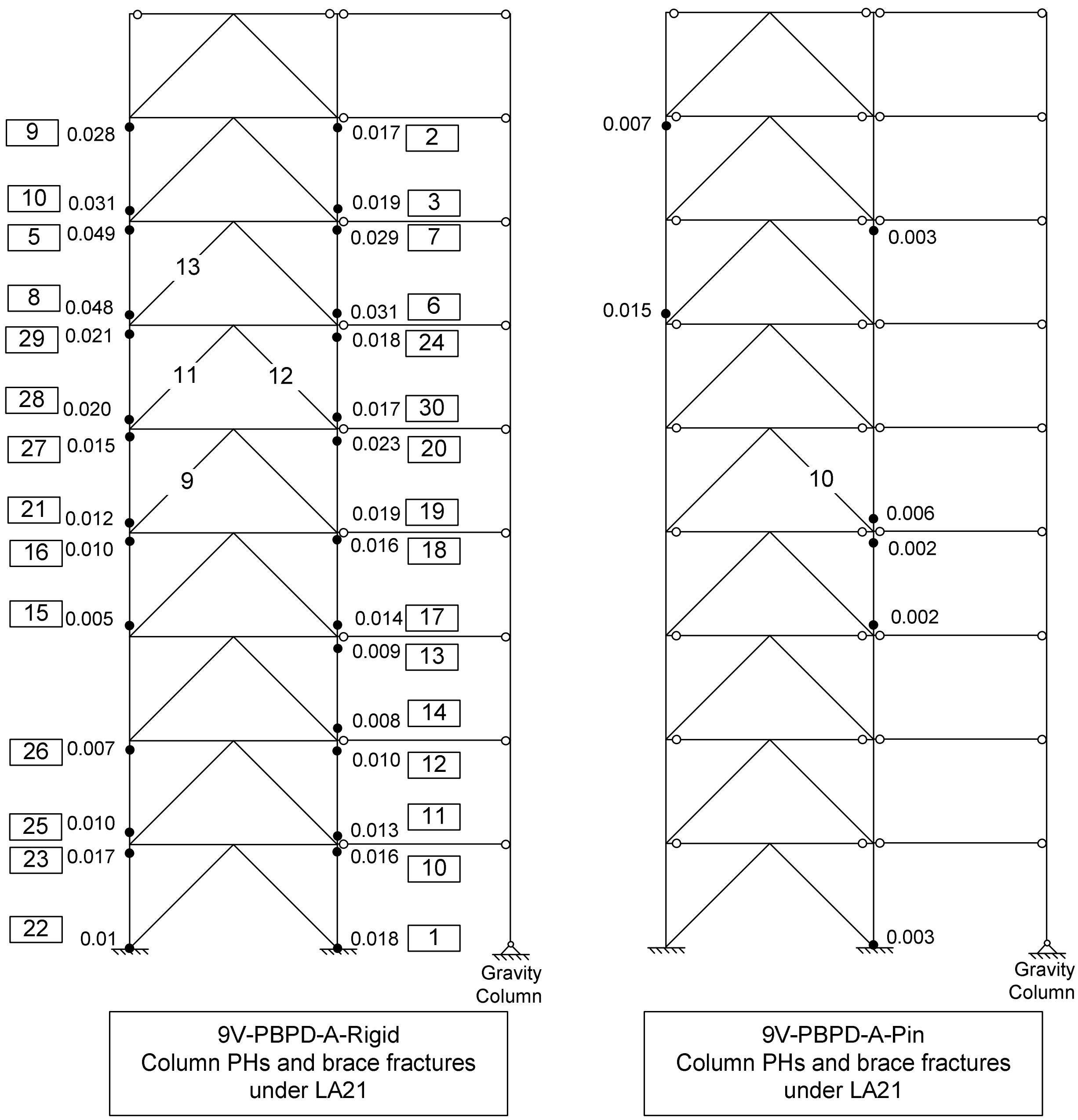

(a) (b)

Figure 3.31. Column PHs and Brace Fractures under LA21 for: (a) 9V-PBPD-A-Pin; and (b) 9V-PBPD-A-Rigid Frames

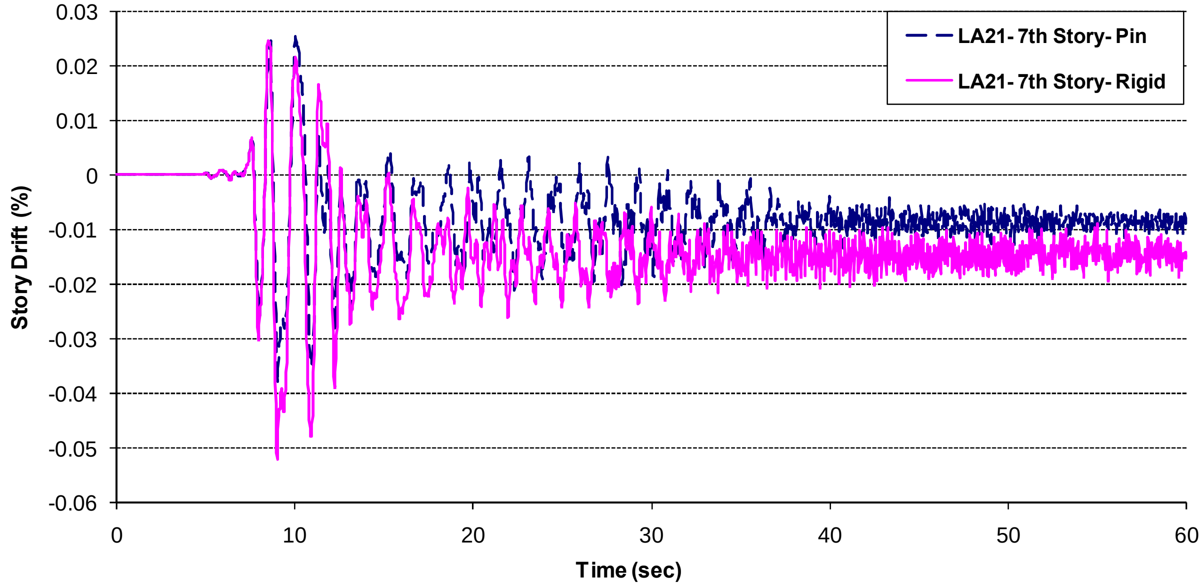

Figure 3.32. Larger Residual Drift for Model with Rigid Connections

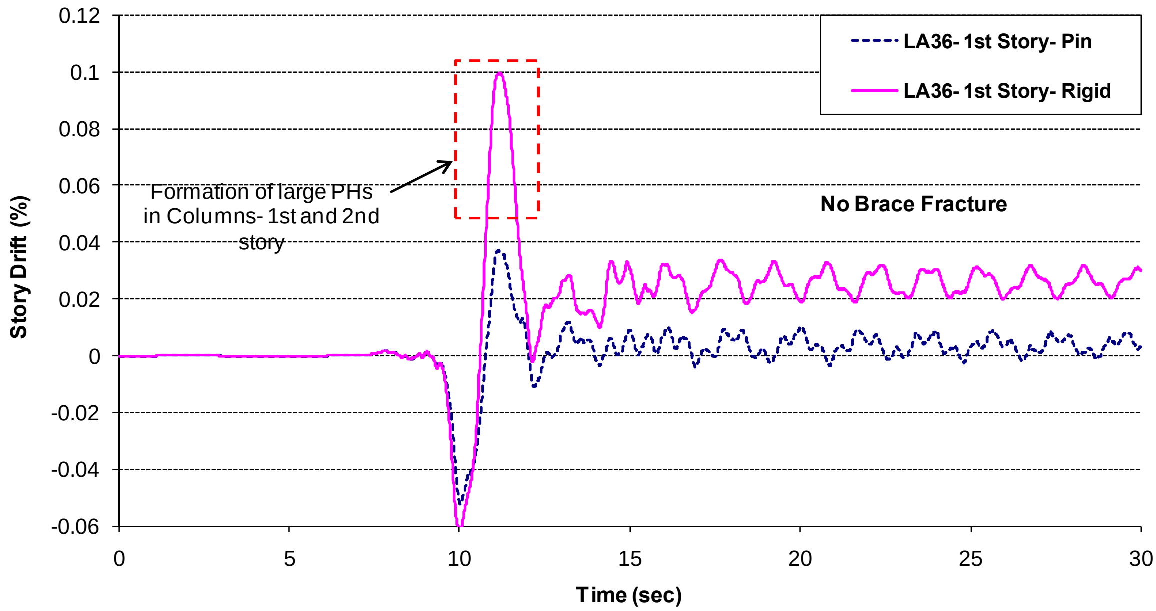

(a)

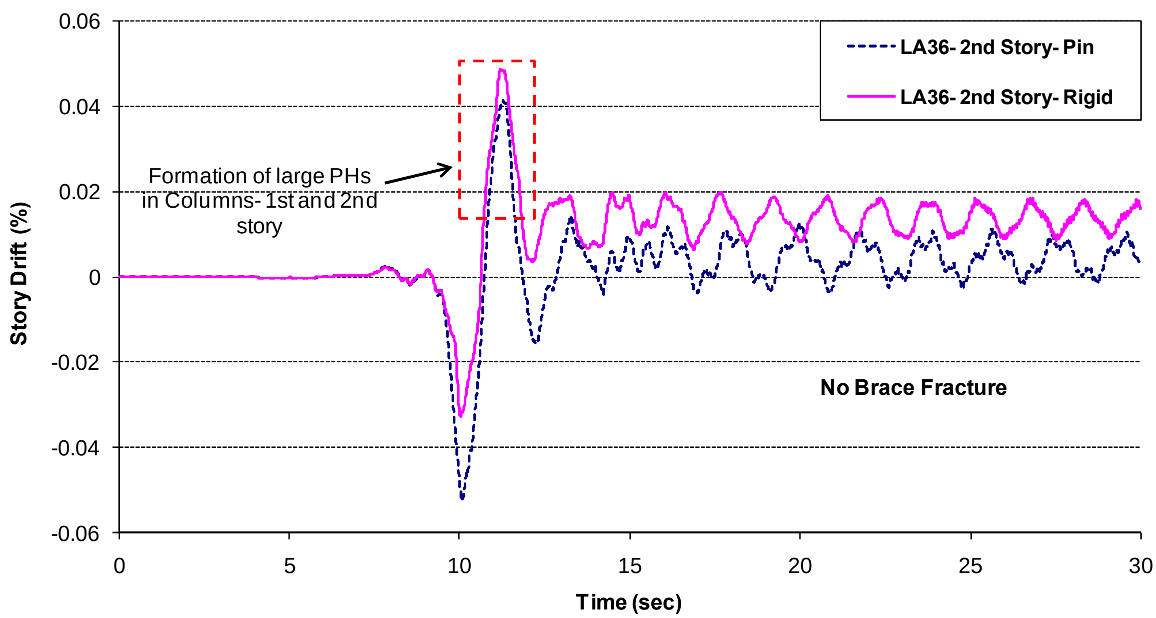

(b)

Figure 3.33. Significant Column PH Formation and Larger Residual Drift under LA36 for 9V-PBPD-A-Rigid Frame

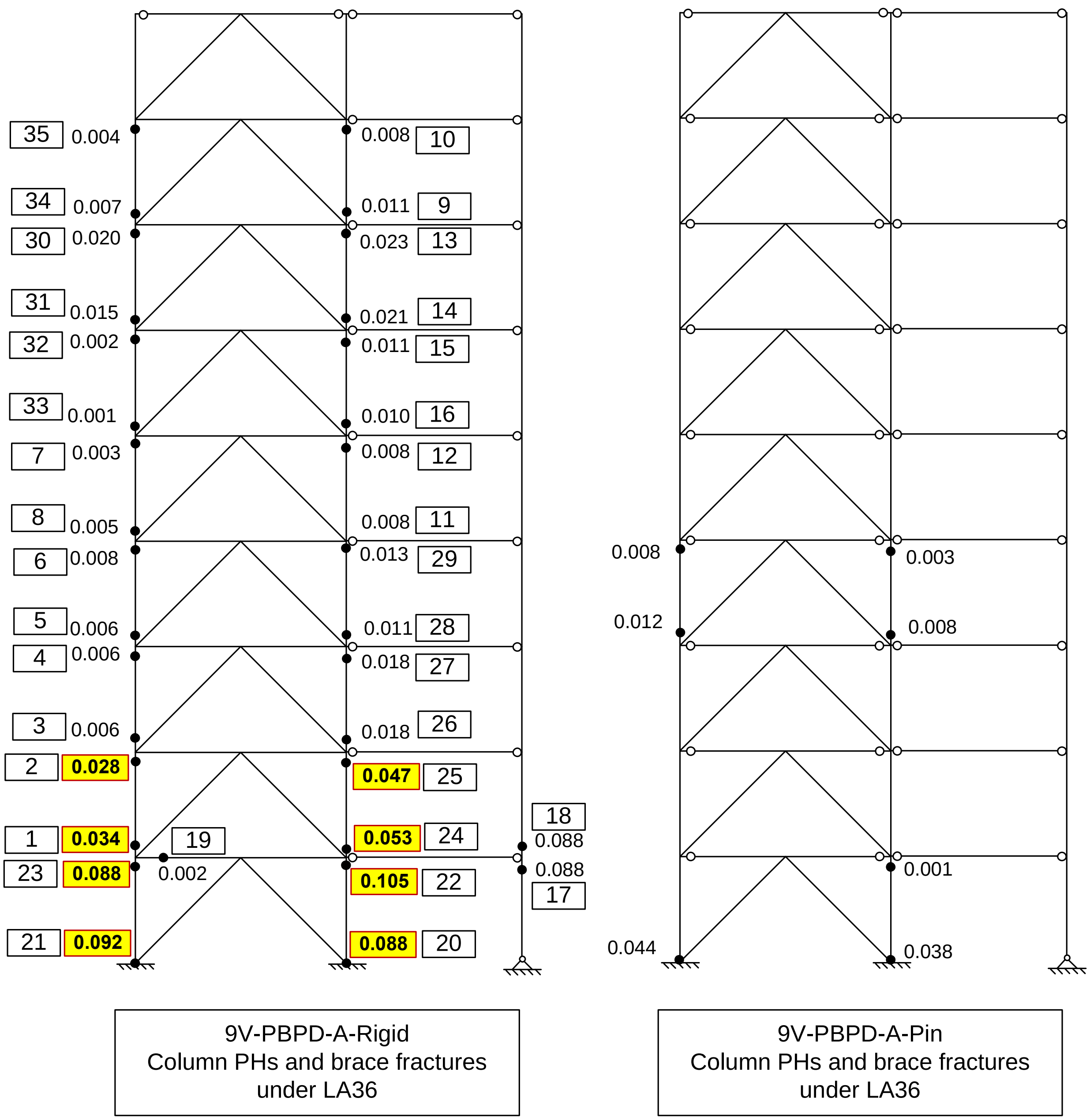

(a) (b)

Figure 3.34. Column PHs under LA36 for: (a) 9V-PBPD-A-Pin; and (b) 9V-PBPD-A-Rigid

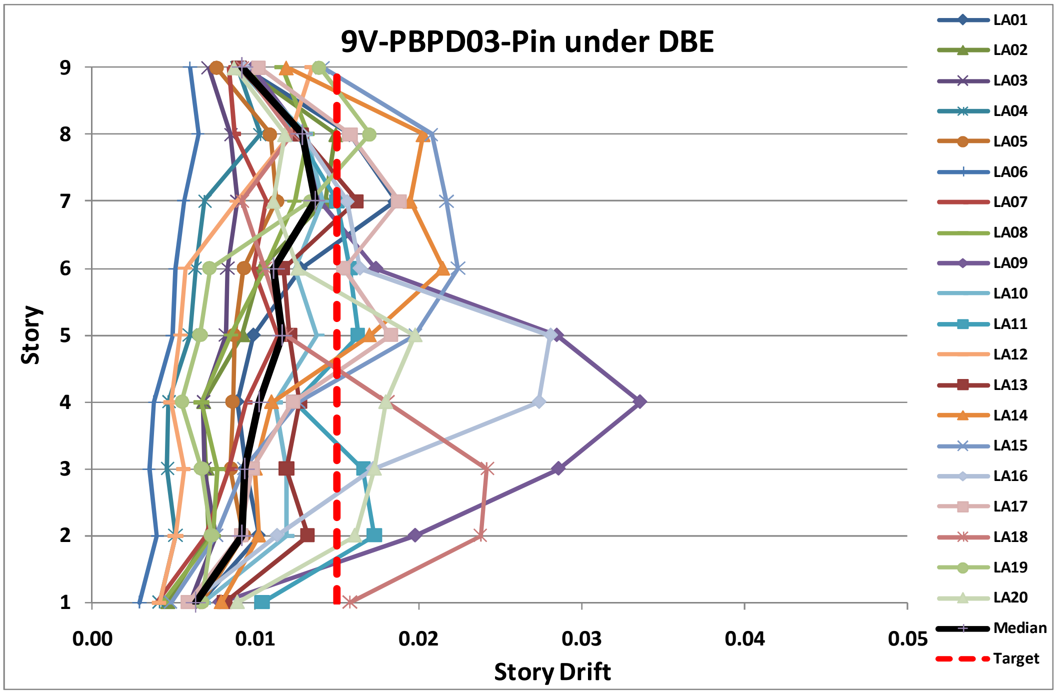

(a)

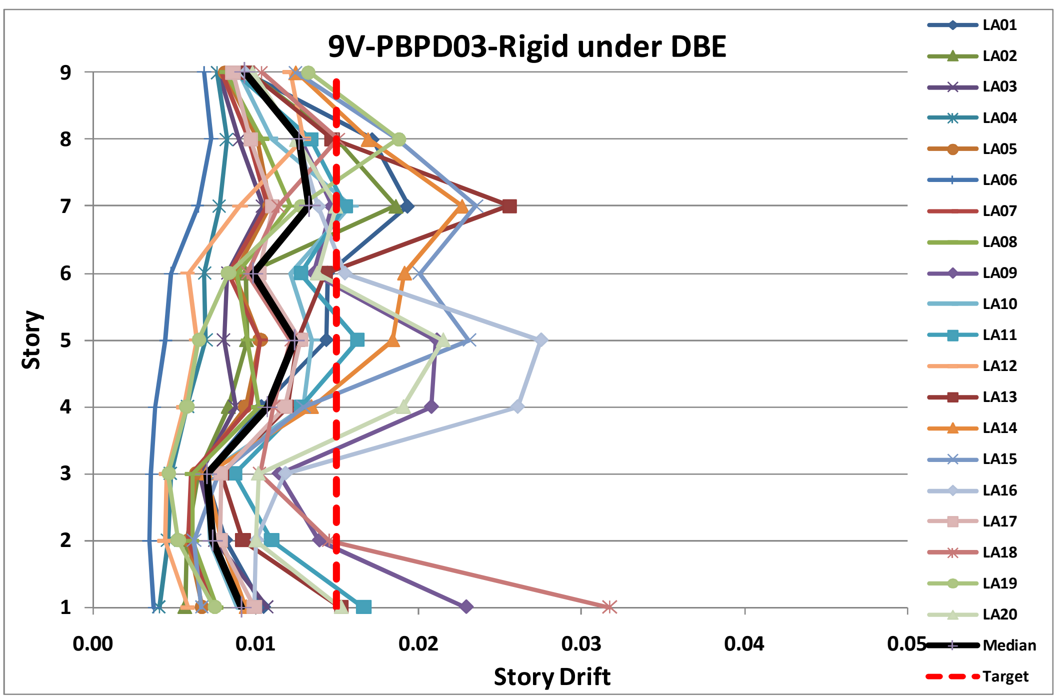

(b)

Figure 3.35. Pin and Rigid models under SAC LA 2/3 MCE ground motions

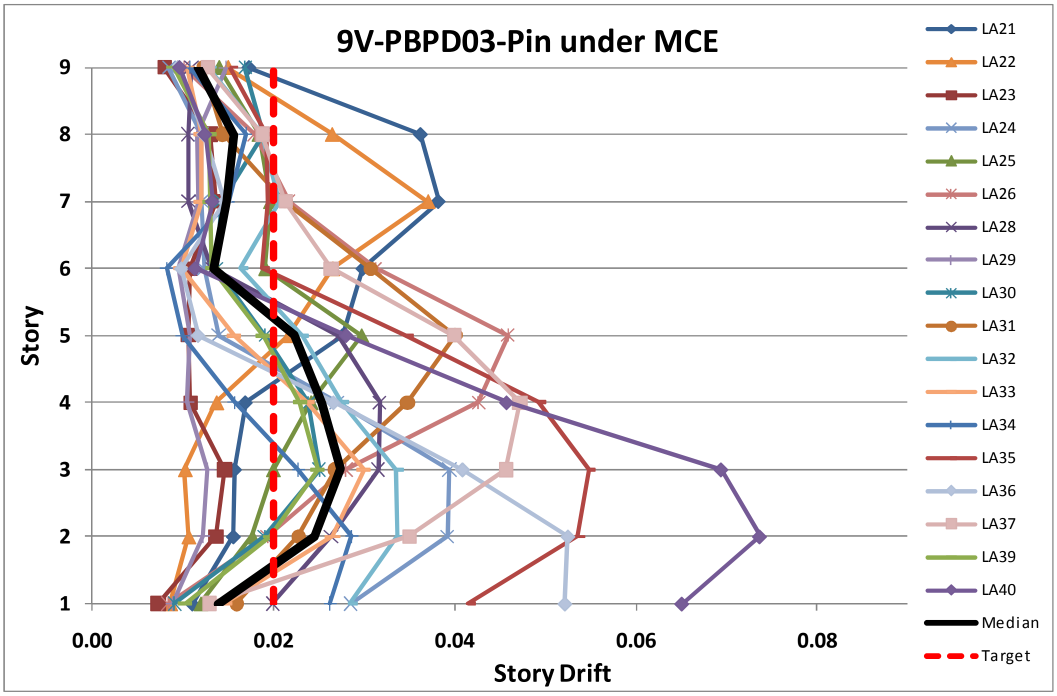

(a)

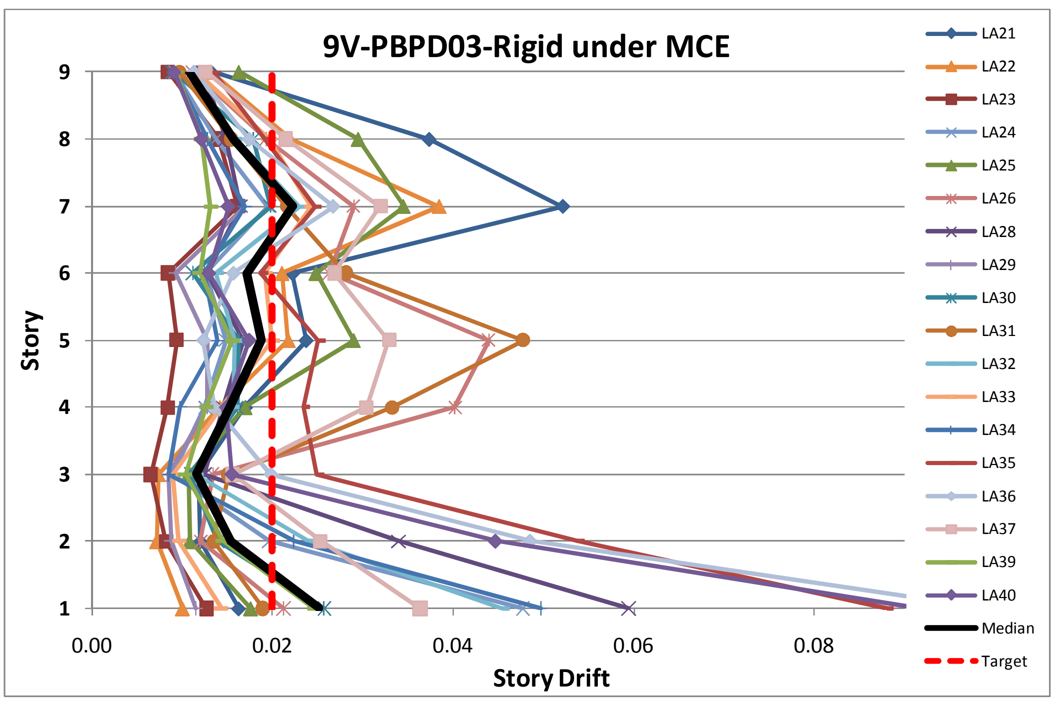

(b)

Figure 3.36. Pin and Rigid models under SAC LA MCE ground motions

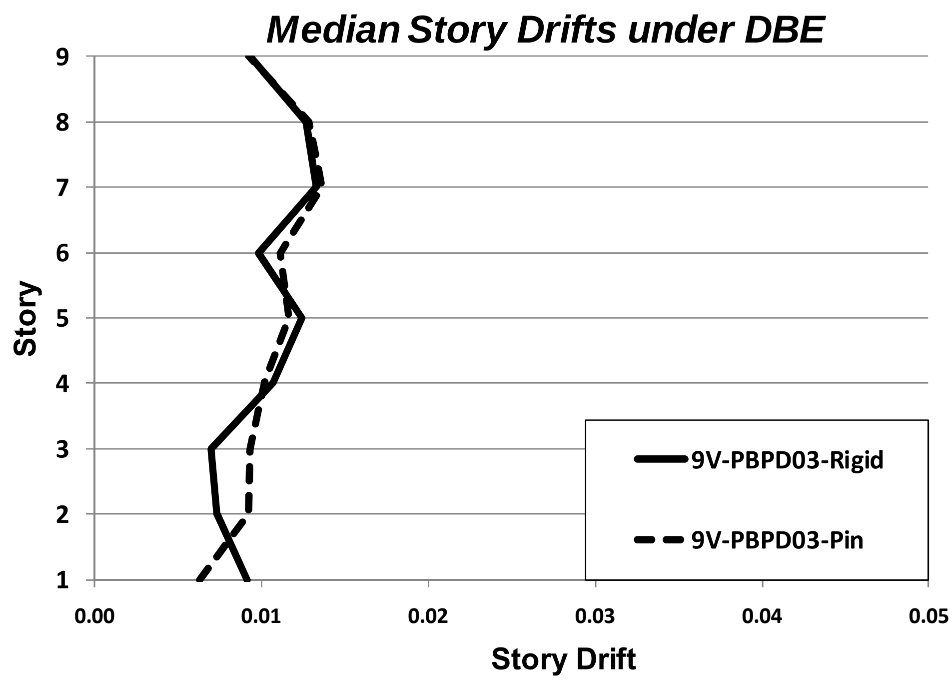

(a)

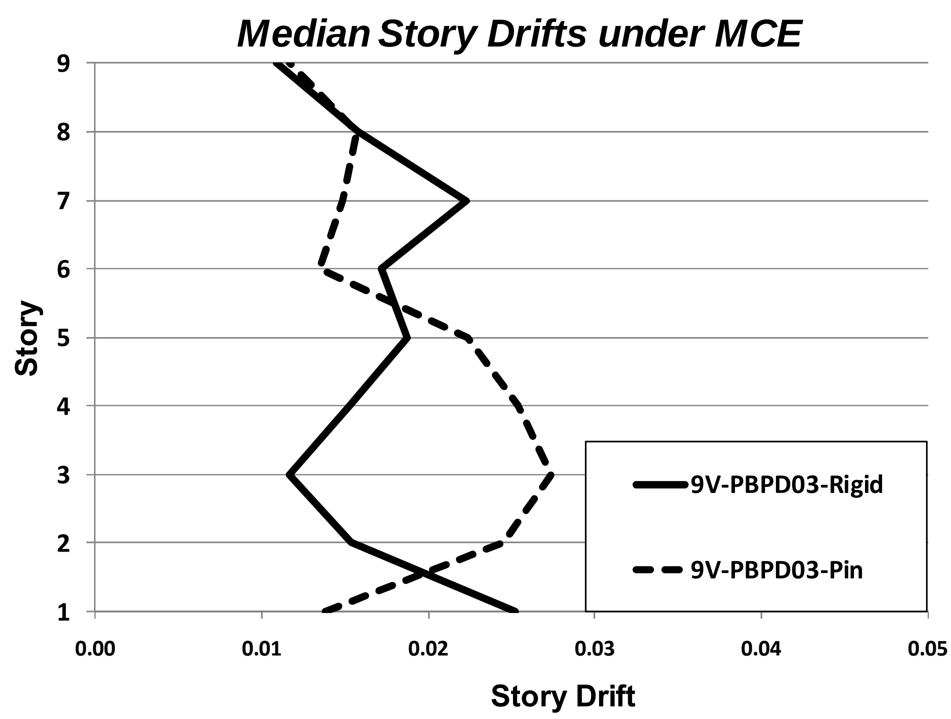

(b)

Figure 3.37. Median Story Drift Values under 2/3 MCE and MCE Hazard Levels

Table 3.21. Comparison of LA21 and LA36 Ground Motion Parameters

Ground Motions	Duration (sec)	PGA
LA21- 1995 Kobe	59.98	1.282g
LA36- Elysian Park (simulated)	29.99	1.101g

CHAPTER 4

Evaluation of Confidence Level against Collapse

4.1 Performance-Based Evaluation of CBF

A reliability framework for seismic performance evaluation of Steel Moment-Resisting Frames (SMRFs) was developed as part of the FEMA/SAC Steel Project (FEMA, 2000b). In this approach, two main performance levels (immediate occupancy and collapse prevention) are considered under specified seismic hazards. The global and the local deformation demands (as obtained from analysis) are then compared with the deformation capacity of the structural system and structural elements, respectively (FEMA, 2000b and Uriz, 2005). Basically, this procedure provides a simple method to estimate the confidence level of structures to meet the given performance level under specified seismic hazard (Yun et al., 2002). In other words, by considering such deformation demands and capacities in probabilistic terms with the assumption of lognormal probability distributions relative to uncertainty parameters (due to all uncertainties and randomness involved), an estimate of the confidence level to achieve the desired performance can be obtained in terms of the probability of the demand being less than the capacity.

Based on these, a demand and capacity factor design (DCFD), similar to the Load and Resistance Factor Design (LRFD), was adopted in FEMA/SAC Steel Project. This reliability-based quantitative approach involves evaluation of site-specific hazard, structural capacity, and structural demand, such that by having the hazard level and performance criteria the confidence level for the structure can be estimated. Hence, the main features in this approach are ground motion hazard curve, dynamic displacements, and displacement capacity. This procedure requires the calculation of a confidence parameter λ which can later be used to determine the confidence level associated with the assumed performance objective (Yun et al., 2002). The confidence parameter can be calculated as:

$$\lambda = \frac{\gamma \cdot \gamma_a \cdot D}{\phi \cdot C} \qquad (4.1)$$

where

C = median estimate of the capacity of the structure, as indicated in FEMA351 (FEMA, 2000b).

D = median demand for the structure, obtained from structural analysis for a specified level of ground motion.

γ = demand variability factor that accounts for the variability inherent in the prediction of demand related to assumptions made in structural modeling and prediction of the character of ground shaking.

γ_a = analytical uncertainty factor that accounts for bias and uncertainty, inherent in the specific analytical procedure used to estimate demand as a function of ground shaking intensity.

ϕ = resistance factor that accounts for the uncertainty and variability inherent in the prediction of structural capacity as a function of ground shaking intensity.

λ = confidence parameter from which a level of confidence can be obtained.

Having calculated the confidence parameter, λ, by using Equation (4.1), the confidence level can be obtained from a table similar to

Table 4.1 (Yun et al., 2002) or directly from the proper probability-based formulation. In this table, β_{UT} is the total uncertainty measure and k is the logarithmic slope of the hazard curve, both of which will be explained later in this chapter.

Uriz and Mahin (2004) used the performance-based earthquake evaluation (PBEE) framework originally developed for SMRFs in FEMA/SAC steel Project (FEMA, 2000b) to assess the performance of CBF and BRBF structures. In their study, the PBEE procedure was applied to four case study buildings; 3-story and 6-story chevron CBFs, and 3-story and 6-story chevron BRBFs. All four frames were originally designed by Sabelli (2000) according to *1997 NEHRP provisions* (FEMA, 1997). In this chapter, only the performances of example CBFs are studied. Also, only the global collapse condition and collapse prevention (CP) performance level are considered. It should be noted, as was mentioned by Uriz and Mahin (2004), that due to lack of supporting experimental data, several significant assumptions are needed when using the PBEE procedure for CBFs. Many parameter values used are approximate for CBFs and as a result, the calculated values for confidence level are only approximate estimates and they may not be as accurate as they are for SMRFs. Nevertheless, they are reasonable enough for comparison purposes since the same parameters have been used for both NEHRP and PBPD designed CBFs.

A summary of the steps in calculating the confidence level with which a structure can achieve its intended performance objective, as outlined by FEMA 351 (FEMA, 2000b), can be given as follows:

1. The performance objective against which the structure should be evaluated is selected. This requires selection of the desired performance level, e.g. Collapse Prevention or Immediate Occupancy, and a desired probability that damage in a period of time will be worse than this performance level. Representative performance objectives may include:

- 2% probability of poorer performance than Collapse Prevention level in 50 years
- 50% probability of poorer performance than Immediate Occupancy level in 50 years.

2. Characteristic motion for the performance objective is determined. For probabilistic performance objectives, an average estimate of the ground shaking intensity at the probability of exceedance identified in the performance objective definition (Step 1) is determined. Ground shaking intensity is characterized by the parameter S_{aT1}, the 5% damped spectral response acceleration at the site for the fundamental period of response of the structure. NEHRP 1997 provides procedures for determining this parameter for any probability of exceedance in a 50-year period.

3. Structural demands for the characteristic earthquake ground motion are determined. A mathematical model is developed to represent the building structure. This model is then subjected to a structural analysis, using any of the methods mentioned in Chapter 3 of FEMA 351 (FEMA, 2000b). This analysis provides estimates of maximum interstory drift demand, maximum column axial compression force demand, and maximum column-splice axial tension force demand, for the ground motion selected in Step 2.

4. Median estimates of structural capacity are determined. Interstory drift capacity for the building frame, as a whole, may be estimated using the default values given in Chapter 3 of FEMA351 for regular structures. Alternatively, the detailed procedures of Section A.6 of FEMA351 (e.g. Incemental Dynamic Analysis or IDA) may be used.

3. A factored-demand-to-capacity ratio, λ is determined. The calculated estimates of demand D and capacity C are determined using Steps 3 and 4, respectively. The corresponding demand (γ) and resistance (ϕ) factors should be determined in accordance with the applicable procedures. Then the confidence parameter λ can be obtained using Equation (4.1).

6. The confidence level is evaluated. The confidence level with regard to the ability of the structure to meet the performance objective should be the lowest value determined using the values of l as determined in accordance with Step 5 above and back-calculated from the equation:

$$\lambda = e^{-b\beta_{UT}(K_X - k\beta_{UT}/2)} \tag{4.2}$$

where:

b = a coefficient relating the incremental change in demand (drift, force, or deformation) to an incremental change in ground shaking intensity, at the hazard level of interest, typically taken as having a value of 1.0,

β_{UT}= an uncertainty measure equal to the vector sum of the logarithmic standard deviation of the variations in demand and capacity resulting from uncertainty,

k = the slope of the hazard curve, in ln-ln coordinates, at the hazard level of interest, i.e., the ratio of incremental change in S_{aT1} to incremental change in annual probability of exceedance,

K_X = standard Gaussian variate associated with probability x of not being exceeded as a function of number of standard deviations above or below the mean found in standard probability tables.

Table 4.1 shows a solution for this equation, for various values of the parameters k, l, and β_{UT}.

The values of the parameter β_{UT} in Table 4.3 are used in Equation (4.2) to account for the uncertainties inherent in the estimation of demands and capacities. Assuming that the amount of uncertainty introduced by each of the assumptions can be characterized, the parameter β_{UT} can be calculated using the equation:

$$\beta_{UT} = \sqrt{\sum_i \beta_{ui}^2} \tag{4.3}$$

where: β_{ui} represents the standard deviation of the natural logarithms of the variation in demand or capacity resulting from each of the various sources of uncertainty.

In the following sections, these steps are followed in order to obtain the confidence level of the five CBFs (3V-NEHRP, 3V-PBPD, 6V-NEHRP, 6V-PBPD, and 9V-PBPD-A) against collapse prevention (CP) performance level under the seismic hazard level of 2% probability of exceedence in 50 years (2%/50yrs).

4.1.1 Determination of Site-Specific Hazard Parameters

In this study, seismic hazard parameters are assumed to be the same as those used in the FEMA/SAC for SMRF case studies (Yun et al., 2002) and the study on CBFs and BRBFs (Sabelli, 2000). Two basic hazard parameters are required for performance evaluation. These are: the intensity as the median 5%-damped linear spectral response acceleration, S_{aT1}, at the fundamental period of the building for the desired hazard level, and the logarithmic slope of the hazard curve, k, at the desired hazard level (FEMA, 2000b). In this study, the building is assumed to be located on firm soil in downtown Los Angeles, California and the seismic hazard parameters are based on the 1997 NEHRP Provisions (FEMA, 1997). Accordingly, twenty ground motions from FEMA/SAC database for the LA site and corresponding to a 2% probability of exceedence in 50 year (hereafter called SAC LA ground motions) are used in dynamic analyses. These ground motions, which consist of LA21 to LA40, are taken from a larger database of representative ground motions developed by Somerville et al. (1997).

The logarithmic slope k of the hazard curve at the desired hazard level is used to determine the resistance factors, demand factors and also the confidence levels. The hazard curve is a plot of probability of exceedance of a spectral amplitude versus the spectral amplitude for a given period, and is usually plotted on a log-log scale (FEMA, 2000b). In functional form it can be represented by the equation:

$$H_{si}(S_i) = k_0 S_i^{-k} \tag{4.4}$$

where:

$H_{Si}(S_i)$ = the probability of ground shaking having a spectral response acceleration greater than S_i,

k_0 = a constant, dependent on the seismicity of the individual site,

k = the logarithmic slope of the hazard curve, and k = 3 can be assumed for Alaska, California and the Pacific Northwest according to Table A.3 of FEMA 351.

4.1.2 Assessment of Structural Demand

The maximum story drift demands were obtained by performing nonlinear dynamic analysis for the suite of 20 SAC LA ground motion (2%/50yrs) which are LA21 to LA40. The analyses were carried out by using the SNAP-2DX program, which has the ability to model the brace behavior under large displacement reversals, as well as fracture life of tubular braces (Rai et al., 1996). In addition, lump gravity columns were included in the model by using continuous leaning columns, which were linked to the braced frame through pin-ended rigid elements. Those gravity columns created significant P-Δ effect under large drifts. Mass proportional critical damping of 2% was considered for all dynamic analyses. It is noted that, due to the presence of gusset plates, the beam ends at all levels (except for the top levels) of the NEHRP frames were modeled by assuming fixed-end condition. All beams and columns of the frame were modeled as beam-column elements. The same modeling technique was used in the study by Sabelli (2000) with the exception of P-Delta modeling. The seismic mass was assumed to be uniformly distributed when assigning such mass properties at the nodes of the braced frame model. The beam-to-column connections of the 3-story and 6-story NEHRP frame (except for roof level) were modeled as moment resisting connections due to the presence of gusset plates. On the other hand, the beam-to-column connections at all levels of the 3-story, 6-story, and 9-story PBPD frames were modeled as pin connections due to the introduction of beam splices (see Figure 2.6). For comparison between performances of NEHRP and PBPD frames under the design level (10%/50yrs) as well as MCE level (2%/50yrs) ground motions the reader is referred to Goel and Chao (2008).

The maximum interstory drifts were considered to be a good indication of the global damage in CBFs. It is well related to the extent of plastic deformations in structural components (local level) as well as the global instability of the whole frame due to *P-Δ* effect. The peak interstory drifts at all stories for the four frames were obtained under each of the 20 SAC LA ground motions. As recommended by FEMA 351, a lognormal probability distribution was considered for these peak interstory drift values. The median and standard deviation values were then obtained for these peak interstory drifts for all ground motions. The median value of these drift demands can be taken as the demand parameter D for use in Equation (4.1). The variability (uncertainty) of dynamic response for this hazard level is represented by the standard deviation of the natural logarithm of the peak drift demands (β_{DR}). Once the value of β_{DR} is determined, the demand variability factor, γ, is calculated from the Equation (4.5) as:

$$\gamma = e^{\frac{k}{2b}\beta_{D_R}^2} \tag{4.5}$$

where:

k = the logarithmic slope of the hazard curve (see section 4.3.1)

b = a coefficient that represents the amount that demand increases as a function of hazard. As mentioned by Uriz (2005), for flexible moment frames, this value is taken as *1.0*, but for stiffer braced frames with shorter periods a value larger than *1.0* might be expected based on the conservation of energy principle (Chopra 1995, Newmark and Hall, 1973).

As can be seen from Table 4.4, the median drift demand for 3-NEHRP is significantly larger than that of 3V-PBPD. The median drift of 3V-PBPD is about 22% of the 3V-NEHRP frame. In the case of 6-story CBFs, the median drift demand of 6V-NEHRP is about 30% larger than that of 6V-PBPD.

The demand uncertainty factor γ_a is based on uncertainties involved in the determination of the median demand, *D*. These uncertainties are mainly coming from the inaccuracies in the analytical modeling and procedure used in demand calculation. The effect of such uncertainties in the recommended performance evaluation procedure can be captured by using an analysis uncertainty factor, γ_a, as given in Equation (4.6):

$$\gamma_a = C_B e^{\frac{k}{2b}\beta_{D_U}^2} \tag{4.6}$$

In this study, the same default values for γ_a recommended in FEMA 351 for SMRFs are used, although this assumption may be unconservative due to the larger scatter of the story drift results in CBFs compared to SMRFs. These analysis uncertainty values are shown in Table 4.2.

4.1.3 Determination of Drift Capacity

Incremental Dynamic Analysis (IDA) procedure developed by Vamvatsikos and Cornell (2002) aims at determining the global drift capacity of structures (FEMA, 2000b). This procedure was utilized in this study to obtain the drift capacities of the study frames. In this method, the maximum interstory drifts were obtained through nonlinear dynamic analyses under varying intensities of twenty 2%/50yrs SAC ground motions (FEMA, 2000b; Vamvatsikos and Cornell, 2002). Having the intensity (in terms of spectral acceleration, S_a) versus maximum story drift plot for each ground motion, the drift capacity for a particular ground motion can be estimated at the point where the slope of the curve falls below one-fifth of its initial slope. Additionally, as an upper bound, the drift capacities cannot be taken greater than 10%. Figure 4.1 and Figure 4.2 show the IDA results for the 3, 6, and 9-story frames, respectively. The drift capacities are shown in these figures by hollow circles on each curve. The numerical values for global drift capacity C and the corresponding resistance factor ϕ are given in Table 4.4.

4.1.4 Confidence Level Assessment

After all the parameters needed in Equation (4-14) to calculate the confidence parameter λ are determined, the confidence level can be obtained for each frame. This can be done either by interpolating the appropriate values from

Table 4.1, or by using the standard Gaussian variate K_X given by the following equation:

$$K_X = \frac{k\beta_{UT}}{2b} - \frac{\ln(\lambda)}{b\beta_{UT}} \tag{4.7}$$

Randomness and uncertainty parameters as well as resulting confidence levels are shown in Table 4.3 and Table 4.4, respectively. As can be seen, confidence level of the 3V-NEHRP frame against global collapse (<<1%) was dramatically improved when it was re-designed by the PBPD method (*i.e.*, 3V-PBPD frame). It is worth mentioning that the enhanced confidence level (>99.9%) is comparable to those of SMFs designed according to 1997 NEHRP provisions (Yun et al., 2002). It can also be seen that although the median drift capacities for the two 3-story frames are somewhat close, the drift demand of the 3V-PBPD frame is only about 22% of the 3V-NEHRP frame. Therefore, most of the improvement in confidence level comes from the reduction in drift demand. Table 4.4 also shows that, the confidence level for 6V-NEHRP frame (23.3%) is higher compared to the 3V-NEHRP frame, but is still much below the 90% satisfactory level suggested by FEMA 351 for SMFs. The confidence level of 86.2%, for the 6V-PBPD frame is also quite close to the desired 90% level. The confidence level for 9V-PBPD-A frame is about 52% which is quite low compared to the 3 and 6-story PBPD frames. Several adjustments to improve the confidence level of the 9-story frame are suggested in Chapter 5.

4.2 Summary and Concluding Remarks

- Reliability-based evaluation by using the FEMA 351 procedure for SMFs, which accounts for randomness and uncertainty in the estimation of seismic demand and drift capacity, showed that steel concentrically braced frames (CBFs) designed by the performance-based plastic design (PBPD) method can have dramatically higher confidence levels against global collapse than those of SCBFs designed by current practice. Also, those confidence levels can be similar to the target confidence levels for SMFs in current practice, *i.e.*, 90% or above.

- Significant improvement in the confidence level (C. L.) can be seen for the 3V-PBPD compared to 3V-NEHRP. This C. L. is indeed comparable to those of MFs designed by 1997 NEHRP code (Yun et al., 2002). On the other hand, the 3V-NEHRP shows extremely low confidence level against global collapse. It can also be seen that although the median drift capacities for the two 3-story frames are somewhat close, they show quite different drift demands under 2/50 ground motions.

-The C.L. for 6V-NEHRP frame was somewhat better than that of the 3V-NEHRP frame, but was still much less than the 90% satisfactory level as suggested by FEMA 351. Significant difference can still be observed between the C.L.s of 6V-NEHRP and 6V-PBPD, with the latter having a confidence level quite close to 90%.

- The C.L. for 9V-PBPD-A came out to be about 52% which is not quite satisfactory when compared to the superior C.L. of 3V-PBPD and 6V-PBPD frames. This can be attributed to larger P-Delta effects and also more brace fractures for this 9-story frame. These issues are further addressed in Chapter 5 and proper modifications are suggested to improve the C.L. of the 9-story CBF, to about the level of 6V-PBPD.

Table 4.1. Confidence Parameter λ, as a Function of Confidence Level, Hazard Parameter k, and Uncertainty β_{UT} (from Yun et al, 2001)

Confidence	2%	5%	10%	20%	30%	40%	50%	60%	70%	80%	90%	95%	99%
						$\beta_{UT}=0.1$							
$k=1$	1.23	1.18	1.14	1.09	1.06	1.03	1.01	0.98	0.95	0.92	0.88	0.85	0.80
$k=2$	1.24	1.19	1.15	1.10	1.06	1.04	1.01	0.98	0.96	0.93	0.89	0.86	0.80
$k=3$	1.25	1.20	1.15	1.10	1.07	1.04	1.02	0.99	0.96	0.93	0.89	0.86	0.80
$k=4$	1.25	1.20	1.16	1.11	1.08	1.05	1.02	0.99	0.97	0.94	0.90	0.87	0.81
						$\beta_{UT}=0.2$							
$k=1$	1.54	1.42	1.32	1.21	1.13	1.07	1.02	0.97	0.92	0.86	0.79	0.73	0.64
$k=2$	1.57	1.45	1.34	1.23	1.16	1.09	1.04	0.99	0.94	0.88	0.81	0.75	0.65
$k=3$	1.60	1.48	1.37	1.26	1.18	1.12	1.06	1.01	0.96	0.90	0.82	0.76	0.67
$k=4$	1.63	1.51	1.40	1.28	1.20	1.14	1.08	1.03	0.98	0.92	0.84	0.78	0.68
						$\beta_{UT}=0.3$							
$k=1$	1.94	1.71	1.54	1.35	1.22	1.13	1.05	0.97	0.89	0.81	0.71	0.64	0.52
$k=2$	2.03	1.79	1.61	1.41	1.28	1.18	1.09	1.01	0.93	0.85	0.74	0.67	0.54
$k=3$	2.12	1.87	1.68	1.47	1.34	1.23	1.14	1.06	0.98	0.89	0.78	0.70	0.57
$k=4$	2.22	1.96	1.76	1.54	1.40	1.29	1.20	1.11	1.02	0.93	0.82	0.73	0.60
						$\beta_{UT}=0.4$							
$k=1$	2.46	2.09	1.81	1.52	1.34	1.20	1.08	0.98	0.88	0.77	0.65	0.56	0.43
$k=2$	2.67	2.27	1.96	1.64	1.45	1.30	1.17	1.06	0.95	0.84	0.70	0.61	0.46
$k=3$	2.89	2.45	2.12	1.78	1.57	1.41	1.27	1.15	1.03	0.91	0.76	0.66	0.50
$k=4$	3.13	2.66	2.30	1.93	1.70	1.52	1.38	1.24	1.12	0.98	0.82	0.71	0.54
						$\beta_{UT}=0.5$							
$k=1$	3.16	2.58	2.15	1.73	1.47	1.29	1.13	1.00	0.87	0.74	0.60	0.50	0.35
$k=2$	3.59	2.92	2.44	1.96	1.67	1.46	1.28	1.13	0.99	0.84	0.68	0.56	0.40
$k=3$	4.06	3.31	2.76	2.22	1.89	1.65	1.45	1.28	1.12	0.96	0.77	0.64	0.45
$k=4$	4.60	3.75	3.13	2.51	2.14	1.87	1.65	1.45	1.27	1.08	0.87	0.72	0.52
						$\beta_{UT}=0.6$							
$k=1$	4.11	3.21	2.58	1.98	1.64	1.39	1.20	1.03	0.87	0.72	0.55	0.45	0.30
$k=2$	4.91	3.85	3.09	2.37	1.96	1.67	1.43	1.23	1.05	0.87	0.66	0.53	0.35
$k=3$	5.88	4.60	3.70	2.84	2.35	2.00	1.72	1.47	1.25	1.04	0.80	0.64	0.42
$k=4$	7.04	5.51	4.43	3.40	2.81	2.39	2.05	1.76	1.50	1.24	0.95	0.77	0.51

Table 4.2. Analysis Uncertainty Parameters

Study Frames	C_B	β_{DU}	γ_a
3V-NEHRP	1.0	0.15	1.03
3V-PBPD	1.0	0.15	1.03
6V-NEHRP	1.0	0.20	1.06
6V-PBPD	1.0	0.20	1.06
9V-PBPD-A	1.0	0.20	1.06

Table 4.3. Randomness and Uncertainty Parameters

Frame	β_{RC}	ϕ_{RC}	β_{UC}	ϕ_{UC}	β_{RD}	β_{UT}
3V-NEHRP	0.537	0.649	0.15	0.967	0.890	0.30
3V-PBPD	0.394	0.793	0.15	0.967	0.545	0.30
6V-NEHRP	0.435	0.753	0.20	0.942	0.663	0.35
6V-PBPD	0.412	0.775	0.20	0.942	0.708	0.35
9V-PBPD-A	0.309	0.866	0.20	0.942	0.515	0.35

* β_{RC}: standard deviation of natural logs of drift capacities due to randomness
* β_{UC}: standard deviation of natural logs of drift capacities due to uncertainty
* β_{RD}: standard deviation of natural logs of drift demands due to randomness
* β_{UT}: vector sum of logarithmic standard deviations for both demand and capacity considering all sources of uncertainty

Table 4.4. Summary of Confidence Level Assessment for 3-Story and 6-Story CBFs

Frame	Median Drift Capacity (from IDA) C	Capacity factor ϕ	Median Drift Demand D	Demand factors		Confidence Parameter	Confidence Level (%)
				γ	γ_a	$\lambda = \dfrac{\gamma \cdot \gamma_a \cdot D}{\phi \cdot C}$	
3V-NEHRP	0.064	0.628	0.068	3.37	1.06	6.04	**<< 1%**
3V-PBPD	0.078	0.766	0.015	1.56	1.06	0.41	**> 99.9%**
6V-NEHRP	0.065	0.709	0.035	1.93	1.06	1.55	**23.3%**
6V-PBPD	0.100	0.730	0.027	2.12	1.06	0.82	**86.2%**
9V-PBPD-A	0.062	0.816	0.0376	1.49	1.06	1.180	**52.1%**

* ϕ : resistance factor that accounts for the randomness and uncertainty in estimation of structural capacity

*γ: demand uncertainty factor;
*γ_a: analysis uncertainty factor

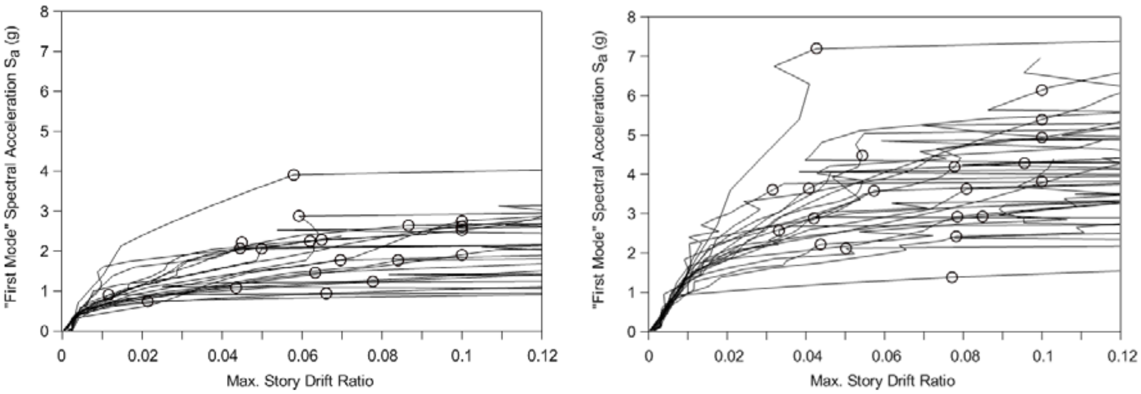

(a) (b)

Figure 4.1. IDA Curves for (a) 3V-NEHRP and (b) 3V-PBPD Frames under 2%/50yrs SAC LA Ground Motions.

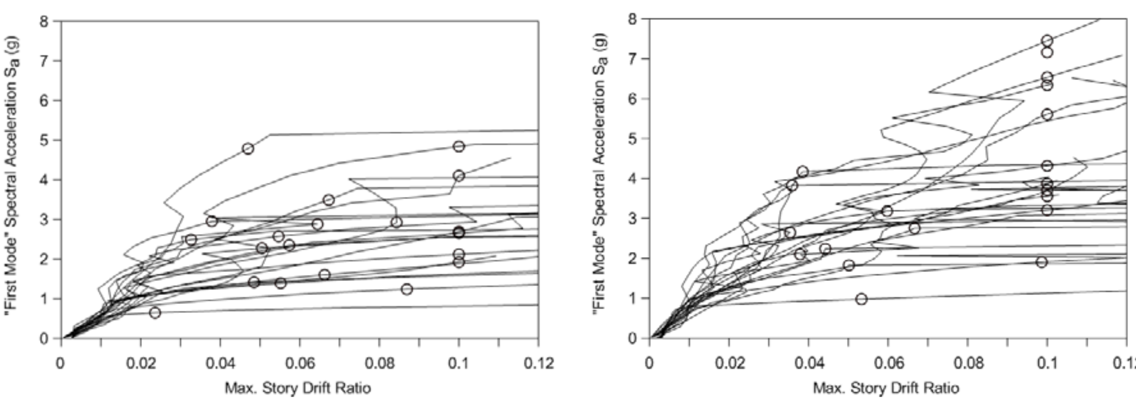

(a) (b)

Figure 4.2. IDA Curves for (a) 6V-NEHRP and (b) 6V-PBPD Frames under 2%/50yrs SAC LA Ground Motions.

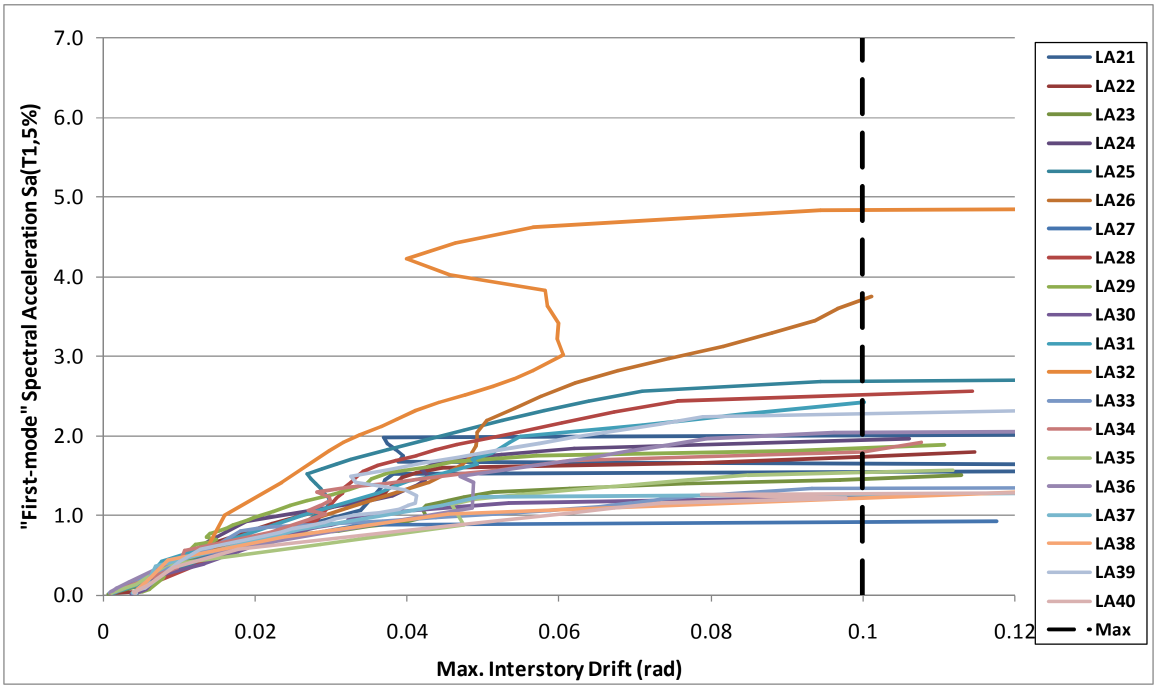

Figure 4.35. IDA Curves for 9V-PBPD03 Frames under 2%/50yrs SAC Ground Motions.

CHAPTER 5

Confidence Level Enhancement of the 9-Story CBF Designed by PBPD

5.1 Introduction

As was presented in Chapter 4, somewhat low confidence level (C.L.) of 52% against collapse was obtained for the 9V-PBPD-A frame designed by the procedure described in Chapter 3, even though the story drifts where within drift limits under design level ground motions. It should also be noted that the C.L. for the 3 and 6-story PBPD frames were excellent with values of 99.9% and 86%, respectively (see Table 4.4).

The main objective in this chapter was to further improve the C.L. of the 9-story CBF (as a representative of mid-rise CBF systems) against collapse. Modifications to improve the C.L. are suggested. These include modification in the PBPD design base shear (DBS) calculation for taller CBF by revising the λ-factor, and considering alternate brace configuration of two story X-pattern (split-X). Also, the effect of increasing the brace fracture life, N_f, on the C.L. is studied.

In general, the main design objectives in the calculation of the required PBPD design base shear are: (1) not exceeding the targeted story drifts under design level ground motions; (2) minimizing potential for collapse under MCE ground motions; (3) achieving satisfactory C.L. against collapse.

Lower C.L. observed for 9V-PBPD-A (compared to 3V-PBPD and 6V-PBPD) is believed mainly due to somewhat low value of DBS used in the design. Therefore, the main focus in this chapter is to suggest way to calculate suitable value of DBS that would result in improved C.L. against collapse. In addition, the effect of using split-X configuration, as well as that of increased N_f on the C.L. are investigated.

5.2 New λ-Factor

The λ-factor approach was introduced in Chapter 3, for calculation of design base shear (DBS) in the PBPD procedure for CBF structures. In this method, the effective target drift is obtained by dividing actual target drift by an appropriate value of λ-factor. This effective target drift is then used along with the modified yield drift (adjusted for column axial deformations) to obtain the effective ductility of the equivalent Elastic-Plastic SDOF system. The PBPD design base shear is then obtained by using this effective ductility.

As was also mentioned in Chapter 3, the estimation for λ-factor in that chapter was an initial attempt. By careful assessment of the parameters involved in the DBS calculation, and also based on observations on the seismic performance and confidence level of the 9V-PBPD-A frame, it was found that the estimation of λ-factor, as used in Chapter 3 (Figure 3.15), can be improved in order to enhance the seismic response of longer period taller CBFs.

The P-Delta effect was not directly accounted for in DBS calculation. In the case of 9V-PBPD-A, the P-Delta forces were later added for the design of braces in order to indirectly capture this second order effect. An alternate method to account for the P-Delta effects can be through suitable modification of the λ-factor, in a way that reflects this effect. By following such approach, enhanced response can be achieved through calculation of appropriate design base shear from the very beginning of the design process.

Therefore, a new and slightly different estimation of λ-factor is proposed here. Figure 5.1 shows this new λ-factor along with the one previously used in Chapter 3. As can be seen, the main difference between the two is for periods larger than 0.7 second which corresponds to mid to high-rise CBF systems. Table 5.1 shows the values of the new λ-factor as a function of T.

Also as can be seen in Figures 5.1 to 5.3, the λ-factor value for periods longer than 1.0 sec is selected to be 1.10 in order to compensate for the P-Delta effect. As a result, it is expected that the new λ-factor would affect mainly the design of mid-rise to high-rise CBF systems.

Figure 5.2 shows comparison between the new λ-factor and the suggested C_2 values from FEMA 356 (2000). As can be seen, the new λ-factor gets closer to the values suggested for Collapse Prevention by FEMA 356 in the range of mid-rise CBFs (T= 0.5 ~ 0.75 second) and comes closer to the values suggested for Life Safety for longer periods. However, such comparison may not be quite fair since the new λ-factor accounts for P-Delta effects, potential brace fractures, as well as pinched hysteretic behavior, whereas the FEMA 356 C_2 factor accounts for the latter only.

As shown in Figure 5.3, the new λ-factor does not exactly follow the mean of displacement ratio for the set of ground motions for stiffness degrading (SD) systems. The reasons are: 1) The mean was obtained for SDOF systems; 2) It does not include the effect of brace fractures; 3) It does not capture P-Delta effect for longer period frames. However, the proposed λ values in general follow the trend of the mean ratios.

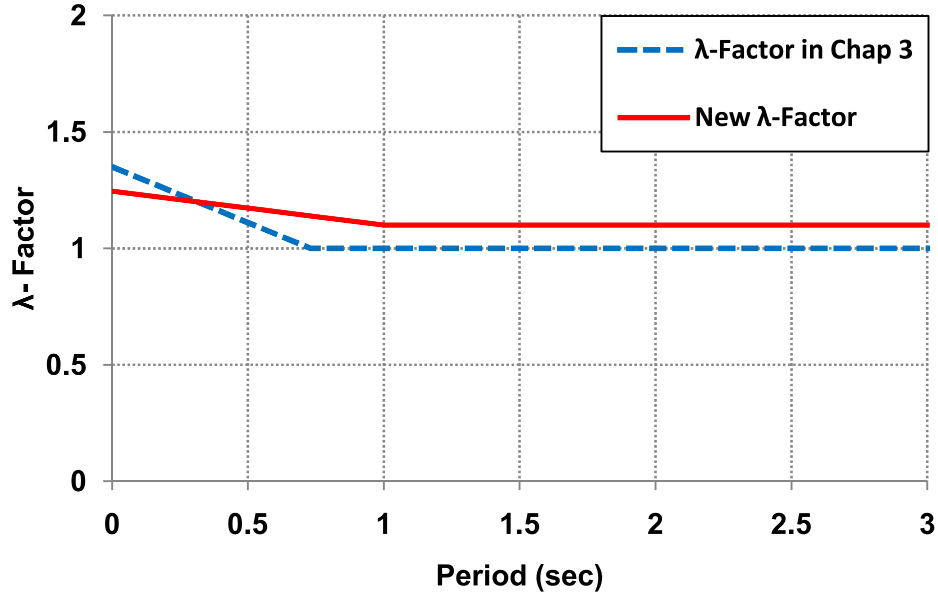

Figure 5.1. New λ-Factor versus λ-Factor used in Chapter 3

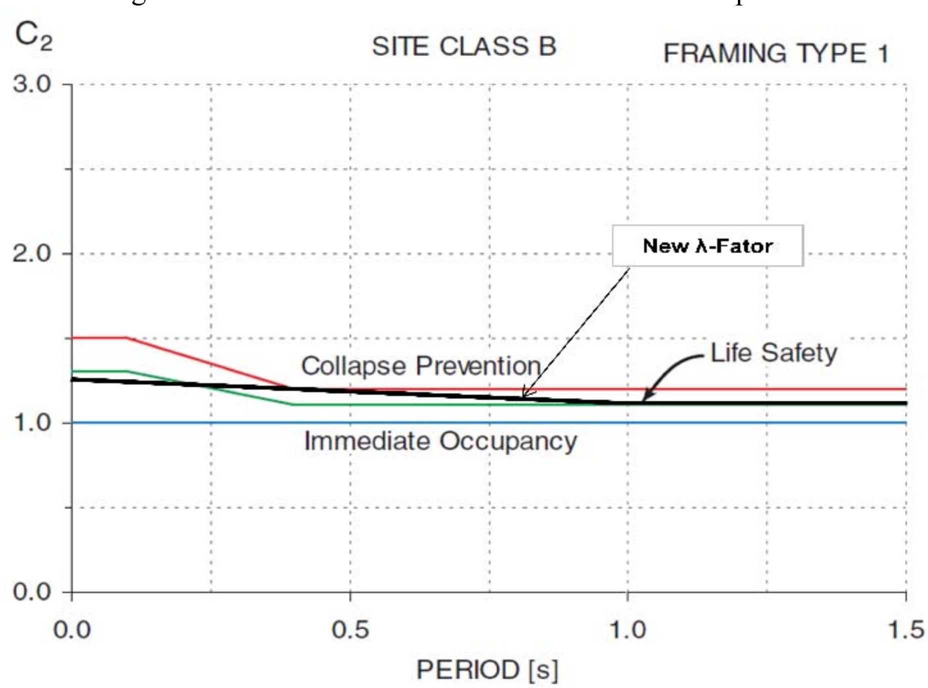

Figure 5.2. Comparison of the New λ-Factor with C_2 values in FEMA 356 (2000)

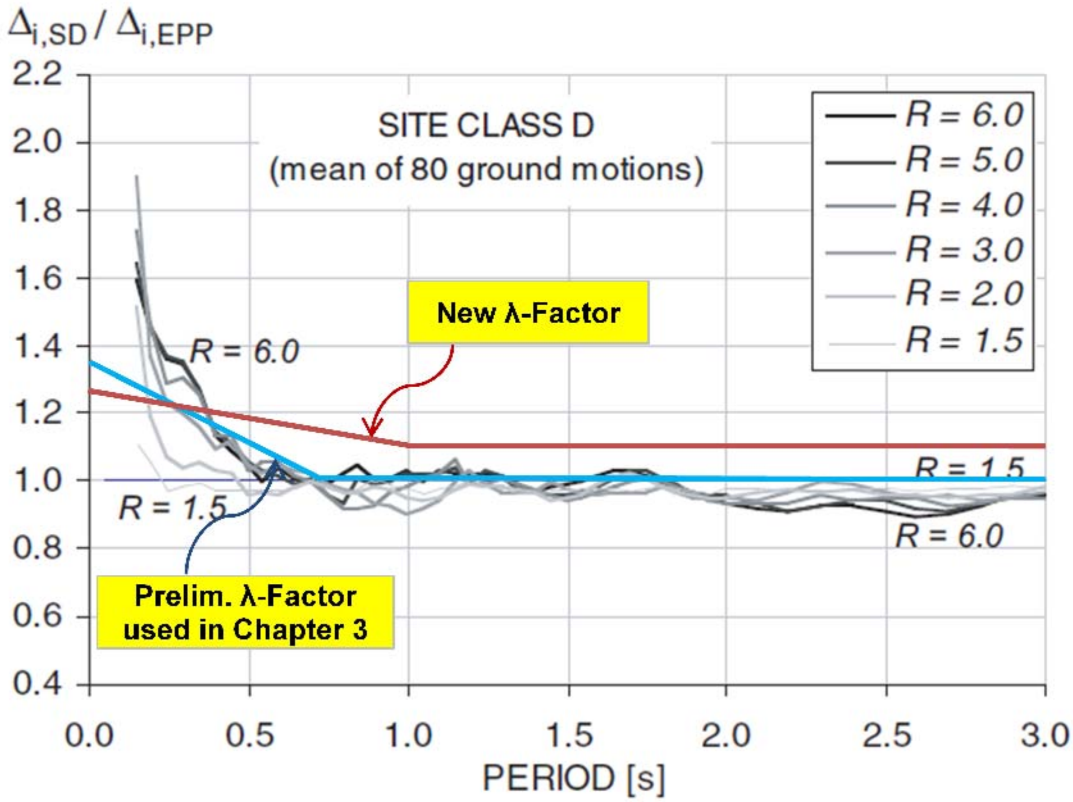

Figure 5.3. New λ-Factor Values for CBF versus Mean Displacement Ratios obtained by Ruiz-Garcia and Miranda (2005)

Table 5.1. New λ-Factor Values as Function of T

$0 \leq T \leq 1.00\,\text{sec}$	$T > 1.00\,\text{sec}$
$\lambda = -0.145T + 1.245$	$\lambda = 1.10$

Calculated *V/W* values by using the new λ-factor are shown and compared with the previous values from Chapter 3 in Figure 5.4 and Tables 5.2 and 5.3. As shown, the percentage increase in the DBS using new λ-factor versus λ-factor in Chapter 3 increases with the period. Considering the case of $k = 0.5$, the DBS for 3-story frame is almost the same with the new λ-factor. DBS increases by 14% for 6-story frame, 32% for 9-story frame, and 25% for 18-story frame.

It should also be mentioned that the DBS for 3 and 6-story frames are almost similar to the previous values as used in Chapter 2.

The Advantages of using this new λ-factor include:

a) Achieving real dual level design for DBE and MCE, meaning for example DBS for DBE level would result in a structure that would satisfy the DBE performance requirements, i.e., targeted drifts, very limited or no brace fracture.

b) When MCE level governs the DBS, that value should be used to satisfy the performance objectives selected for both levels. That has also been found to result in enhanced C.L. against collapse. If one chooses to only satisfy the DBE level requirements, design can be based on DBE base shear alone.

c) Any value of the k factor (for lateral force distribution) between 0.5 and 0.75 can be used. However, it is recommended that for taller frames smaller value be used, which results in smaller drifts in the upper stories.

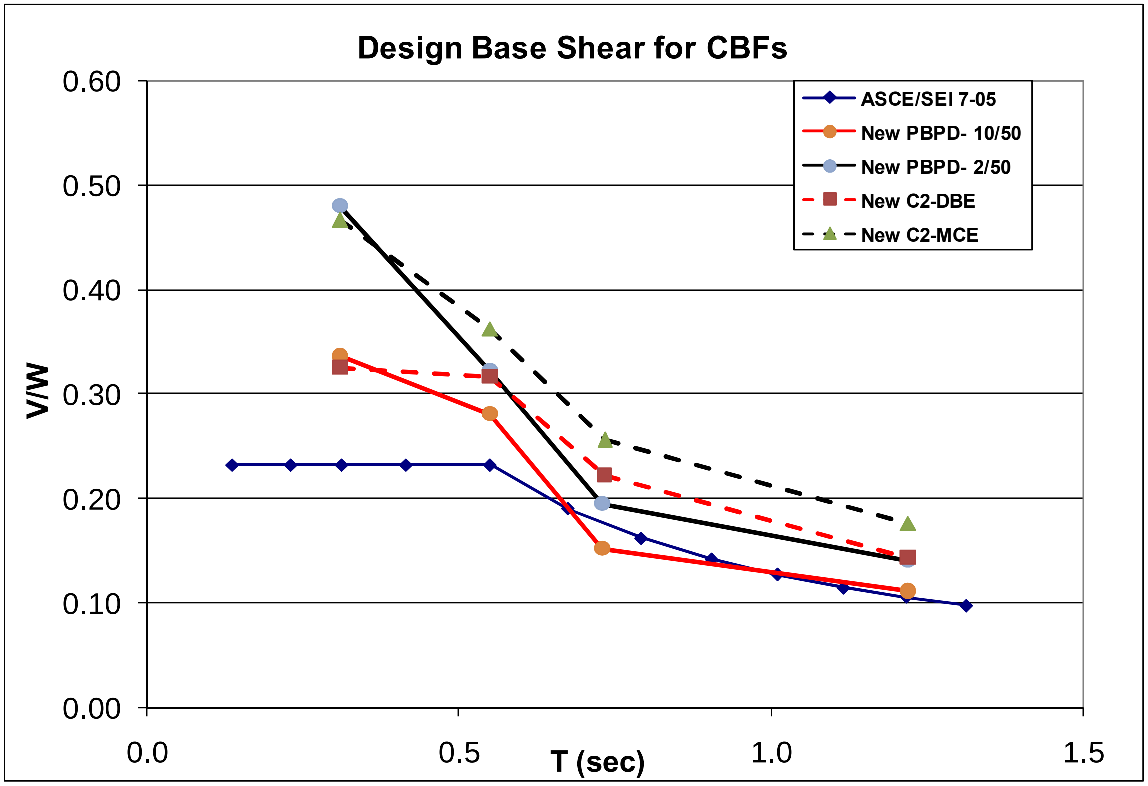

Figure 5.4. Comparison of Design Base Shear from PBPD versus ASCE/SEI 7-05 (values obtained using $k = 0.75$)

Table 5.2. PBPD Design Base Shear using $k = 0.75$

Frame	Period T (sec)	λ-factor in Chap 3		New λ-factor		$(V/W)_{New\,\lambda} / (V/W)_{\lambda\ in\ Chap\,3}$
		DBE	MCE	DBE	MCE	
3V	0.31	0.336	0.480	0.325	0.466	0.97
6V	0.55	0.281	0.322	0.317	0.362	1.12
9V	0.734	0.166	0.195	0.222	0.256	1.31
18V	1.22	0.111	0.141	0.144	0.176	1.25

Table 5.3. PBPD Design Base Shear using $k = 0.50$

Frame	Period T (sec)	λ-factor in Chap 3		New λ-factor		$(V/W)_{New\ \lambda} / (V/W)_{\lambda\ in\ Chap\ 3}$
		DBE	MCE	DBE	MCE	
3V	0.31	0.311	0.447	0.305	0.438	0.98
6V	0.55	0.260	0.298	0.296	0.337	1.13
9V	0.734	0.154	0.180	0.206	0.237	1.32
18V	1.22	0.103	0.130	0.134	0.163	1.25

5.3 Re-Design of the 9-Story CBF (9V-PBPD-B)

The 9-story SAC building with Chevron CBF as described in Chapter 3 is redesigned in this section. The main differences of this design compared with the previous design in Chapter 3 are: (1) Modified DBS is used here by using the new λ-factor; (2) Six braced bays in each direction are used in this design instead of four bays in the 9V-PBPD-A, Figure 5.5.

Value of $k = 0.5$ was used for the lateral distribution parameter. As can be seen from Table 5.3, the MCE design base shear governs the design. Hence, $V/W = 0.237$ for the MCE hazard was used for the design. Lateral design forces, selected sections for the braces, beams and columns along with the fracture life of braces are given in Tables 5.4, 5.5, and 5.6.

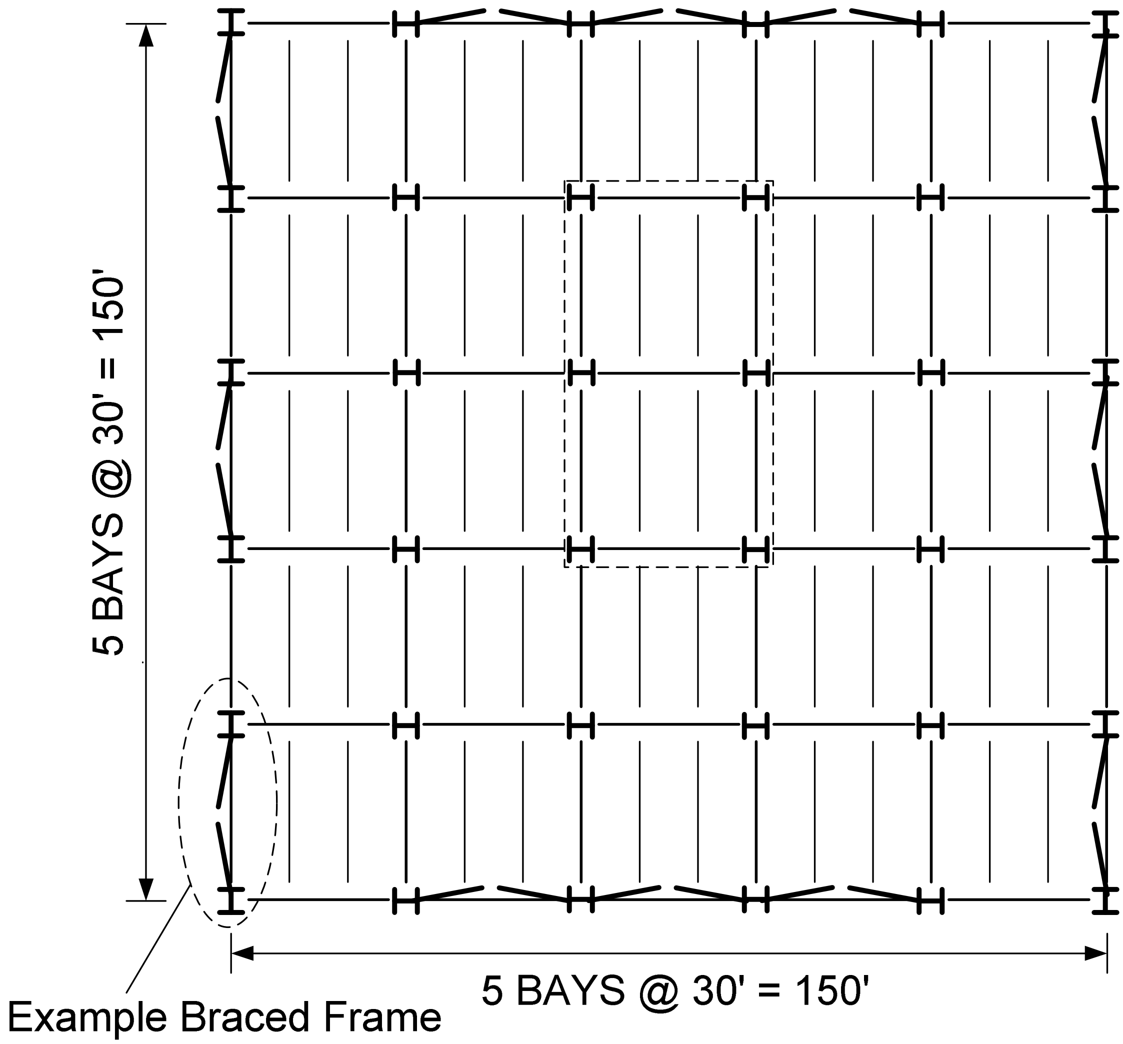

Figure 5.5. Plan View of 9-Story SAC Building: 9V-PBPD-B Design

Table 5.4. Lateral Force Distribution ($k = 0.50$) for 9V-PBPD-B

Floor	F_i (kips)	F_i (kips)	Story Shear (kips)
	Full Structure	one CBF	one CBF
9	1356.9	339.2	339.2
8	513.7	128.4	467.6
7	365.8	91.5	559.1
6	278.2	69.6	628.6
5	215.1	53.8	682.4
4	164.7	41.2	723.6
3	121.7	30.4	754.0
2	83.2	20.8	774.8
1	48.3	12.1	786.9

Table 5.5. Required Brace Strength and Selected Sections for 9V-PBPD-B

Floor	α	***Vi/0.9cos(α)* kips**	**Brace Section**	**Strength $P_y+0.5P_{cr}$**	**Area**	F_{cr}	$0.5P_{cr}$	P_y
9	41	499	**2HSS4×4×5/16**	500	8.2	29.93	122.7	377.2
8	41	688	**2HSS4-1/2x4-1/2x3/8**	683	10.96	32.67	179.0	504.2
7	41	823	**2HSS4-1/2x4-1/2x1/2**	861	13.9	31.83	221.2	639.4
6	41	926	**2HSS5×5×1/2**	997	15.76	34.49	271.8	725.0
5	41	1005	**2HSS5×5×1/2**	997	15.76	34.49	271.8	725.0
4	41	1065	**2HSS6×6×1/2**	1266	19.48	37.97	369.8	896.1
3	41	1110	**2HSS6×6×1/2**	1266	19.48	37.97	369.8	896.1
2	41	1141	**2HSS6×6×1/2**	1266	19.48	37.97	369.8	896.1
1	50	1360	**2HSS6×6×5/8**	1482	23.4	34.68	405.8	1076.4

Table 5.6. Design of Beams for 9V-PBPD-B.

Floor	w_u (k/ft)	R_yP_y	$0.5P_{cr}$	F_h	F_v	P_u	M_u	Beam Section
9	0.95	528.1	122.7	491.2	265.9	245.6	1785.2	**W36x135**
8	1.13	705.8	179.0	667.8	345.6	333.9	2310.0	**W40x167**
7	1.13	895.2	221.2	842.6	442.1	421.3	2925.4	**W40x199**
6	1.13	1014.9	271.8	971.1	487.6	485.5	3215.1	**W40x215**
5	1.13	1014.9	271.8	971.1	487.6	485.5	3215.1	**W40x215**
4	1.13	1254.5	369.8	1225.9	580.4	612.9	3807.0	**W40x249**
3	1.13	1254.5	369.8	1225.9	580.4	612.9	3807.0	**W40x249**
2	1.13	1254.5	369.8	1225.9	580.4	612.9	3807.0	**W40x249**
1	1.21	1507.0	405.8	1229.5	843.5	614.7	5492.0	**W40x324**

Table 5.7. Design of Columns for 9V-PBPD-B

Floor	$P_{trans.}$	P_{beam}	$0.5P_{cr}Sin\ \alpha$	$0.5F_v$	P_u	P_u (cumulative)	Column Section
9	32.88	28.5	0	133	194	194	**W14x109**
8	37.56	33.9	81	173	325	519	**W14x109**
7	37.56	33.9	117	221	410	929	**W14x109**
6	37.56	33.9	145	244	460	1390	**W14x211**
5	37.56	33.9	178	244	494	1883	**W14x211**
4	37.56	33.9	178	290	540	2423	**W14x211**
3	37.56	33.9	243	290	604	3027	**W14x398**
2	37.56	33.9	243	290	604	3632	**W14x398**
1	37.56	36.3	243	422	738	4370	**W14x398**

5.4 Design of the 9-Story CBF with Split-X Configuration (9X-PBPD-B)

In this section, the effect of using Spli-X brace configuration on seismic performance and also C.L. of the 9-story CBF is investigated. Other design assumptions such as pin ended beams, fixed base, and use of double HSS for braces are the same as before.

The design parameters are kept the same for this configuration as for chevron braced frame in the previous section. Therefore, the same MCE design base shear of $V/W=0.237$ applies and is used for this design as well. The same bracing members are used since the story shears are the same as the chevron configuration. However, much smaller unbalanced force on the beams, and therefore much lighter beam sections (more reasonable design) are obtained for the Split-X frame. Column sections remain about the same as in the Chevron design. The free-body diagrams used for capacity design of beams and columns are shown in Figure 5.6. Expected yield forces, R_yP_y, and post-buckling strength of braces, $0.5P_{cr}$, are considered in tension and compression, respectively, to obtain the design forces for beams and columns. P_L and P_R represent lateral forces due to other sources, such as frame action, inertia forces, etc. Those forces were assumed to be zero when designing beam case B. The same assumption was used for columns and only axial forces due to truss action were used for the design.

Important design parameters of different 9-story PBPD frames studied herein are given in Table 5.8.

Beam and column sections for the design with Split-X configuration, 9X-PBPD-B, are shown in Tables 5.9 and 5.10, respectively. It can be seen that the beams in two different designs for Split-X configuration are significantly lighter than those of Chevron configuration. The column sections are almost the same, except in the 4th story where the Split-X design needed W14x398 based on capacity design requirements. The difference between 9X-PBPD-B and 9X-PBPD-B1 is just in their beam sizes, as will be discussed later in this section.

Generally, the performance of 9X-PBPD-B was found to be somewhat more stable than the Chevron design under MCE ground motions (e.g. 9V-PBPD-B frame showed dynamic instability under LA21 but 9X-PBPD-B frame did not.

The Split-X configuration (9X-PBPD-B frame) mainly involves axial behavior of all members, but the Chevron frame has significant flexural component, especially in the beams after buckling of the compression braces. That is why large beam sizes are needed in the Chevron frame.

As mentioned earlier, beams sizes in the Split-X configuration are considerably smaller compared to the Chevron configuration, making the Split-X frame lighter in weight. However, local inelastic activity, such as large beam plastic hinge rotation, was observed in the response of the 9X-PBPD-B frame, especially under MCE ground motions. Further investigation showed that it was due to small axial design forces for the beams. Nevertheless, local inelastic activity in the beams did not have much effect on the global behavior of the frame.

Larger beam sizes with higher strength and stiffness are needed to prevent or minimize such local inelastic activity. As shown in Table 5.9, W18x175 beam sections were used in the revised design at all floor levels except at the roof level (W36x135), and the 1st floor beam which is W24x176 (due to larger vertical unbalanced forces). Use of those beam sizes successfully eliminated the local inelastic activity. The 9X-PBPD-B1 design was used for further evaluation. As shown in Table 5.10, the column sections are almost similar for the Chevron and Split-X configurations.

Larger unbalance forces on the beams than those obtained by capacity design considering free-body diagrams of Figure 5.6 were observed in the results from time history analyses. These unbalanced forces could cause plastic hinges at the mid-span of the beams in case B. However, formation of these plastic hinges did not affect the global drift response of the structure, as also observed by Lacerte and Tremblay (2006).

The results also imply that the assumed initial ultimate force pattern for capacity design of beams was unconservative. However, it should be mentioned that floor slabs, when present, do provide significant contribution to resist in-plane beam forces. Such contribution was neglected in this study. Final beam sections for the 9X-PBPD-B1 frame was done through some trial and error. More representative estimate of beam design forces in the Split-X configuration of CBF warrants further study.

Table 5.8. Different Designs/Models used for 9-story PBPD CBF

9-Story CBF Designs	**DBS**	**Brace Configuration**	N_f	**Notes**
9V-PBPD-A*	Based on λ-factor in Chapter 3	Chevron	regular	
9V-PBPD-B	Based on New λ-factor	Chevron	regular	
9V-PBPD-B-Nf	Based on New λ-factor	Chevron	increased	Same as 9V-PBPD-B, only with increased N_f
9X-PBPD-B	Based on New λ-factor	Split-X	regular	Small beam sizes, showed local instability in beams (Table 5.9)
9X-PBPD-B1	Based on New λ-factor	Split-X	regular	Modified: only beam sized increased to W18x175 (Table 5.9)
9X-PBPD-B1-Nf	Based on New λ-factor	Split-X	increased	Same as 9V-PBPD-B, only with increased N_f

* Suffix A at the end of model designation indicates that design base shear is obtained by using the preliminary λ-factor in Chapter 3, whereas B indicates that the design base shear is obtained using new λ-factor suggested in Chapter 5.

Table 5.9. Beam Sections for Different Designs

Floor Level	**Beam Sections**		
	9V-PBPD-B	**9X-PBPD-B**	**9X-PBPD-B1**
Roof	W36x135	W36x135	W36x135
8	W40x167	W18x65	W18x175
7	W40x199	W27x84	W18x175
6	W40x215	W18x65	W18x175
5	W40x215	W18x65	W18x175
4	W40x249	W18x65	W18x175
3	W40x249	W18x65	W18x175
2	W40x249	W18x65	W18x175
1	W40x324	W24x176	W24x176

Table 5.10. Column Sections for Different Designs

Story	**Column Sections**		
	9V-PBPD-B	**9X-PBPD-B**	**9X-PBPD-B1**
9	W14x109	W14x109	W14x109
8	W14x109	W14x109	W14x109
7	W14x109	W14x109	W14x109
6	W14x211	W14x211	W14x211
5	W14x211	W14x211	W14x211
4	W14x211	W14x398	W14x398
3	W14x398	W14x398	W14x398
2	W14x398	W14x398	W14x398
1	W14x398	W14x398	W14x398

Table 5.11. Different Fracture Life, N_f, Values Used

9-story CBF Model / Story	9V-PBPD-B 9X-PBPD-B1 (regular N_f)	9V-PBPD-B-Nf 9X-PBPD-B1-Nf (increased N_f)
9	152	237
8	157	237
7	329	329
6	224	224
5	224	224
4	132	227
3	132	227
2	132	227
1	245	245

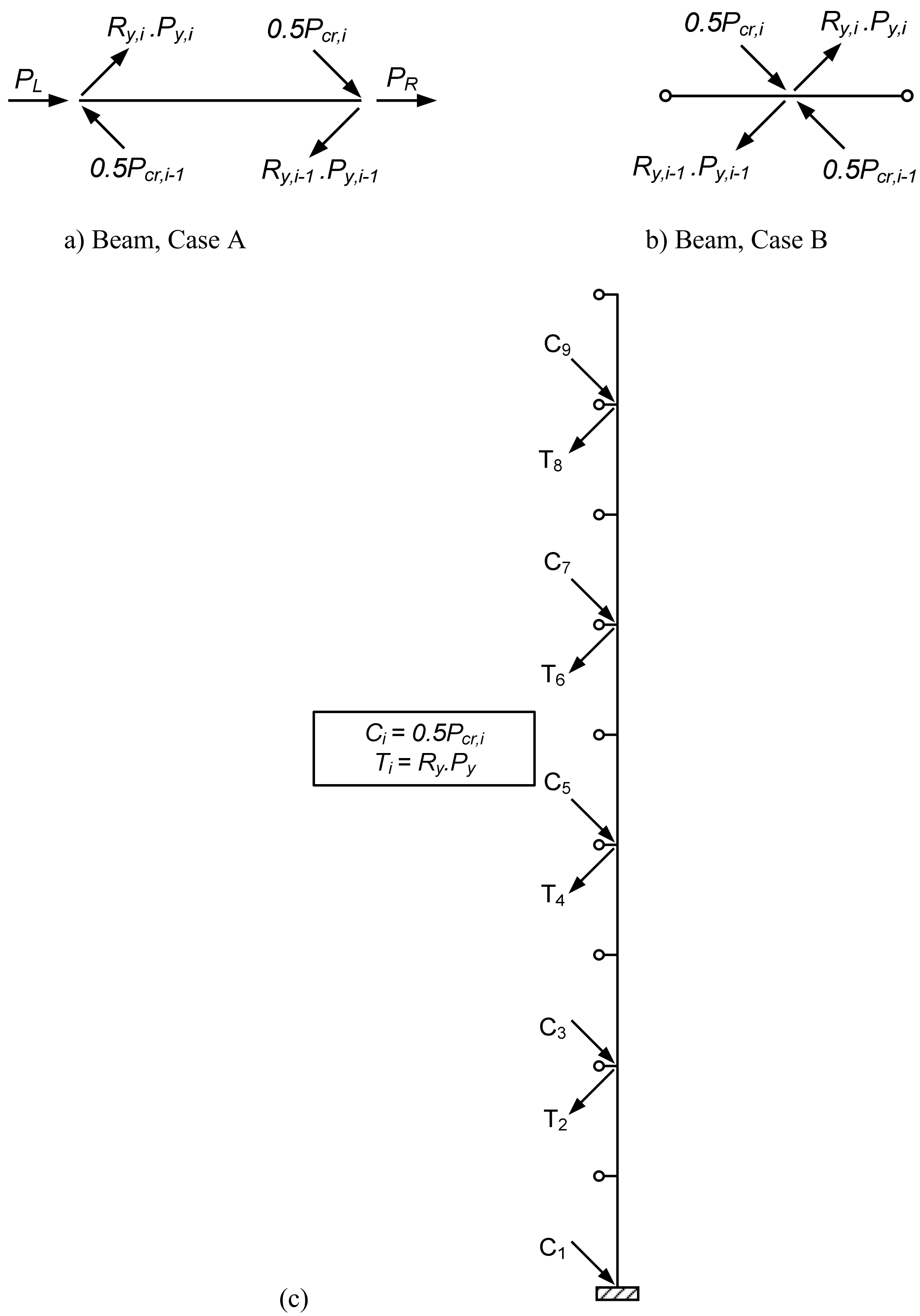

Figure 5.6. Capacity Design of Beams and Column in Split-X Configuration: (a) Beam, Case A; (b) Beam, Case B; and (c) Column Tree.

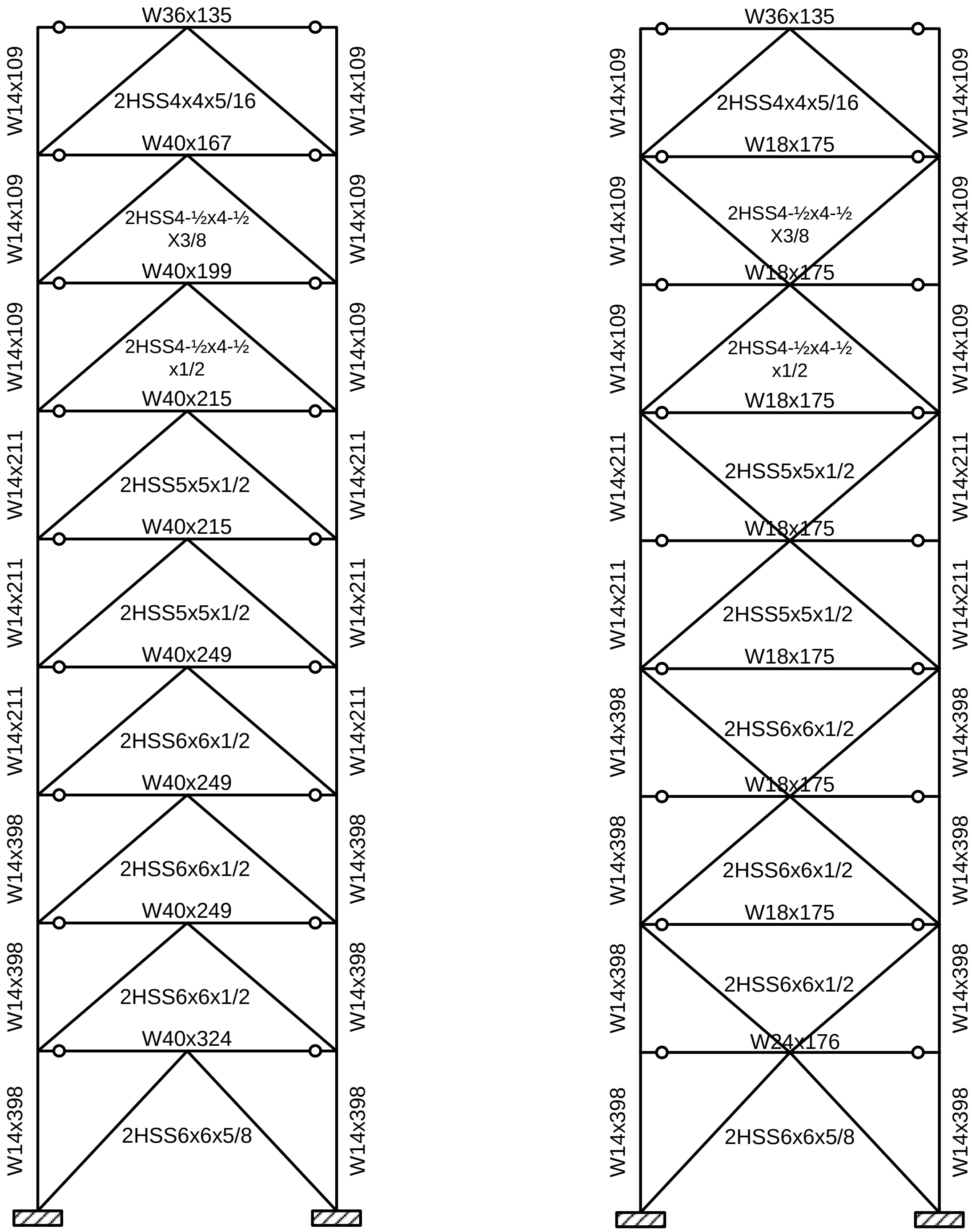

9V-PBPD-B **9X-PBPD-B1**

(a) (b)

Figure 5.7. Member Sections for 9-Story CBF Designed by PBPD: (a) Chevron Configuration; and (b) Split-X Configuration.

5.5 Evaluation of Seismic Performance

In this section, performance of the 9V-PBPD-B and 9X-PBPD-B1 frames (designed by using the new λ-factor) under DBE and MCE level SAC LA ground motions is evaluated. In addition, the confidence level of these frames are calculated and compared with that of the previous design in Chapter 3.

SNAP-2DX software was used as was done in Chapter 3 and 4. The same modeling assumptions used for 9V-PBPD-A were also made for these frames, which include consideration of gravity and P-Delta column as well as beam-end releases and eccentricities.

In the following Sections 5.5.1 the time-history response and maximum story drifts of the new Chevron and Split-X braced frames are shown. The confidence levels against collapse of these new frames are then evaluated by using the FEMA 351 (2000b) procedure in Section 5.5.2.

To evaluate the effect of increasing the fracture life, N_f, on dynamic response as well as confidence level, the N_f values for 9V-PBPD-B and 9X-PBPD-B1 were increased to the levels greater than 200 for all brace sections. The corresponding models are called 9V-PBPD-B-Nf and 9X-PBPD-B1-Nf, respectively. The results with increased values of N_f are discussed in Section 5.5.3.

5.5.1 *Performance Comparison of 9V-PBPD-B and 9X-PBPD-B1 vs. 9V-PBPD-A*

Maximum story drifts under SAC LA ground motions for the redesigned 9V-PBPD-B and 9X-PBPD-B1 frames based on the new λ-factor are shown in Figures 5.8 and 5.9, respectively, for DBE and MCE ground motions.

The median drift values can also be seen in Figure 5.10. The median story drifts under DBE level are close to each other for all three frames, with 9V-PBPD-B and 9X-PBPD-B1 showing smaller drifts at upper levels. The median drifts fall well within the target drift limit used in the design. The 9V-PBPD-B and 9X-PBPD-B1 frames show smaller median drifts, especially at lower levels. This shows that the increase in design base shear resulted in lower drift demands for these designs under MCE ground motions. Also, 9X-PBPD-B1 frame shows somewhat more uniform distribution over the height.

The number of brace fractures were almost the same for all three models (9V-PBPD-A, 9V-PBPD-B, and 9X-PBPD-B1) under both DBE and MCE ground motions. However, models with increased N_f, 9V-PBPD-B-Nf and 9X-PBPD-B1-Nf, showed much less and also delayed brace fractures compared to their corresponding models with original N_f values. Therefore, the increase in design base shear did not have much effect on brace fractures. Such fractures, however, could be prevented by using a minimum N_f of 200 for taller CBF structures, instead of 100 as used earlier in Chapter 2.

The ground motions under which each design showed collapse are shown in Table 5.12. As can be seen, the Split-X configuration shows more stable behavior. In addition, the 9V-PBPD-B model designed by using the new λ-factor shows somewhat more stable response compared with 9V-PBPD-A frame designed in Chapter 3 based on original λ-factor.

It can be seen that the collapse of 9V-PBPD-B was due to brace fracture since this model did not show collapse when N_f was increased. However, under LA38, the increase in N_f value did not affect the time at which the collapses occurred, indicating that the collapses were not caused by brace fractures.

Figure 5.11 shows the 3rd story drift time-history response of 9V-PBPD-B frame under LA28. Such response can be considered as the typical response of the 9-story frames designed by PBPD under those ground motions that cause some brace fractures. Due to near-field nature of the MC level SAC LA ground motions, most of the earthquake energy is transferred to the frames through large velocity pulses in a rather short time interval in the early stages of the record. Maximum story drifts of PBPD 9-story frames occur mostly under such velocity pulses, except for 9V-PBPD-B model under LA21 which showed collapse due to extensive brace fracture (Figure 5.12.a). Brace fractures, which are due to low-cycle fatigue, occurred at later stages of the ground motion. As a result, even for ground motions under which some brace fractures were observed, the maximum story drifts under MCE ground motions had occurred before the fracture of braces started.

Figure 5.12.a shows the exception to the trend mentioned above. In this case, the peak story drift occurred at about 10 seconds past the start of the ground motion. However, at about t = 45 seconds, the frame became unstable due to excessive brace fractures and eventually collapsed after formation of soft stories.

Figure 5.12.b shows the 4th story drift versus time for the same frame as in 5.12.a, but with increased N_f values in stories 2,3,4, and 5 (model 9V-PBPD-B-Nf). As can be seen, this model survived under LA21 even though there were brace fractures. The increase in N_f delayed fracture of braces 7 and 8 for about 7 seconds, which was enough in this case for the structure to survive the earthquake.

Figure 5.12.c shows 4th story drift versus time response of the Split-X configuration model 9X-PBPD-B1 (with original N_f values) under LA21. As shown, only minor brace fractures occurred at the end of the ground motion.

Table 5.12. Collapse Cases under Time History Analyses

Model	9V-PBPD-A	9V-PBPD-B	9V-PBPD-B-Nf	9X-PBPD-B1	9X-PBPD-B1-Nf
Ground Motions caused Collapse	LA27 (t=46.8sec) LA38 (t=12.7sec)	LA21 (t=51.3sec) LA38 (t=36.7sec)	LA38 (t=36.7sec)	LA38 (t=50.2sec)	LA38 (t=50.2sec)

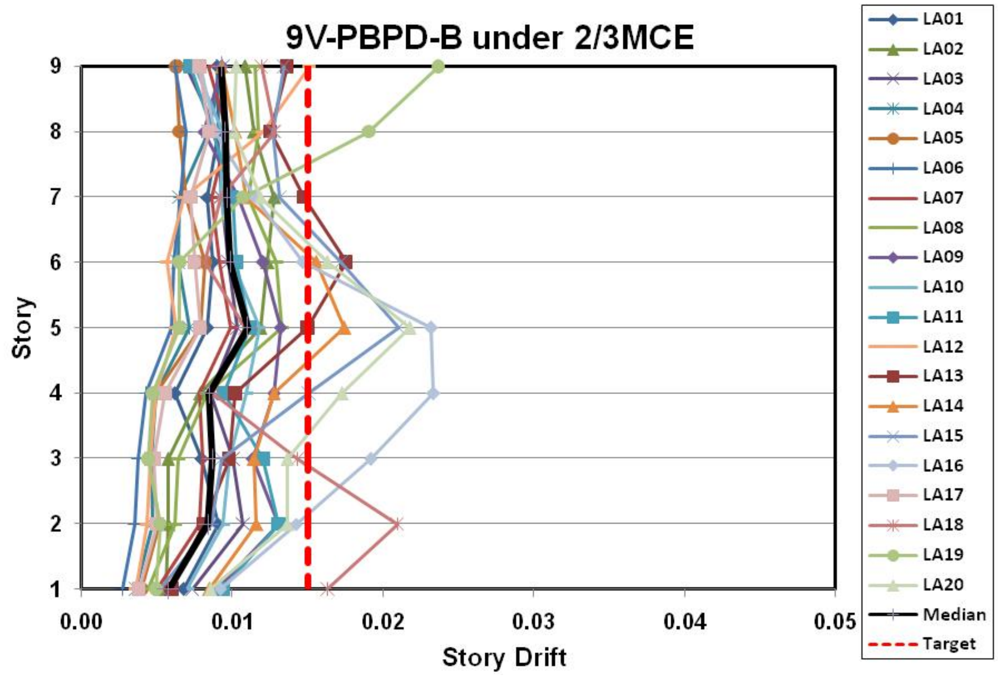

a) 9V-PBPD-B

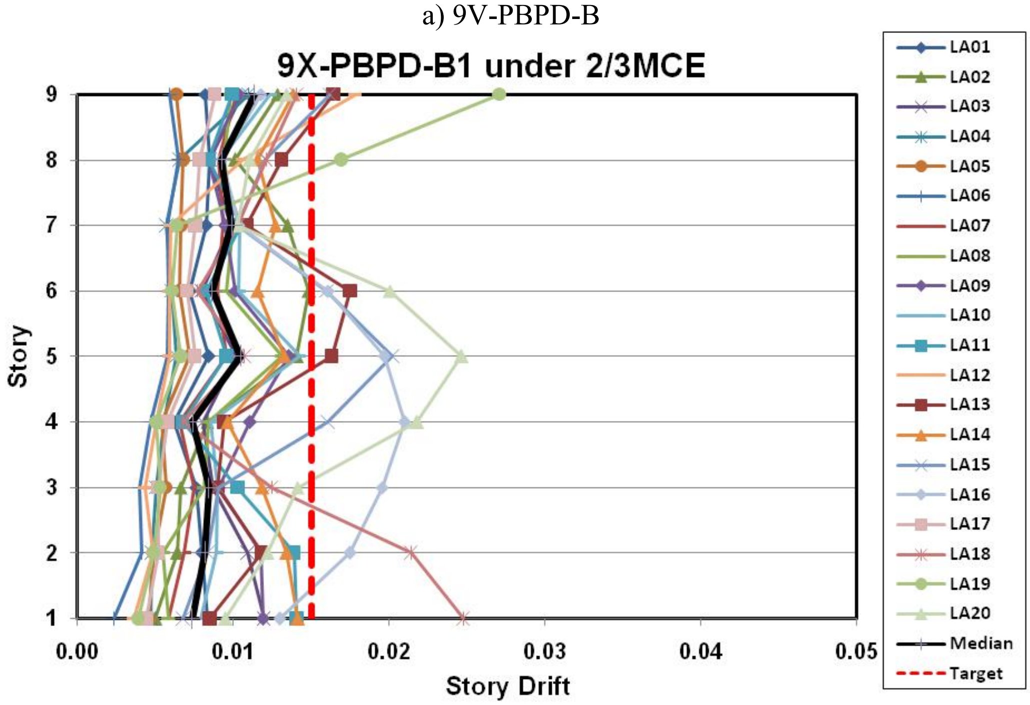

b) 9X-PBPD-B1

Figure 5.8. Maximum Story Drifts under SAC DBE Ground Motions

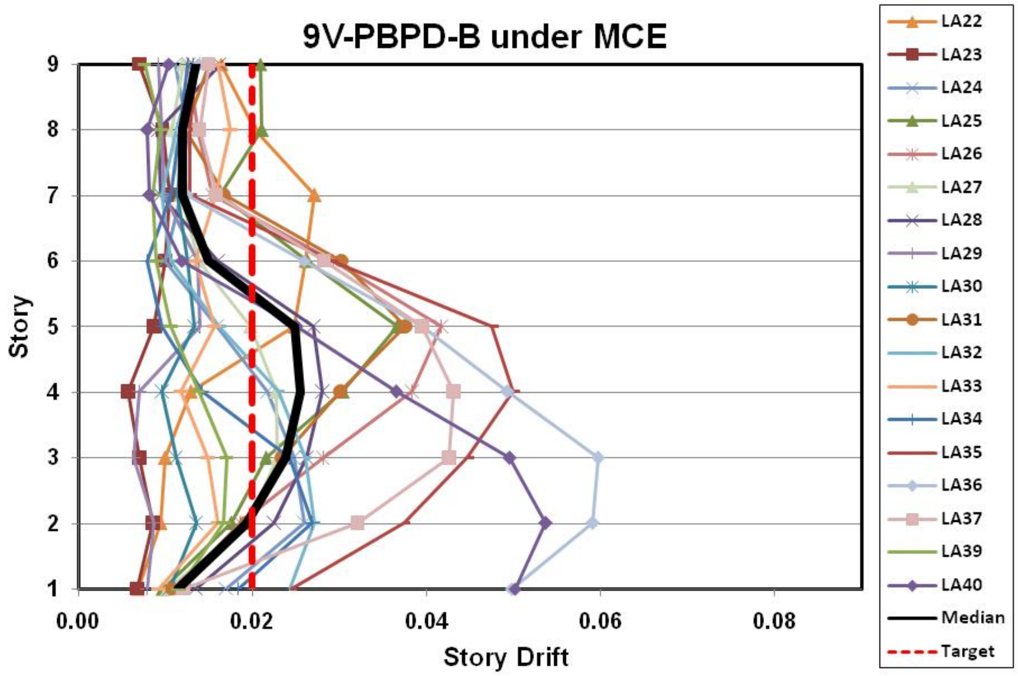

a) 9V-PBPD-B

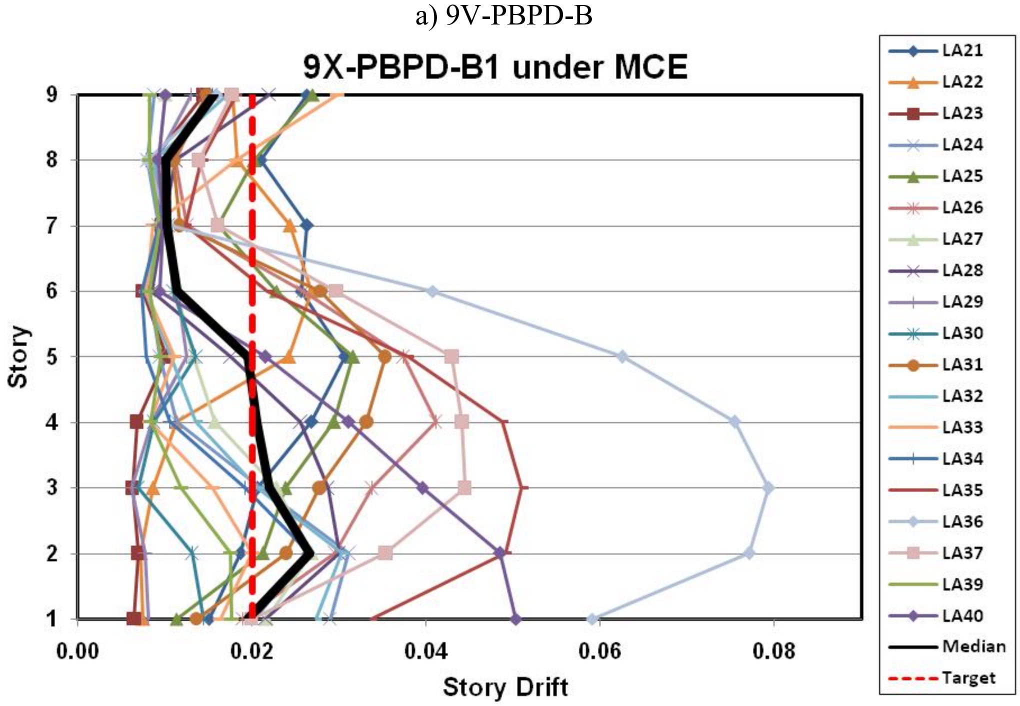

b) 9X-PBPD-B1

Figure 5.9. Story Drifts under SAC MCE Ground Motions

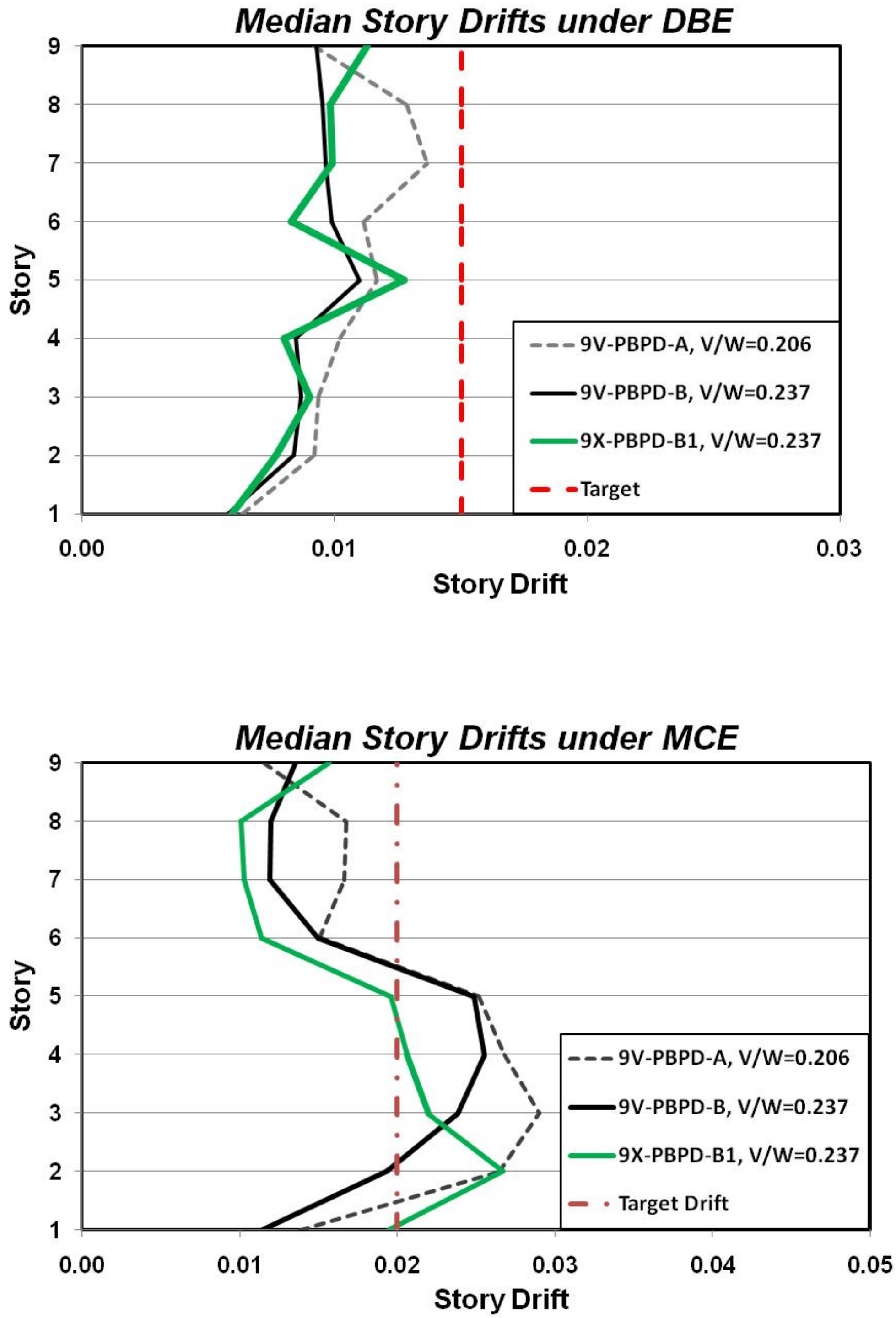

Figure 5.10. Median Story Drifts for Different Designs under DBE and MCE Ground Motions

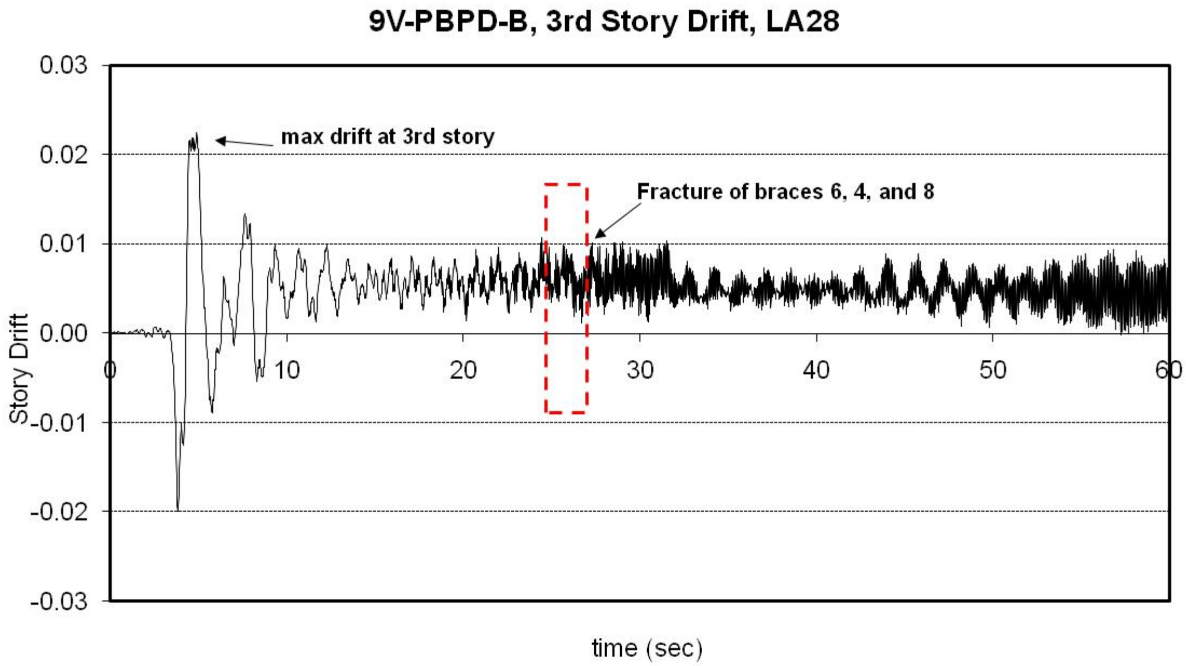

Figure 5.11. Story Drift vs. Time for 3rd Story and Brace Fractures for 9V-PBPD-B under LA28

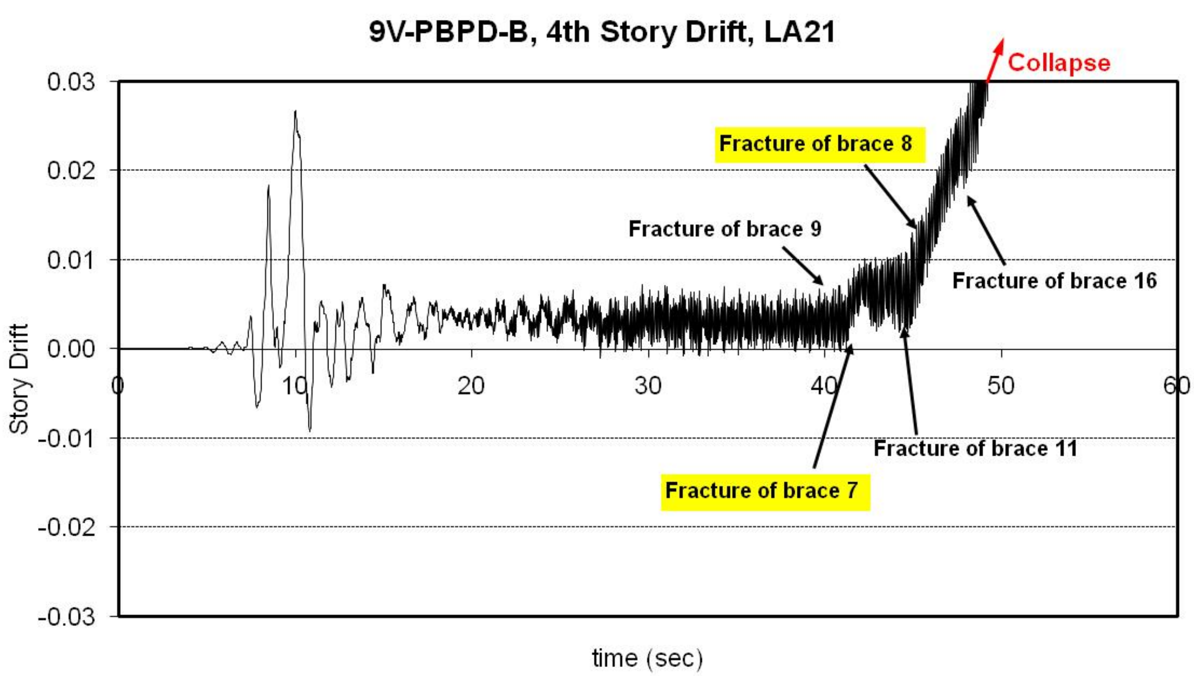

(a)

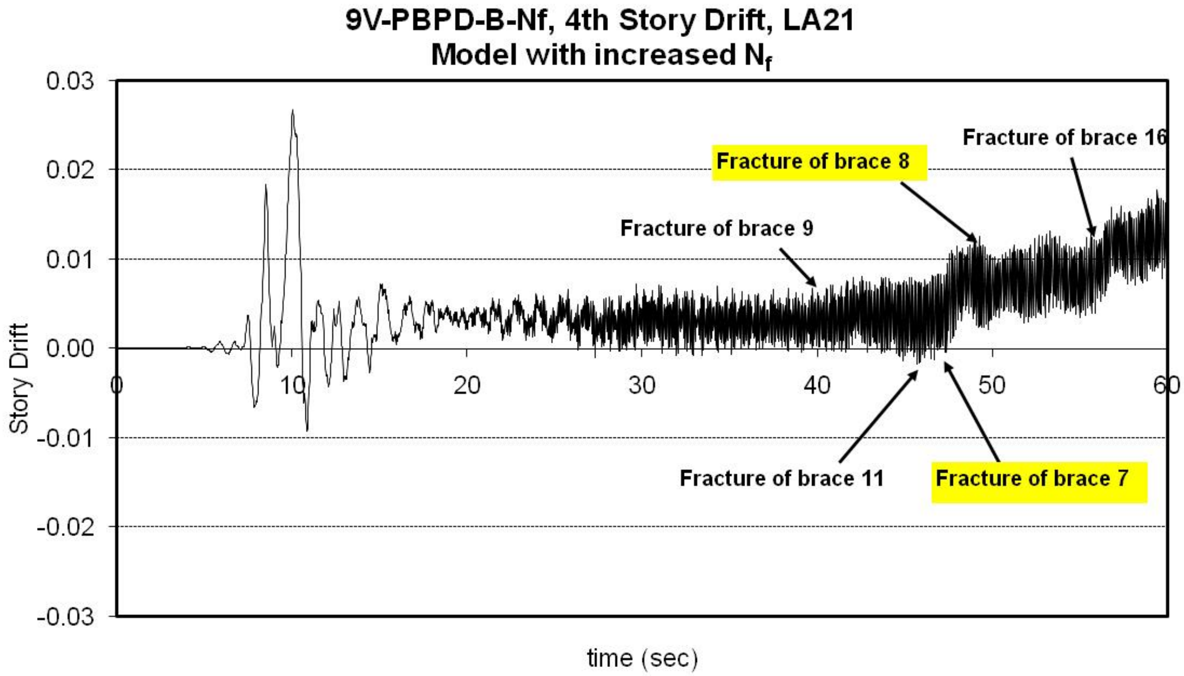

(b)

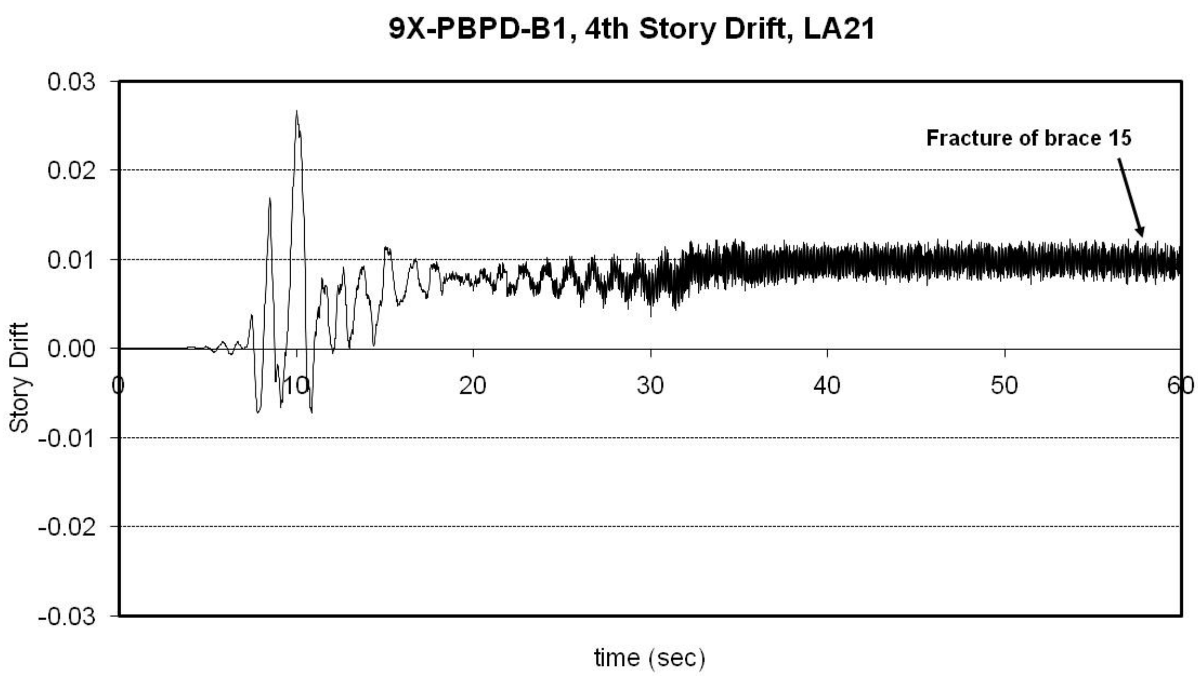

(c)

Figure 5.12. 4th Story Drift vs. Time: (a) 9V-PBPD-B; (b) 9V-PBPD-Nf; and (c) 9X-PBPS-B1

5.5.2 Confidence Level Evaluation of 9V-PBPD-B and 9X-PBPD-B1 Frames

The confidence levels of the 9V-PBPD-B and 9X-PBPD-B1 frames were evaluated by following the FEMA 351 (2000b) procedure as described in Chapter 4. Tables 5.12 to 5.14 show the parameters used in confidence level evaluation. Figure 5.13 shows the IDA curves for these two designs under MCE set of SAC LA ground motions. It can be seen from Table 5.14 that the new designed frames show improvement in confidence level against collapse. The confidence level for 9V-PBPD-B came out to be 68.6% versus 52.1% of the original 9V-PBPD-A frame (Chapter 4). This 16.5% increase in the confidence level comes mainly from the increase in the design base shear using new λ-factor.

It can also be seen that the brace configuration has significant effect on the confidence level. The 9X-PBPD-B1 frame has same brace sections as 9V-PBPD-B, but only with different configuration. The confidence level of the Split-X frame is about 10% better than the corresponding Chevron frame (77.4% versus 68.6%). This was mainly due to smaller scatter in drift demand for the Split-X frame under MCE ground motions. It should be noted that the beams sizes in the Split-X frame are considerably smaller compared to those of Chevron frame, but still the Split-X design shows better confidence level.

5.5.3 *The Effect of Increasing N_f on the Confidence Level*

It was seen that the brace fractures, e.g., under LA21 ground motion led to instability or quite large story drifts. Thus far, main focus of the study presented in this chapter was on evaluation of the effect of increasing the design base shear on the seismic performance of the 9-story frames. In this section, an increased level of N_f for 9V-PBPD-B and 9X-PBPD-B1 designs is considered in order to minimize the adverse effects of lower N_f on the performance and confidence level of these frames. This can be achieved by increasing N_f to values more than 200 (for braces with N_f smaller than 200) without any change in other properties of the model. The increased values of N_f are shown in Table 5.11 which shows increase in stories 2, 3, 4, 8, and 9. Such increases in fracture life for hollow structural sections can be achieved by various methods as mentioned in section C13.2d of AISC Seismic Provisions (AISC, 2005a). Filling with plain concrete can be used as an effective way of reducing the severity of local buckling and delay fractures hollow tubular braces (Liu and Goel, 1988; Lee and Goel, 1987). Goel and Lee (1992) developed an empirical equation to estimate the effective width-to-thickness ratio of concrete-filled HSS braces. As another method, longitudinal stiffeners such as rib plates or small angle sections in a hat configuration can be used on tube walls (Liu and Goel, 1987).

Therefore, the N_f values for braces in 9V-PBPD-B and 9X-PBPD-B1 frames were increased to over 200 (stories 2, 3, 4, 8, 9). As shown in Table 5.8, these new models are designated 9V-PBPD-B-Nf and 9X-PBPD-B1-Nf, respectively. The time-history response as well as confidence level analysis were carried out for these frame models as well.

The maximum story drifts for the models with increased N_f were found to be essentially the same as the models with regular N_f, except for 9V-PBPD-B model under LA21 ground motions. 9V-PBPD-B frame collapsed under LA21, but the increased N_f model 9V-PBPD-B-Nf survived without collapse with about 3.4% maximum story drift. For other ground motions, the maximum story drifts did not change with increase in N_f. However, brace fractures were delayed by about 4 to 14 seconds (depending on ground motion), and in some cases the fractures were totally eliminated in the increased N_f models.

The values of confidence level are shown in Table 5.13 to 5.15. Also, Figure 5.15 shows the IDA curves for these two models under MCE set of SAC LA ground motions. As can be seen, the increase in N_f value increases the confidence level of 9V-PBPD-B by about 11% from 68.6% tp 79.4%. The main reason for this increase was that 9V-PBPD-B-Nf model showed smaller scatter in drift demand compared to 9V-PBPD, even though the two models had the same median drift demand. For the Split-X configuration, both the drift demand and its scatter essentially remained unchanged with increase in N_f. However, 9X-PBPD-B1-Nf model showed slightly larger drift capacity which resulted in somewhat higher confidence level. As can be seen from Table 5.15, confidence level increased 5.3% (from 77.4% to 82.7%) by increasing N_f to values more than 200 for the Split-X configuration.

5.6 Summary and Conclusions

The main objective of the study presented in this chapter was to improve the confidence level against collapse (C.L.) for the 9-story CBF against collapse. Several modifications were suggested. The first modification was in the design base shear (DBS) calculation. A slightly larger λ-factor was suggested for mid to high-rise CBF frames to offset the detrimental effect of P-Delta overturning forces in the calculation of DBS.

The effect of using Split-X (two story X bracing) configuration on seismic performance and C.L. of CBF was also studied. In addition, the effect of increasing brace fracture life, N_f, on seismic performance and C.L. was evaluated.

The main conclusions from the results presented in this chapter are:

1- Higher values of design base shear (DBS) for 9-story (and taller) CBF were obtained using the proposed new λ-factor in PBPD method. This new λ-factor results in larger design base shear for mid to high-rise CBF structures.

2- The 9-story Chevron CBF design based on the new DBS showed smaller story drifts under both DBE (10%/50 yrs) and MCE (2%/50 yrs) ground motions compared to the 9V-PBPD-A frame designed in Chapter 3.

3- Higher levels of confidence level (C.L.) against collapse were obtained using the new DBS for Chevron configuration. The C.L. of 52% obtained in Chapter 4 for 9V-PBPD-A increased to 68.6% by using the new DBS in 9V-PBPD-B.

4- Improvement was seen in C.L. of the Chevron frame designed by using increased N_f (of more than 200) for fracture life of the braces. This increase in N_f resulted in increase of C.L. of the 9-stoy Chevron CBF from 68.6% to 79.4% (about 11%).

5- It was shown that C.L. of 9-story CBF improved by only changing the brace configuration to Split-X. The C.L. increased from 68.6% to 77.4% (about 10%) by using Split-X instead of Chevron configuration. The same brace sections were used. However, much lighter beams are needed in the Split-X configuration. The C.L. obtained for the Split-X design with original N_f values was almost equal to that of Chevron design with increased N_f.

6- Increasing the design base shear did not have much effect on drift capacity of the 9-story CBF frames obtained from IDA. However, larger design base shear resulted in lower drift demands with reduced scatter under MCE ground motions which basically translates into higher confidence level.

7- Increase in design base shear based on the new λ-factor was seen to be the main factor in reducing the story drifts under MCE level ground motions. Better controlled drift demand results in higher confidence level.

8- Increase in N_f value (brace fracture life factor) did not have significant effect on drift response under MCE level SAC LA ground motions since the maximum story drifts generally occur at the early stages for such near-field ground motions.

Table 5.13. Analysis Uncertainty Parameters

Study Frames	C_B	β_{DU}	γ_a
3V-NEHRP	1.0	0.15	1.03
3V-PBPD	1.0	0.15	1.03
6V-NEHRP	1.0	0.20	1.06
6V-PBPD	1.0	0.20	1.06
9V-PBPD	1.0	0.20	1.06

Table 55.14. Randomness and Uncertainty Parameters

Frame	β_{RC}	ϕ_{RC}	β_{UC}	ϕ_{UC}	β_{RD}	β_{UT}
3V-NEHRP	0.537	0.649	0.15	0.967	0.890	0.30
3V-PBPD	0.394	0.793	0.15	0.967	0.545	0.30
6V-NEHRP	0.435	0.753	0.20	0.942	0.663	0.35
6V-PBPD	0.412	0.775	0.20	0.942	0.708	0.35
9V-PBPD-A	0.309	0.867	0.20	0.942	0.515	0.35
9V-PBPD-B	0.266	0.899	0.20	0.942	0.622	0.35
9V-PBPD-B-Nf	0.258	0.905	0.20	0.942	0.559	0.35
9X-PBPD12-B1	0.226	0.927	0.20	0.942	0.522	0.35
9X-PBPD12-B1-Nf	0.225	0.927	0.20	0.942	0.498	0.35

*β_{RC}: standard deviation of natural logs of drift capacities due to randomness
*β_{UC}: standard deviation of natural logs of drift capacities due to uncertainty
*β_{RD}: standard deviation of natural logs of drift demands due to randomness
*β_{UT}: vector sum of logarithmic standard deviations for both demand and capacity considering all sources of uncertainty

Table 5.15. Summary of Confidence Level Assessment for 3-Story, 6-Story, and 9-Story CBFs

Frame	Median Drift Capacity (from IDA), C	Capacity factor, ϕ^*	Median Drift Demand, D	Demand factors		Confidence Parameter $\lambda = \frac{\gamma \cdot \gamma_a \cdot D}{\phi \cdot C}$	Confidence Level (%)
				γ^*	$\gamma_a{}^*$		
3V-NEHRP	0.064	0.628	0.068	3.37	1.06	6.04	<< 1%
3V-PBPD	0.078	0.766	0.015	1.56	1.06	0.41	> 99.9%
6V-NEHRP	0.065	0.709	0.035	1.93	1.06	1.55	23.3%
6V-PBPD	0.100	0.730	0.027	2.12	1.06	0.82	86.2%
9V-PBPD-A	0.062	0.816	0.0376	1.49	1.06	1.180	52.1%
9V-PBPD-B	0.061	0.847	0.0276	1.79	1.06	1.015	68.6%
9V-PBPD-B-Nf	0.061	0.852	0.0276	1.60	1.06	0.902	79.4%
9X-PBPD-B1	0.0604	0.873	0.0305	1.51	1.06	0.924	77.4%
9X-PBPD-B1- Nf	0.0646	0.873	0.0305	1.51	1.06	0.832	82.7%

* ϕ: resistance factor that accounts for the randomness and uncertainty in estimation of structural capacity
*γ: demand uncertainty factor;
*γ_a: analysis uncertainty factor

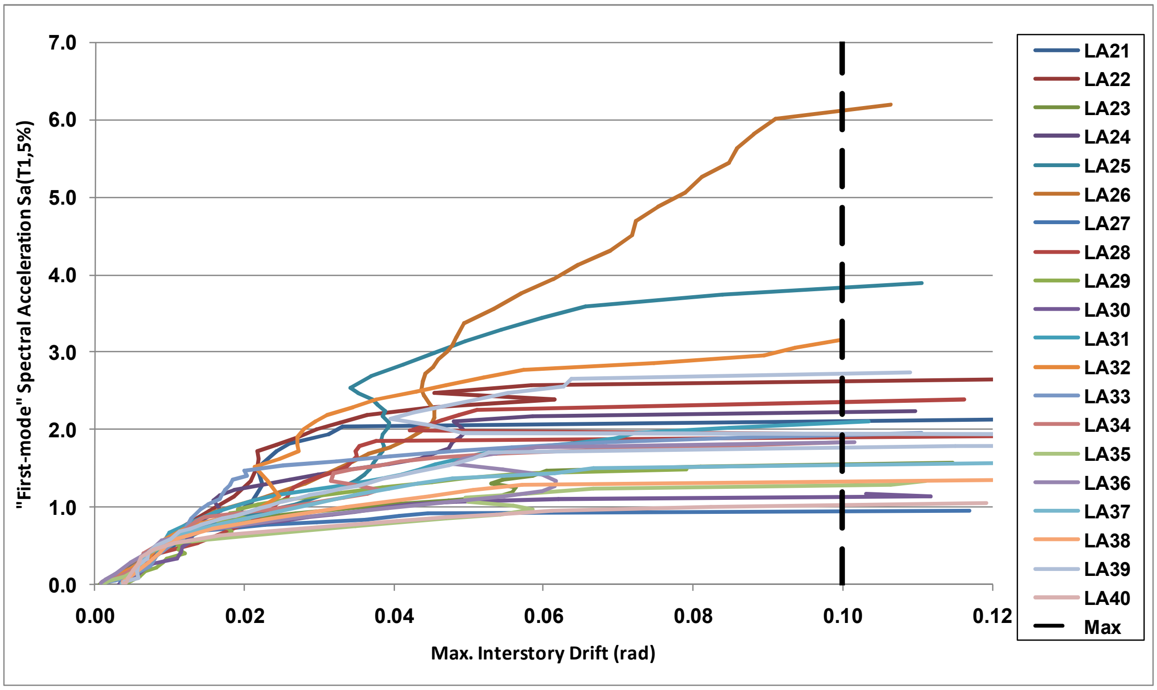

a) Original Nf

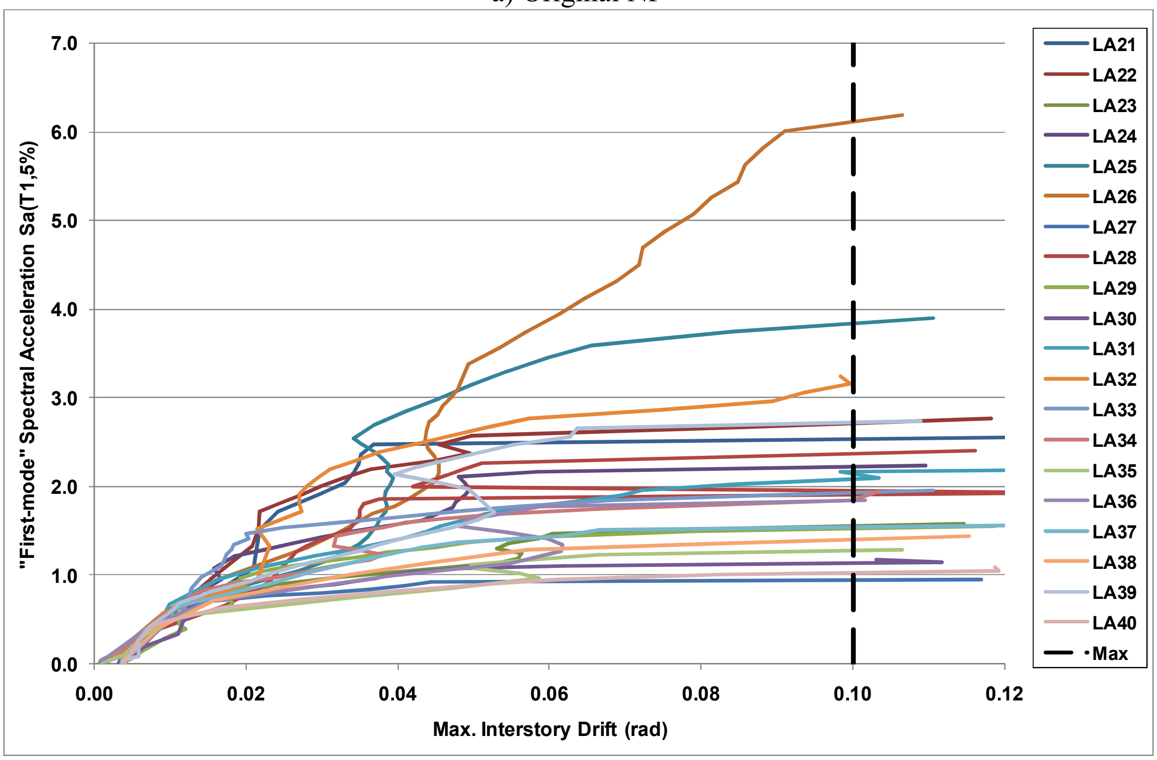

b) Increased Nf

Figure 5.13. IDA Plots for: (a) 9V-PBPD-B-Nf; and (b) 9V-PBPD-B.

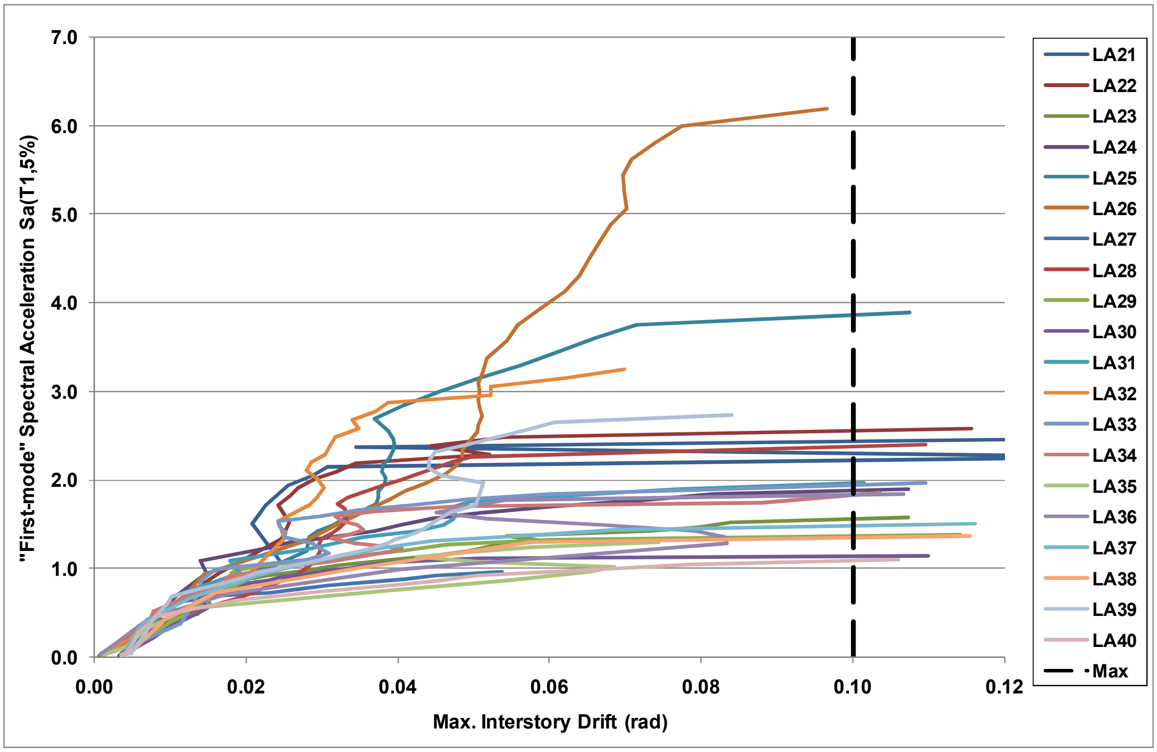

a) Original Nf

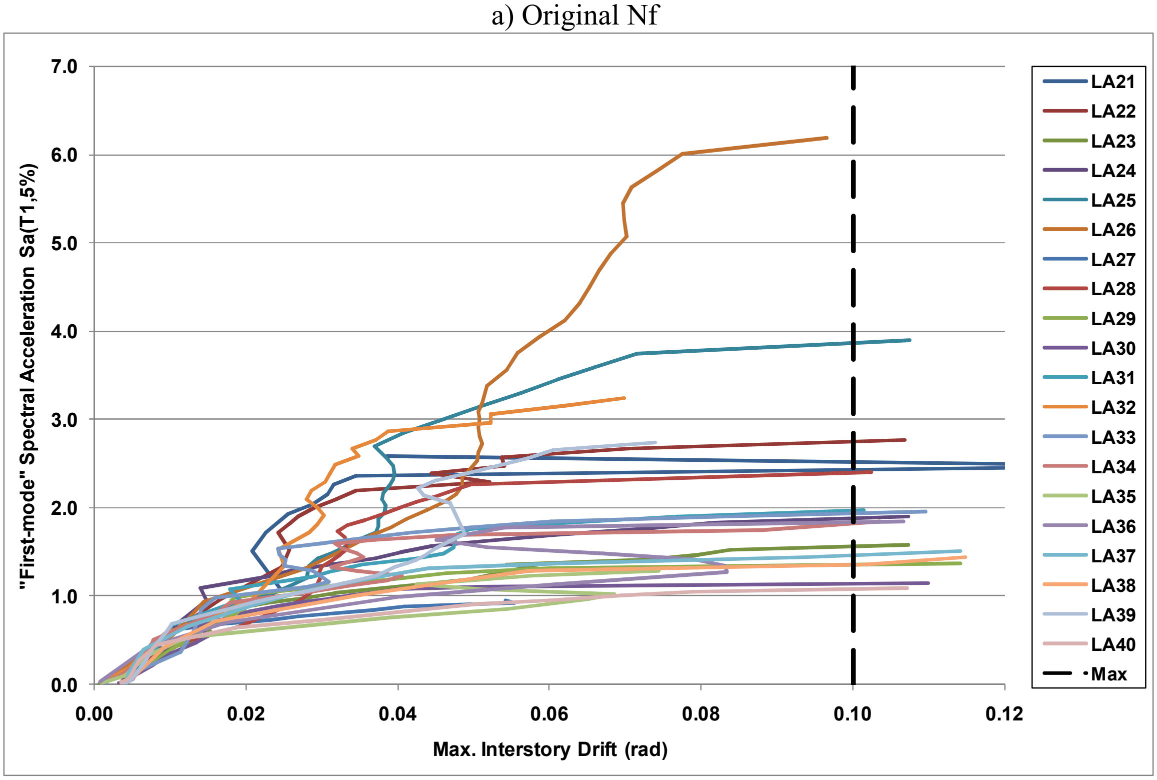

b) Increased Nf

Figure 5.14. IDA Plots for: (a) 9X-PBPD-B1-Nf; and (b) 9X-PBPD-B1.

CHAPTER 6

Summary and Conclusions

6.1 Summary

Application of the PBPD method to seismic design of CBF is presented in this report. The PBPD method directly accounts for inelastic behavior by using pre-selected target drift and yield mechanism as key performance limit states. As a result, control of drift and yielding is built into the design process from the very start, eliminating or minimizing the need for lengthy iterations to arrive at the final design.

The overall PBPD procedure for design of CBF was presented in Chapter 2. One procedure developed earlier to calculate the PBPD design base shear by using the concept of energy modification factor, η, was discussed. In addition, several related design recommendations were proposed in order to improve the seismic performance of CBF systems and to avoid undesirable failure modes. Those recommendations include: Use of beam shear splices to minimum moment transfer into the columns; using double HSS sections for braces instead of single HSS, and direct consideration of the fracture criterion along with strength and compactness criteria for the design of braces. Two CBF systems, 3 and 6-story frames previously designed based on 1997 NEHRP, were redesigned using the PBPD procedure. The redesigned frames showed dramatic improvement in their seismic performance. Unlike the NEHRP frames, the PBPD frames showed no brace fractures, no column plastic hinges (except at the base), and smaller residual story drifts.

New findings based on more recent research work on PBPD procedure for CBF systems were presented in Chapter 3. A new configuration for the gusset plate connection, in which the brace gusset plate is only connected to the column, is proposed in order to minimize the flexural rigidity of the brace-beam-column connection. Also, the current capacity design method for columns in CBF based on the cumulative axial forces was evaluated by comparing the column moments from the pushover and dynamic analyses.

In addition, an alternative method to account for pinched hysteretic behavior of CBF, which can also be applied to other systems with degrading hysteretic behavior was introduced. In this method, a modification factor, called λ-factor, is directly applied on the target drift to account for the effect of pinching. The λ-factor is the ratio between the maximum displacement of a pinched SDOF system (representing CBF) to that of an equivalent elastic-plastic SDOF. By dividing the design target drift for the CBF by this factor, an effective target drift is obtained which is then used to calculate the PBPD design base shear. Also, for design base shear calculation in CBF systems, a procedure to estimate the varying yield drift ratio (due to flexural deformation caused by axial deformation of columns) at the beginning of design for braced systems is introduced. The target drift ratio for such systems is modified accordingly, based on the original definition of the target drift for use in the work-energy equation in PBPD. Finally, the suggested PBPD procedure was applied to design the 9-story SAC building by using Chevron-type

CBF as the lateral force resisting system. The performance of this design was then evaluated using both DBE and MCE level SAC LA ground motions.

In Chapter 4, the reliability-based performance evaluation (confidence level analysis) was carried out for the study CBF structures, the NEHRP designs (Sabelli, 2000) and the PBPD designs. The NEHRP frames were shown to have very low confidence levels against collapse by Uriz and Mahin (2004). For reference, a summary of the reliability-based performance evaluation procedure developed as part of the FEMA/SAC Steel Project (FEMA, 2000) was also presented.

The main objective of the study presented in Chapter 5 was to improve the confidence level against collapse (C.L.) for the 9-story CBF against collapse. Several modifications were suggested. The first modification was in the design base shear (DBS) calculation. A slightly larger λ-factor was suggested for mid to high-rise CBF frames to offset the detrimental effect of P-Delta overturning forces in the calculation of DBS.

The effect of using Split-X (two story X bracing) configuration on seismic performance and C.L. of CBF was also studied. In addition, the effect of increasing brace fracture life, Nf, on seismic performance and C.L. was evaluated.

6.2 Major Conclusions and Findings

Based on the study presented in this report, following conclusions can be drawn:

1. The basic PBPD method has been successfully adapted for CBF systems by making appropriate modifications.
2. The seismic performance and confidence level against collapse under severe ground motions can be dramatically enhanced by using the PBPD procedure as developed herein.
3. Results from nonlinear time-history analyses carried out on example frames designed by PBPD method showed the frames met all desired performance objectives, including the intended yield mechanism and story drifts, while preventing brace fractures and undesirable column yielding under varied hazard levels.
4. Application of the PBPD method for taller CBF systems was achieved by using the proposed modifications in PBPD design base shear calculation as demonstrated in Chapter 3. The proposed modifications included, accounting for pinched hysteretic behavior, varying yield drift and selection of proper target drift.
5. It was shown in Chapter 3 that the dual hazard level design based on appropriate target drift for each hazard level can be easily and reliably implemented in the PBPD procedure to obtain the desired performance at different hazard levels for CBF systems.

Other major findings from the study presented in Chapter 3 are:

a) Although there is some eccentricity in the proposed connection Type II of gusset plate to column, the total unbalanced moments transferred to the columns are smaller as compared with those in the connection Type I where beam shear splice is used. This is due to the fact that the shear connection in this configuration is much closer to the column centerline. Also, the moments produced by the axial force in the brace and those produced by the shear force in the beam act in opposite directions. Since the columns in CBF are generally designed for axial force only, having less moment demand on columns would ensure better performance.

b) Even with considering only axial forces in column design in CBF, good performance can still be expected for the PBPD frame. The main reason is that although moments were not considered in columns during the design, maximum moments and maximum axial forces in the columns generally do not occur at the same time. Also, the axial force used in column design is based on the assumption that all braces buckle and yield at the same time, which is quite conservative. A practical implication is that since there would be some bending moments in the columns it is better to use somewhat deeper sections whenever possible in order to have some reserve bending capacity.

c) A new approach (λ-factor method) was used to account for the pinched hysteretic behavior of CBF systems in PBPD procedure. The method can be easily applied to other degrading systems as well. This method gave reasonable design base shear values for low-rise as well as high-rise CBF structures. The proposed modifications on yield drift and target drift should also be included in the modified procedure.

d) The proposed modifications were applied in the design of the 9-story SAC LA frame with CBF as the lateral system. The results from nonlinear static and time-history analyses showed excellent performance of the designed structure under both DBE and MCE hazard levels, proving that the dual level design concept worked well.

Following conclusions are drawn from the study presented in Chapter 4:

a) Reliability-based performance evaluation by using the FEMA 351 procedure, which accounts for randomness and uncertainty in the estimation of seismic drift demand and capacity, showed that CBF designed by the proposed Performance-Based Plastic Design (PBPD) method can have dramatically higher confidence levels against global collapse than those of SCBF designed by current practice. Also, those confidence levels can be similar to the target levels for SMF in current practice, i.e., 90% or above.
b) Dramatic improvement in the confidence level was seen for the 3V-PBPD frame, comparable with those of MF designed by 1997 NEHRP code (Yun et al., 2002). On the other hand, the 3V-NEHRP frame showed extremely low confidence level against global collapse (less than 1%). It was also be seen that although the median drift capacities for the two 3-story frames were somewhat close, they showed quite different drift demands under 2/50 ground motions.
c) The confidence level for 6V-NEHRP frame was somewhat better than that of the 3V-NEHRP frame, but was still much less than the 90% satisfactory level as suggested by FEMA 351. Large difference was still observed in the confidence

levels of 6V-NEHRP and 6V-PBPD frames, with the latter having a confidence level quite close to 90%.

Following conclusions are drawn from the study presented in Chapter 5:

a) Higher values of design base shear (DBS) for 9-story (and taller) CBF were obtained using the proposed new λ-factor in PBPD method. This new λ-factor results in larger design base shear for mid to high-rise CBF structures.

b) The 9-story Chevron CBF design based on the new DBS showed smaller story drifts under both DBE (10%/50 yrs) and MCE (2%/50 yrs) ground motions compared to the 9V-PBPD-A frame designed in Chapter 3.

c) Higher levels of confidence level (C.L.) against collapse were obtained using the new DBS for Chevron configuration. The C.L. of 52% obtained in Chapter 4 for 9V-PBPD-A increased to 68.6% by using the new DBS in 9V-PBPD-B.

d) Improvement was seen in C.L. of the Chevron frame designed by using increased N_f (of more than 200) for fracture life of the braces. This increase in N_f resulted in increase of C.L. of the 9-stoy Chevron CBF from 68.6% to 79.4% (about 11%).

e) It was shown that C.L. of 9-story CBF improved by only changing the brace configuration to Split-X. The C.L. increased from 68.6% to 77.4% (about 10%) by using Split-X instead of Chevron configuration. The same brace sections were used. However, much lighter beams are needed in the Split-X configuration. The C.L. obtained for the Split-X design with original N_f values was almost equal to that of Chevron design with increased N_f.

f) Increasing the design base shear did not have much effect on drift capacity of the 9-story CBF frames obtained from IDA. However, larger design base shear resulted in lower drift demands with reduced scatter under MCE ground motions which basically translates into higher confidence level.

g) Increase in design base shear based on the new λ-factor was seen to be the main factor in reducing the story drifts under MCE level ground motions. Better controlled drift demand results in higher confidence level.

h) Increase in N_f value (brace fracture life factor) did not have significant effect on drift response under MCE level SAC LA ground motions since the maximum story drifts generally occur at the early stages for such near-field ground motions.

REFERENCES

AISC. (1997), Seismic Provisions for Structural Steel Buildings, American Institute of Steel Construction, Chicago, Illinois.

AISC. (2005a), ANSI/AISC 341-05, *Seismic Provisions for Structural Steel Buildings*, American Institute of Steel Construction, Chicago, Illinois.

AISC. (2005b), ANSI/AISC 360-05, *Specification for Structural Steel Buildings*, AmericanInstitute of Steel Construction, Chicago, Illinois.

ASCE. (2000), "Prestandard and Commentary for the Seismic Rehabilitation of Buildings," FEMA 356 Report, prepared by the American Society of Civil Engineers, published by Federal Emergency Management Agency, Washington, D. C.

ASCE. (2005), Minimum Design Loads for Buildings and Other Structures, SEI/ASCE 7-05, American Society of Civil Engineers, Reston, VA.

Astaneh-Asl, A. (1998), "Seismic Design And Behavior of Gusset Plates." Structural Steel And Education Council (Steel Tips), 209 Vernal Drive, Alamo, California 94507.

Astaneh-Asl, A., Goel, S., and Hanson, R. D. (1985), "Cyclic out-of-plane buckling of double-angle bracing." *ASCE Journal of Structural Engineering*, 111(5), 1135- 1153.

Bayat, M.R., Chao, S-H., and Goel, S.C. (2010), "Further Development of Performance-Based Plastic Design Method for Concentrically Braced Frame." *9th US National and 10th Canadian Conference on Earthquake Engineering, July 2010, Toronto, Canada.*

Bayat, M.R. (2010), "Performance-Based Plastic Design of Earthquake Resistant Steel Structures: Concentrically Braced Frames, Tall Moment Frames, and Plate Shear Wall Frames" *Ph.D. Dissertation*, University of Texas at Arlington.

Calvi, G. M., Priestley, M. J. N., Sullivan, T. J., and Happold, B. (2006), "Development of Displacement-Based Design and Assessment Methods; Progress Review: Year 1." *Presentation, European Centre for Training and Research in Earthquake Engineering (EUCENTRE), Nov 2006. (url:* http://www.reluis.it*).*

Chao, S.-H., and Goel, S. C. (2005), "Performance-Based Seismic Design of EBF Using Target Drift and Yield Mechanism as Performance Criteria," *Report No. UMCEE 05-05*, Department of Civil and Environmental Engineering, University of Michigan, Ann Arbor, MI.

Chao, S-H., and Goel, S. C., (2006a), “Performance-Based Plastic Design of Seismic Resistant Special Truss Moment Frames (STMF).” *Report No. UMCEE 06-03*, Department of Civil and Environmental Engineering, University of Michigan, Ann Arbor, MI.

Chao, S-H., and Goel, S. C., (2006b). “A seismic design method for steel concentric braced frames for enhanced performance.” *4th International Conference on Earthquake Engineering, Taipei, Taiwan.*

Chao, S.-H., and Goel, S.C., Lee, S.-S., (2007), “A Seismic design lateral force distribution based on inelastic state of structures.” *Earthquake Spectra* 23 (3), 547-569.

Chao, S.-H., Bayat, M. R., and Goel, S.C., (2008), “Performance-Based Plastic Design of steel concentric braced frames for enhanced confidence level.” *14th World Conference on Earthquake Engineering, Beijing, China.*

Federal Emergency Management Agency, FEMA (2000a), FEMA 356, *Prestandard and Commentary for the Seismic Rehabilitation of Buildings,* Washington, D. C.

Federal Emergency Management Agency, FEMA (2000b), FEMA 351, *Recommended Seismic Evaluation and Upgrade Criteria for Existing Welded Steel Moment Frame Buildings*, , Federal Emergency Management Agency, Washington, D. C.

Federal Emergency Management Agency, FEMA (2004), FEMA 440, *Improvement of Inelastic Seismic Analysis Procedures*, Federal Emergency Management Agency, Washington, D. C.

Federal Emergency Management Agency, FEMA (2009), FEMA P695, *Recommended Methodology for Quantification of Building System Performance and Response Parameters*, prepared for the Federal Emergency Management Agency, prepared by the Applied Technology Council, Redwood City, CA

Foutch, D. and Shi, S. (1998), “Effects of Hysteresis Type on the Seismic Response of Buildings.” *Proceedings of the 6th US National Conference on Earthquake Engineering*.

Goel, S. C. (1992a), “Earthquake Resistant Design of Ductile Braced Steel Structures,”
Stability and Ductility of Steel Structures under Cyclic Loading, CRC Press, Boca Raton, FL., pp. 297-308.

Goel, S.C., (1992b). “Earthquake Resisitant Design of Ductile Braced Steel Structures.” In *Stability and Ductility of Steel Structures under Cyclic Loading*. Ed. Y. Fukumoto and G. C. Lee. Boca Raton, FL: CRC Press: 297-308.

Goel, S.C., and Lee, S. (1992), “A Fracture Criterion for Concrete-Filled Tubular Bracing Members Under Cyclic Loading.” *Proceedings of the 1992 ASCE Structures Congress*, ASCE, pp. 922-925, Reston, VA.

Goel, S.C. and Chao, S-H., 2008. *Performance-Based Plastic Design: Earthquake Resistant Steel Structures*, International Code Council.

Gupta, A. and Krawinkler, H. (1999). “Seismic Demands for Performance Evaluation Steel Moment Resisting Frame Structures.” *Report No. 132*, The John A. Blume Earthquake Engineering Center, Dept. of Civil and Env Eng., Stanford University.

Gupta, B and Kunnath, S.K. (1998), “Effects of Hysteresis Model Parameters on Inelastic Seismic Demands.” *Proceedings of the 6th US National Conference on Earthquake Engineering.*

Hassan, O. F., and Goel, S. C. (1991). "Modeling of Bracing Members and Seismic Concentrically Braced Frames." *UMCE 91-1*, University of Michigan, College of Engineering, Ann Arbor, MI 48109-2125.

Lacerte, M., Tremblay, R. (2006), “Making Use of Brace Overstrength to Improve the Seismic Response of Multistory Split-X Concentrically Braced Steel Frames.”, *Canadian Journal of Civil Engineering*, 33 (8), 1005-1021.

Lee, S-S, and Goel, S. C. (1987), “Seismic Behavior of Hollow and Concrete-Filled Square Tubular Bracing Members,” *Report No. UMCE 87-11*, Department of Civil and Environmental Engineering, University of Michigan, Ann Arbor, MI.

Lee, H.-S, and Goel, S. C. (1990), “Seismic Behavior of Steel Built-Up Box-Shaped Bracing Members and Their Use in Strengthening Reinforced Concrete Frames,” *Report No. UMCE 90-7*, Department of Civil and Environmental Engineering, University of Michigan, Ann Arbor, MI.

Lee, S.-S. and Goel, S.C. (2001). “Performance-Based Design of Steel Moment Frames Using Target Drift and Yield Mechanism”, *Report No. UMCEE 01-17*, Dept. of Civil and Environmental Engrg, University of Michigan, Ann Arbor, MI.

Leelataviwat, S.(1998), “Drift and Yield Mechanism Based Seismic Design and Upgrading od Steel Moment Frames”, *PhD Dissertation*, University of Michigan, Ann Arbor, MI.

Liu, Z. and Goel, S.C. (1987), “Investigation of Concrete Filled Steel Tubes under Cyclic Bending and Buckling.” *Report No. UMCEE 87-03*, Department of Civil and Environmental Engineering, University of Michigan, Ann Arbor, MI.

Liu, Z. and Goel, S.C. (1988), “Cyclic Load Behavior of Concrete-Filled Tubular Braces,” *Journal of the Structural Division*, ASCE, Vol. 114, No. 7, Reston, VA.

MacRae, G.A., Kimura, Y., Roeder, C. (2004), “Effect of Column Stiffness on Braced Frame Seismic Behavior.” Journal pf Structural Engineering, 130(3), 381-391.

Medina, R. A. and Krawinkler, H. (2004). "Influence of Hysteretic Behavior on the Nonlinear Response of Frame Structures", *Proceedings of the 13th World Conference on Earthquake Engineering*, 13WCEE, Vancouver, B.C., Canada, Paper # 239, August 1-6.

NCREE website, National Center for Research on Earthquake Engineering, Taipei, Taiwan, *url:* http://w3.ncree.org/

NEHRP (National Earthquake Hazards Reduction Program). (1997). FEMA 302: Recommended Provisions for Seismic Regulations for New Buildings and Other Structures. Washington, D.C., Federal Emergency Management Agency.

Rai, D.C., Goel, S. C. and Firmansjah, J. (1996). “SNAP-2DX: General Purpose Computer Program for Static and Dynamic Nonlinear Analysis of Two Dimensional Structures.” *Report No. UMCEE 96-21*, Dept of Civil and Environmental Engrg, University of Michigan, Ann Arbor, MI.

Rahnama, M., and Krawinkler, H. (1993), “Effects of soft soil and hysteresis model on seismic demands”, *Report No. 108,* John A. Blume Earthquake Engineering Center Department of Civil and Environmental Engineering, Stanford University, Stanford, California.

Redwood, R. G., and Channagiri, V. S. (1991), “Earthquake Resistant Design of Concentrically Braced Steel Frames,” *Canadian Journal of Civil Engineering*, Vol. 18, pp. 839-850.

Richards, P. 2008. Seismic column demands in ductile frames. *Journal of Structural Engineering*, 135 (1), 33-41.

Ruiz-Garcia, J., Miranda, E. (2005), “Performance-based assessment of existing structures accounting for residual displacements”, *Report TR-153*, The John A. Blume Earthquake Engineering Center, Stanford University, Stanford, CA.

Sabelli, R., 2000. “Research on Improving the Design and Analysis of Earthquake Resistant Steel Braced Frames”, FEMA/EERI Report, Washington, D. C.

Sabelli, R., Mahin, S., and Chang, C. (2003), “Seismic Demands on Steel Braced Frame Buildings with Buckling-Restrained Braces,” *Engineering Structures*, Vol. 25, pp. 655-666.

Sabelli, R., and Bruneau, M. 2007. *Steel Plate Shear Walls (AISC design guide # 20)*, American Institute of Steel Construction, Chicago.

Shaback, B., and Brown, T. (2003),” Behaviour of Square Hollow Structural Steel Braces with End Connections under Reversed Cyclic Axial Loading,” *Canadian Journal of Civil Engineering*, Vol. 30, pp. 745-753.

Somerville, P.G., Smith, M., Punyamurthula, S. and Sun, J. (1997). “Development of Ground Motion Time Histories for Phase 2 of the FEMA/SAC Steel Project”, *Report No. SAC/BD-97/04*, SAC Joint Venture, Sacramento, CA.

Tang, X., and Goel, S. C. (1987), “Seismic Analysis and Design Considerations of Braced Steel Structures,” *Report No. UMCEE 87-04*, Department of Civil and Environmental Engineering, University of Michigan, Ann Arbor, MI

Tang, X., and Goel, S. (1989). "Brace Fractures and Analysis of Phase I Structure."*ASCE Journal of Structural Engineering*, 115(8), 1960-1976.

Tremblay, R., Bruneau, M., Nakashima, M., Prion, H. G. L., Filiatrault, A., and Devall, R. (1996), “Seismic Design of Steel Buildings: Lessons from the 1995 Hyogo-Ken Nanbu Earthquake,” *Canadian Journal of Civil Engineering*, Vol. 23, pp. 727-756.

Tremblay, R. and Robert, N. (2000), “Seismic Design of Low- and Medium-Rise Chevron Braced Steel Frame.” *Canadian Journal of Civil Engineering*, 27(6), 338-360.

Uriz, P., Mahin, S.A. (2004). “Seismic Performance Assessment of Concentrically Braced Frames”. Paper No. 1639, *13th World Conference on Earthquake Engineering*, Vancouver, B. C., Canada.

Uriz, P. (2005). “Towards Earthquake Resistant Design of Concentrically Braced Steel Structures”, *Ph.D. Thesis*, University of California, Berkeley.

Vamvatsikos, D. and Cornell, C.A. (2002), "Incremental Dynamic Analysis." *Earthquake Engineering and Structural Dynamics*, 31, 491-514.

Yun, S.-Y., Hamburger, R.O., Cornell, C.A. and Foutch, D.A. (2002), "Seismic Performance Evaluation for Steel Moment Frames." *Journal of Structural Engineering*, 128: 4, 534-545.